# Molecular Dynamics Simulation Studies of Piperazine Activated MDEA Absorption Solution with Methane and Carbon Dioxide


Master of Science Thesis in

Process Technology - Separation

by

Amir Hajiahmadi Farmahini

Department of Physics and Technology

University of Bergen - Norway

June 2010

**بنام خدا**

To my parents

تقدیم به پدر و مادر نازنینم

## Abstract

Regenerative chemical absorption process is widely used in industry for removal of carbon dioxide from natural gas, with activated aqueous solutions of alkanolamines considered a beneficial blend. One of the most promising blends is the aqueous mixture of methyldiethanolamine (MDEA) activated by small amount of piperazine, due to the fairly high rate of reaction of piperazine as a cyclic diamine with carbon dioxide and the low heat of regeneration of MDEA as a tertiary alkanolamine. However, mechanisms involved in absorption of carbon dioxide by means of aqueous piperazine activated MDEA solution are not well understood and available knowledge within the open literature is limited.

This thesis aimed to extend our knowledge of the topic by providing insights into the intermolecular interactions involved in mechanisms governing the absorption of $CO_2$. Furthermore, understanding of the processes associated with the undesired trapping of methane was an additional objective. Characterization of the blend to analyze the distribution of the absorbent and absorbate molecules inside the amine solution was yet another goal for this work. In general, a better understanding of intermolecular interactions and correlations between molecular constituents of the amine solution during the overall process of carbon dioxide absorption from natural gas was expected from this work.

To achieve this purpose, MD simulation was chosen as the scientific method to study the system on the molecular scale but prior to starting the simulation, the following had to be accomplished.

Initially, an extensive literature review was carried out to determine the speciation of the solution in thermodynamic conditions relevant for absorption units in amine gas treating plants. Moreover, the natural gas was simplified to an impurity free binary mixture of methane and carbon dioxide during the simulation.

In order to study the system on the molecular level, we obtained missing force-field parameters by combining the OPLS parameter with ab-initio calculations for piperazine molecule, piperazine carbamate, protonated piperazine and molecular MDEA. To investigate the most important torsional angles in MDEA and piperazine carbamate, geometry of the molecules was optimized and rigid coordinate scan was performed to define true torsional angles, so that ultimately, new functions for dihedral angles of these molecules were derived. In order to calculate the partial atomic charges for all the above mentioned models, Mulliken,

Löwdin and CM4 partial atomic charges were computed using 6-31G** basis set and SM8 solvation model. Given the reliability and accuracy of the CM4 charges, they were chosen to be implemented into the final models. Other models for carbon dioxide, methane and water molecules needed for the simulations were taken from literature.

Constraint MD simulation was performed at constant temperature using MDynaMix Ver.5.1 for one primary and four reference systems.

It was observed that the MDEA was separated from aqueous phase and positioned alongside the gas-liquid interface. Moreover, it was determined that piperazine molecules were spread within MDEA phase, while protonated piperazine and piperazine carbamate mainly dissolved in the water bulk. Hydrogen bond network inside the solution was studied based on geometric definition of hydrogen bonding. It was demonstrated that nitrogens and oxygens in amine, alcohol and carboxylate groups were capable of forming hydrogen bonds, so that piperazine carbamate, protonated piperazine and MDEA formed considerable number of hydrogen bonds with surrounding water in their vicinity. It was also shown that such a hydrogen bonding network has important influence on molecular distribution in the system.

Performance of piperazine was observed in accelerating mechanism of carbon dioxide absorption. This simulation highlighted the important role of piperazine and piperazine carbamate in regard with absorption of carbon dioxide. It was demonstrated that piperazine activated solution of MDEA becomes very efficient for absorption of $CO_2$in accordance with enhanced solubility of carbon dioxide in the amine solution. Moreover, it was indicated that MDEA has high loading capacity for removal of carbon dioxide.

Several investigations were carried out in various systems to evaluate the affinity of carbon dioxide and methane towards different functional groups in piperazine and MDEA molecules. It was demonstrated that carbon dioxide shows higher affinity towards the amine and alcohol groups compared to methane. Methane was almost inert towards alcohol groups in MDEA while, it was found to be somewhat attracted by amine groups of both piperazine and MDEA molecules. Consequently, it was deduced that amine groups are mainly responsible for absorption of carbon dioxide.

These simulations have also shown that this kind of blend contributes to undesired trapping of methane, which is regarded as a crucial drawback for the ultimate goal of absorption process in natural gas treating plant. In this regard, sandwich packing of methane molecules by a pair

of piperazine rings was investigated as a possible mechanism affecting the absorption process of carbon dioxide. It was found that most probably this is not the major mechanism for entrapment of methane at low loading; however, it was turned out that amine groups carry the main responsibility for the observed sandwich candidates in trapping of methane in current study.

## Acknowledgments

I owe my deepest gratitude to my supervisor Prof. Bjørn Kvamme. He offered me this opportunity to work on the subject of current research and attracted my attention for the first time to the exciting world of quantum chemistry and molecular simulation. His extensive knowledge over the issue in addition to his inspiring character was always a great help in every single step of the work. I learnt many things under his supervision during my master studies.

It is also an honor for me to thank my co-supervisor Prof. Tatiana Kuznetsova. This thesis would not have been possible unless her every day assistance. She was always welcoming and patient about my interminable questions.

I am greatly indebted to PhD. Student Bjørnar Jensen - my peer research group - who generously helped me during entire last year. He shared with me his deep knowledge of quantum chemistry and molecular simulation. We had many useful discussions around different parts of the work which was undeniably instructive for me. Bjørnar reviewed my entire thesis and gave me several useful comments with his pinpoint accuracy. Moreover, I would like to thank him specifically for his great help in writing scripts for VMD program. It was close to impossible for me to cope with the programming issue without his extensive programming knowledge. At the same time, I would like to show my gratitude towards PhD student Mohammad.T.Vafaei for his useful comments and suggestions on my thesis.

In addition, employees at Bergen Center for Computational Science (BCCS) which followed my application for access to Hexagon super computers until it was available, I am also thankful to them.

The last but of course not the least, this master study - far from home - was not possible without my parents supports. I even cannot express my deep appreciation of what they have done for me. Hereby, I would love to thanks Mom and dad and also my kind sisters for everything during these two years.

## Abbreviations

| | |
|---|---|
| AMBER | Assisted Model Building and Energy Refinement |
| AO | Atomic Orbital |
| BASF | Badische Anilin- und Soda-Fabrik chemical company |
| BCCS | Bergen Center for Computational Science |
| BEA | Buthyl Ethanol Amine |
| BET | Brunauer-Emmett-Teller |
| B3LYP | Beck-3-Lee-Yang-Parr |
| CHARMM | Chemistry at HARvard Molecular Mechanics |
| CM4 | Charge Model class 4 |
| DEA | Di Ethanol Amine |
| DFT | Density Functional Theory |
| DGA | Di Glycol Amine |
| DIPA | Di Iso  Propanol Amine |
| DOW | Dow Chemical Company |
| DZ | Double Zeta basis sets |
| EXXON | Exxon Mobil Corporation |
| GGA | Generalized Gradient Approximation |
| GTO | Gaussian Type Orbital |
| GUI | Graphical User Interface |
| HF | Hartree-Fock |
| IFT | Interfacial Tension |
| KE | Kent-Eisenberg |
| KS | Kohn-Sham |
| La | The Hume Linear Algebra Tcl Package |
| LCAO | Linear Combination of Atomic Orbitals |
| LDA | Local Density Approximation |

| | |
|---|---|
| L-J | Lennard-Jones |
| LPA | Löwdin Population Analysis |
| LSDA | Local Spin Density Approximation |
| MD | Molecular Dynamics |
| MDEA | Methyl Di Ethanol Amine |
| MEA | Mono Ethanol Amine |
| MM | Molecular Mechanics |
| MO | Molecular Orbital |
| MPA | Mulliken Population Analysis |
| NAM | N-Acetyl Morpholine |
| NFM | N-Formyl Morpholine |
| NMR | Nuclear Magnetic Resonance |
| NRTL | Non-Random Two-Liquid |
| OPLS-aa | Optimized Potentials for Liquid Simulations-all atom |
| PBC | Periodic Boundary Condition |
| PDB | Brookhaven Protein Databank |
| PDE | Partial Differential Equation |
| PES | Potential Energy Surface |
| PZ | Piperazine |
| PZCOO | Piperazine carbamate |
| PZH | Protonated piperazine |
| QM | Quantum Mechanics |
| RDF | Radial Distribution Function |
| RLPA | Redistributed Löwdin Population Analysis |
| SCF | Self Consistent Field |
| SM | Solvation Model |
| SPC/E | Extended Simple Point Charge |

| | |
|---|---|
| SPE | Single Point Energy |
| STO | Slater Type Orbital |
| SV | Split Valence basis set |
| Tcl | Tool Command Language |
| TEA | Tri Ethanol Amines |
| TNO | The Netherlands Organisation for Applied Scientific Research |
| TZ | Triple Zeta basis sets |
| VLE | Vapor Liquid Equilibrium |
| VMD | Visual Molecular Dynamics |

# Contents

# 1 Introduction

Carbon dioxide capture is one of the major issues in many industrial process plants. A set of technical, economical and environmental reasons supports the idea of carbon dioxide capture. This technology concerns separation of carbon dioxide from gaseous stream either in combustion units as flue gas or in the natural gas treatment plants.

One of the most common technologies used for capturing the carbon dioxide is absorption-desorption process within which different kind of physical and/or chemical solvents are used to separate carbon dioxide from gaseous streams. This process takes place in two different process units usually called absorption and stripper columns. The former is responsible for separation of carbon dioxide from gas stream and the latter facilitates regeneration of the solvents.

Among different kind of chemical absorbents so called alkanolamine solutions are widely used to remove the acid gases like carbon dioxide ($CO_2$) and hydrogen sulfide ($H_2S$) from several types of gas streams such as natural gas, flue gas, synthesis gas and refinery gases (Bottinger et al. 2008). As a case in point monoethanolamine (MEA), diethanolamine (DEA), diisopropanolamine (DIPA) and N-methyldiethanolamine (MDEA) are industrially important for regenerative chemical absorption processes (Samanta and Bandyopadhyay 2007). Moreover, blended solutions of these alkanolamines have also been under consideration to improve absorption of acid gases. More recently activated amine solutions became popular since they benefit a combination of various advantages by mixing the primary, secondary and tertiary amines. This includes relatively high rate of reaction and low heat of regeneration during process of absorption and desorption respectively.

Aqueous solution of piperazine activated MDEA is one of the popular promoted blends. Despite broad application of this kind of blend, reactions, mass transport phenomena and mechanisms involved in absorption of carbon dioxide are not well known. On the other hand, based on high mobility of interface in such systems, several undesired pitfalls such as “flooding, foaming and liquid entrainment” may happen (Poplsteinova 2004). One of the major difficulties attracted the utmost attention is undesired trapping of other molecules during the absorption process. In the case of natural gas treating, trapping of methane molecules is considered as an undesired process. It can lead to the loss of considerable

amount of methane which has apparently a significant impact on the overall process efficiency and the cost issue.

This individual work specifically undertakes investigation of aqueous piperazine activated MDEA solution in molecular scale to provide more insight into the mechanisms and intermolecular interactions which are involved in absorption process of carbon dioxide from natural gas. Alternatively, investigation of undesired trapping of methane during this process is of current work's interest. This research tries to point out some of the phenomena or mechanisms - in microscopic scale - which may potentially give rise to the undesired trapping of methane.

As such, molecular dynamics (MD) simulation approach was chosen to investigate the molecular distribution of the system inside the absorption solution and to study intermolecular interactions for different primary and reference systems. This necessitated to step into the molecular modeling and quantum mechanics world.

Initially a comprehensive literature review had to be done to specify composition of the system in liquid phase and to determine true concentration of each species inside the solution. In other words, this was necessary to approximate speciation of the mixture according experimental determinations.

The next step involved modeling of different species which have major concentration inside the solution. This part required to choose an appropriate force field which fits requirements of liquid mixture. To serve this purpose, OPLS-all atom[1] force field was chosen. Having this, modeling of the molecules or species was followed performing a set of quantum mechanical calculations including geometry optimization, dihedral angle investigation and partial atomic charge calculation.

Once modeling part of the work was finished for five decided models (molecular piperazine (PZ), protonated piperazine (PZH), piperazine carbamate (PZCOO) and methyldiethanolamine (MDEA)), molecular dynamics simulation was performed for four reference systems as well as one primary system. Thermodynamic conditions of the systems were set to be close to the one for absorption unit to be able to replicate the real absorption criteria.

[1] Optimized Potentials for Liquid Simulations (OPLS)

Regarding structure of the current thesis, everything has been categorized in 12 chapters. After introduction (chapter 1), chapter 2 briefly explains justification and importance of the current thesis and describes which targets were expected to be achieved.

Chapter 3 introduces subject of carbon dioxide capture and sets out issue of acid gas removal as a part of gas purification technology. Later, it focuses on the absorption process and application of alkanolamine solutions for removal of carbon dioxide. Finally, aqueous solution of piperazine activated MDEA will be introduced exclusively so that special attention will be paid to the chemical reactions, modeling and complexity of the system.

Chapter 4 turns to the quantum mechanics and molecular modeling world. Principles of quantum mechanics in addition to computational chemistry methods for modeling of molecular systems will be discussed in this chapter. Moreover, a detail description concerning topic of molecular dynamics simulation, concepts and computational techniques will be argued.

Chapter 5 reviews open literature in the area of current thesis and introduces previous researches which have been conducted in this regard.

Chapter 6 presents the road map to the final expected destination by explaining strategy of present work through the subsequent chapters by which contribution of current research to the scientific achievements is introduced.

At this point current writing turns to the practical part of the thesis. Chapter 7 explains methodology, limitations and assumptions in regard with composition of the amine solution and specifies speciation of the liquid phase.

Chapter 8 concerns modeling of the molecular systems in details which includes all the quantum mechanical calculations in this regard. Chapter 9 explains different reference and primary systems precisely in addition to initial simulation set-up for MD.

Finally, chapter 10 is allocated to the outcomes of current thesis so that simulation results will be argued comprehensively in this chapter. Chapter 11 summarizes overall conclusions of the current study and chapter 12 proposes further works based on what have been achieved in this thesis.

# 2 Justification of the work, goals and choice of method

## 2.1 Justification

The regenerative chemical absorption systems which employ piperazine activated N-methyldiethanolamine (MDEA) solution for absorption of carbon dioxide still involve processes and mechanisms which need further studies. Reactions and mechanisms governing the process of mass transport across the gas-liquid interface are quite complex and dynamic so that available models for these phenomena are not perfect yet. Considering experimental data are really limited for these systems, more experimental investigations are required to shed more light on the shadows. Exactly at this point, significance of simulation works emerges. Smart simulations can direct further experimental determinations to the right direction with much lower expenditure.

Accordingly, current research aimed to investigate process of carbon dioxide absorption in molecular scale to provide more insight into the issue and to extend our understanding about the mechanisms which are responsible for this process. Alternatively, it is of great interest for this research to be able to simulate one of the most important drawbacks associated with absorption of carbon dioxide. Undesired trapping of methane during absorption of carbon dioxide is a major pitfall which is industrially and economically crucial. As we know from experimental determinations, methane is highly insoluble inside the water while for the above mentioned activated systems it shows an unusual solubility inside the solution. Technically this is an undesirable process because it wastes capacity of the absorption solution. In addition to that, methane entrapment has a significant cost impact on the overall process cost, since simultaneous trapping of methane in such a system is equal to a huge amount of methane loss per year when absorbed carbon dioxide is used or deposited under the ground.

Consequently, results from this work can provide us with fundamental understanding of the dynamics involved in the uptake of carbon dioxide as well as the mechanisms which govern the undesired trapping of methane. These results can be used to extend our insight into such processes and to improve design of the plants for removal of carbon dioxide from natural gas.

## 2.2 Goals

Absorption of carbon dioxide in alkanolamine systems takes place across a very dynamic interface between the gas and liquid phases. Due to this dynamics, distribution of the solvens and absorbate molecules are quite complex along the interface. Understanding of mechanisms which lead to the absorption of carbon dioxide and unusual trapping of methane molecules

depends on the correct identification of this distribution and characterization of the interface. For current master thesis underlying goals are defined:

- Molecular distribution for both absorbent and absorbate molecules within the gas-liquid interface and inside the liquid bulk will be analyzed. It is of great importance for this work to know how and why amine solvents as well as absorbed gaseous components (methane and carbon dioxide) distribute along the gas-liquid interface and inside the liquid phase. How is this distribution interrelated with other phenomena such as hydrogen bond network in the solution and what is the correlation between different constituents of the gas stream versus various functional groups of amine solvents.
- Significance of hydrogen bond network and ionic characterization of different species will be studied for the molecular distribution of the system.
- Process of carbon dioxide absorption will be studied to identify importance and responsibility of each solvent in uptake of carbon dioxide in connection with chemical reactions and reaction rates presented in literature.
- Effectiveness of aqueous activated piperazine MDEA solution for enhancing the solubility of carbon dioxide will be analyzed.
- Entrapment of methane molecules from binary mixture of natural gas into the activated amine solution will be investigated, so that relevant evidence and related indications from responsible mechanisms will be inspected for further studies.

## 2.3 Choice of method

Considering this work undertakes investigation of activated amine solution in microscopic scale in order to study intermolecular interactions and atomic correlations among different molecules and functional groups, during the process of carbon dioxide absorption, combination of quantum mechanical methods and molecular dynamics simulation were considered to be employed as proper techniques.

Quantum mechanics will be only utilized for modeling of the individual molecules in this work, because simulation of the large systems is not possible by performing ab initio calculations due to humongous computational requirements. On the other hand, molecular dynamics (MD) simulation is suitable for investigation of large systems because of the less computational requirements and time evolutionary characteristic of this method. Hence,

simultaneous application of these two methods will be an appropriate approach which is beneficial for current study.

# 3 Carbon Capture and Acid Gas Removal

## 3.1 Introduction

Gas purification is one of the most significant parts of any gas processing plant since there is always variety of impurity contents in the gas stream. In principle purification process is designed based on type of the impurities and application of the final product. Table 3-1 lists the most important gas phase impurities in gas treating plants.

**Table 3-1: Major Gas Phase Impurities (Kohl and Nielsen 1997)**

| No. | Major Gas Phase Impurities |
|---|---|
| 1 | Hydrogen Sulfide |
| 2 | Carbon Dioxide |
| 3 | Water Vapor |
| 4 | sulfur dioxide |
| 5 | Nitrogen oxides |
| 6 | Volatile organic compounds (VOCs) |
| 7 | Volatile chlorine compounds (e.g., HC1, C12) |
| 8 | Volatile fluorine compounds (e.g., HF, SiF4) |
| 9 | Basic nitrogen compounds |
| 10 | Carbon monoxide |
| 11 | Carbonyl sulfide |
| 12 | Carbon disulfide |
| 13 | Organic sulfur compounds |
| 14 | Hydrogen cyanide |

Among different gas impurities mentioned above some of them are considered as sour gases or acidic gases. Hydrogen sulfide is the best known example for sour impurities because of the smell due to its sulfur content. This substance is both very harmful and corrosive for process equipments and has to be removed from main gas streams to avoid potential problems. Similar to hydrogen sulfide, carbon dioxide is considered as another dominant acidic gas in many gas treating facilities including the natural gas processing units.

Since the focus of this work is merely on the removal of carbon dioxide from natural gas, the focus of following descriptions concerns separation of carbon dioxide rather than other impurities inside the gas stream.

In fact, carbon dioxide capture is an important subject in many different sectors of industry, which produces significant amount of carbon dioxide emissions. Basically all of the hydrocarbon base energy facilities and natural gas processing units have to deal with the issue of carbon dioxide removal. In fossil fuel power plants capturing of the carbon can be accomplished either by separation of $CO_2$ from flue gases or by utilizing different processing methods such as integrated gasification combined cycle (IGCC). Similarly, in natural gas processing units, different technologies can be employed to achieve carbon capturing goals.

A broad range of considerations from technical and economical point of view to even environmental solicitudes necessitate establishment of carbon capture facilities at the aforementioned industrial plants. For instance in technical point of view corrosion of process equipments due to the acidic characterization of the carbon dioxide is one the important issues while on the other hand, presence of carbon dioxide can occupy useful capacity of the pipeline which is needed for transportation of natural gas. Similarly for ammonia plants, carbon dioxide has to be removed in some stages since the ammonia synthesis catalysts can be poisonous in presence of carbon dioxide.

Alternatively, economical concerns play an undeniable role in the issue of carbon dioxide capture. As an illustration, carbon dioxide decreases heating value of natural gas in combustion units which is clearly of no interest. Furthermore, it is now proven that carbon dioxide is the main contributor among other greenhouse gases to the global warming problem (Watson et al. 2001). This fact that carbon dioxide has been the main participant of the recent climate changes since industrial revolution has attracted tremendous attentions from around the world. Currently a global debate has arisen out of the global warming effects of carbon dioxide to control the carbon emission by following different carbon mitigation strategies.

## 3.2 General View

As previously mentioned, acid gas removal refers to a group of separation methods by which the most important acidic constituents of the gas stream are removed. This includes various traditional and newly developed purification technologies which are currently available for gas processing industry. In principle following categorization (Kohl and Nielsen 1997) can be considered as the main purification technologies for carbon dioxide removal:

1. Absorption into the solution
2. Adsorption on a solid surface
3. Permeation through a membrane

4. Methanation

### 3.2.1 Absorption

Absorption is separation of the gas constituents based on their solubility into a liquid environment. Indeed, since different components of the gas mixture have various solubility inside the liquid phase, selective dissolution of the impurities is possible.

Principally, absorption process is the first stage of a absorption-desorption cycle in gas treating plants. This process takes place inside the absorption column to separate the acid gases from gaseous stream using different types of solvents. On the other hand, second stage concerns regeneration of the solvents within stripper (regenerator) column where solvents are regenerated from enriched absorbent solution. Figure 3-1 illustrates absorption-desorption cycle for amine systems.

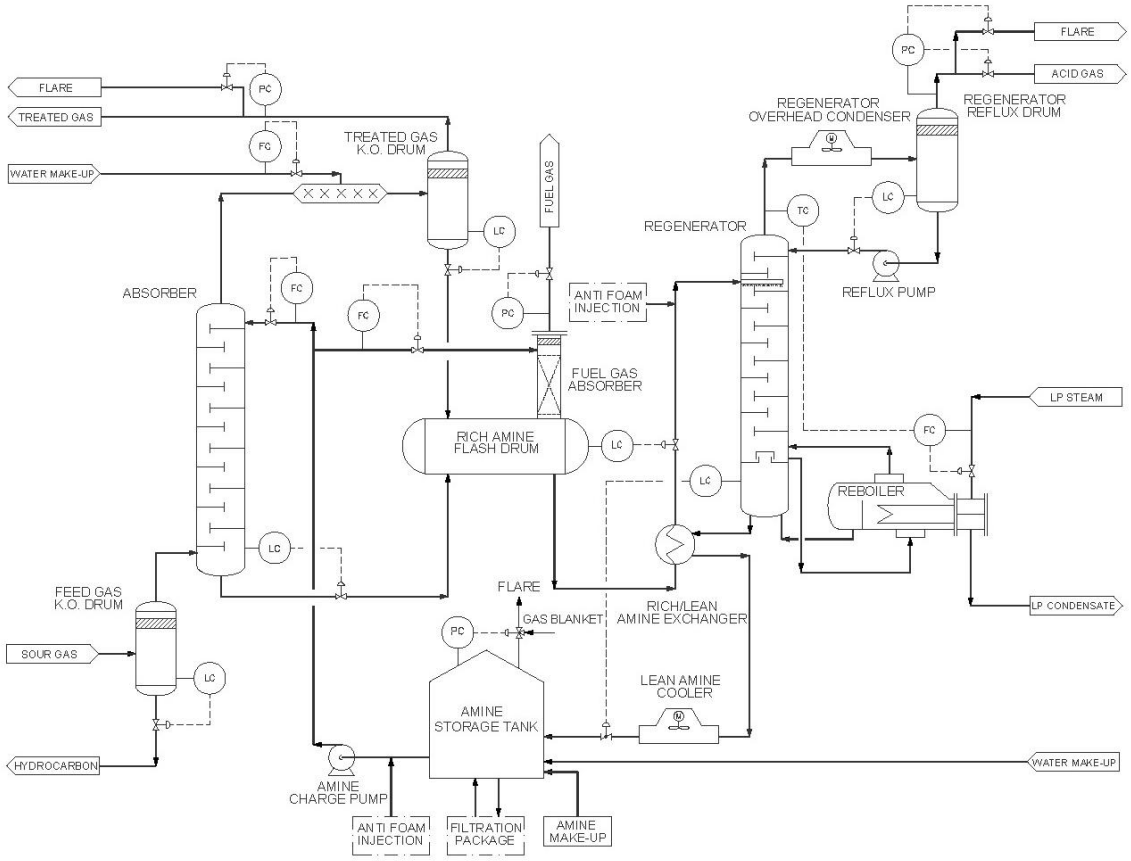


**Figure 3-1: Schematic process flow diagram for absorption amine system (Mahdi and Dannie 2007)**

These unit columns provide a very large contact area between the gas and liquid phases. Gas absorption contactors usually provide this vast area utilizing three various techniques (Kohl and Nielsen 1997):

1. "dividing the gas into small bubbles in a continuous liquid phase (bubble cap trays)
2. spreading the liquid into thin films that flow through a continuous gas phase (packed columns)
3. forming the liquid into small drops in a continuous gas phase (spray chambers)"

There are two major types of absorption process, namely physical and chemical absorption or in other words, non-reactive and reactive absorption. Physical absorption has lower capacity in comparison with chemical absorption however it benefits from easier regeneration of the solvent during desorption process. To elaborate, three types of solvents are used for absorption process as following:

- Non-reactive physical solvents (e.g. SELEXOL, NAM, NFM)
- Acid-base reacting solvents (e.g. MDEA)
- Reactive solvents which produce carbamate (e.g. MEA, DEA, DIPA, Piperazine)

Physical solvents are polar organic compound having affinity towards acid gases (Jou et al. 2003). As mentioned, a famous example for these solvents is SELEXOL made of dimethyl ether of polyethylene glycol which is ideal for removal of hydrogen sulfide as well as carbon dioxide (Kohl and Nielsen 1997). Similarly, N-acetyl morpholine (NAM) and N-formyl morpholine (NFM) are other examples for physical absorbents which are currently being used in acid gas removal industry.

Application of physical absorbents is limited. This is because transfer of acidic components through the gas-liquid interface is rate limiting, meaning long queues of absorbate molecules are formed behind the interface in the gas side while reactions between absorbent molecules with acid gases are not enough fast to carry them into the liquid side. Hence, the partial pressure emerges as an important factor that can justify application of this type of solvents. The same limitation exists for acid-base reactive solvents because they are only slightly reactive. For instance in the case of MDEA, depressurization causes system undergoes opposite direction reaction and solvent is regenerated.

In contrary, carbamate reactive solvents have higher capacity to dissolve the absorbate molecules. They have higher rate of reactions so that they are able to overcome the mass

transport limitation through the interface. In principle quick reactions remove the absorbate molecules readily from interface and give empty space for new molecules. Since this process is exothermic, the process of regeneration is costly and energy demanding.

In general, physical absorption is more suitable for conditions in which the partial pressure is high enough. Different values between 4 to 13 bar have been suggested by different researchers as the boundary between favorable and unfavorable area for physical absorption (Kohl and Nielsen 1997).

### 3.2.2 Adsorption

Adsorption is a process in which molecules of adsorbate adhere to the surface of adsorbent so that a selective separation is feasible. Primarily in gas purification, gas stream has to be passed through a bed of microporous solid surface having proper velocity, pressure and temperature. Initially, when the gas touches the adsorbent surface there are numerous free sites on which the adsorbate molecules can be adsorbed. As the time passes, concentration of adsorbate molecules increases on the "internal surfaces of the adsorbent"(Kohl and Nielsen 1997). This continues until the system reaches equilibrium. Afterwards, the adsorbent has to be regenerated by applying pressure drop and/or temperature increase.

The forces between the adsorbent and the adsorbed molecules are usually very weak (physical adsorption) so that they may even lead to a kind of agglomeration among the molecules forming the liquid phase. Generally in physical adsorption, interactions are only within the intermolecular range due to the Van der Waals forces (Barnes and Gentle 2005). In less industrially important type of adsorption chemical reactions between the adsorbate molecules and the adsorbent surface may happen. In this so called *chemisorptions* process, adsorbent material cannot be regenerated without chemical reactions(Kohl and Nielsen 1997). In principle, the number of chemisorbed layers is limited to one; while in case of physical adsorption several adsorbed layers are possible. Moreover, in suitable conditions a physical adsorption on the chemisorbed layer is also possible (Barnes and Gentle 2005).

The most frequently used treatment describing the monolayer adsorption has been introduced by Irving Langmuir (1916) which explains the relation between the coverage of the absorbent surface by the adsorbate molecules and the gas pressure for the monolayer chemisorptions process. Langmuir adsorption model is formulated by Equation (3-1) (Barnes and Gentle 2005).

$$relative\ adsorption = \frac{n_{ads.}}{n_{ads.}^{tot.}} = \frac{\alpha p}{1 + \alpha p} \quad \textbf{(3-1)}$$

Where;

$$\alpha = \frac{a_1}{b_1 \exp\left(-\frac{E}{RT}\right)} = \left(\frac{a_1}{b_1}\right) exp\left(\frac{E_1}{RT}\right)$$

Also;

$$\text{Rate of adsorption } = a_1 p A_0$$

$$\text{Rate of desorption } = b_1 A_1 exp\left(-\frac{E_1}{RT}\right)$$

$n_{ads.}$ is amount of adsorbed material, $n_{ads.}^{tot.}$ monolayer adsorption capacity, $p$ actual gas pressure, $T$ temperature, $E_1$ enthalpy of adsorption, R universal gas constant, $A_0$ area of bare surface and $A_1$ area occupied by one adsorbed layer. $a_1$ and $b_1$are adsorption and desorption factors respectively.

The expanded form of the Langmuir equation (BET) was introduced by Brunauer, Emmett and Teller which includes the multilayer form of the adsorption. This equation is widely used to explain the process of gas adsorption and is given by Equation (3-2) (Barnes and Gentle 2005).

$$\frac{n_{ads.}}{n_{ads.}^{tot.}} = \frac{Zp}{(p^0 - p)\left\{1 + (Z - 1)\left(\frac{p}{p^0}\right)\right\}} \quad \textbf{(3-2)}$$

Where;

$$Z \approx exp\{(E_1 - E_V)/RT)\}$$

$p^0$ is saturation pressure and $E_V$ enthalpy of the vaporization of the adsorbate.

It also can be pointed out that the so called *molecular sieves* which nowadays are widely used in many different areas of industry or science are being produced based on the concept of above mentioned adsorption process.

### 3.2.3 Membrane Permeation

Membrane permeation process is used as both gas purification and gas separation method. It works based on the different rates of permeation for gas components through the membrane. The partial pressure difference of the gaseous components is governing here as the driving force so that each component which is passing through the membrane will leave the system with much lower pressure than the feed stream.

Similarly, with other gas separation methods there are a range of advantages and disadvantages for membrane permeation technology. The most considerable deficiency of such systems is the existence of some impurities in the final product which may need further processing. In addition to that, since the pressure is used as driving force in membrane separation, substantial amount of energy might be required for "gas compression". On the other hand, a list of advantages including the "low capital investment", "ease of operation", "flexibility" and "reliability" can be considered for this technology (Kohl and Nielsen 1997).

The mechanism within which membrane separates the gas components is called "solution-diffusion mechanism" (Kohl and Nielsen 1997). This mechanism can be divided into four individual processes (Kohl and Nielsen 1997):

1. Adsorption of the gaseous components on the membrane surface
2. Solution of the adsorbed components into the membrane
3. Diffusion of the gas across the membrane medium
4. Desorption of the gas from opposite surface of the membrane

Several models for the above mentioned permeation process (solution-diffusion) have been proposed. According Kohl and Nielsen (1997) the simplest model which neglects the first process of this quaternary mechanism can be described by Henry's law and Fick's first law of diffusion. Simply it means concentration of the gas components on the membrane walls can be explained by Henry's law signifying the proportionality of the partial pressure in the gas phase and the surface concentration for each component. While Fick's first law governs the rate of diffusion through the membrane. Combining corresponding equations from these two laws, following formulation is deduced (Kohl and Nielsen 1997):

$$J_i = \frac{P_i \Delta p_i}{l} \quad \textbf{(3-3)}$$

Where;

$J_i$ is steady-state flux of component $i$, $P_i$is the permeability coefficient, $\Delta p_i (= p_{i,feed} - p_{i,permeate})$ is partial pressure difference across the membrane and $l$ is the membrane thickness. Permeability coefficients of gaseous components are given in Barrer unit.[2]

There is also a more complicated model called "dual system model". This postulates the adsorption of the gas components on the "microporous cavities" of membrane wall based on Langmuir adsorption isotherm, in addition to dissolution of the components in the "dense regions of membrane surface " according to Henry's law (Kohl and Nielsen 1997).

In principle, permeation rate of individual components are affected by temperature, pressure and composition of the gas mixture. Another parameter which is also important for design of membrane units is "separation factor" which is shown by Equation (3-4) (Kohl and Nielsen 1997).

$$\propto_{ij} = \frac{P_i}{P_j} \quad \textbf{(3-4)}$$

Where $\propto_{ij}$presents capability of the membrane unit to separate the gas components $i$ and $j$. In this regard, very low or very high values signify the condition for "easy separation" while values around unity demonstrates a situation in which there is no chance for separation (Kohl and Nielsen 1997).

### 3.2.4 Methanation

Catalytic conversion of carbon monoxide and carbon dioxide using hydrogenation method for production of synthesis methane is called *methanation*. This process is usually employed to remove the small amount of carbon dioxide or carbon monoxide remaining from other processes such as $CO_2$ absorption in which concentration of contaminant gases is maximum

[2] One Barrer equals $\frac{10^{-10}(cm^3\{STP\})(cm)}{(cm^2)(sec)(mmHg)}$

about 2.5 mole% (Kohl and Nielsen 1997). Following reactions govern process of methanation.

$$CO + 3H_2 \rightarrow CH_4 + H_2O \quad \textbf{(3-5)}$$

$$CO_2 + 4H_2 \rightarrow CH_4 + 2H_2O \quad \textbf{(3-6)}$$

As we can see in these reactions, carbon monoxide and carbon dioxide are hydrogenated to produce methane. Figure 3-2 illustrates the flow diagram for methanation process.

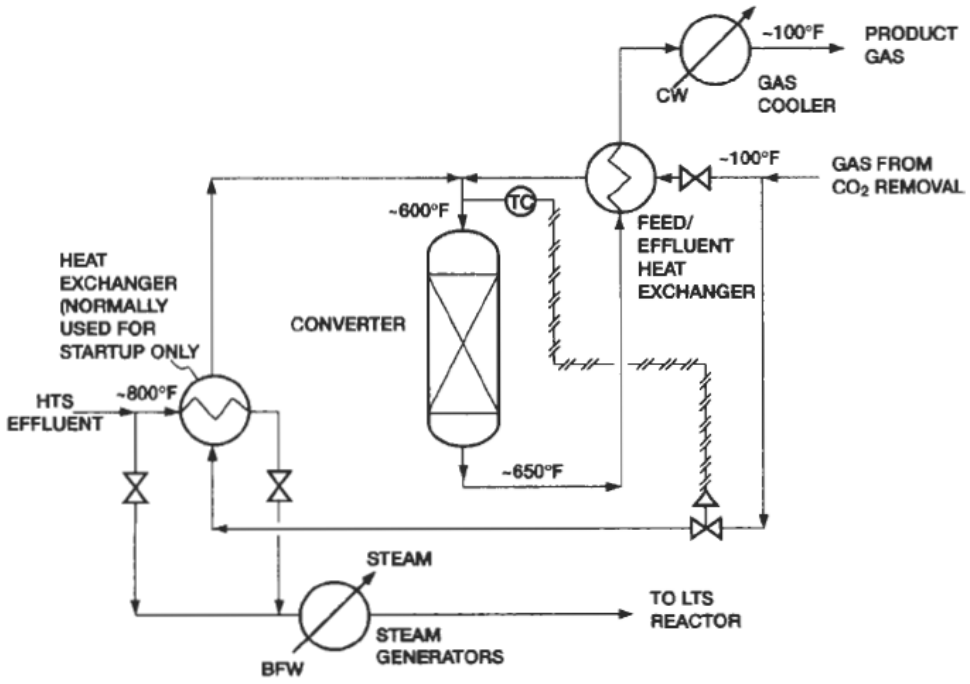


**Figure 3-2:Methanation Unit (Kohl and Nielsen 1997)**

## 3.3 Alkanolamine Systems

Nowadays, amine-type absorbents are recognized as well suited solvents for removal of carbon dioxide in absorption processes. Among this family of chemical compounds, *Alkanolamine* absorbents have attracted an enormous attention during the recent decades.

Initially alkanolamines were introduced as absorbents for acid gas removal applications by R. R. Bottoms (1930), and triethanolamines (TEA) was the first compound that was

commercially used (Kohl and Nielsen 1997). Within less than a century, several kinds of alkanolamines were used industrially; including MEA (monoethanolamine), DEA (Diethanolamine), TEA (triethanolamine), MDEA (methyldiethanolamine), DGA (diglycolamine) and DIPA (diisopropanolamine).

Furthermore, several patented mixtures of alkanolamines, using various sorts of additives, have been introduced for industrial applications by different companies such as DOW Chemical Company, UOP LLC, Huntsman Corporation and BASF Aktiengesellschaft. Apart from those chemical compounds mentioned above, particular class of solvents named as *sterically hindered* amines have been recently produced by EXXON Research and Engineering Company which are used to control the carbon dioxide-amine reaction. Various solutions of this family of acid gas absorbents are called Flexsorb (Kohl and Nielsen 1997).

### 3.3.1 Categorization of Alkanolamines

Alkanolamines are a group of ammonia derivatives consisting at least one hydroxyl group and one amine group. The amine group can be divided into different subcategories based on the number of substituents on the nitrogen atom. Considering this general definition, it is normal to distinguish between the following classes of alkanolamines:

1. Primary alkanolamines: In this subcategory, nitrogen atom carries one substituent group (ethanol group) and two hydrogen atoms which are directly bonded to the nitrogen. MEA (monoethanolamine) is an example for this subcategory.

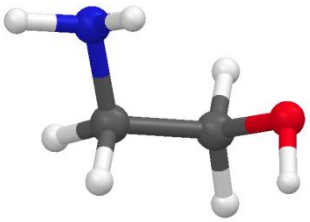

**Figure 3-3: Molecular structure of monoethanolamine, $C_2H_7NO$**

2. Secondary alkanolamines: In this group of alkanolamines, two hydrogens of the amine group have been replaced by two ethanol groups. The best example is DEA (diethanolamine).

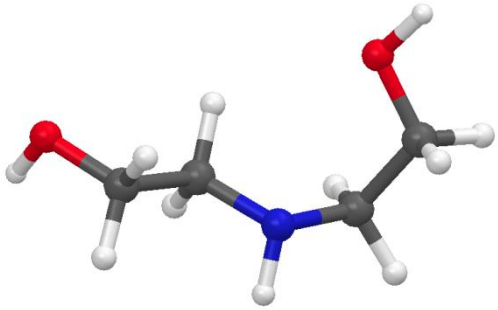

**Figure 3-4: Molecular structure of diethanolamine, $C_4H_{11}NO_2$**

3. Tertiary alkanolamines: These alkanolamines possess no hydrogen atom directly bonded to the nitrogen, meaning all the hydrogen atoms have been replaced by the substituent groups (alkyl or alkanol groups) such as MDEA (methyldiethanolamine).

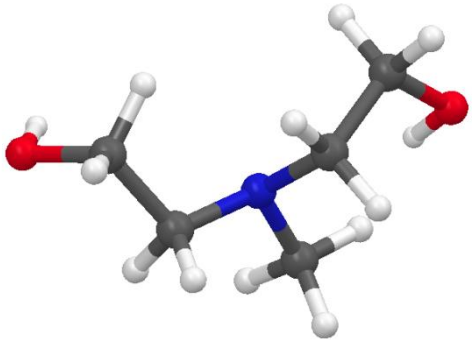

**Figure 3-5: Molecular structure of methyldiethanolamine, $CH_3N(C_2H_4OH)_2$**

4. Sterically hindered (alkanol)amines: They are "structurally primary amines in which the amino group is attached to a tertiary carbon atom or secondary amines in which the amino group is attached to a secondary or tertiary carbon atom"(Sartori and Savage 1983). Some of these amines are depicted in Figure 3-6.

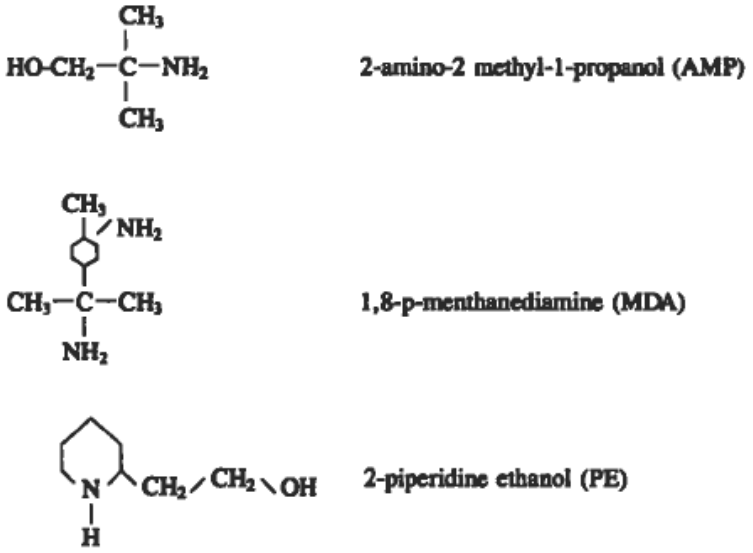


**Figure 3-6: typical sterically hindered amines (Sartori and Savage 1983)**

Reaction of primary and secondary alkanolamines with carbon dioxide follows the overall reaction (3-7) leading to the formation of carbamates (Derks 2006).

$$2Am + CO_2 \Leftrightarrow AmH^+ + AmCOO^- \quad \textbf{(3-7)}$$

While reaction of tertiary alkanolamines with $CO_2$ does not form carbamate species and should be considered as a "hydrolysis catalyzed reaction" which is shown by reaction (3-8) (Derks 2006).

$$Am + CO_2 + H_2O \Leftrightarrow AmH^+ + HCO_3^- \quad \textbf{(3-8)}$$

It also should be mentioned that primary and secondary alkanolamines posses higher rates of reaction while tertiary alkanolamines have higher capacity and require lower heat of regeneration (Derks 2006).

### 3.3.2 Improvements of (alkanol)amine systems

Conventional alkanolamine systems have limited applications due to several technical and economical factors. It is challenging for these systems to achieve high loading much beyond the 0.5 $\frac{mol_{CO2}}{mol_{amine}}$ (Sartori and Savage 1983). Low rate of absorption in systems such as those with physical solvents or MDEA involved solutions, in addition to high rate of reaction, high

volatility and high rates of degradation in very active solutions, like those with MEA and DEA solvents, are the most common drawbacks that necessitate improvements of these systems.

Currently, promoted solutions of alkanolamines are used to improve the systems working at high partial pressure of carbon dioxide such as natural gas cleaning processes. However at low partial pressure other improvements have to be done on the account of using more active alkanolamines like MEA or DEA.

Over the course of the past years, many research groups either within the industry or the academic sector have been working on development of more efficient technologies. Piperazine activated solutions are one of the significant improvements introduced for the better recovery of carbon dioxide in the early eighties. More recently, several research studies have been conducted within three major research groups mentioned bellow.

Mitsubishi has developed "more efficient tower packing materials with low pressure drops" (Svendsen et al. 2001). On the other hand, TNO[3], Kværner[4] and Gore[5] have developed "membrane absorber contactors", advantageous for improvement of $CO_2$recovery. At the same time different groups have been working on developing "new improved absorbents". Among those are Mitsubishi Company in Kansai-Japan and Prof. Amit Chakmas group at University of Regina. Mitsubishi has produced new proprietary absorbents, commercially called KS1, KS2 and KS3 with lower energy requirement and waste production in comparison with common MEA based processes (Svendsen et al. 2001).

### 3.3.3 Piperazine Activated Methyldiethanolamine solution

Application of conventional alkanolamines faces several limitations due to their low rates of reaction or large values for heats of regeneration. In this regard, addition of small amount of primary and secondary alkanolamines has found widely use to combine the higher rates of reaction from primary and secondary alkanolamines with lower heats of regeneration and higher stoichiometric loading capacity of the tertiary amines together into the blended systems.

[3] The Netherlands Organisation for Applied Scientific Research.
[4] Norwegian engineering company joined with Aker ASA in 2005, currently known as Aker Solution.
[5] W. L. Gore & Associates, Inc.

One of the popular mixtures in this category for removal of carbon dioxide from industrial gases, including natural gas, is aqueous blend of piperazine activated methyldiethanolamine (MDEA) which is patented by BASF in early eighties (Apple et al. 1982).

"Piperazine has been shown to be an effective promoter in MEA, MDEA and potassium carbonate due to its rapid formation of carbamates with $CO_2$"(Idem et al. 2009) so that it behaves as a successful rate accelerator in such solutions.

It has been found that MDEA has high capacity for removal of carbon dioxide but since it is a tertiary amine, its reaction with $CO_2$ cannot lead to formation of carbamates (Bottinger et al. 2008). Therefore addition of small amount of piperazine into the aqueous solution of MDEA accelerates the reactions and increases the solubility of carbon dioxide inside the solution while at the same time maintains the heat of regeneration in relatively low level as MDEA systems.

## 3.4 Carbon dioxide absorption in PZ activated MDEA solution: Mechanisms and Modeling

### 3.4.1 Reactions and Mechanisms of piperazine effect

Piperazine is a cyclic diamine (Figure 3-7) with promising effects on the conventional solution of MDEA. The addition of small amount of piperazine increases the absorption rate of carbon dioxide (acceleration effect) and enhances solubility of $CO_2$in the solution (loading upturn).

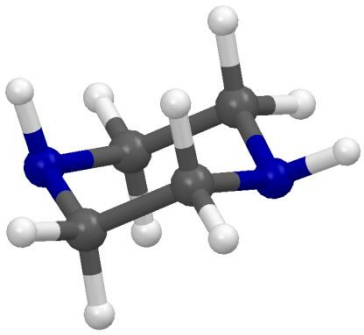

**Figure 3-7: Molecular structure of piperazine, ($C_4H_{10}N_2$)**

The acceleration effect of piperazine highly depends on the partial pressure of carbon dioxide in the gas mixture and the molar fraction of accelerator (van Loo et al. 2007).

In general, exact determination of liquid composition in such a system is a challenging issue. Speciation of this system differs to some extent from liquid bulk to the gas-liquid interface. It is governed by the chemical reactions happening inside the liquid phase as well as initial concentrations of piperazine and MDEA, the loading factor, vapor-liquid equilibrium (VLE) and physical properties of the system such as temperature and pressure.

One way to determine the complex speciation of the aqueous piperazine activated MDEA solution is to study composition of the solution in more basic systems such as aqueous solution of piperazine or aqueous solution of MDEA alone.

Based on these kinds of studies, different papers suggest almost similar set of reactions for the absorption of carbon dioxide in aqueous solution of PZ-MDEA blend. However they have sometimes minor variations regarding the intermediate reactions.
Primarily, reactions between carbon dioxide and piperazine activated solution of MDEA ($CO_2 + PZ + MDEA + H_2O$) which forms piperazine carbamate and piperazine bicarbamate are regarded for absorption rate of $CO_2$(Idem et al. 2009). Nevertheless this is not a general rule since different versions of this rule have been introduced by different researchers considering the diversity of the systems (for instance look at following set of reactions proposed by (Derks 2006) which neglects the reaction involved in production of piperazine bicarbamate). Similarly, dominant products of the governing reactions may vary depending on some factors – such as loading factor – which can affect the reaction rates and final concentration of the products. All of these needed to be taken into account. As a case in point, it has been shown for aqueous piperazine ($CO_2 + PZ + H_2O$) that there are two different reaction zones in which at low loading, the main reaction products are piperazine carbamate and protonated piperazine while at high loading, the dominant reaction product is protonated piperazine carbamate (Bishnoi and Rochelle 2000).

In this thesis, reactions and mass transfer model proposed by Derks (2006) was used extensively to be able to present a comprehensive view of the overall kinetic and mass transfer problem in such amine systems. On the other hand, considering speciation of amine solution in current master thesis has been decided mostly based on the experimental data from Derks (2006), this decision will help to stay consistent with related definitions and criteria in his work.

As such, following reactions are considered inside the liquid phase (Derks 2006):

The reaction between MDEA and $CO_2$ is a base catalyzed hydration reaction within which the tertiary amine catalyzes the formation of carbonate.

$$CO_2 + MDEA + H_2O \overset{k_{MDEA}}{\Longleftrightarrow} MDEAH^+ + HCO_3^- \quad \textbf{(3-9)}$$

The next reaction is production of bicarbonate due to the reaction of $CO_2$ with hydroxide ion:

$$CO_2 + OH^- \overset{k_{OH}}{\Longleftrightarrow} HCO_3^- \quad \textbf{(3-10)}$$

Formation of piperazine carbamate is governed by the overall reaction (3-11):

$$CO_2 + 2PZ \overset{k_{PZ}}{\Longleftrightarrow} PZCOO^- + PZH^+ \quad \textbf{(3-11)}$$

Similarly, piperazine carbamate and protonated piperazine react with carbon dioxide leading to production of piperazine bicarbamate and zwitterion ion, protonated piperazine carbamate:

$$CO_2 + PZCOO^- + B \Leftrightarrow PZ(COO^-)_2 + BH^+ \quad \textbf{(3-12)}$$

$$CO_2 + PZH^+ + B \Leftrightarrow H^+PZCOO^- + BH^+ \quad \textbf{(3-13)}$$

Where B can be MDEA, piperazine or $OH^-$.[6]

Reactions (3-9), (3-10), (3-11), (3-12) and (3-13) are a group of reactions with "finite reaction rates". But there is another group of reactions involving only "proton transfer" that can be assumed at "equilibrium" and "instantaneously fast"(Derks 2006).

$$MDEA + H_3O^+ \Leftrightarrow MDEAH^+ + H_2O \quad \textbf{(3-14)}$$

$$OH^- + H_3O^+ \Leftrightarrow 2H_2O \quad \textbf{(3-15)}$$

[6] Alternative reactions for (3-11), (3-12) and (3-13) can be found at: Bishnoi, S. and G. T. Rochelle (2000). "Absorption of carbon dioxide into aqueous piperazine: reaction kinetics, mass transfer and solubility." Chemical Engineering Science **55**(22): 5531-5543.

$$CO_3^{2-} + H_3O^+ \Leftrightarrow HCO_3^- + H_2O \quad \textbf{(3-16)}$$

$$PZ + H_3O^+ \Leftrightarrow PZH^+ + H_2O \quad \textbf{(3-17)}$$

$$PZCOO^- + H_3O^+ \Leftrightarrow H^+PZCOO^- + H_2O \quad \textbf{(3-18)}$$

$$PZH^+ + H_3O^+ \Leftrightarrow PZH_2^{2+} + H_2O \quad \textbf{(3-19)}$$

It has been shown that reaction (3-11) is the main contributor to the overall absorption rate of carbon dioxide (Derks 2006). Moreover, it has been demonstrated that contribution of reactions (3-12), (3-13), (3-18) and (3-19) to the overall absorption rate are not significant and can be neglected (Derks 2006). It should be noted here, by neglecting reaction (3-12), reactivity of the second amine group in piperazine molecule is not taken into account. However, it seems that this second amine group will play more important role only at high loading (Derks 2006).

The mechanism within which formation of piperazine carbamate takes place is assumed to be same as reaction of carbon dioxide with primary and secondary alkanolamines which is the so-called *zwitterion* mechanism (Derks 2006; Idem et al. 2009). In this mechanism the protonated piperazine carbamate ($H^+PZCOO^-$) is formed as zwitterion so that subsequently it is deporotonated by any base existing in the liquid ($PZ$, $PZH^+$, $PZCOO^-$, $OH^-$, $H_2O$). Zwitterion mechanism is presented by reactions (3-20) and (3-21) (Derks 2006).

$$PZ + CO_2 \Leftrightarrow H^+PZCOO^- \quad \textbf{(3-20)}$$

$$H^+PZCOO^- + B \Leftrightarrow PZCOO^- + BH^+ \quad \textbf{(3-21)}$$

In contrary reaction of MDEA as a tertiary alkanolamine with carbon dioxide only involves a proton transfer mechanism (Idem et al. 2009), since MDEA lacks the N-H bond necessary for the formation of carbamate ion. Hence it is not able to react with carbon dioxide directly and only encourages hydrolysis of carbon dioxide in aqueous solution to form bicarbonate and protonated amine (Rinker et al. 2000). This mechanism is based on the reaction (3-9) in which the reaction rate is limited to the value of $k_{MDEH}$ and the kinetics is very poor (Rinker et al. 2000). Table 3-2 compares the values for reaction rates of carbon dioxide with hydroxyl ion, MDEA and piperazine molecules signifying the limited reaction rate of MDEA with $CO_2$ and the ability of piperazine to react with $CO_2$ based on a much higher reaction rate.

**Table 3-2: Kinetic rates constant for carbon dioxide reactions (Derks 2006)**

| Reaction | Kinetic rate constants | Value | Unit |
|---|---|---|---|
| $CO_2 + MDEA$ | $k_{MDEA}$ | $5.3 \times 10^{-3}$ | $m^3 kmol^{-1} s^{-1}$ |
| $CO_2 + OH^-$ | $k_{OH}$ | 8.4 | $m^3 kmol^{-1} s^{-1}$ |
| $CO_2 + PZ$ | $k_{PZ}$ | 76 | $m^3 kmol^{-1} s^{-1}$ |

### 3.4.2 Modeling of piperazine MDEA systems

Modeling of the system provides us with the ability to predict behavior of the system under various conditions. In general, for modeling of the absorption process within the gas-liquid interface we need to establish the thermodynamic vapor-liquid equilibrium (VLE) model first, giving equilibrium composition of the liquid phase. Subsequently, the speciation data from this thermodynamic model should be used as input data for the mass transfer (kinetic) model.

#### 3.4.2.1 Thermodynamic model

To account non-ideality of the liquid phase for equilibrium composition of the solution, an equilibrium thermodynamic model has to be defined. Many thermodynamic models are available in the literature to describe equilibrium solubility of the acid gases in aqueous blends of amine solutions. Some of the best known thermodynamic models are mentioned as following:

- Kent-Eisenberg (KE) empirical model
- Li-Mather electrolyte model
- Non-Random Two-Liquid (NRTL) model

Therefore vapor-liquid model is achieved through thermodynamic modeling of the equilibrium system in which equilibrium reactions are taken into account. In absence of the thermodynamic model, still equilibrium composition of the liquid bulk can be determined at

any temperature using values of the loading factor and initial amine concentrations along with overall mass balances. However non-ideality of the liquid phase will not take into account anymore so that input data for kinetic mass transfer model cannot be precise enough.

#### 3.4.2.2 Mass transfer model

Following modeling of the system has been proposed by Derks (2006) based on the reactions and mechanisms described in Section 3.4.1.

First of all there are five equations governing the conservation of mass for each species in addition to the electro-neutrality condition:

Overall MDEA balance:

$$C_{MDEA} + C_{MDEAH^+} = C_{MDEA,0} \quad \textbf{(3-22)}$$

Overall piperazine balance:

$$C_{PZ} + C_{PZH^+} + C_{PZCOO^-} = C_{PZ,0} \quad \textbf{(3-23)}$$

Overall water-hydrogen balance:

$$C_{H_2O} + C_{H_3O^+} + C_{OH^-} + C_{HCO_3^-} + C_{PZH^+} + C_{MDEAH^+} = C_{H_2O,0} \quad \textbf{(3-24)}$$

Overall carbon dioxide balance:

$$\alpha_{CO_2}(C_{PZ} + C_{PZH^+} + C_{PZCOO^-} + C_{MDEA} + C_{MDEAH^+}) = C_{CO_2} + C_{HCO_3^-} + C_{CO_3^{2-}} + C_{PZCOO^-} \quad \textbf{(3-25)}$$

Where $\alpha_{CO_2}$ is the loading factor.

Electro-neutrality criterion:

$$C_{PZH^+} + C_{MDEAH^+} + C_{H_3O^+} = C_{OH^-} + C_{HCO_3^-} + 2C_{CO_3^{2-}} + C_{PZCOO^-} \quad \textbf{(3-26)}$$

Furthermore, there are six independent equilibrium equations in this model:

$$K_{H_2O} = \frac{C_{OH^-} C_{H_3O^+}}{C_{H_2O} C_{H_2O}} \quad \textbf{(3-27)}$$

$$K_{HCO_3^-} = \frac{C_{HCO_3^-}}{C_{OH^-} C_{CO_2}} \quad \textbf{(3-28)}$$

$$K_{CO_3^{2-}} = \frac{C_{OH^-} C_{HCO_3^-}}{C_{CO_3^{2-}} C_{H_2O}} \quad \textbf{(3-29)}$$

$$K_{PZCOO^-} = \frac{C_{PZ} C_{HCO_3^-}}{C_{PZCOO^-} C_{H_2O}} \quad \textbf{(3-30)}$$

$$K_{PZ} = \frac{C_{PZ} C_{H_3O^+}}{C_{PZH^+} C_{H_2O}} \quad \textbf{(3-31)}$$

$$K_{MDEA} = \frac{C_{MDEA} C_{H_3O^+}}{C_{MDEAH^+} C_{H_2O}} \quad \textbf{(3-32)}$$

Equations (3-22) - (3-32) builds a system of 11 linear equations. Simultaneous solution of this system for 11 unknown concentrations results in the equilibrium composition of the liquid bulk which does not take into account non-ideality of the solution.

Next step for the modeling of this system is developing a mass transfer model explaining the kinetics and absorption rate of carbon dioxide into the amine solution. A diffusion-reaction based mass transfer model has been developed by Derks (2006) describing the complete process of diffusion as well as the reactions:

$$\frac{dC_i}{dt} = D_i \frac{d^2 C_i}{dx^2} + \sum_i^n \nu_i R_i \quad \textbf{(3-33)}$$

Where $C_i$ , $D_i$, $\nu_i$ and $R_i$ are concentration of specie $i$ in the liquid bulk, diffusion coefficient of specie $i$, stoichiometric factor and reaction rate of any reaction in which the species $i$ takes place respectively. Reaction rate $R_i$ is calculated for each reaction based on the corresponding reaction and equilibrium constants.

Developing Equation (3-33) for all the 11 reactions explained earlier [reactions (3-9) - (3-19)], results in a set of 11 non-linear partial differential equations (PDE) which can be solved for all the 11 components, by applying the boundary and initial conditions of the system.

### 3.4.3 Complexity of interfacial mass transfer

Gas – liquid interface in reactive absorption systems – including the piperazine activated systems - involves complexity within the "diffusion-reaction" zone due to the "hydrodynamic irregularities" brought about by the simultaneous diffusion and chemical reactions (Kutepov et al. 2001). This fact has been reflected in Equation (3-33) as two distinct diffusion and reaction terms on the right hand side.

There are various optical methods for observation of the interfacial mass transfer. Since this phenomenon takes place in "all spatial scales" in two phase systems, most of these methods have to be utilized simultaneously to be able to study the process of mass transfer within the interface. For instance, "holographic interferometry" is employed for "large scale mass fluxes" while "polarization interference microscopy" and "modified fluctuation spectroscopy" are suitably applicable in micro scale study of the interface and boundary layer (Kutepov et al. 2001).

Figure 3-8 illustrates development of the carbon dioxide absorption by MEA as the solvent.

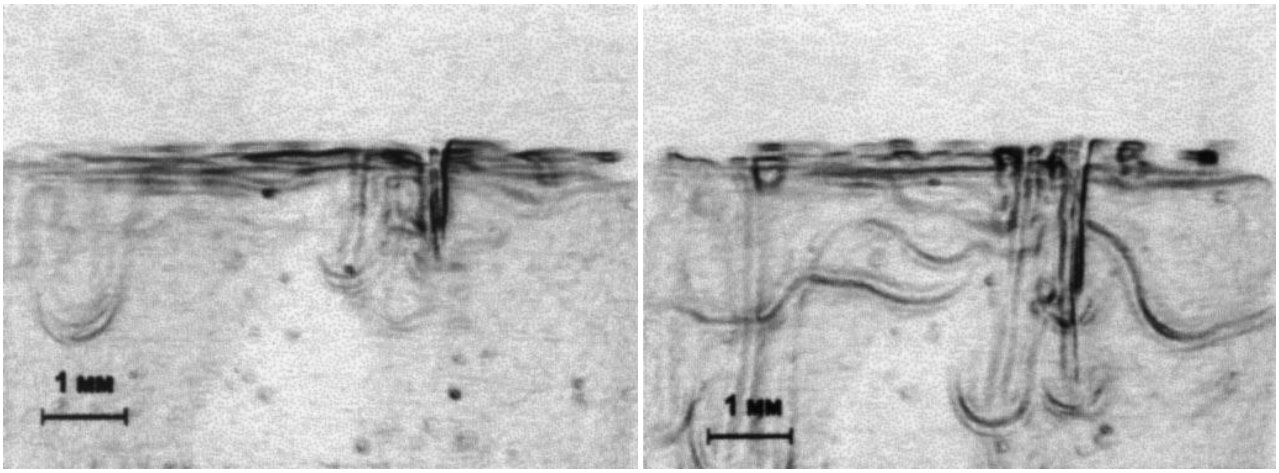


**Figure 3-8: Development of the carbon dioxide absorption by MEA (Kutepov et al. 2001)**

### 3.4.4 Further Complexities

The highly dynamic nature of the interface in alkanolamine systems due to the capillary waves in addition to the common irregularities of reactive two phase systems mentioned above give rise to different difficulties during the process of carbon dioxide absorption. Briefly speaking following drawbacks can be listed:

- **Foaming:** This problem arises out of the contaminated solutions of alkanolamines and is considered as one of the "most common operating problems" (Kohl and Nielsen 1997). The contaminants can be "condensed hydrocarbon", "acidic amine degradation products", "lubricating oil aerosols" and "surface active agents"(Kohl and Nielsen 1997). Foaming can lead to the formation of a resistant phase in the contactor, filling the volume of the system which gradually decreases capacity and efficiency of the absorption process (Lebedev et al. 1997). Since components acting as surfactant cause foaming problem, potentially amine solvents with surfactant characteristics can give rise to this phenomenon (da Silva 2005).
- **Volatility losses:** Volatility losses of amine are usually considered to be a reason which increases the process cost. It depends on the temperature of the system and vapor pressure of amine.
- **Entrainment:** This phenomenon can be defined as entrapment of a substance into another one when there is no equilibrium between them, such that both substances may be in the same or different phases. In amine systems entrainment of amines due to

the “inefficient mist extraction” or “foaming” is a major deficiency which gives rise to the amine loss problem (Kohl and Nielsen 1997).

- **Methane entrapment:** Undesired trapping of methane into the aqueous solution of piperazine activated MDEA is another deficiency of such systems. This leads to a significant amount of methane loss in natural gas cleaning plants which of course is not economically favorable. Despite extensive effect of methane entrapment on the overall economy of the absorption process, there is no data available in this regard in open literature. As such current thesis decided to provide some insight into this problem.

# 4 Computational Methods

In scientific researches, different methods are employed to investigate a hypothesis or to explore an unknown area of the subject. In general, experimental works provide most reliable results but on the other hand, they are limited by various considerations. It is usually very expensive and time consuming to conduct experiments for diversified areas of researchers interests. Mainly expensive equipments and accurate apparatus are needed for experimental works. Moreover, the equipment usually needs to be calibrated for every individual experiment, a procedure which is mostly very time consuming and even sometimes complicated.

Considering this, computational methods can provide a great progress towards the academic researches beyond the limitation of experimental methods. This approach employs the basic theories from physics and chemistry sciences accompanied with mathematical techniques for problem solving and utilizes principles of computer science to investigate the issue.

Intrinsically, computational methods yield approximate results due to the many approximations applied in different parts of them. This comprises all the mathematical approximations applied in the problem solving techniques in addition to the various estimations exploited in connection with scientific theories. Consequently, results from this approach always need to be validated towards experimental works. Still, there are several noticeable benefits in its application. Considering the broad area of application where computational methods can be employed from chemistry and physics to biology and medical sciences, in addition to the capability and flexibility of this technique to predict results in many different conditions, it should be regarded as a strong and useful tool that can be used complimentarily or in parallel with experimental approach to extend the area of investigation.

Basically, the computational approach seems very helpful for examining the scientific hypotheses or prediction of the prospective results. This can specially be very useful for the experimentalist by directing the future experiments.

There are different types of computational methods using quantum mechanics or classical mechanics as their approach. Quantum mechanics itself can be divided to *ab-initio* and *semi-empirical* methods as two main computational methods in this field. In ab-initio calculation only an electronic *wavefunction* model is chosen to solve the *Schrödinger equation*. Fundamental constants and atomic numbers of the nuclei are used as input values. On the other hand, semi-empirical methods utilize simplified form of the *Hamiltonian operator* with

some parameters taken from experiments. While the former is computationally very expensive and time consuming for the large systems of particles and its accuracy merely depends on the employed model for the wavefunction, the latter approach is less accurate but more reasonable to be used for large systems (Atkins and Friedman 2005).

As a computational method, molecular simulation is also a very useful tool, which provides the possibility to investigate the behavior of matter in molecular scale. Depending on the simulation method, time dependant thermodynamic properties of the system as well as configuration of the particles at any time can be determined appropriately.

## 4.1 Quantum Mechanics (QM)

Quantum mechanics which is structured based on five postulates can explain "behavior of all known forms of the matter"(Atkins and Friedman 2005) . It concerns the behavior of molecules as well as the electrons, nucleus and other subatomic particles. The most fundamental concept of QM is the wavefunction which can be explained through the first postulate of the quantum mechanics. According this, "state of a system is fully described" by the wavefunction $\Psi(r_1, r_2, \dots, t)$ which contains "information about all the properties of the system that are open to experimental determination"(Atkins and Friedman 2005).

Still, the core postulate of QM is the fifth and final postulate describing time dependant "dynamical evolution of the wavefunction"(Atkins and Friedman 2005). This is the well-known Schrödinger equation represented by Equation (4-1) as a partial differential equation:

$$i\hbar \frac{\partial \Psi}{\partial t} = H\Psi \qquad \textbf{(4-1)}$$

Where H is the Hamiltonian operator corresponding to the total energy of the system and ħ is the reduced Planck's constant.

This is equivalent to Equation (4-2) presenting the total kinetic and potential energies explicitly in cartesian coordinate system.

$$i\hbar \frac{\partial \Psi}{\partial t} = -\frac{\hbar^2}{2m}\nabla^2\Psi + V(x, y, z)\Psi \qquad \textbf{(4-2)}$$

Exact solution of the Schrödinger equation for large systems is impossible and for small systems even very complicated. The simplest form of the wavefunction belongs to the

*hydrogenic atoms* which can be defined as "one electron species with arbitrary atomic number Z"(Atkins and Friedman 2005).

Another basic concept needs to be introduced before going further, is *atomic orbitals* (AO). The atomic orbitals are "one-electron wavefunctions in atoms". Historically they are labeled by letters s, p, d, f, (...) so that for instance an electron occupying a s-orbital is called s-electron. Similarly for other orbitals there are p-electrons in p-orbitals and so on(Atkins and Friedman 2005).

Solution for the Schrödinger equation can be claimed if we know the exact form of the wavefunction $\Psi_{nlm_l}$, where $n$, $l$ and $m_l$ are called *quantum numbers*. According Atkins and Friedman (2005), these quantum numbers are introduced as following:

- $n$ is the principle quantum number ranging from 1, 2, 3… specifying the number of electronic shells on the atomic structure. This number also decides about the energy of the shell according Equation (4-3) and controls range of the $l$ quantum numbers from 0 to $n-1$.

$$E_n = -\left(\frac{Z^2 \mu e^4}{32\pi^2 \varepsilon_0^2 \hbar^2}\right)\frac{1}{n^2} \qquad \textbf{(4-3)}$$

  Where Z is the atomic number, μ is reduced mass and $\varepsilon_0$is vacuum permittivity.

- Each electronic shell is composed of n number of subshells which are the atomic orbitals with quantum number $l$. $l$ is also defined as the *orbital angular momentum* quantum number giving the orbital angular momentum of the electron through Equation (4-4). Moreover, this quantum number controls the range of $m_l$ between $-l$ and $l$.

$$Magnitude\ of\ the\ angular\ momentum = \{l(l+1)\}^{\frac{1}{2}}\hbar \qquad \textbf{(4-4)}$$

- $m_l$ is called *magnetic quantum number*, and is defined as component of the orbital angular momentum of an electron. This quantum number is represented by individual orbitals so that there are $2l+1$ individual orbitals in each subshell.

### 4.1.1 Approximate form of the atomic orbital (AO) and SCF method

As mentioned earlier, there is no analytical solution for Schrödinger equation in many electron atoms to find the exact form of the atomic orbitals. Therefore, the best way to approach the solution is numerical approximation of the wavefunction. We usually need a set of approximate atomic orbitals to be able to model the true wavefuntions.

One of these approximate forms of the atomic orbitals are called *Slater type orbitals* (*STO*) which have been defined by Equation (4-5) in spherical polar coordinates:

$$\psi_{nlm_l}(r,\theta,\phi) = N.r^{n_{eff}-1}.e^{-\frac{z_{eff}\rho}{n_{eff}}}.Y_{lm_l}(\theta,\phi) \qquad \textbf{(4-5)}$$

Where N and $Y_{lm_l}$are defined as normalization constant and *spherical harmonic*[7] function respectively. $\rho$ is equal to $\frac{r}{a_0}$ ($a_0$: Bohr radius). Moreover, effective principal quantum number $n_{eff}$ and effective nuclear charge $Z_{eff}$ can be found in reference books (Atkins and Friedman 2005).

As mentioned, the best way to calculate the atomic orbitals is to solve the Schrödinger equation numerically. There is an effective procedure serving for numerical solution of Schrödinger equation, which is called *Self-consistent field* (*SCF*).

In this method Schrödinger equation is solved iteratively, nevertheless, at least one approximation of the atomic orbitals should be known beforehand! SCF method presumes the spherical average of the all electrons and nucleus except the electron of interest, as a single charge on the nucleus. It also assumes that electron of interest moves in this potential field. Based on this method, wavefunctions of the all electrons other than the electron of interest are already known. For example, Slater type orbitals can be used as an approximate form of the wavefunction for this group of electrons. Subsequently, the Schrödinger equation is solved for the only unknown electron (electron of interest) and the average potential which is positioned on the nucleus. Once the wavefunction of the individual electron is calculated the procedure should be repeated for other electrons. This continues until a set of new approximations are obtained for all the electrons. This is considered as one cycle in SCF method. Similar procedure should be taken iteratively until the difference between the outcome of the cycle

[7] Spherical harmonic functions are solutions of the Schrödinger equation under the conditions that no radial movement is allowed. Simply meaning, the electron can only move over the surface of a sphere in which the nuclei has been placed at the center.

and initial approximation of the same cycle is insignificant. Here is the point where the iteration can stop and the final set of functions can be considered as convincing approximations for the atomic orbitals of a many electron specie (Atkins and Friedman 2005).

### 4.1.2 Molecular orbitals (MO) and Basis sets

Understanding of the molecular structure is the most fundamental part of the chemistry so that it will help us to comprehend the reasons of chemical reactions and to know the energy path which molecules follow during a chemical reaction. It is necessary to know which forces govern behavior of the constituent elements of the molecules. How are the atoms held together under a specific geometry? And how do they transform from one conformation to another?

To step into this area we need to define electronic structure of the molecules by solving the Schrödinger equation for even more complicated systems. Within the molecular structure of molecules, a set of atoms exist each with many electrons. Hence, it is not very difficult to guess how complicated the solution of Schrödinger equation can be for molecules. Again the remedial approach will be the approximation. Apart from the *Born-Oppenheimer* approximation, which assumes the nuclei at fixed position and tries to solve the Schrödinger equation for electrons within the nuclei potential fields (Atkins and Friedman 2005), there is another important approximation on which the molecular structure is built up. *Molecular Orbital theory* presumes that electronic structure of the molecules can be resembled as the linear combination of atomic orbitals (LCAO) within the molecule. Since we already have good approximation for the atomic orbitals, it can be a very helpful initial point towards the modeling of the electronic structure of the molecules.

Equation (4-6) represents the LCAO:

$$\psi = \sum_{r} C_r \phi_r \qquad \textbf{(4-6)}$$

This sum "extends over all the atomic orbitals of the atoms in the molecule" (Atkins and Friedman 2005). These atomic orbitals are called *Basis Sets.* In general, going from basic atomic orbitals to the more extended basis sets can lead to a higher accuracy for approximation of molecular orbitals. Since it is not possible to use the infinite number of basis functions to construct the extremely accurate form of the molecular orbital, there will be always an error due to this limitation. This deviation is called *Basis set truncation error*. Several considerations should be taken into account for selection of the basis sets.

Necessarily, smart selections have to be made to keep the computational effort at its lowest possible level, while the accuracy of the calculations is always concerned and only small truncation error should be generated simultaneously.

Since the application of STOs as basis functions in equation (4-6) is not computationally reasonable due to the high computational requirement, a new form of basis functions has been developed. These are called *Gaussian-type orbitals* (*GTO*). Gaussian orbitals are computationally less demanding but their accuracy is lower in comparison with Slater types. Roughly speaking, to be able to model one STO, three times GTOs are required in terms of quantity to produce the same accuracy (Jensen 2006). This fact is shown by Figure 4-1.

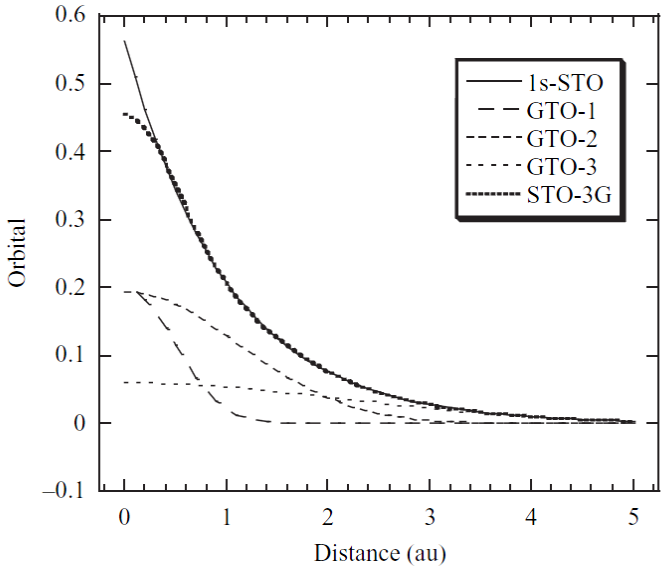


**Figure 4-1: One STO can be resembled by linear combination of three GTOs**

**(Jensen 2006)**

Gaussian-type orbitals are defined in Cartesian coordination according Equation (4-7):

$$\theta_{ijk}(r_1 - r_c) = (x_1 - x_c)^i (y_1 - y_c)^j (z_1 - z_c)^k e^{-\beta |r_1 - r_c|^2} \quad \textbf{(4-7)}$$

In this equation $(x_c, y_c, z_c)$ are Cartesian coordinates of the center of the Gaussian function at $r_c$ ; $(x_1, y_1, z_1)$ are Cartesian coordinates of an electron at $r_1$; $i, j, k$ are non-negative integers and $\beta$ is positive exponent. The Cartesian Gaussian will be an s-type Gaussian when $i = j = k = 0$, it will be a p-type in the case $i + j + k = 1$ and if $i + j + k = 2$ the Gaussian type will

be a d-type. The same logic applies for the rest of the Gaussian types (Atkins and Friedman 2005). Figure 4-2 illustrates cross-section through the three Gaussian orbitals.

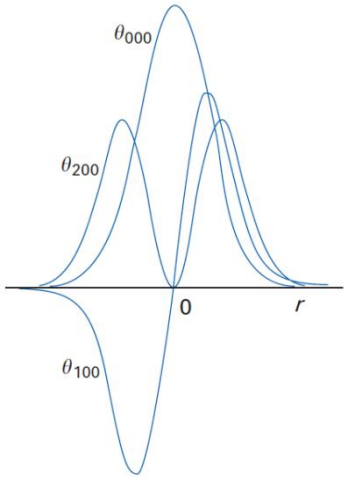


**Figure 4-2: Cross-section through three Gaussian Orbitals**

**(Atkins and Friedman 2005)**

The GTOs can decrease number of integrals, which of course leads to the less computational effort. The number of integrals are reduced due to this fact that product of two GTOs can be resembled by another GTO centered between the centers of original GTOs (Atkins and Friedman 2005). This is illustrated by Figure 4-3. On the other hand, GTOs doesn't represent the orbitals at the nucleus perfectly (Atkins and Friedman 2005). As an illustration for hydrogenic atoms, 1s-orbital has a "cusp" at the nucleus but GTO cannot represent this behavior at this point (Figure 4-4). To avoid this deficiency *contracted Gaussian functions* are used, which basically are linear combination of the *primitive Gaussian functions*.

$$\chi_j = \sum_i d_{ji}\, g_i \qquad \textbf{(4-8)}$$

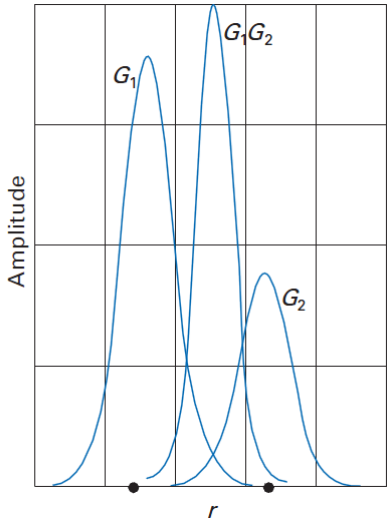


**Figure 4-3: Product of two Gaussians which lies between the original functions (Atkins and Friedman 2005)**

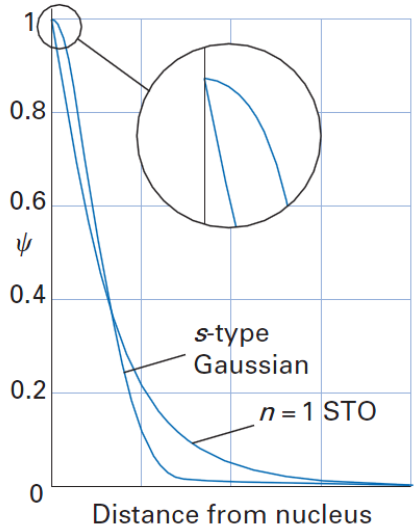


**Figure 4-4: Existence of the cusp at the nucleus for the hydrogenic 1s-orbital (Atkins and Friedman 2005)**

The most basic basis set is called *minimal basis set* using only one function for the orbitals. There are also more accurate types of basis sets like *double-zeta basis sets* (*DZ*) or *triple-zeta basis sets* (*TZ*) in which the former uses two basis functions to represent the orbitals and the latter applies three basis functions. In addition, there is *split-valence basis set* (*SV*) utilizing the multi basis functions (double, triple, etc.) for the valence shell (the outermost shell) and only one basis function for orbitals within the inner shells.

Addition of extra functions such as *polarization* or *diffuse* functions can be made to the basis sets to represent the true wavefunction more accurately. In the case of polarization, basis functions with higher angular momentum values are used. For example, addition of the p-type basis functions can represent polarization of the s-orbitals. Polarization is due to the deformation of the atomic orbitals by neighboring atoms during formation of covalent bonds (Atkins and Friedman 2005). Polarization functions are represented by ” * “ and ” ** “ signs for heavy atoms and hydrogen atoms inclusion respectively. On the other hand, inclusion of diffuse functions are made to provide the accurate models for large distribution of the charges like having formal negative charges on the molecule or to be able to handle the molecular properties depending on the regions far from the nucleus (Hinchliffe 2008). Similarly diffuse functions are represented by “ + “ and ” ++ “ signs for heavy atoms and hydrogen atoms inclusion respectively.

Application of contracted Gaussians instead of primitive Gaussians is very useful on the account of decreasing the number of unknown coefficients in HF calculation and as a result saving a considerable amount of computer time. Given equations (4-6) and (4-8), this fact is easily understandable. Suppose we have a basis set including N number of primitive Gaussians. Solution of equation (4-6) then will depend on the N number of $C_r$ coefficients that have to be computed within the HF calculation. But on the other hand, assuming contracted Gaussians rather than primitives each made of M number of primitive basis functions (Look at equation 4-9), leads to determination of only $\frac{N}{M}$ number of coefficients.

There are different sorts of methods to construct the contracted Gaussian basis sets. These methods are usually called *Contraction Scheme* (Atkins and Friedman 2005). One of the contraction schemes is defined as an expansion of the STO basis set in terms of the N primitive Gaussian basis functions. This contraction scheme is addressed as STO-NG. Alternatively, there is another contraction scheme that is categorized as split-valence type of basis sets. As an illustration, 6-31G basis set comprises 1 contracted Gaussian consisted of 6 primitive Gaussians for every orbital within the inner shells. In addition, it is composed of two basis functions for each orbital in valence shell including one contracted Gaussian made of 3 primitive Gaussians and one individual primitive Gaussian(Atkins and Friedman 2005). Polarization and diffuse functions can also be added to this basis set such as $6-31G^{**}$or $6-31+G^{**}$.

### 4.1.3 Density Functional Theory (DFT)

There are various numerical methods to determine the electronic structure of the molecules, such as Hartree-Fock (HF) method. However, this method does not take into account the effect of electron correlation. It means that the instantaneous coulombic interactions as well as the "quantum mechanical effects on the electron distributions" are neglected (Atkins and Friedman 2005). Consequently, in molecules with many electron atoms, HF methods does have accuracy limitations.

A brilliant method, which is widely being used in this regard, is *Density functional theory*. This method does consider the important effect of electron correlation and simultaneously is applicable to big molecules while it has smaller computational requirements.

It has been shown that ground-state energy of the system is a functional of density(Hohenberg and Kohn 1964). It means energy of an electronic system can be mathematically described by electron probability density of the system, E[$\rho$] (Atkins and Friedman 2005).

Assuming a system in which paired electrons are defined by the same spatial one-electron orbitals, Equation (4-9) will describe exact ground state energy of the system based on DFT theory(Atkins and Friedman 2005):

$$E[\rho] = -\frac{\hbar^2}{2m_e}\sum_{i=1}^{n}\int \psi_i^*(r_1)\nabla_1^2\psi_i(r_1)dr_1 - j_0\sum_{I=1}^{N}\frac{Z_I}{r_{I1}}\rho(r_1)dr_1 + \frac{1}{2}j_0\int\frac{\rho(r_1)\rho(r_2)}{r_{12}}dr_1dr_2 + E_{XC}[\rho] \quad \textbf{(4-9)}$$

In this Kohn-Sham equation, $\psi_i$ is the one-electron spatial orbital.

The exact ground-state electron density also can be written as following(Atkins and Friedman 2005):

$$\rho(r) = \sum_{i=1}^{n}|\psi_i(r)|^2 \quad \textbf{(4-10)}$$

It is important and should be noted that the first, second, third and final terms in the right hand side of Equation (4-9) signify kinetic energy of the electrons $T_S[\rho]$, electron-nucleus attraction $E_{ne}[\rho]$, coulomb interaction between total charge distribution $J[\rho]$ and *exchange-correlation energy* $E_{XC}[\rho]$ respectively (Atkins and Friedman 2005).

$$E_{DFT}[\rho] = T_S[\rho] + E_{ne}[\rho] + J[\rho] + E_{XC}[\rho] \quad \text{(Jensen 2006)} \quad \textbf{(4-11)}$$

Since we do not know the exact form of the exchange-correlation energy $E_{XC}[\rho]$, calculation of the ground-state energy of the system again needs some approximations. In this regard, several approximations have been introduced. One approximation is Local density approximation (LDA) by which the exchange-correlation term is described as following:

$$E_{XC} = \int \rho(r)\varepsilon_{XC}[\rho(r)]dr \qquad \textbf{(4-12)}$$

Where $\varepsilon_{XC}[\rho(r)]$ is exchange-correlation energy per electron in a homogeneous electron gas of constant density (Atkins and Friedman 2005).

Since accuracy of the energy diminishes by changing the electron density and because equation (4-12) does not take into account variation of $[\rho(r)]$, this equation overestimates the energy for inhomogeneity conditions. In such cases, a gradient correction is required in the LDA equation. This correction usually is called *Generalized gradient approximation* (*GGA*).

There are also other types of exchange-correlation functionals like *Local-spin density approximation* (*LSDA*), which is used to describe open-shell atoms. Since in valence shell of these atoms individual electrons with spin-up or spin-down exist, LSDA takes into account the density of these electrons possessing opposite spins as well as the total electron *density*(Atkins and Friedman 2005*).*

One of the widely used exchange-correlation functional, which uses LSDA and GGA, is *Beck-3-Lee-Yang-Parr* (*B3LYP*). B3LYP is derived by the hybrid method that includes the exact exchange part of the functional (Jensen 2006).

$$E_{XC}^{B3LYP} = (1-a)E_X^{LSDA} + aE_X^{exact} + b\Delta E_X^{B88} + (1-c)E_C^{LSDA} + cE_C^{LYP} \qquad \textbf{(4-13)}$$

Where the $E_X$ and $E_C$ are pure exchange and pure correlation parts of the exchange-correlation functional respectively. In addition to that $E_X^{B88}$ is a GGA correction to LSDA exchange energy proposed by A.D.Beck. The a, b and c parameters are determined by fitting to experimental data.

To summarize, density functional theory (DFT) employs the self-consistent approach to calculate the Kohn-Sham (KS) orbitals $\psi_i(r)$ in Equations (4-9) and (4-10) (Atkins and Friedman 2005). This procedure is illustrated in Figure 4-5.

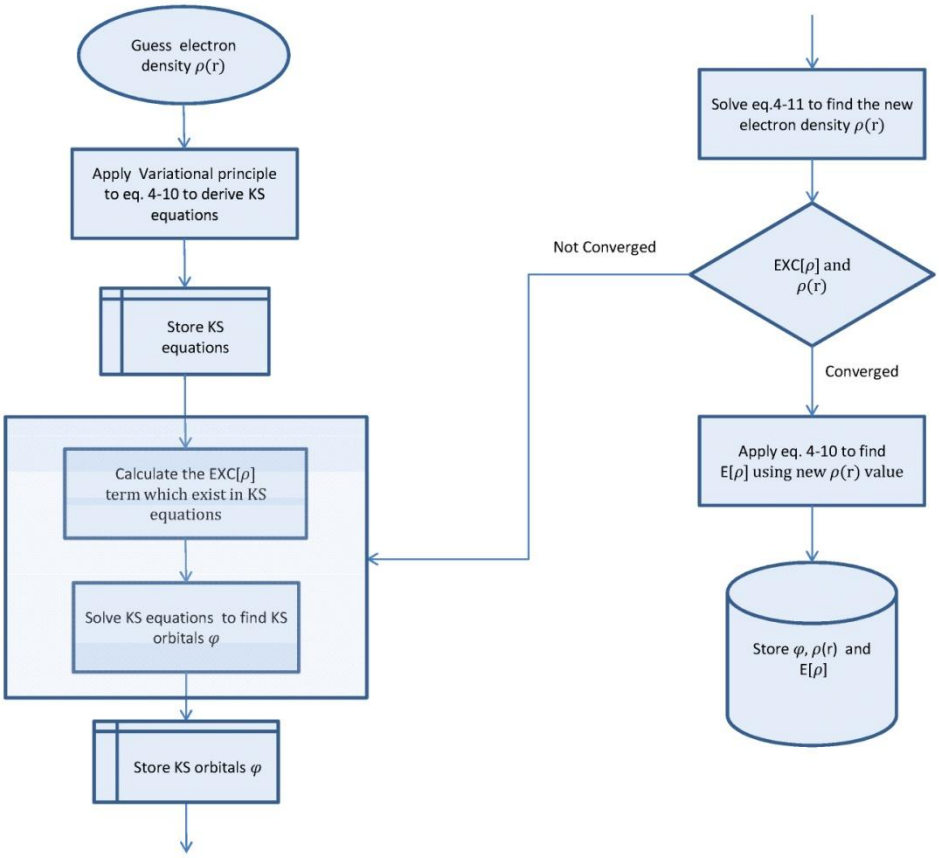


**Figure 4-5: DFT computation procedure**

### 4.1.4 Solvation Model

Since the chemical reactions usually do not take place in vacuum we always need to take into account the effect of environment. In the case of this thesis, an effective medium - water - does exist which needs to be considered. Water as a solvent always plays an important role in chemical reactions. Considering the polarity of water molecules, the solvent effect is very important, especially when we aim to calculate the partial charges of the solute. Based on Jensen (2006), effect of solvation can be regarded under two different categories:

- Non-specific (long-range) solvation which consists of polarization and dipole orientation
- Specific (short-range) solvation including hydrogen bonds, Van der Waals interactions, charge transfer effects and so on.

Solvation effects can be modeled by considering the solvent molecules explicitly. This approach is computationally very demanding due to the large number of solvent molecules

which are needed to be considered. To be able to overcome the computational limitations, another type of models have been proposed which "treat the solvent as a continuous medium"(Jensen 2006). These models, which are called *continuum solvation models*, only treat the solute molecules explicitly. They assume the solvent "as an uniform polarizable medium" with a specific dielectric constant which contains a cavity of solute molecules (Jensen 2006). Desired shape of the cavity should be same as the molecular shape but on the account of limitations based on computational resources, in many cases, only simple cavity shapes like a sphere are used. A continuum salvation model having simple sphere cavity for the solute is illustrated by Figure 4-6.

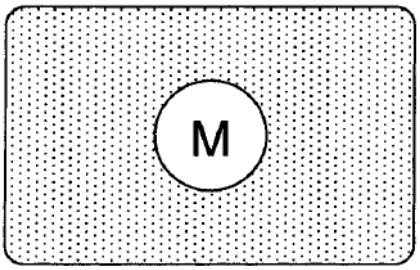


**Figure 4-6: Continuum solvation model (Jensen 2006)**

In this thesis a recently improved version of Solvation Model (SM version 8.0) has been employed. SM8 is a universal model, which means it is applicable to all solvents. As an implicit or continuum model it is also suitable for any charged or uncharged solute composed of hydrogen, carbon, nitrogen, oxygen fluorine, silicon, phosphorus, sulfur, chlorine and bromine in any solvent or liquid medium (Marenich et al. 2007). It is recommended for SM8 model to be used with "self-consistently polarized class IV charges" such as CM4 charges (Marenich et al. 2007). This type of charges will be introduced in the following section.

### 4.1.5 Partial atomic charges

Calculation of the partial atomic charges within the molecules is a problematic issue. Since positions of the electrons around the atoms are not fixed and other neighboring atoms continuously affect the electrons - especially when there is a solvent environment available – electron distribution takes place asymmetrically along the bond length. Due to this uncertainty in electron distribution, procedures for calculation of the partial charges and assigning a fraction of this distribution to each atom can be a challenging task.

One of the approaches towards calculation of the partial atomic charges is definitely utilizing the quantum chemistry methods as a promising tool. Within this area several schemes have been proposed. The simplest scheme is called *Mulliken population analysis* (*MPA*), which partitions the electronic distribution among the atoms based on contribution of atomic orbitalls (Mulliken 1955). Results from this method are not considered reliable due to the non-realistic assumptions or consequences in many situations (Cramer 2004). As an illustration, this method predicts orbital occupancies with values less than zero or higher than 2, which are obviously of no physical meaning. In addition, MPA neglects the effect of electronegativity of various atoms, since it assumes the electrons are divided evenly along the bond length between different atoms. Moreover, MPA is very dependant to the size of basis sets (Cramer 2004).

To avoid the deficiencies of MPA, P.O. Löwdin mentioned the problem of non-orthogonality in regard with atomic orbitals (Lowdin 1950). In his improvement on mulliken population analysis, he proposed application of a symmetric orthogonalization scheme. Considering Equation (4-14) as gross charge on atom $i$, *Löwdin population analysis* (*LPA*) can be defined by Equation (4-15).

$$q_i = Z_i - N_i \qquad \text{(Cramer 2004)} \qquad \textbf{(4-14)}$$

Where, $Z_i$ is the nuclear charge and $N_i$ is atomic population.

$$N_i = \sum_i S_{ii}^{\frac{1}{2}} P_{ii} S_{ii}^{\frac{1}{2}} \qquad \text{(Baker 1985)} \qquad \textbf{(4-15)}$$

Where, $P_{ii}$ density matrix, $S_{ii}$ overlap matrix and $S_{ii}^{\frac{1}{2}} P_{ii} S_{ii}^{\frac{1}{2}}$ is Löwdin density matrix.

Löwdin charges themselves are not stable with very large basis functions such as diffuse functions. To alleviate this problem *Redistributed Löwdin population analysis* (*RLPA*) has been proposed (Thompson et al. 2002). This method modifies the part of the LPA that comes from diffuse functions and therefore diminishes sensitivity of this method towards the diffuse functions (Thompson et al. 2002; Cramer 2004).

MPA and LPA schemes are categorized as class II charge models in which molecular wavefunctions (MO) are partitioned into contributor atomic orbitals (AO). Another class of

charge models, which is interesting for this thesis, is class IV from which CM4 charge scheme has been employed to be used with SM8 solvation model for calculation of partial charges.

Class IV charge models have been developed to avoid the errors existing in the class II and class III of charges. For instance, class II of charges are obtained based on the computation of wavefunction and class III stands for physical observables. But class IV is derived by a "semi-empirical mapping" of class II or class III charges (Cramer 2004; Kelly et al. 2005). CM4 model, which is one of the class IV charge models, has been designed to provide an accurate charge distribution and is defined by Equation (4-16). This charge model has been recommended to be used with the SM8 solvation model.

$$q_k^{CM4} = q_k^0 + \sum_{k \neq k'} (D + CB_{k,k'})B_{k,k'} \qquad \textbf{(4-16)}$$

Where sum goes over atoms $k$ in the molecule, $q_k^0$ is partial atomic charge from Class II which is LPA for non-diffuse basis sets and RLPA for diffuse basis sets and $B_{k,k'}$ is the *Mayer bond order* between atoms $k$ and $k'$. In addition, C and D are empirical parameters (Olson et al. 2007). It also should be noted that Mayer Bond order is defined based on Equation (4-17).

$$B_{k,k'} = \sum_{\mu \in k} \sum_{\nu \in k'} (PS)_{\mu\nu} . (PS)_{\nu\mu} \qquad \textbf{(4-17)}$$

Where P and S are previously defined density and overlap matrices.

## 4.2 Molecular Mechanics (MM)

Solution of the Schrödinger equation for multi atomic molecules leads to introduction of the *Potential energy surface* (*PES*) concept. Once molecular wavefunction and its corresponding energy are known, potential energy surface of the molecule will be defined.

Since the chemistry can be understood by knowing the "energy as a function of the nuclear coordinates" (Jensen 2006), once the PES is known many physical and chemical properties can be calculated. The link between properties of the microscopic system where, atoms and molecules are considered explicitly and macroscopic observables such as temperature and entropy is established by *Statistical mechanics*.

The main interesting points on the PES are those with zero first derivatives in respect to all the coordinates. Such points are usually called *Stationary points* (Leach 1996). These points

are very interesting for chemist because the forces on all the atoms are zero here. There are different types of stationary points. One is called *minimum points* corresponding to the stable conformations of the molecule. Another type of stationary points is called *Saddle Points* which are the "highest points on the pathway between two minima" (Leach 1996). Both of these points are of great interest in chemistry since investigation of the former can lead to finding the most stable structure of the molecule (*Global minimum*) from which the equilibrium geometry of the molecule can be specified. This is the task being done by *Geometry optimization* within which *conformation search* is performed to find the global minimum corresponding to the optimized (equilibrium) structure of the molecule. On the other hand, investigation of the saddle points can specify the *transition states* between two different conformations.

According to the Born-Oppenheimer approximation, nuclei are massive enough to have negligible quantum mechanical behavior while this is not true about electrons. Electrons are much lighter and faster than the nuclei within the molecular structure so that any fluctuation in the nuclear positions will be followed immediately by their associated electronic distributions. Therefore electronic wavefunction depends mainly on the nuclear positions (Jensen 2006). Considering this, potential energy surface (PES) can be defined as a multidimensional surface by which variations of the potential energy of the system (nuclei conformations) are represented (Leach 1996).

Neglecting the explicit contribution of the electrons into the molecular energy, we are allowed to assume the atoms (nuclei) as single points. Considering that nuclei only have very insignificant quantum mechanical behavior, it is possible to use classical mechanics to explain the potential energy of such a system. Here, classical definitions of the potential energy are employed - such as the simple ball and spring model for intra-molecular potential energy of a given molecule - to be able to simplify modeling of the molecular structure.

MM is computationally less demanding than the QM but on the other hand, it lacks description of the electronic structure of the molecule. Therefore, those cases in which atomic or molecular orbitals play an important role, cannot be explained by MM. Considering this fact, recent developments of the computational methods have been directed towards the QM/MM approach, so that quantum mechanical description of the system is available in the areas of interest while simultaneously MM is utilized in other parts of the system to save the computer time.

### 4.2.1 Molecular Modeling

Molecular modeling concerns various techniques which are widely used in molecular design technology within chemical, pharmaceutical and agrochemical industries. At the same time, it is an important stage ahead of any molecular simulation, because it is necessary to have validated models for molecules and species which are supposed to be employed during the simulation.

Molecular modeling involves modeling of the various types of potential interactions by which behavior of the molecules are explained. As mentioned earlier, in molecular mechanics (MM), classical definitions of potential energy are used. In this regard, two main types of molecular interactions are distinguished: *Intermolecular* interactions which occur among the individual molecules and *intra-molecular* interactions that are contributions of atoms into the potential energy within each molecule.

#### 4.2.1.1 Intermolecular interactions

Intermolecular potential interactions relate to the non-bonded interactions among various atoms from different molecules. This class of interactions can be categorized as *long-range* and *short-range* interactions which means how fast they fall off with respect to distance. *Electrostatic* interactions and *Van der Waals* interactions are two contributors in this part.

##### 4.2.1.1.1 Electrostatic interactions and Ewald summation

Electrostatic interactions or long-range interactions are a group of non-bonded interactions which follow the Coulomb's law. In other words, partial or formal charges (in the ionized molecules) of the atoms cause this type of interactions. Therefore mutual potential energy is defined by Equation (4-18).

$$U_{AB} = \frac{1}{4\pi\varepsilon_r\varepsilon_0} \cdot \frac{q_A q_B}{R_{AB}} \qquad \textbf{(4-18)}$$

Where $\varepsilon_0$ is vacuum permittivity and $\varepsilon_r$ is relative permittivity.

Calculation of the electrostatic interactions between all the atom pairs is not computationally favorable, since the interactions over very long distances within the periodic boundary condition[8] are negligible. To reduce the computational requirement reasonably *Cut-off* distances are proposed to be employed. Nevertheless, truncation of the interactions beyond

[8] Periodic boundary condition (PBC), can be imagined as a periodic array of simulation boxes in which every box has been surrounded by other (replicated) boxes in all directions.

the cut-off distance does lead to some serious mathematical problems, such as discontinuity within the interaction profile. In order to diminish the computational effort as low as possible and to simultaneously keep the accuracy high enough, the *Ewald summation* method is utilized. This method is able to calculate the electrostatic energy "exactly" (Jensen 2006) and to include "all the effects of long-range forces into a computer simulation"(Leach 1996).

Application of Equation (4-18) for all the atom pairs within the periodic boundary condition can be redefined as following(Leach 1996).

$$U_{el} = \frac{1}{2} \sum_{|n|=0}^{\infty\,'} \sum_{i=1}^{N} \sum_{j=1}^{N} \frac{q_i q_j}{4\pi\varepsilon_0 |r_{ij} + n|} \qquad \textbf{(4-19)}$$

Here a cluster of cubic cells has been assumed so that $n$ is position of the box within the cubic lattice, N is the number of charges in each box and $r_{ij}$ is the minimum distance between charge $i$ and $j$. The prime on the first sum signifies interactions of $i = j$ are excluded for $n = 0$.

Figure 4-7 illustrates that electrostatic interactions consist of the interactions within the central box ($n = 0$) and the interactions between the central box with all the image boxes(Leach 1996).

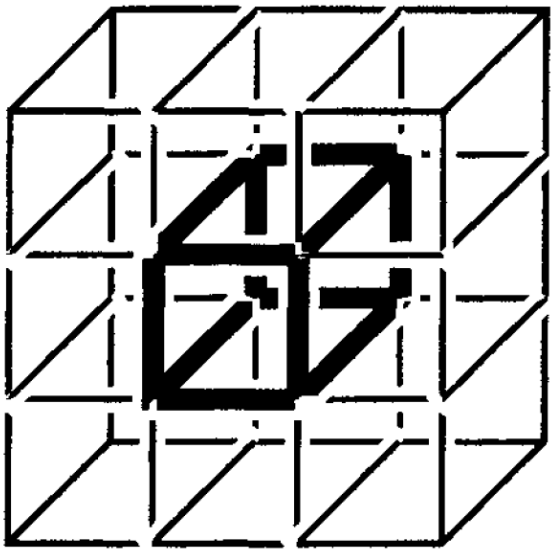

**Figure 4-7: illustration of the central box inside a cluster of image boxes due to the PBC application (Jensen 2006)**

Equation (4-19) is a very slow converging equation; hence, it is converted into two other series of equations that can be converged much faster. Here is exactly the point that Ewald summation emerges. It presumes that each charge is surrounded by a neutralizing charge distribution. Therefore one term is added into the total potential equation to include the contribution of this neutralizing charge. This neutralizing potential term is described by *Gaussian functions*. Summation of the potential interactions between the charges plus the neutralizing distribution is called *real space* summation.

Moreover, to compensate the addition of the neutralizing charge distribution, a counteractive potential term is also needed which is performed in *Reciprocal space*. At the end, some correction terms for the total potential equation are also considered to exclude the interaction of each Gaussian with itself and to include the effect of surrounding medium.

The final equation for total potential energy based on Ewald summation method is demonstrated by Equation (4-20) (Leach 1996).

$$U_{el}^{tot} = \frac{1}{2}\sum_{i=1}^{N}\sum_{j=1}^{N}\left\{\begin{array}{c} \sum_{|\boldsymbol{n}|=0}^{\infty'} \frac{q_i q_j}{4\pi\varepsilon_0}\frac{erfc(\alpha|r_{ij}+n|)}{|r_{ij}+n|} \\ +\sum_{k\neq 0}\frac{1}{\pi L^3}\frac{q_i q_j}{4\pi\varepsilon_0}\frac{4\pi^2}{k^2}exp\,(-\frac{k^2}{4\alpha^2})\cos\,(k.r_{ij}) \\ -\frac{\alpha}{\sqrt{\pi}}\sum_{k=1}^{N}\frac{{q_k}^2}{4\pi\varepsilon_0} \\ +\frac{2\pi}{3L^3}\left|\sum_{k=1}^{N}\frac{q_k}{4\pi\varepsilon_0}r_k\right|^2 \end{array}\right. \qquad \textbf{(4-20)}$$

Inside the brace, first term from top indicates the contribution from real space summation, second term demonstrates the contribution from reciprocal space, third term is correction due to the self interaction of the Gaussian functions in real space and the last term shows the correction because of surrounding medium effect when the medium is vacuum ($\varepsilon_r = 1$).

To clarify about the notation, $q_i, q_j, q_k$are charges of particles $i, j, k$ respectively, ercf is the complementary error function, $n$ is the cubic lattice point vector, $r_{ij}$ is minimum distance vector between charge $i$ and $j$, $\alpha$ is exponent in Gaussian function, vectors $k$ are reciprocal

vectors so that $k = 2\pi n/L^2$, L is the box size, N is the number of particles and $U_{el}^{tot}$ is the total electrostatic potential energy.

#### 4.2.1.1.2 Short range interactions

Short range interactions are predicated upon a variety of dipole-dipole, induced dipole and dispersion interactions in combination with the repulsive contribution. The first three contributions are those with attractive effect due to the attraction between the dipoles (permanent, induced or instantaneous one). It should be stressed that dispersion interaction - also known in conjunction with *London forces* - is a quantum mechanical phenomenon caused by instantaneous fluctuations of the electron distribution which give rise to the formation of temporary dipole moments. These dipole moments - in turn - can induce some other dipoles among the electron distribution of the neighboring atoms which contribute to the dispersion interactions.

Repulsive contribution to the short-range interactions, in contrary, arises from electron clouds overlap when the distances are not long enough. In such a situation "negatively charged electrons repel each other" (Jensen 2006) and "positively charged nuclei become less well shielded" (Hinchliffe 2008) and cause the repulsion. Repulsive potential falls off exponentially with respect to inter-atomic distances (Hinchliffe 2008).

Historically, the short-range interactions are known under the name of *Van der Waals energies*(Jensen 2006). A famous mathematical description which models the short-range interactions is *Lennard-Jones* (*L-J*) potential model explained by Equation (4-21).

$$U_{L-J} = 4\varepsilon[\left(\frac{\sigma}{R}\right)^{12} - \left(\frac{\sigma}{R}\right)^{6}] \qquad \textbf{(4-21)}$$

Here, $\varepsilon$ is the minimum potential energy or in other words the maximum attraction potential, known as potential well depth, while $\sigma$ is the distance at zero potential and R is inter-atomic distance. The first term with the power of 12 represents the repulsive interaction which falls off dramatically as the distance increases. Repulsion interaction can be illustrated better by an exponential function but it has been simplified here by using the $12^{th}$ power of the inverse of distance. The second term in L-J potential expression represents the attraction interaction which falls off much slower than the repulsion one.

Considering the above mentioned behavior of the L-J potential, at long distances they are totally negligible. Therefore, in order to save the computer time, molecular simulators usually prefer to truncate them when interacting particles are very far from one another. However, as stressed earlier, this so called cut-off option can give rise to some serious mathematical problems based on the discontinuity issue. As such, some circumventing methods are essential.

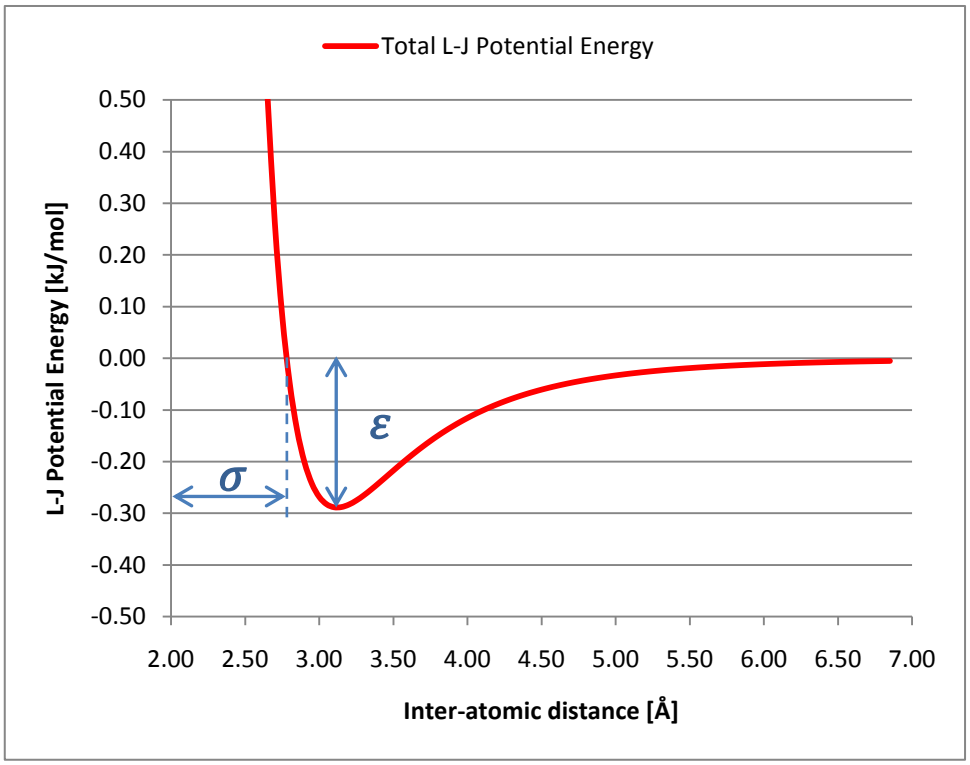


**Figure 4-8: L-J 12-6 potential energy for Neon atom**

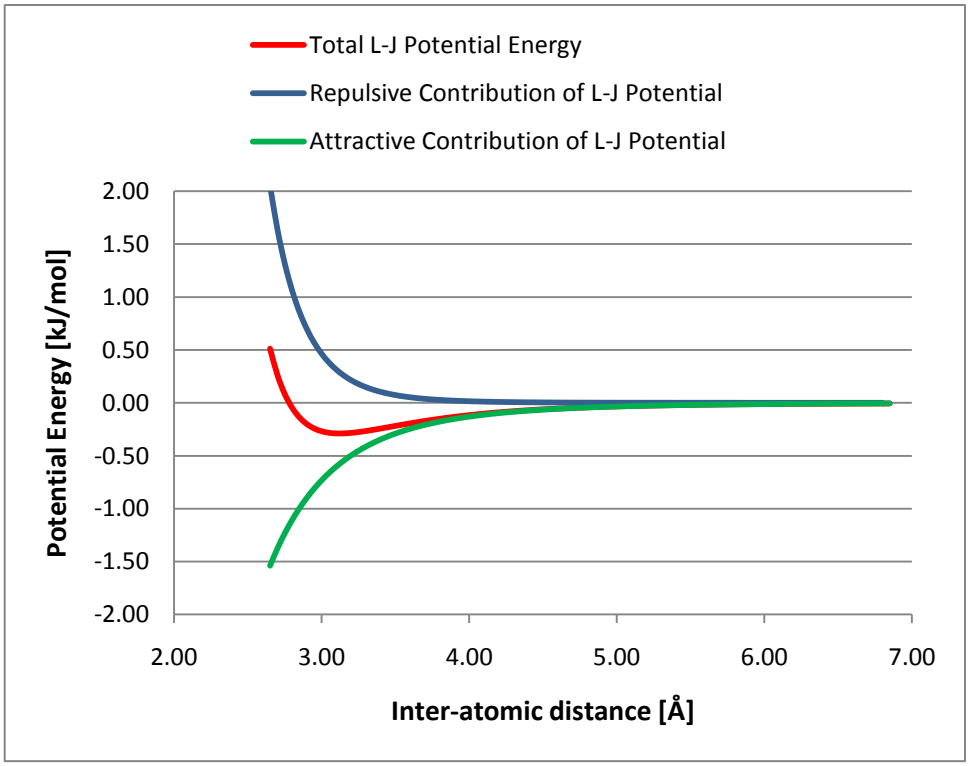


**Figure 4-9: L-J 12-6 potential energy for Neon atom with its repulsive and attractive contributions**

Clearly, Lennard-Jones potential energy between two atomic sites depends on the values of $\sigma$ and $\varepsilon$ (apart from their separation) which are broadly available in literature for pure substances. Problem arises when polyatomic molecules are needed to be considered. In this case, cross-interactions between unlike atoms have to be calculated. Since calculation of L-J parameters for unlike atoms is difficult, so-called mixing rule (*Lorentz-berthelot's rule*) is used to calculate their L-J parameters based on the parameters for pure materials. In this rule collision diameter $\sigma_{ij}$ is calculated as an arithmetic mean value of $\sigma$ for two pure species while well depth $\varepsilon_{ij}$ is given as a geometric mean value of $\varepsilon$ for two pure species(Leach 1996). Equations (4-22) and (4-23) explain collision diameter $\sigma_{ij}$ and well depth $\varepsilon_{ij}$ respectively.

$$\sigma_{ij} = \frac{1}{2}(\sigma_{ii} + \sigma_{jj}) \qquad \textbf{(4-22)}$$

$$\varepsilon_{ij} = \sqrt{\varepsilon_{ii}.\varepsilon_{jj}} \qquad \textbf{(4-23)}$$

#### 4.2.1.2 Intra-molecular interactions

Basically intra-molecular interactions concern the potential interactions among the atomic components of every molecule. This includes the *Bond stretching*, *Angle bending*, *Dihedral motions* (*torsional rotation*) and *Out of plane bending* (*inversion*) potentials. Moreover, Van der Waals interactions between all the atoms which are not separated by three or more covalent bonds should be also taken into account.

##### 4.2.1.2.1 Bond stretching

Potential energy between two sample atoms can be resembled using the classical harmonic spring model known as Hook's law.

$$U_{AB} = \frac{1}{2} k_{AB} (R_{AB} - R_{eq,AB})^2 \qquad \textbf{(4-24)}$$

Where $U_{AB}$ is the spring potential energy (stretching potential) between atoms A and B, $R_{AB}$ is the instantaneous inter-nuclear distance between A and B, and $R_{eq,AB}$ is the inter-nuclear distance at equilibrium. Moreover, $k_{AB}$ is called force constant or bond strength, which can be calculated using QM calculations or by conducting experimental measurements. Figure 4-10, illustrates the classical covalent bond model based on Hook's Equation (4-24).

**Figure 4-10: Classical covalent bond model**

This is actually the simplest bond stretching model. More elaborate models have been proposed to introduce more accuracy into the obtained results. One of the most popular models in this sense is *Morse potential* which is defined by Equation (4-25).

$$U = D_e \left\{ 1 - \exp\left[ - \left( \frac{\omega_e}{2} \sqrt{\frac{2\mu}{D_e}} \right) (R - R_e) \right] \right\}^2 \qquad \textbf{(4-25)}$$

Where $D_e$is potential well depth, μ is reduced mass and $\omega_e$is equilibrium angular frequency. $R$ and $R_e$has the same definition as in the harmonic potential case.

#### 4.2.1.2.2 Angle bending

In almost the same way, the angle between two bonds, i.e. three atoms, can be modeled using the classical definition of Hook's law. In this case, the angle can vibrate harmonically depending on the external forces which are experienced.

$$U_{ABC} = \frac{1}{2} k_{ABC} (\theta_{ABC} - \theta_{eq,ABC})^2 \quad \textbf{(4-26)}$$

Where $U_{ABC}$ is the angle bending potential energy, $\theta_{ABC}$is the instantaneous angle between atoms A, B and C, $\theta_{eq,ABC}$ angle at equilibrium and $k_{ABC}$ is the angle force constant. Figure 4-11 shows a classical harmonic model for angle bending.

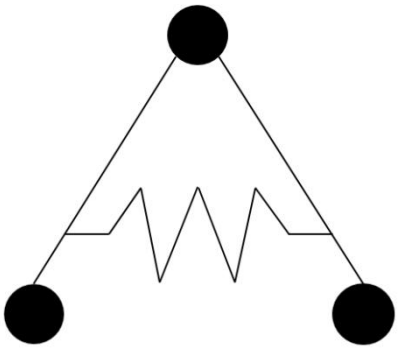

**Figure 4-11: Classical harmonic spring as an angle bending model**

#### 4.2.1.2.3 Dihedral (torsional) motion

Dihedral motion can be considered as torsion of the four bonded molecules along the dihedral angle ABCD according Figure 4-12.

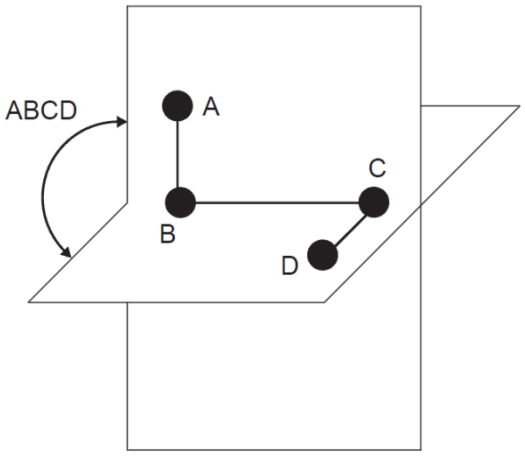


**Figure 4-12: Torsional motion around the dihedral angle ABCD (Hinchliffe 2008)**

Similarly, a range of various models have been proposed for torsional potential. As a case in point, OPLS force field employs Equation (4-27) for torsional potential.

$$U_{dih} = \frac{V_1}{2}(1 + cos\varphi) + \frac{V_2}{2}(1 - cos2\varphi) + \frac{V_3}{2}(1 + cos3\varphi) + \frac{V_4}{2}(1 - cos4\varphi) \quad \textbf{(4-27)}$$

Where $V_1$ , $V_2$ , $V_3$ and $V_4$ are Fourier coefficients for dihedral angles from OPLS-aa force field and $\varphi$ is the torsional angle (Watkins and Jorgensen 2001).

#### 4.2.1.2.4 Out of plane bending interactions

According Figure 4-13, when four atoms ABCD prefer to lie down on the plane, any deviation of atom D from indicated plane gives rise to another type of potential energy, called *out of plane bending* energy or *inversion potential*. This potential can be modeled as a harmonic term concerning the out of plane angle $\Psi$ or as quadratic function of the height $d$ (Jensen 2006).

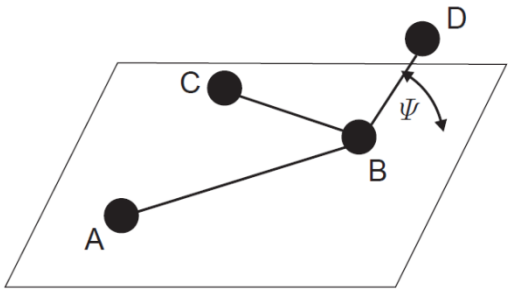


**Figure 4-13: Out of plane (inversion) potential (Hinchliffe 2008)**

$$U_{oop}(\Psi) = K\Psi^2 \quad \textbf{(4-28)}$$

Or

$$U_{oop}(\Psi) = K'h^2 \quad \textbf{(4-29)}$$

Where $K$ and $K'$ in above equations are force constants and $h$ in Equation (4-29) represents the height of atom D above the plane ABC.

#### 4.2.1.2.5 Non-bonded interactions inside the molecule

As explained in preceding sections, non-bonded interactions occur due to the electrostatic potential or Van der Waals forces. Sometimes this class of interactions has to be taken into account for intra-molecular interactions as well, especially when the large molecules such as proteins are to be considered. In these cases, non-bonded potentials between atoms of the same molecule should be added to the total intra-molecular potential energy of the molecule. Different force fields pick various strategies to define the separation distance between the non-bonded atoms. However, it is more common to choose atoms separated by three or more covalent bonds for intra-molecular non-bonded interactions (Jensen 2006).

Consequently, the intra-molecular interactions of one sample molecule can be visualized as Figure 4-14.

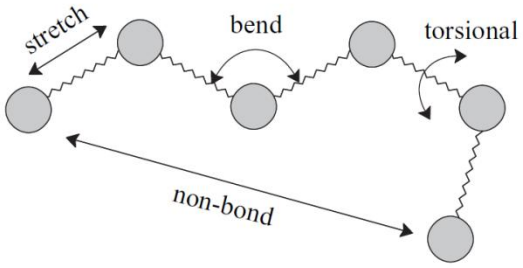


**Figure 4-14: Intra-molecular interactions**

### 4.2.1.3 Force fields

As expressed earlier, in order to define the molecular structures in MM, molecular potential energy and its corresponding parameters are treated by employing the classical definitions of energy. Considering that electronic structures of the atoms are not taken into account in MM, partial atomic charges have to be calculated separately by QM approach.

In principle, a set of specific equations for calculating the potential energy between atoms and functional groups in combination with related parameters and partial atomic charges are called force field. The idea behind the force field method is based on the "observation that molecules tend to be composed of units that are structurally similar in different molecules"(Jensen 2006). Simply meaning bond length, bond angles, torsional angles and other force field parameters for specific atom types or functional groups are roughly the same even within different molecules. This is what usually called *transferability* property in the force fields. However, different force fields can be optimized for specific desires such as OPLS force field which is optimized for simulation of liquids.

Standard modern force fields choose similar definitions with slight variations to define total potential energy as equation **(4-30)** (Hinchliffe 2008):

$$U = \sum_{Stretch} U_{ij} + \sum_{Bend} U_{ijk} + \sum_{dihedral} U_{ijkl} + \sum_{Out\ of\ plane} U_{ijkl} + \sum_{L-J} U_{ij} + \sum_{Electrostatic} U_{ij} \quad \textbf{(4-30)}$$

There are numerous force fields developed for different desires. Among those are MM2, MM3, MM4, AMBER, CHARMM, OPLS, etc.

For this thesis OPLS all atom force field - which OPLS is an acronym for *Optimized Potentials for Liquid Simulations* - was chosen due to the focus of this research on the simulation of liquid solution of amine systems.

### 4.2.2 Molecular Dynamics Simulation (MD)

Calculation of thermodynamic properties of the system needs the PES to be quantified. Nevertheless, this is only possible for very small systems such as individual small molecules in gas phase by performing energy minimization (Leach 1996). Considering the real systems in which we are interested are very sophisticated, such as liquid systems consisting of too many molecules, this approach is practically impossible. Having said that, molecular simulation is found to be a useful tool for calculation of the properties of the large systems.

Molecular Dynamics (MD) is a simulation technique based on time evolution of the system. A microscopic replication of the macroscopic system is treated as a manageable box of the molecules in order to predict the configurations and properties of the system in any time in future (Leach 1996). MD employs an initial configuration of the molecules as input, and then computes the molecular forces based on interaction parameters of a given force field. Subsequently, it determines velocities and positions of the molecules by integrating the Newton's law of motion. Data collected from any preceding step is used to calculate the new forces, velocities and positions for the ensuing configuration after a very small time interval. This procedure is followed by the same cycle to predict the configuration of the system at any time in future. This means that MD generates a *Trajectory* of the system with respect to time. Having this information, thermodynamic averages of the system can be calculated by applying statistical mechanics approach to resemble the thermodynamic properties of the macroscopic system of interest.

#### 4.2.2.1 MD algorithms

Once the total mutual potential energies of the molecules are determined in the system (Equation (4-31)), corresponding force can be calculated based on Equation (4-32).

$$U_{ij}^{tot} = \sum_{j=i+1}^{N} U_{ij} + \sum_{j=i+1}^{N-1} \sum_{k=j+1}^{N} U_{ijk} + \cdots \qquad \textbf{(4-31)}$$

Equation (4-31) does not assume pair wise additivity, therefore second, third and (…) terms in this equation are to include the effect of other molecules in the total mutual potential energy of two specific molecules such as $i$ and $j$.

$$F_i = -gradU_i \quad \textbf{(4-32)}$$

Where $U_{ij}$ is total mutual potential energy between molecule $i$ and $j$ while $F_i$ represents the total force on molecule $i$.

Given total force $F_i$ on any specific molecule, MD applies Newton's second law to determine the velocity and position of that molecule by numerical integration of Equation (4-33).

$$F_i = m_i \frac{d^2 r_i}{dt^2} \quad \textbf{(4-33)}$$

There are several types of algorithms in the literature to integrate Equation (4-33) numerically. Two of those well known algorithms are *Verlet* and *Leapfrog* algorithms, however, the latter is considered as "the most accurate and stable technique for use in molecular dynamics"(Hinchliffe 2008).

#### 4.2.2.1.1 Leapfrog algorithm

Writing the well-known *Taylor expansion* for velocity of the molecule $i$ in following form we will have (Hinchliffe 2008):

$$V_i\left(t + \frac{\Delta t}{2}\right) = V_i(t) + \left(\frac{dV_i}{dt}\right)_t \frac{\Delta t}{2} + \frac{1}{2}\left(\frac{d^2 V_i}{dt^2}\right)_t \left(\frac{\Delta t}{2}\right)^2 + \cdots \quad \textbf{(4-34)}$$

$$V_i\left(t - \frac{\Delta t}{2}\right) = V_i(t) - \left(\frac{dV_i}{dt}\right)_t \frac{\Delta t}{2} + \frac{1}{2}\left(\frac{d^2 V_i}{dt^2}\right)_t \left(\frac{\Delta t}{2}\right)^2 + \cdots \quad \textbf{(4-35)}$$

Subtracting Equations (4-34) and (4-35) with some rearrangements leads to Equation (4-36) which is one of the leapfrog equations (Hinchliffe 2008).

$$V_i\left(t+\frac{\Delta t}{2}\right)=V_i\left(t-\frac{\Delta t}{2}\right)+a_i(t)\Delta t+\cdots \quad \textbf{(4-36)}$$

Similarly writing a Taylor expansion for position of molecule $i$ leads to Equation (4-37) which is another leapfrog equation for MD simulation (Hinchliffe 2008).

$$r_i(t+\Delta t)=r_i(t)+V_i\left(t+\frac{\Delta t}{2}\right)\Delta t+\cdots \quad \textbf{(4-37)}$$

The procedure is clear. Initially, acceleration $a_i$ is calculated at time $t$ from Equation (4-33). Subsequently, velocity $V_i$ is calculated at time $t+\frac{\Delta t}{2}$ by means of the first leapfrog equation (Equation (4-36)). Having the velocity at this time, position $r_i$ is determined at time $t+\Delta t$ based on Equation (4-37). This procedure is continued to develop time evolution of the system. In these equations, $\Delta t$ is so-called *time step* or *time increment* of MD simulation.

#### 4.2.2.1.2 Verlet algorithm

Verlet algorithm stems from Taylor expansion for position of the molecule $i$ as following (Hinchliffe 2008):

$$r_i(t+\Delta t)=r_i(t)+\left(\frac{dr_i}{dt}\right)_t\Delta t+\frac{1}{2}\left(\frac{d^2r_i}{dt^2}\right)_t(\Delta t)^2+\cdots \quad \textbf{(4-38)}$$

$$r_i(t-\Delta t)=r_i(t)-\left(\frac{dr_i}{dt}\right)_t\Delta t+\frac{1}{2}\left(\frac{d^2r_i}{dt^2}\right)_t(\Delta t)^2+\cdots \quad \textbf{(4-39)}$$

Assuming third and higher order derivatives in above equations are negligible, Verlet algorithm appears to be such as Equation (4-40) (Hinchliffe 2008).

$$r_i(t+\Delta t)=2r_i(t)-r_i(t-\Delta t)+\left(\frac{d^2r_i}{dt^2}\right)_t(\Delta t)^2 \quad \textbf{(4-40)}$$

As one can see, by using the Verlet algorithm, MD has to calculate the acceleration at time $t$ from Equation (4-33). Then, positions of the molecule are calculated at time $t$ and $t-\Delta t$ (instead of calculating the velocity in leapfrog algorithm) in order to determine new position of the molecule at $t+\Delta t$ .

#### 4.2.2.2 Constraint dynamics

There are various techniques to increase the speed of simulation. In general, simulation of rigid molecules is much easier than the flexible ones. This is because simulation of flexible molecules involves the intra-molecular interactions which can affect the molecular conformation more strongly, while neglecting the flexibility of the molecule decreases the problem to solution of a system involving merely intermolecular interactions.

One of the appropriate approaches to increase the speed of simulation is to eliminate the high frequency motions in the system, because they attract less attention due to their little role in the major conformational variation rather than the low frequency motions (Leach 1996). Doing this, it is possible to increase the time step and consequently speed up the simulation.

High frequency motions can be removed for example by defining a new geometric coordinates - called *Generalized coordinates* - which exclude those degrees of freedom that count for high frequency motions (Field 2007). There is always 3N-6 degrees of freedom for a common system with N particles, in which 3N is connected with degrees of freedom of each particle (3) multiplied by the number of molecules (N) and 6 excluded degrees of freedom is associated with translational and rotational motion of center of mass of the system. For a system with the new geometric coordinates (which is supposed to neglect the high frequency motions), a number of $N_c$ degrees of freedom should also be excluded from total degree of freedom of the system (Field 2007). This gives the reason for Equation (4-41).

$$Degree\ of\ freedon = 3N - 6 - N_c \qquad \textbf{(4-41)}$$

Where $N_c$ is the number of high frequency motions.

However, the problem is that solution of involved equations for generalized coordinates is complicated and expensive.

Alternatively, another approach can be considered to eliminate the high frequency motions of the system, and simultaneously avoid the above mentioned complexity of the generalized coordinates. This can be accomplished by putting constrain on those degrees of freedom which are responsible for "generating the high frequency motions" (Field 2007). Under these criteria, bond lengths or bond angles have to adopt themselves with specific values of constraint, taking into account also some tolerance on their vibrational motions. This is what is called constraint dynamics in which the equation of motion is solved, while simultaneously the constraints of the system have to be satisfied (Leach 1996).

Introducing constraints to the system alters the dynamics of the simulation, so that equation of the motion will change. This is due to addition of constraint forces in Equation (4-42).

$$m\frac{d^2r}{dt^2} = -F_{pot} - F_{const.} \quad \textbf{(4-42)}$$

Where $F_{pot}$ is the total force due to the potential interactions while $F_{const.}$ is the total force due to the imposed constraint on the system.

Application of MD algorithms - for instance Verlet algorithm - based on this new equation of motion generates a set of functions comprising $N_c$number of equations which can be solved iteratively.

One of the well-known algorithms, which are widely used in MD simulation, is the *SHAKE* algorithm. This algorithm considers the constraints in turn and tries to solve the involved equations iteratively within some tolerance (Leach 1996). Several variants of SHAKE algorithm have also been developed such as MSHAKE or P-SHAKE algorithms.

#### 4.2.2.3 Periodic boundary condition (PBC)

Periodic boundary condition (PBC) can be imagined as a periodic array of simulation boxes in which every box has been surrounded by other (replicated) boxes in all directions. Figure 4-15 illustrates two-dimensional representation of PBC.

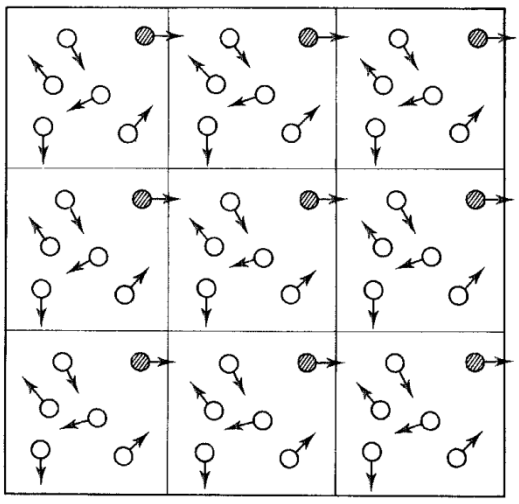

**Figure 4-15: 2-D periodic boundary condition (Leach 1996)**

Applying PBC in MD simulation is useful because we can simulate the bulk environment by means of only limited number of molecules. In such a case, if for instance one molecule

leaves the simulation box the same molecule emerges from opposite side of the box. This behavior has been shown in Figure 4-16.

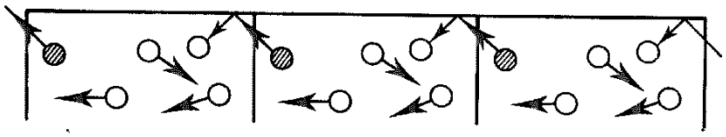

**Figure 4-16: Behavior of particles under the PBC (Leach 1996)**

Various shapes of PBCs can be used within MD simulation. Depending on the configuration of the system and shapes of the molecules, shape of the periodic boundary condition can be decided. In general five shapes are appropriate for MD simulation since they can fill all the space by translation operation of the central box in three dimensions: simple cubic box, hexagonal prism, truncated octahedron, rhombic dodecahedron and elongated dodecahedron. Different types of PBC are shown in Figure 4-17 (Leach 1996).

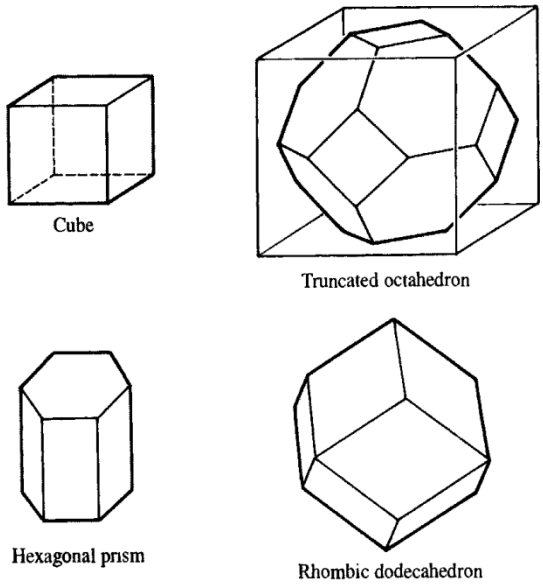


**Figure 4-17: Different periodic cells in computer simulation**

It is also important to decide about the box size in the simulation. In principle, size of the simulation box should be appropriately chosen so that the box can contain dimensions of the fluctuations or interactions which are supposed to be observed during the simulation. As a case in point, short-range L-J interactions can be usually fitted into the boxes larger than $6\sigma$ on each side (Leach 1996) but this will be more problematic for long-range interactions.

#### 4.2.2.4 Phase space and ensembles in molecular simulation

Phase space in molecular simulation is an unphysical space where states of the system are defined as explicit points. For a system consisted of N atoms 6N values are needed to have the state of the system fully defined. In principle, state of each atom is realized by 3 values regarding its position components and 3 values associated with its momentum components. This clearly signifies 6N values for N atoms in the phase space. State of the system in phase space does not concern the time of the system. However, in specific form of simulation such as molecular dynamics, trajectory of the system evolution can be observed as a path of successive states which are connected by time.

Any collection of the points (microstates) in phase space, which solely concerns macroscopic properties of the system, is defined as an *Ensemble*. To be specific, ensemble is a particle free concept in classical thermodynamics (Hinchliffe 2008) by which no attention is to be paid to the microscopic properties of the system. The only thing that is important here is macroscopic and average properties of the system over the ensembles. In general, ensembles comprise many numbers of exact replicas which are only similar in macroscopic level and represent the concept of bulk properties.

Despite molecular dynamics is traditionally performed in NVE (or NVEP)(Leach 1996), there are variety of ensembles which are available to be used. Four important ensembles in statistical thermodynamics are regarded as following:

- NVT or *canonical* ensemble in which number of molecules (N), Volume (V) and temperature (T) are kept constant.
- NVE or *microcanonical* ensemble that keeps the Energy (E) constant rather than the temperature in canonical ensemble.
- NTP or *isothermal-isobaric* ensemble that retains the number of molecule (N), temperature (T) and pressure (P) as constant.
- VT$\mu$ or *grand canonical* ensemble by which the volume (V), temperature (T) and chemical potential are constant.

Based on the *ergodic theorem,* average values over the ensembles is exactly the same as time averages of the original system in molecular dynamics (Hinchliffe 2008). In other words, this hypothesis assumes that the average calculated for a large number of molecule over a short time is equal with the average obtained by following a small number of molecules for a long time (Jensen 2006) . Here is the point where statistical mechanics plays its important role and

establishes the connection between the properties from microscopic level to the properties in macroscopic level, using the concept of ensemble. Indeed, this is what is done by *partition functions* in statistical mechanics. For the N interacting particles in condense phase the partition function $Q$ is calculated by Equation (4-43).

$$Q = \sum_{i}^{\infty} e^{\frac{-E_i}{k_B T}} \quad \textbf{(4-43)}$$

Where $E_i$ is energy of the state, $T$ is temperature and $k_B$ is the Boltzmann constant. It is important to note that $Q$ describes the entire system comprising N particles, and that $E_i$ belongs to the all energy states for whole of the system (Jensen 2006).

The brilliant point about partition function is its relation with thermodynamic functions, such as internal energy and Helmholtz free energy. Apparently, having these thermodynamic functions, the other ones like Gibbs free energy, entropy, enthalpy, pressure, etc. can be derived accordingly. Just for the sake of argument, Equations (4-44) and (4-45**)** have been given here to demonstrate connection of the partition function $Q$ with thermodynamic functions.

$$A = -k_B T ln Q \quad \textbf{(4-44)}$$

$$U = k_B T^2 \left(\frac{\partial ln Q}{\partial T}\right)_V \quad \textbf{(4-45)}$$

Where A and U are Helmholtz free energy and internal energy respectively (Jensen 2006).

#### 4.2.2.5 MD in constant temperature (application of Nosé Hoover thermostat)

In many cases, it is of great interest to perform the simulation in constant temperature. For instance, sometimes we need to compare the results from same systems but in different temperatures or we may need to investigate evolution of the system under specific temperatures. At this point, *temperature scaling* is a technique that can be employed to achieve this goal. The simplest way of doing temperature scaling in MD is *velocity scaling* by

which the velocity of the system is scaled at each level by the factor λ given by Equation (4-46).

$$\lambda = \sqrt{\frac{T_{Req.}}{T_{Curr.}}} \quad \textbf{(4-46)}$$

Since velocity of the system is connected with kinetic energy and the kinetic energy itself is associated with the temperature of the system based on Equation (4-47), scaling the velocity gives rise to the temperature scaling of the system (Leach 1996).

$$\langle E_K \rangle_{NVT} = \frac{3}{2} N k_B T \quad \textbf{(4-47)}$$

Where $E_K$ is time average of the kinetic energy for an unconstrained system.

Having Equations (4-46) and (4-47), temperature variation due to the velocity scaled by a factor of λ is predictable (Leach 1996):

$$\Delta T = (\lambda^2 - 1) T(t) \quad \textbf{(4-48)}$$

Where T(t) is temperature at time $t$ and $\Delta T$ is temperature change.

Alternatively, another method for temperature scaling is the one using a *heat bath* coupled to the system, so that it provides or removes energy from the system to keep the temperature constant based on following equation (Berendsen et al. 1984).

$$\frac{dT(t)}{dt} = \frac{1}{\tau} (T_{bath} - T(t)) \quad \textbf{(4-49)}$$

In this equation $\tau$ signifies the coupling parameter which dictates how tightly the system and the heat bath are coupled. The less the magnitude of this parameter the tighter the coupling of bath and the system.

Even in this method velocity is scaled due to the change of thermal energy imposed by the heat bath. Here, Equation (4-50) is defined as the Equation (4-46)'s successor for factor λ (Berendsen et al. 1984).

$$\lambda = [1 + \frac{\delta t}{\tau}\left(\frac{T_{bath}}{T(t)} - 1\right)]^{\frac{1}{2}} \quad \textbf{(4-50)}$$

Despite that the above mentioned temperature scaling methods can keep the average temperature of the system constant, they introduce some deficiencies into the system. To elaborate, averages over the canonical ensemble (NVT) are not precise, so that energy is not distributed evenly among different types of molecule. As such the solvent usually possesses much higher temperatures than the solute.

One of the popular solutions to avoid the unequal energy distribution in the system is called *extended system* method which is reputed as *Nosé-Hoover* method. This method was first proposed by Nosé (Nosé 1984), later simplified by Hoover (Hoover 1985) and developed more recently with some improvements (Martyna et al. 1992).

Extended system of Nosé-Hoover is actually a thermal reservoir (heat bath) integrated with the physical system. This reservoir was introduced initially by Nosé possessing one extra degree of freedom $s$, in addition to its conjugate momentum $p_s$, which acts as an external system (Nosé 1984). This reservoir has potential energy as well as the kinetic energy. Energy can flow between reservoir and the system to keep the temperature constant.

Nosé-Hoover introduces modified forms of the equations of motion for the extended system according to following equations(Hoover 1985):

$$\frac{dq_i}{dt} = \frac{p_i}{m_i} \quad \textbf{(4-51)}$$

$$\frac{dp_i}{dt} = F(q_i) - \xi p_i \quad \textbf{(4-52)}$$

$$\frac{d\xi}{dt} = \frac{[\sum_i \frac{{p_i}^2}{m_i} - X k_B T]}{Q} \quad \textbf{(4-53)}$$

In these three equations, $q_i$ is position of particle $i$, $p_i$ momentum of particle $i, m_i$ mass of particle $i$, F($q_i$) force on the particle $i$ due to the potential energy of the system, $\xi$ thermodynamic friction coefficient, $k_B$ Boltzmann constant, $X$ number of degree of freedom

and $Q$ is the parameter which determines the speed of temperature control with dimension of "energy $\times (time)^2$ that can be considered the fictitious mass of extra degree of freedom(Leach 1996)."

In Equation (4-53) time derivative of ξ is calculated by difference between kinetic energy of the system ($\sum_i \frac{{p_i}^2}{m_i}$) and its average value ($Xk_BT$) divided by Q . This Q itself is an important parameter which controls the system's response to the variations in temperature, with the large Q values causing the system to respond slowly, and small values of Q leading to rapid temperature fluctuations (Frenkel and Smit 2001).

Equations (4-51), (4-52) and (4-53) are known as Nosé-Hoover thermostat and time development of the system is fully described by them (Nosé 1991).

#### 4.2.2.6 Radial distribution functions (RDF)

*Radial distribution functions (RDF)* play an important role in the theory of simple fluids considering many thermodynamic properties in addition to the structure of the system can be identified from them (Leach 1996; Field 2007).

There are RDFs in different levels such as the triple radial distribution functions or pair radial distribution functions. However, mostly RDF aims the latter. Pair radial distribution functions can be defined as a useful tool which measures "the probability of finding a particle as a function of distance from a typical particle relative to that expected from a completely uniform distribution, i.e. an ideal gas with density $\frac{N}{V}$," (Jensen 2006).

Equation (4-54) demonstrates the above mentioned definition mathematically (Jensen 2006).

$$g(r, \delta r) = \frac{V}{N^2} . \frac{\langle N(r, \delta r) \rangle_M}{4\pi r^2 \delta r} \qquad \textbf{(4-54)}$$

Where $g(r, \delta r)$ is dimensionless pair distribution function, $N(r, \delta r)$ is the number of particles in spherical shell, subscript $M$ signifies the average (mean) value, $V$ is volume of the system , $N$ is number of particles in the system and $4\pi r^2 \delta r$ is volume of the spherical shell with thickness $\delta r$ which is calculated as following.

$$V_{shell} = \frac{4}{3}\pi(r+\delta r)^3 - \frac{4}{3}\pi r^3$$

$$= 4\pi r^2\delta r + 4\pi r\delta r^2 + \frac{4}{3}\pi\delta r^3 \qquad \textbf{(4-55)}$$

$$\approx 4\pi r^2\delta r$$

In other words, $g(r,\delta r)$ is the ratio of the actual density at distance $r$ to the mean density $\rho = \frac{N}{V}$ (Dill and Bromberg 2003). Figure 4-18 illustrates a typical radial distribution function from molecular dynamics simulation of the liquids. In this special case, MD simulation was performed for 256 Argon atoms inside a cubic box possessing 23Å side dimension at 100 $°K$ for 150 ps. However, only the first 7 ps of the simulation has been illustrated in this figure as equilibration phase. As one can observe, there are some maxima and minima in this figure. For instance, the first peak at $r = 3.75$ Å possesses value of 3.27 implying that it is 3.27 times more likely to find two atoms with this separation in comparison with ideal gas. And for the first minimum at $r = 5.47$ Å with the value of 0.48 it is obviously less likely to find any pair of atoms at the mentioned separation. It is also important to notice that the probability of finding of any atom pair within the distances shorter than the atomic diameter is zero due to the highly repulsive forces (Leach 1996). In contrary, the probability tends towards 1 as the inter-atomic distance increases, signifying the liquid is approaching the ideal gas limit.

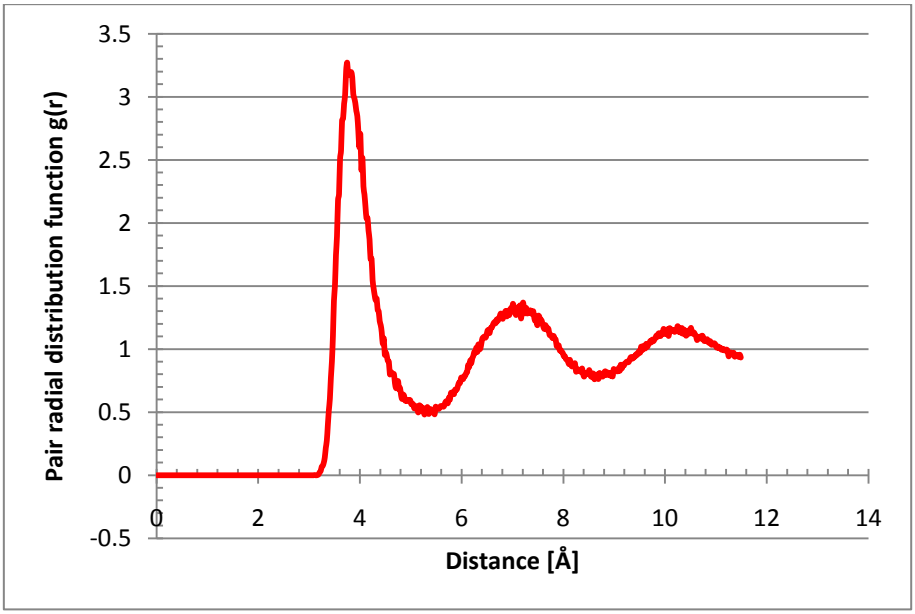


**Figure 4-18: RDF from MD simulation of liquid Argon**

In order to calculate the pair radial distribution function from MD simulation, the neighborhood of each atom is considered within discrete distances, where the average number of the particles are counted over the whole simulation time (Leach 1996).

The total number of surrounding atoms within the first shell of the particle of interest can be calculated by integration of the pair radial distribution (correlation) function over distance, according to Equation (4-56) (Dill and Bromberg 2003).

$$Number\ of\ nearest\ neighbors = \int_0^B \rho g(r) 4\pi r^2 dr \quad \textbf{(4-56)}$$

Where B is the distance of first minimum in the pair correlation function.

# 5 Literature review and previous works

Studies of piperazine activated MDEA solution systems lack enough experimental data. Despite recently published scientific works by different groups of researchers, still the kinetics of involved processes in such systems are not very well known. Furthermore, mechanisms which are responsible for the mass transport of carbon dioxide through the interface needs to be investigated more deeply. The situation for methane trapping processes is even worse. There is no individual research published in open literature for unusual trapping of methane in activated alkanolamine systems. However, many parts of this master thesis benefit from several experimental studies, which have been conducted on similar systems. As a case in point, speciation of the amine solution in current study was decided based on various experimental data available in the literature. At this place, the most important studies from open literature, which have been used in connection with current thesis are introduced as following.

❖ Experimental studies:

- Kinetics of carbon dioxide absorption was investigated by (Xu et al. 1992) for piperazine activated MDEA solutions.
- Beneficial effect of piperazine on carbon dioxide loading in MDEA solutions was studied by the same group more recently (Xu et al. 1998). They also investigated solubility of carbon dioxide in such systems (Liu et al. 1999).
- Studies of interfacial mass transfer systems were carried out by (Kutepov et al. 2001). He also investigated evolution of the irregularities in diffusion-reaction region for chemical absorption of carbon dioxide by using optical methods. In this work MEA and KOH solution were employed.
- Investigation of kinetics and reactions for aqueous piperazine systems in absorption of carbon dioxide was carried out by (Bishnoi and Rochelle 2000). In this work they measured solubility and absorption rate of carbon dioxide into aqueous piperazine solutions. They extended their studies later to the quaternary system of piperazine-MDEA-water and carbon dioxide to study speciation of the solution, vapor-liquid equilibrium and carbon dioxide solubility in such systems (Bishnoi and Rochelle 2002a). They also reported that aqueous blend of piperazine and MDEA absorbs carbon dioxide faster than MEA or DEA blends with MDEA at similar concentrations (Bishnoi and Rochelle 2002b).

- Extension of equilibrium thermodynamic model for carbon dioxide-water-piperazine system was made by (Álvaro Pérez-Salado et al. 2003) to cover the quaternary system including the MDEA. Prediction of solubility data was compared with experimental measurements afterwards.
- Employing H-NMR spectroscopy method, speciation of aqueous solution of piperazine and carbon dioxide was quantified by (Ermatchkov et al. 2003). They also determined equilibrium constants for the formation of piperazine carbamate, piperazine dicarbamate and protonated piperazine carbamate, which are important constituents of the piperazine involved reactions.
- Speciation of various alkanolamines (BEA, MDEA and MEA) with different amount of dissolved carbon dioxide were measured performing NMR studies by (Jakobsen et al. 2005). This reference was specifically useful for current thesis to decide about initial concentration of the protonated MDEA inside the liquid.
- Derks (2006) conducted a comprehensive research as his PhD dissertation concerning aqueous blends of piperazine-MDEA. Amine diffusion, kinetics of absorption and solubility of carbon dioxide were determined for both blends of aqueous piperazine and aqueous piperazine activated MDEA. NMR studies were also performed for quaternary systems to provide more experimental data for speciation of such systems. Composition of the quaternary system for this master thesis simulation has been mainly based on experimental determinations provided by Derks in his PhD research.
- Kinetics of reaction between carbon dioxide and aqueous solution of piperazine was studied by (Samanta and Bandyopadhyay 2007). Moreover, concentration profile of different species in the solution was analytically calculated in a liquid film close to the gas-liquid interface. Results from this part of work were also very crucial for current master thesis, because this paper provides detail data about concentration of the solvents within the interface.
- Quantitative speciation of both tertiary ($CO_2 + MDEA + H_2O$) and quaternary ($CO_2 + MDEA + Piperazine + H_2O$) systems were determined using H and C NMR spectroscopy by (Bottinger et al. 2008). These measurements were very important for the current master thesis, considering this paper provides significant amount of speciation data.
- Kinetics and degradation rate of concentrated aqueous piperazine were studied by (Freeman et al. 2009). It was concluded that this kind of solvent can be used

preferably for absorption of carbon dioxide due to its fast kinetics and low rate of degradation.

❖ Computational studies:

- OPLS interaction parameters were used extensively from a broad range of computational data (1984-2004), provided by Prof. William L.Jorgensen research group at university of Yale.
- Computational chemistry method was used by (da Silva 2005) to provide predictive models for carbon dioxide absorption in aqueous amine systems. In his PhD thesis, he tried to model the solvent effects by means of quantum mechanical calculations and molecular simulations. Reaction mechanisms – including the carbamate formation – and equilibrium constants were studied in this PhD dissertation. For the current master thesis, it was very instructive to compare application of the computational details such as basis sets for different QM calculations with his work. Moreover, it was very promising to be able to compare the results for partial charge calculations with this reference.
- Removal of carbon dioxide from natural gas was studied by (van Loo et al. 2007), using simulation method for mixtures of MDEA with various primary or secondary activators, but not with piperazine. Optimal number of trays in the tray column in addition to the amount of activator was investigated by him.

# 6 Strategy for current research

As stated earlier, the main purpose of this thesis is to extend our knowledge about characterization of the gas-liquid interface in terms of the molecular distribution of the amine solution, in addition to understanding of the mechanisms which give rise to the absorption of carbon dioxide and unusual trapping of methane.

To serve the purpose, molecular simulation should be establish, so that it can replicate true behavior of the physical system in actual life. In this regard, correct initial set-up of the system will be necessary.

Two steps ahead of simulation part are determination of the system composition and modeling of the molecular components. Speciation of the solution should be specified accurate enough in such a way an acceptable approximation of that can be used as initial composition of the system. Required information for speciation of the system are available in literature; therefore a literature review will be done in order to approximate correct composition of the liquid phase. Once speciation of the system is well defined, procedure can be followed to the modeling part of the work.

Molecular modeling of the specified molecules or species for the solution will be the next stage of this work. This will need to decide about an appropriate force field from which interaction parameters will be employed. This step will be followed by a series of quantum mechanical calculations to investigate the important torsional angles and to calculate the partial atomic charges.

Once the models are ready, initial set-up of the simulation can be decided. Simulation box in MD can be divided into two gas and liquid phases. This is to form a gas-liquid interface. Gas phase will contain a simplified mixture of natural gas with methane and carbon dioxide. However, the natural gas will be assumed to be impurity free. On the other hand, liquid phase contains aqueous solution of PZ-MDEA blend. Subsequently, NVT constraint MD simulation will be performed in thermodynamic conditions close the ones in absorption units. Several reference systems with similar thermodynamic conditions will be run in parallel, in such a way comparative analyses at the end of simulation will be possible.

The final stage of current study will concern interpretation of the simulation results. Several in-house codes for Matlab and VMD[9] programs will be used to analyze the results.

[9] Visual Molecular Dynamics Ver.1.8.7 which is a "visualization program for animating and analyzing large biomolecular systems using 3-D graphics and built-in scripting". http://www.ks.uiuc.edu/Research/vmd/

# 7 Speciation of the system

System composition is an important issue for any studies involving simulation of the alkanolamine systems. In order to replicate true behavior of the system in actual life, speciation of the system needs to be determined accurately. On the other hand, modeling of the molecular entities in first place requires information about composition of the system because major molecules and species which have the higher concentrations in the system have to be modeled.

This includes both liquid and gas phases. For the gas phase, natural gas was simplified to a binary mixture of methane and carbon dioxide so that concentration of impurities was disregarded. However, for the liquid phase or - in other words - the amine solution, speciation of system was difficult to specify. As mentioned in Section 3.4.1, speciation of piperazine activated MDEA solution is a challenging issue, which involves a certain level of complexity, because the complete mechanism and reaction intermediates of such a system are not identified perfectly. In this work, data taken from literature which are based on experimental measurements have been used to decide about speciation of the solution. Due to the lack of enough experimental data for a broad range of loading value, temperature and pressure, it was very problematic to find exact speciation of the system in temperature, pressure and molarities of interest. Considering this, approximation of liquid composition around the available experimental data, which are close to the condition of interest, had to be made.

Speciation of the liquid phase in this thesis has been determined mainly based on reactions and experimental data given by Derks (2006) in his PhD research (Section 3.4.1).

Derks (2006) has been determined concentration of piperazine species in the liquid phase for 4.0 $kmol.m^{-3}$aqueous MDEA activated by 1.0 $kmol.m^{-3}$ piperazine at 298 K for different loading values performing NMR. Loading value 0.07 was chosen for the system of our interest considering availability of other experimental data (concentration of other species rather than piperazine species) in the literature. Concentration of piperazine species corresponding to loading value of 0.07 are given in Table 7-1.

**Table 7-1: Liquid phase speciation of a 4.0 M MDEA and 1.0 M PZ at 298.15 K as determined by NMR (Derks 2006)**

| $CO^2$ loading $[mol.mol^{-1}]$ | PZ:MDEA | $C_{PZ} + C_{PZH^+}$ $[kmol.m^{-3}]$ | $C_{PZCOO^-} + C_{H^+PZCOO^-}$ $[kmol.m^{-3}]$ | $C_{PZ(COO^-)_2}$ $[kmol.m^{-3}]$ |
|---|---|---|---|---|
| 0.07 | 0.24 | 0.67 | 0.30 | 0.029 |

Considering Equations (3-22) to (3-32), composition of the system will be fully identified, once concentrations of the all eleven species are known. However, many of these species are not present in considerable mole fractions inside the solution, so that they do not contribute significantly to the molecular interactions inside the solution. Consequently, only species possessing higher concentrations are needed to be considered.

At this stage concentration of following groups of molecules and species can be calculated according following procedure:

Having concentration of 3 groups of piperazine species given in Table 7-1, in addition to the density of amine solution - 4.0 $kmol.m^{-3}$ MDEA plus 1.0 $kmol.m^{-3}$ piperazine - at 298.15 K, which is determined by experiment ($\rho$ = 1044.61 $kg.m^{-3}$ (Derks 2006)), it is possible to estimate mole fractions of different species inside the solution. Estimated mole fractions of different species are given in Table 7-2.

**Table 7-2: Mole fraction of different groups of species inside the bulk liquid**

| Specie | Mole fraction |
|---|---|
| $C_{PZ} + C_{PZH^+}$ | 0.0224 |
| $C_{PZCOO^-} + C_{H^+PZCOO^-}$ | 0.011 |
| $C_{PZ(COO^-)_2}$ | $9.6823 \times 10^{-4}$ |
| $C_{MDEA} + C_{MDEAH^+}$ | 0.13897 |
| $C_{H_2O} + C_{H^+} + C_{OH^-}$ | 0.8257 |
| $C_{CO_2} + C_{HCO_3^-} + C_{CO_3^{-2}}$ | $1.9765 \times 10^{-3}$ |

In order to decide about concentration of every individual species given in table above, some complementary data were needed. It was always very difficult to find experimental data for

systems exactly similar to the system of our interest in the literature. Therefore results from approximately similar systems were used to estimate concentration of each species in Table 7-2. By similar, initial concentrations of the amine solvent (MDEA - PZ) in addition to thermodynamic conditions are meant.

According to (Bishnoi and Rochelle 2000) at low solution loading of aqueous piperazine, piperazine carbamate ($PZCOO^-$) and protonated piperazine ($PZH^+$) are dominant products. From this we know the concentration of zwitterion (protonated piperazine carbamate $H^+PZCOO^-$) and piperazine bicarbamate ($PZ(COO^-)_2$) are most likely negligible. However, it does not say anything about concentration of molecular piperazine ($PZ$). Derks (2006) showed that reactions involved in production of piperazine bicarbamate (reaction (3-12)) and protonated piperazine carbamate (reaction (3-13) can be neglected. This is why concentrations of these two species did not appear among the equations (3-22) and (3-32). Similarly, concentration of piperazine bicarbamate was observed to be negligible by (Bottinger et al. 2008) performing NMR investigations.

NMR studies by (Jakobsen et al. 2005) showed concentration of protonated MDEA ($MDEAH^+$) is much smaller than molecular MDEA. Therefore the former can be neglected as well.

Analytical calculation of concentration profile for the liquid film close to interface was determined by (Samanta and Bandyopadhyay 2007). This data signify approximately equal concentrations of molecular piperazine and protonated piperazine. Moreover, It was shown that concentration of dissolved carbon dioxide, bicarbonate ion ($HCO_3^-$) and hydronium ion ($H_3O^+$) are not significant.

Ultimately, based on above mentioned experimental observations, in addition to the composition of liquid phase given in Table 7-2, following speciation of the amine solution was determined. In comparison with Table 7-2 some of the species are neglected or included in the mole fraction of water. Final mole fractions are given in table Table 7-3.

**Table 7-3: Final calculated mole fractions of different species for the system of interest**

| Specie | Mole fraction |
|---|---|
| $C_{PZ}$ | 0.011 |
| $C_{PZH^+}$ | 0.011 |
| $C_{PZCOO^-}$ | 0.011 |
| $C_{MDEA}$ | 0.13897 |
| $C_{H_2O} + C_{H^+} + C_{OH^-}$ | 0.82767 |

# 8 Modeling of the molecules

Once speciation of the system is determined, modeling of the decided molecules / species can be started. As it was stated completely in section 4.2.1, procedure for modeling of the molecules involves three main steps. First of all interaction parameters have to be decided through a suitable force field, second optimization of the molecular geometry and at last calculation of partial charges.

For this research seven different molecules or species had to be modeled. These were piperazine, MDEA, water, methane and carbon dioxide molecules in addition to protonated piperazine and piperazine carbamate species. Among these, carbon dioxide, water and one-site methane molecules had already been modeled but for rest of the molecules / species new models were constructed for the first time in this work. Moreover, in order to resemble behavior of the methane in more precise manner, a five-site model was chosen. Interaction parameters for this five-site model were taken from literature.

## 8.1 Interaction parameters and OPLS force field

Current research utilizes all-atom version of OPLS (optimized potentials for liquid simulations) force field. The main reason for choosing this force field for the present research was that OPLS is optimized specifically for simulations in liquid state. Considering that focus of current work belongs to the interface and liquid bulk, OPLS would be an appropriate choice for such a simulation. Moreover we know that OPLS is a well known, reliable and validated force field which is being used successfully in many researches involving application of molecular simulation.

Complete set of OPLS all-atom force field has already been received from Prof. William L. Jorgensen – the main author of the force field – by the research group at the department of process technology. References to OPLS all-atom are given below:

(Jorgensen et al. 1996; Wolfgang et al. 1997; Jorgensen and McDonald 1998; McDonald and Jorgensen 1998; Rizzo and Jorgensen 1999; Melissa et al. 2001; Watkins and Jorgensen 2001; Jorgensen et al. 2004; Jensen and Jorgensen 2006)

Interaction parameters including Lennard-Jones 12-6 parameters, bond stretching parameters, angle bending parameters and dihedral angle Fourier coefficients (except for two torsional angles in MDEA and PZCOO) were taken from OPLS-AA force field while the partial charges were calculated independently using quantum mechanical calculations. These parameters have been given in Table 8-1 to Table 8-4 for MDEA molecule.

**Table 8-1: OPLS L-J 12-6 interaction parameters for MDEA molecule**

| Atom label | Atom type | Sigma [Å] | Epsilon [kJ/mol] |
|---|---|---|---|
| NT | N tertiary amines | 3.30 | 0.71128 |
| CT | CH3(N) tertiary aliphatic amines | 3.50 | 0.276144 |
| CT | CH2(N) tertiary aliphatic amines | 3.50 | 0.276144 |
| CT | CH2 all-atom C: alkanes | 3.50 | 0.276144 |
| HC | H(C) for carbons directly bonded to N in amines, diamine | 2.50 | 0.06276 |
| HC | H all-atom H: alkanes | 2.50 | 0.12552 |
| HO | H(O) alcohols | 0.00 | 0.0000 |
| OH | O alcohols | 3.07 | 0.71128 |

**Table 8-2: OPLS bond stretching parameters for MDEA molecule**

| Bond | Equilibrium bond length [Å] | Force constant [$\frac{kJ}{mol.Å^2}$] |
|---|---|---|
| CT-NT | 1.448 | 1598.288 |
| CT-CT | 1.529 | 1121.312 |
| CT-HC | 1.090 | 1422.560 |
| CT-OH | 1.410 | 1338.880 |
| HO-OH | 0.945 | 2313.752 |

**Table 8-3: OPLS angle bending parameters for MDEA molecule**

| Angle | Equilibrium angle [degree] | Force constant $[\frac{kJ}{mol.rad^2}]$ |
|---|---|---|
| HC-CT-OH | 109.50 | 146.4400 |
| CT-OH-HO | 108.50 | 230.1200 |
| CT-CT-HC | 110.70 | 156.9000 |
| HC-CT-NT | 109.50 | 146.4400 |
| CT-NT-CT | 107.20 | 216.7312 |
| HC-CT-HC | 107.80 | 138.0720 |
| CT-CT-NT | 109.47 | 235.1408 |
| CT-CT-OH | 109.50 | 209.2000 |

**Table 8-4: OPLS torsional parameters for MDEA molecule**

| Dihedral angle | V1 $[\frac{kJ}{mol}]$ | V2 $[\frac{kJ}{mol}]$ | V3 $[\frac{kJ}{mol}]$ | V4 $[\frac{kJ}{mol}]$ |
|---|---|---|---|---|
| NT-CT-CT-HC | -4.24 | -2.97 | 1.98 | 0.00 |
| CT-NT-CT-HC | 0.00 | 0.00 | 0.00 | 0.00 |
| CT-NT-CT-CT | 1.74 | -0.54 | 2.91 | 0.00 |
| HC-CT-NT-CT | 0.00 | 0.00 | 0.00 | 0.00 |
| CT-CT-OH-HO | -1.49 | -0.73 | 2.06 | 0.00 |
| HC-CT-CT-HC | 0.00 | 0.00 | 1.26 | 0.00 |
| HC-CT-CT-OH | 0.00 | 0.00 | 1.96 | 0.00 |
| CT-CT-NT-CT | 1.74 | -0.54 | 2.91 | 0.00 |
| HC-CT-OH-HO | 0.00 | 0.00 | 1.47 | 0.00 |

Parameters for torsional angle NT-CT-CT-OH were not given in Table 8-4. Due to significance of this angle among other dihedrals in MDEA, associated parameters for that were calculated specifically by performing quantum mechanical calculations. Details of this are given in Section 8.3.2.

Similarly interaction parameters for piperazine species (molecular piperazine, protonated piperazine and piperazine carbamate) taken from OPLS-AA force field are given in Table 8-5 to Table 8-8.

**Table 8-5: OPLS L-J 12-6 interaction parameters for PZ, PZH and PZCOO**

| Atom label | Atom type | Sigma [Å] | Epsilon [kJ/mol] | Remark |
|---|---|---|---|---|
| NT | N secondary amines | 3.30 | 0.71128 | PZ, PZH, PZCOO |
| CT | CH2(N) secondary aliphatic amines | 3.50 | 0.276144 | PZ, PZH, PZCOO |
| H | H(N) secondary amines | 0.00 | 0.00000 | PZ, PZH, PZCOO |
| HC | H(C) for carbons directly bonded to N in amines, diamine | 2.50 | 0.06276 | PZ, PZH, PZCOO |
| NT* | N tertiary amines | 3.30 | 0.71128 | PZCOO |
| C | C in COO- carboxylate | 3.75 | 0.43932 | PZCOO |
| O2 | O: O in COO- carboxylate | 2.96 | 0.87864 | PZCOO |

**Table 8-6: OPLS bond stretching parameters for PZ, PZH and PZCOO**

| Bond | Equilibrium bond length [Å] | Force constant $[\frac{kJ}{mol.Å^2}]$ | Remark |
|---|---|---|---|
| CT-NT | 1.448 | 1598.288 | PZ, PZH, PZCOO |
| CT-CT | 1.529 | 1121.312 | PZ, PZH, PZCOO |
| CT-HC | 1.090 | 1422.560 | PZ, PZH, PZCOO |
| H-NT | 1.010 | 1815.856 | PZ, PZH, PZCOO |
| C-NT* | 1.522 | 1326.328 | PZCOO |
| C-O2 | 1.250 | 2744.704 | PZCOO |

**Table 8-7: OPLS angle bending parameters for PZ, PZH and PZCOO**

| Angle | Equilibrium angle [degree] | Force constant $[\frac{kJ}{mol.rad^2}]$ | Remark |
|---|---|---|---|
| CT-CT-NT | 109.47 | 235.1408 | PZ, PZH, PZCOO |
| CT-CT-HC | 110.70 | 156.9000 | PZ, PZH, PZCOO |
| CT-NT-H | 109.50 | 146.4400 | PZ, PZH, PZCOO |
| CT-NT-CT | 107.20 | 216.7312 | PZ, PZH, PZCOO |
| HC-CT-NT | 109.50 | 146.4400 | PZ, PZH, PZCOO |
| HC-CT-HC | 107.80 | 138.0720 | PZ, PZH, PZCOO |
| C-NT*-CT | 111.10 | 263.5920 | PZCOO |
| NT*-C-O | 120.40 | 334.7200 | PZCOO |
| O2-C-O2 | 126.00 | 334.7200 | PZCOO |
| H-NT-H | 106.40 | 182.4224 | PZH |

Since there was no data available for angle equal NT-C-O2 in OPLS-AA, equivalent parameters for NT-C-O were used in instead of that (Look at Table 8-7).

**Table 8-8: OPLS torsional parameters for PZ, PZH and PZCOO**

| Dihedral angle | V1 $[\frac{kJ}{mol}]$ | V2 $[\frac{kJ}{mol}]$ | V3 $[\frac{kJ}{mol}]$ | V4 $[\frac{kJ}{mol}]$ | Remark |
|---|---|---|---|---|---|
| CT-CT-NT-CT | 1.74 | -0.54 | 2.91 | 0.00 | PZ, PZH, PZCOO |
| CT-CT-NT-H | -0.79 | -1.74 | 1.75 | 0.00 | PZ, PZH, PZCOO |
| CT-NT-CT-CT | 1.74 | -0.54 | 2.91 | 0.00 | PZ, PZH, PZCOO |
| CT-NT-CT-HC | 0.00 | 0.00 | 0.00 | 0.00 | PZ, PZH, PZCOO |
| HC-CT-CT-HC | 0.00 | 0.00 | 1.26 | 0.00 | PZ, PZH, PZCOO |
| HC-CT-CT-NT | -4.24 | -2.97 | 1.98 | 0.00 | PZ, PZH, PZCOO |
| HC-CT-NT-H | 0.00 | 0.00 | 1.67 | 0.00 | PZ, PZH, PZCOO |
| NT-CT-CT-NT | 46.17 | -4.05 | 1.13 | 0.00 | PZ, PZH, PZCOO |
| CT-CT-NT*-C | 0.00 | 1.93 | 0.00 | 0.00 | PZCOO |
| HC-CT-NT*-C | 0.00 | 0.00 | -0.58 | 0.00 | PZCOO |

Parameters for torsional angle CT-NT*-C-O2 were not given in Table 8-8. Due to significance of this angle among other dihedrals in PZCOO, associated parameters were calculated

specifically for that by performing quantum mechanical calculations. Details of this are given in Section 8.3.1.

## 8.2 Geometry optimization

Modeling of the molecules and species were carried out using *Schrödinger package*[10]. *Maestro Ver.9.0.211* was used as the unified graphical interface of this package for drawing the molecules. Later, generated geometries of each molecule / specie through Maestro GUI were optimized by doing quantum mechanical calculations to determine the equilibrium structure of them. This was necessary because in its following steps, quantum mechanical calculations for partial charges and dihedral angles were to be performed. Considering in quantum mechanics the minima are investigated, the initial configuration of the system had to be already in a minimum point on the PES. That is why equilibrium structures of the molecules had to be computed initially. Geometry optimization was performed using *Jaguar Ver.7.6* software which is Schrödinger's ab initio calculation module. Once geometry of the molecules are optimized, the final structure is dumped into the *Brookhaven Protein Databank* (PDB) file format. These files later are used in Maestro to generate input files for Jaguar which does the quantum mechanical calculations. Table 8-9 was used to demonstrate the Jaguar set-up for optimization of the energy.

**Table 8-9: Geometry optimization set-up in Jaguar**

| Molecule | Basis set | Theory | Functional |
|---|---|---|---|
| MDEA | 6-31G** | DFT | Hybrid B3LYP |
| PZ | 6-31G** | DFT | Hybrid B3LYP |
| PZH | 6-31G** | DFT | Hybrid B3LYP |
| PZCOO | 6-31++G** | DFT | Hybrid B3LYP |

Molecular structures of the molecules and species which have been drawn by Maestro and optimized in Jaguar were illustrated Figure 8-1 to Figure 8-4.

[10] Schrödinger is a scientific software package in computational drug design for pharmaceutical and biotechnology research. Access at: http://www.schrodinger.com/

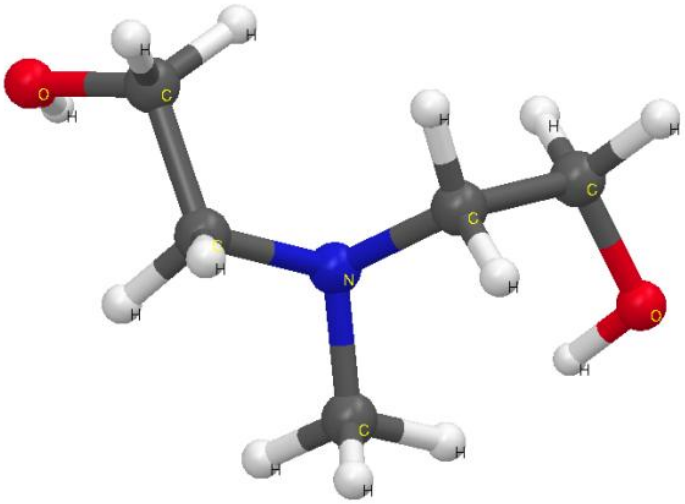

**Figure 8-1: Molecular structure of MDEA molecule**

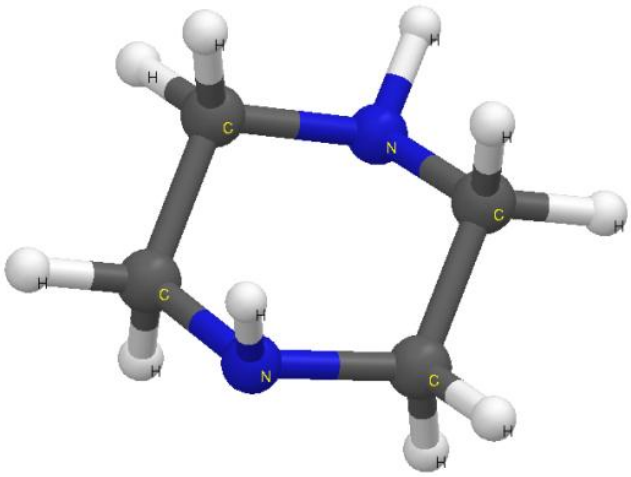

**Figure 8-2: Molecular structure of piperazine molecule**

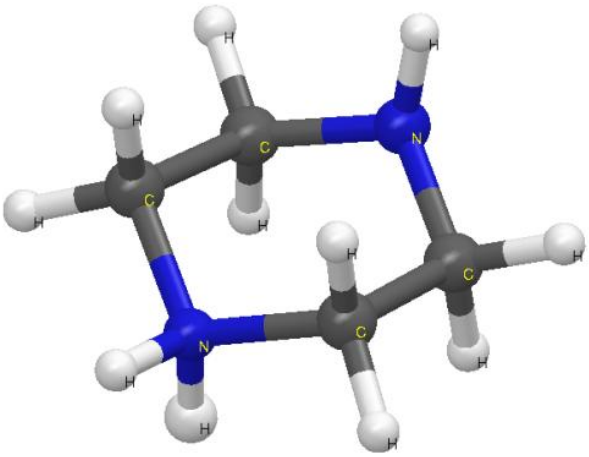

**Figure 8-3: Molecular structure of protonated piperazine**

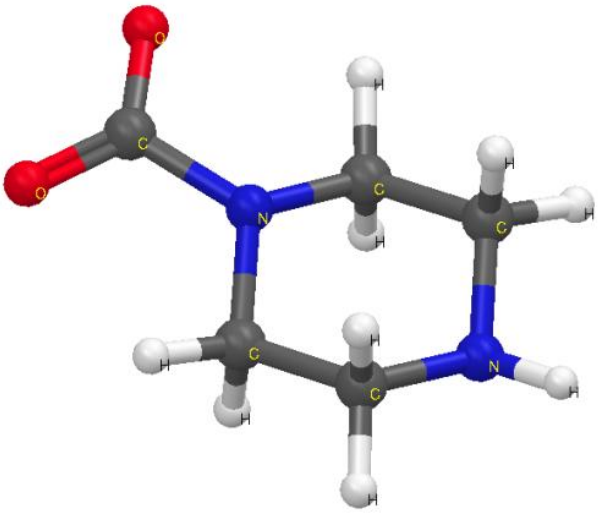

**Figure 8-4: Molecular structure of piperazine carbamate**

## 8.3 Parameterization of Torsional energy

As it was mentioned in section 8.1, for two dihedral angels – one in MDEA and another one in piperazine carbamate – OPLS parameters have not been used. Due to the importance of these torsional angles I decided to build my own force field parameters for them by doing quantum mechanical calculations to obtain more accurate results.

In this regard, quantum mechanical calculations were carried out by performing *rigid coordinate scan* using Schrödinger's Jaguar application. Simulations were performed on

*Fimm* Linux clusters at Parallab, BCCS[11]. In rigid coordinate scan method, Jaguar performs a series of calculations to compute energy of the molecule with the varying torsional angle while, it keeps the other coordinates fixed in the molecule. In other words, the torsional energies are calculated when the dihedral angle of interest varies from zero to 359°. Having the torsional energies for one complete cycle, it is possible to show their variation as a function of angle. Using *least squares method* mathematical definition of this function can be determined. Parameters of the final form of this fitted function are used as the force field parameters for that specific angle of interest. This procedure was carried out for C-N-C-O and N-C-C-O dihedral angles in piperazine carbamate and MDEA respectively.

### 8.3.1 C-N-C-O/C-N-C=O dihedral angles in piperazine carbamate

There are two C-N-C-O and C-N-C=O important dihedral angles in piperazine carbamate as we can see in **Figure 8-4**. Both of them have been evaluated by performing quantum mechanical calculations in Jaguar using rigid coordinate scan method. Simulation set-up mentioned in Table 8-10 was applied at this stage in Jaguar.

**Table 8-10: Rigid coordinate scan set-up in Jaguar for two C-N-C-O dihedral angles in PZCOO**

| Molecule | Basis set | Theory | Functional |
|---|---|---|---|
| PZCOO | 6-31+G** | DFT | Hybrid B3LYP |

Computed torsional energies from quantum mechanics then was compared with potentials obtained from Equation (4-27) and OPLS parameters for this specific angle. This comparison has been demonstrated in figure Figure 8-5 . The fitted functions also have been added to the same graph to facilitate simultaneous comparison among them. As this graph demonstrates a perfect fitting was achieved.

[11] The Bergen Center for Computational Science (BCCS), which is a department of Uni Research affiliated with University of Bergen (UiB).

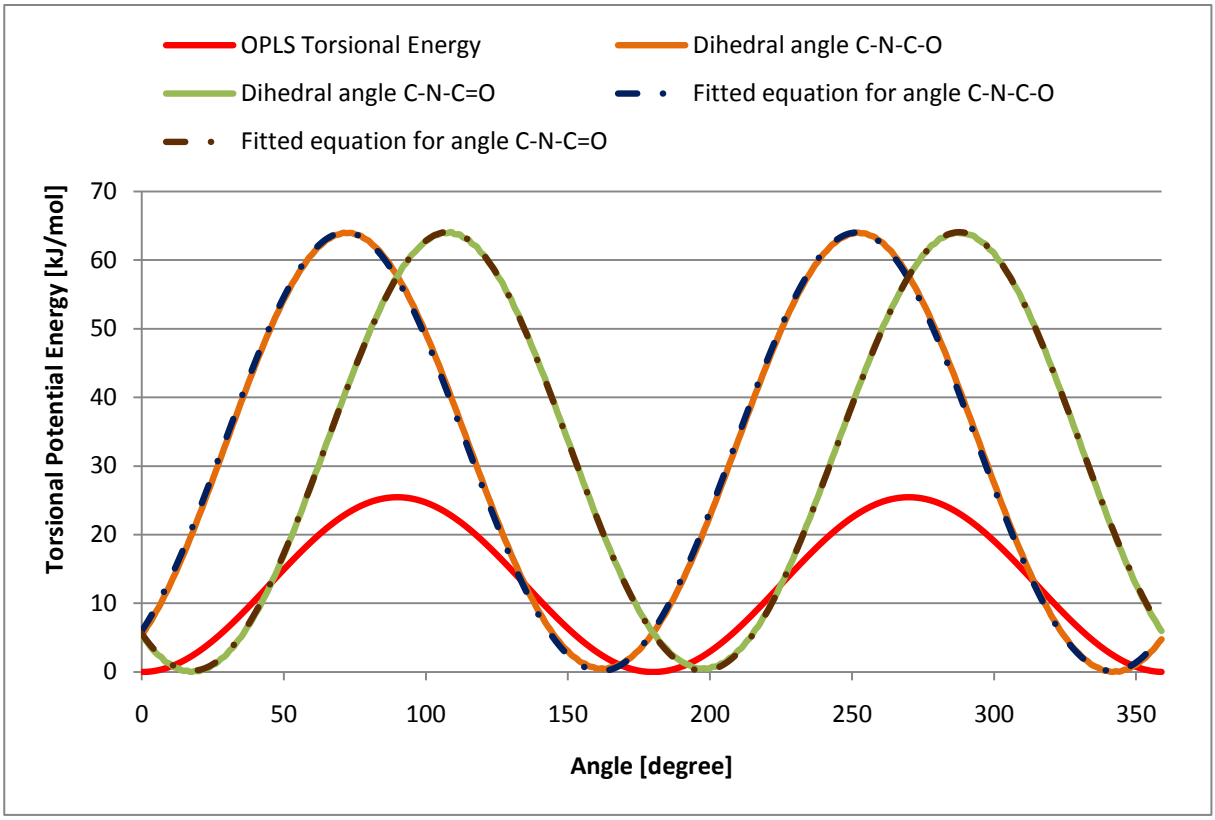


**Figure 8-5: Comparison of torsional energy from QM calculation with the one from OPLS**

From Figure 8-5 it is clear that OPLS torsional energy cannot replicate true behavior of C-N-C-O or C-N-C=O dihedrals. It simply fails to resemble the energy at maxima and shows a noticeable difference. Clearly speaking the amplitude (difference between minimum and maximum) in OPLS is about 25 kJ/mol while, this value for each of computed torsional energies are approximately 64 kJ/mol which are significantly different. From a molecular structure point of view, this means, that OPLS does not predict very high potential barriers at about 90° or 270° while, according QM calculations there are two high peaks at around 71° and 252° for C-N-C-O dihedral angle and two peaks with same height at around 106° and 287° for C-N-C=O dihedral angle which both of them are resembling a real potential barrier after the minima. Actually if the dihedral angle is located between two maxima, it will be very energy consuming for the molecular structure to be able to overcome the barrier and pass the maxima but OPLS completely underestimates the potential barrier. Consequently the fitted function obtained based on QM calculations in this section was used as the true description of C-N-C-O/C-N-C=O torsional energy for the MD simulation. Equation (8-1 is mathematical illustration of this function and Table 8-11 describes the fitted parameters of that. The same

function has been already used in Bjørnar Jensen's master thesis in the research group and he had already implemented this function into the MD code for the molecular dynamics simulation. Therefore, at this stage I did not have to implement the function again. Credit for application of this function for the first time and its implementation into the MD code goes back to his work (Jensen 2009).

$$U_{tors.} = V_1(1 + \cos(2\varphi + f_1)) + V_2(1 - \cos(2\varphi + f_2)) + V_3(1 + \cos(4\varphi + f_3)) \quad \textbf{(8-1)}$$

**Table 8-11: Fitted parameters for Equation (8-1)**

| Fitted parameters | $V_1$ [kJ/mol] | $f_1$ [degree] | $V_2$ [kJ/mol] | $f_2$ [degree] | $V_3$ [kJ/mol] | $f_3$ [degree] |
|---|---|---|---|---|---|---|
| C-N-C-O | -0.666427 | 34.5829 | 31.2892 | 35.4451 | 0.728444 | 70.6008 |
| C-N-C=O | 0.136553 | 43.9283 | 31.9823 | -35.1870 | -0.732692 | 108.0740 |

### 8.3.2 N-C-C-O dihedral angle in MDEA

The same procedure was taken performing quantum mechanical calculations by doing rigid coordinate scan in Jaguar for N-C-C-O dihedral angle in MDEA molecule. There are two identical angles of this dihedral in MDEA. Simulation set-up for Jaguar is mentioned in Table 8-12.

**Table 8-12: Rigid coordinate scan set-up in Jaguar for two N-C-C-O dihedral angles in MDEA**

| Molecule | Basis set | Theory | Functional |
|---|---|---|---|
| MDEA | 6-31+G** | DFT | Hybrid B3LYP |

In almost the same way as piperazine carbamate, torsional energies were computed initially and then by using least squares method, best fit for the computed torsional potential energy was obtained. Ultimately, the fitted function was implemented into the MD code for further applications. Mathematical description of the fitted function, in addition to the fitted parameters is given in Equation (8-2) and Table 8-13 respectively.

$$U_{tors.} = \frac{V_1(1+\cos(\varphi+f_1))}{2} + \frac{V_2(1-\cos(2\varphi+f_2))}{2} + \frac{V_3(1+\cos(3\varphi+f_3))}{2} + \frac{V_4(1-\cos(0.5\varphi+f_4))}{2} + V_5 \quad (8\text{-}2)$$

**Table 8-13: Fitted parameters for Equation (8-2)**

| Angle | $V_1$ [kJ/mol] | $f_1$ [degree] | $V_2$ [kJ/mol] | $f_2$ [degree] | $V_3$ [kJ/mol] | $f_3$ [degree] | $V_4$ [kJ/mol] | $f_4$ [degree] | $V_5$ [kJ/mol] |
|---|---|---|---|---|---|---|---|---|---|
| N-C-C-O | 14.4177 | -34.9575 | -12.1999 | 0.841773 | 14.7394 | 15.9052 | 17.048 | -64.6709 | -0.8 |

Moreover, comparison between QM result, fitted function and the OPLS prediction is illustrated in Figure 8-6.

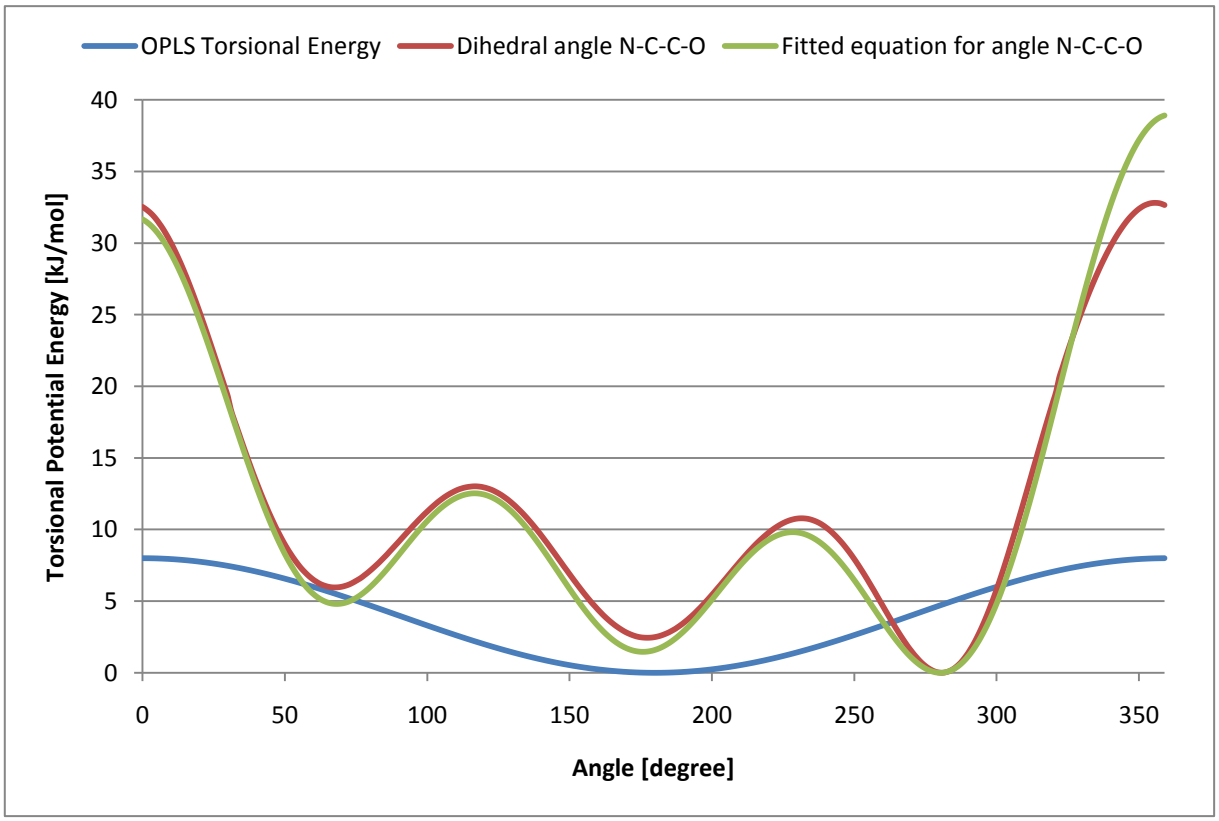


**Figure 8-6: Comparison of torsional energy from QM calculation with the one from OPLS**

Again and as it is obvious here, OPLS underestimates the torsional energy of the dihedral and cannot replicate the true form of the minima and maxima in the energy profile. Two local

minima are observed at around 69° and 178° while the global minima is located at 281°. Moreover, a high potential barrier exist at 356° exactly after global minima which shows 32.8 kJ/mol difference.

## 8.4 Calculation of partial atomic charges

Next and final step in modeling of the molecules / species was calculation of partial atomic charges. To serve the purpose of this stage, ab initio quantum mechanical calculations were performed using Schrödinger's Jaguar application. Mulliken Population Analysis (MPA), Löwdin Population Analysis (LPA) and Charge Model class 4 (CM4) schemes were employed for calculation of partial atomic charges. Results from these calculations were compared with each other at the end. As it was mentioned in Section 4.1.5, MPA is not able to calculate reliable results for partial atomic charges and LPA is not stable with very large basis sets such as diffuse functions. On the other hand, CM4 scheme provides accurate charge distribution and is compatible with continuum solvation model SM8. Since in this research, behavior of molecules inside the solution (liquid phase) is under observation, effect of surrounding medium is not negligible. Considering water as the dominant solvent in aqueous alkanolamine systems and polarity of its molecule, partial atomic charges have to be calculated taking into account effect of this medium. Referring Section 4.1.4, this was already emphasized that SM8 solvation model is an appropriate continuum model for the system of interest in this work. SM8 can be used - at the same time – for both charged and uncharged solutes composed of hydrogen, carbon, nitrogen and oxygen in any solvent or liquid medium. In this regard, it should be reminded that aqueous blends of piperazine and MDEA also contain both charged and uncharged species.

According what mentioned above, the following simulation set-up (Table 8-14) for Jaguar application was used to perform single point energy (SPE) calculation.

**Table 8-14: Single point calculation set-up in Jaguar**

| Molecule | Basis set | Theory | Functional |
|---|---|---|---|
| MDEA | 6-31G** | DFT | Hybrid B3LYP |
| PZ | 6-31G** | DFT | Hybrid B3LYP |
| PZH | 6-31G** | DFT | Hybrid B3LYP |
| PZCOO | 6-31G** | DFT | Hybrid B3LYP |

Diffuse basis set 6-31+G** was tried for piperazine carbamate (PZCOO) because this specie possesses formal negative charge on one of the oxygen atoms. Surprisingly and despite the Jaguar manual for version 7.6, the CM4 charge model was not available for diffuse basis sets and SM8 model started to use Löwdin charges instead of CM4. Based on this limitation the basis set 6-31G** was chosen for PZCOO eventually.

Table 8-15 to Table 8-18 presents computed partial atomic charges for each molecule and species that have been modeled in this work.

**Table 8-15: Partial atomic charges calculated for MDEA using 3 different schemes**

| Atom | MPA | LPA | CM4 | Atom | MPA | LPA | CM4 |
|---|---|---|---|---|---|---|---|
| N1 | -0.46013 | -0.19702 | -0.46258 | H12 | 0.09469 | 0.09825 | 0.05337 |
| C2 | -0.16432 | -0.22775 | -0.00278 | H13 | 0.12202 | 0.11344 | 0.07352 |
| H3 | 0.11847 | 0.10917 | 0.06274 | O14 | -0.57709 | -0.35763 | -0.48039 |
| H4 | 0.11185 | 0.10673 | 0.06005 | H15 | 0.32501 | 0.22577 | 0.31673 |
| H5 | 0.08830 | 0.07969 | 0.03748 | C16 | -0.04059 | -0.11617 | 0.06112 |
| C6 | -0.05649 | -0.13928 | 0.03249 | C17 | 0.04654 | -0.04938 | 0.06983 |
| H7 | 0.06342 | 0.07176 | 0.02954 | H18 | 0.10118 | 0.09037 | 0.04852 |
| H8 | 0.11454 | 0.11133 | 0.06565 | H19 | 0.10822 | 0.09691 | 0.05437 |
| H9 | 0.07888 | 0.07918 | 0.03789 | O20 | -0.56651 | -0.36062 | -0.49044 |
| C10 | 0.06906 | -0.05336 | 0.06754 | H21 | 0.33075 | 0.23240 | 0.32242 |
| H11 | 0.09220 | 0.08620 | 0.04292 | | | | |

**Table 8-16: Partial atomic charges calculated for piperazine using 3 different schemes**

| Atom | MPA | LPA | CM4 | Atom | MPA | LPA | CM4 |
|---|---|---|---|---|---|---|---|
| C1 | -0.04494 | -0.13372 | 0.04385 | H9 | 0.11413 | 0.10965 | 0.06458 |
| C2 | -0.05667 | -0.12607 | 0.05419 | H10 | 0.08922 | 0.09267 | 0.04785 |
| C3 | -0.05669 | -0.12752 | 0.05274 | H11 | 0.07603 | 0.07231 | 0.03022 |
| C4 | -0.04494 | -0.13399 | 0.04359 | H12 | 0.10708 | 0.10742 | 0.06275 |
| H5 | 0.07591 | 0.07175 | 0.02965 | N13 | -0.53651 | -0.29572 | -0.58745 |
| H6 | 0.10736 | 0.10799 | 0.06333 | H14 | 0.25172 | 0.17477 | 0.28535 |
| H7 | 0.08947 | 0.09316 | 0.04834 | N15 | -0.52638 | -0.28888 | -0.58130 |
| H8 | 0.11408 | 0.10885 | 0.06377 | H16 | 0.24114 | 0.16733 | 0.27854 |

**Table 8-17: Partial atomic charges calculated for piperazine carbamate using 3 different schemes**

| Atom | MPA | LPA | CM4 | Atom | MPA | LPA | CM4 |
|---|---|---|---|---|---|---|---|
| C1 | -0.03902 | -0.12251 | 0.05474 | H10 | 0.05102 | 0.06642 | 0.02490 |
| C2 | 0.01618 | -0.12053 | 0.05709 | H11 | 0.07175 | 0.07387 | 0.03180 |
| C3 | 0.01601 | -0.12015 | 0.05749 | H12 | 0.11930 | 0.10726 | 0.06271 |
| C4 | -0.03896 | -0.12323 | 0.05403 | N13 | -0.51931 | -0.29944 | -0.58704 |
| H5 | 0.07161 | 0.07326 | 0.03119 | H14 | 0.25134 | 0.17263 | 0.28296 |
| H6 | 0.11933 | 0.10722 | 0.06266 | N15 | -0.55732 | -0.21256 | -0.47952 |
| H7 | 0.05107 | 0.06700 | 0.02548 | C16 | 0.58155 | 0.12315 | 0.41829 |
| H8 | 0.08355 | 0.10667 | 0.06889 | O17 | -0.68076 | -0.50273 | -0.61708 |
| H9 | 0.08350 | 0.10665 | 0.06883 | O18 | -0.68083 | -0.50299 | -0.61741 |

**Table 8-18: Partial atomic charges calculated for protonated piperazine using 3 different schemes**

| Atom | MPA | LPA | CM4 | Atom | MPA | LPA | CM4 |
|---|---|---|---|---|---|---|---|
| C1 | -0.07148 | -0.10275 | 0.06204 | H10 | 0.12610 | 0.10751 | 0.06198 |
| C2 | -0.08444 | -0.11862 | 0.06166 | H11 | 0.17468 | 0.13158 | 0.08630 |
| C3 | -0.08439 | -0.11906 | 0.06123 | H12 | 0.19144 | 0.14515 | 0.10147 |
| C4 | -0.07163 | -0.10221 | 0.06258 | N13 | -0.43636 | 0.00650 | -0.34428 |
| H5 | 0.17468 | 0.13172 | 0.08644 | N14 | -0.53021 | -0.27374 | -0.56959 |
| H6 | 0.19143 | 0.14527 | 0.10158 | H15 | 0.26313 | 0.18313 | 0.29360 |
| H7 | 0.12638 | 0.10830 | 0.06278 | H16 | 0.38804 | 0.25416 | 0.35686 |
| H8 | 0.13460 | 0.12847 | 0.08299 | H17 | 0.37350 | 0.24604 | 0.34926 |
| H9 | 0.13454 | 0.12856 | 0.08309 | | | | |

CM4 partial atomic charges for molecular piperazine and protonated piperazine specie were compared with results obtained by (da Silva 2005) which has reproduced the partial charges using CM2 scheme, basis set 6-31G* and salvation model SM 5.42R (which R denotes using rigid geometries during parameterization). Table 8-19 and Table 8-20 demonstrate this comparison.

**Table 8-19: Comparison of partial atomic charges for molecular piperazine**

| Current thesis | | | Da Silva (2005) | | |
|---|---|---|---|---|---|
| Atom label | MPA | CM4 | Atom label | MPA | CM2 |
| N13 | -0.536510 | -0.587450 | N1 | -0.94 | -0.53 |
| H14 | 0.251720 | 0.285350 | One associated H | 0.43 | 0.27 |
| C1, C4 | -0.044940 | 0.043720 | C1, C2 | 0.23 | -0.19 |
| H5, H6, H11, H12 | 0.091595 | 0.092975 | Four associated H | 0.00 | 0.08 |
| N15 | -0.526380 | -0.581300 | N2 | -1.07 | -0.54 |
| H16 | 0.241140 | 0.278540 | One associated H | 0.47 | 0.28 |
| C2, C3 | -0.056680 | 0.053465 | C3, C4 | 0.35 | -0.20 |
| H7, H8, H9, H10 | 0.101725 | 0.112270 | Four associated H | -0.02 | 0.08 |

**Table 8-20: Comparison of partial atomic charges for protonated piperazine**

| Current thesis | | | Da Silva (2005) | | |
|---|---|---|---|---|---|
| Atom label | MPA | CM4 | Atom label | MPA | CM2 |
| N13 (Protonated) | -0.436360 | -0.344280 | N1 (Protonated) | -0.32 | -0.32 |
| H16, H17 | 0.380770 | 0.353060 | Two associated H | 0.39 | 0.35 |
| C1, C4 | -0.071560 | 0.062310 | C1, C2 | -0.14 | -0.16 |
| H5, H6, H11, H12 | 0.183058 | 0.093948 | Four associated H | 0.14 | 0.16 |
| N14 | -0.530210 | -0.569590 | N2 | -1.09 | -0.53 |
| H15 | 0.263130 | 0.293600 | One associated H | 0.52 | 0.29 |
| C2, C3 | -0.084420 | 0.061445 | C3, C4 | 0.28 | -0.15 |
| H7, H8, H9, H10 | 0.130405 | 0.072710 | Four associated H | 0.06 | 0.15 |

In Table 8-19 and Table 8-20, average values have been calculated for rows which contain more than one atom.

Presented results in Table 8-19 and Table 8-20 for partial atomic charges signify almost a good agreement between results from current thesis and da Silva (2005). But as mentioned in Section 4.1.5, the results from MPA scheme are not reliable since this method is very sensitive to the size of basis set. It was pointed earlier that Da silva (2005) has used basis set 6-31G* while in current thesis a bigger basis set with more polarization function (6-31G**) has been utilized. In general in present work not only more comprehensive basis set for

piperazine and protonated piperazine have been used but a higher level of theory (CM4 Scheme) and more modern solvation model (SM8) have been employed.

In following distribution of partial atomic charges for amine molecules is illustrated by Figure 8-7.

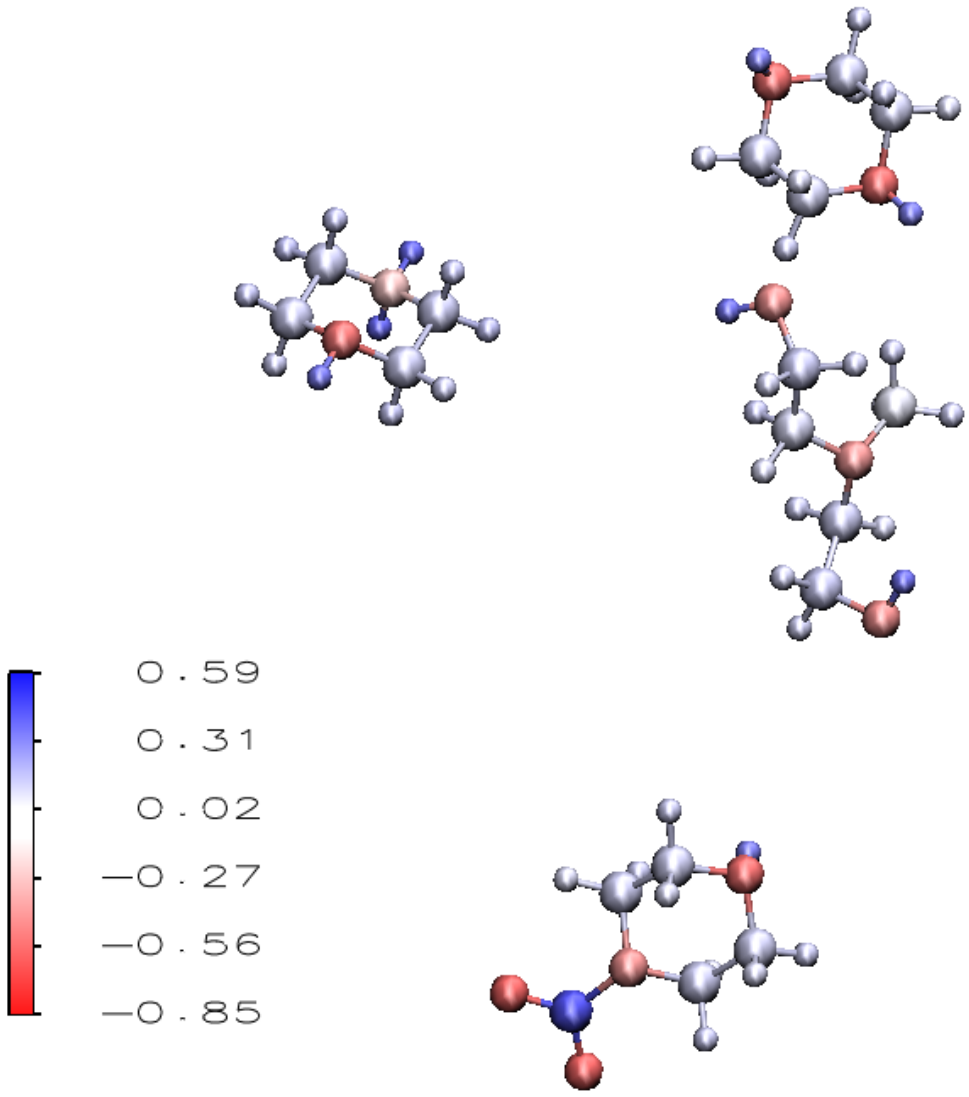


**Figure 8-7: Charge distribution of amine molecules**

## 8.5 Other Models

Models for water, methane and carbon dioxide were taken from literature since there were already good models which have been utilized many times for different simulations.

### 8.5.1 Water model

*Extended simple point charge* model (SPC/E) was used for water. This model is characterized by three point masses with OH bond length of 1 Å and HOH angle equal to tetrahedral angle. Charges are located on oxygen and hydrogen atoms equal -0.8476 and +0.4238 respectively(Berendsen et al. 1987) while the Lennard-Jones 12-6 potential is positioned only on oxygen molecule. SPC/E model is detailed in Table 8-21 and Table 8-22.

**Table 8-21: SPC/E water model**

| Site ID | Atom name | Charge [e] | Sigma [Å] | Epsilon [kJ/mol] |
|---|---|---|---|---|
| 1 | Oxygen | -0.8476 | 3.166 | 0.6507 |
| 2 | Hydrogen | +0.4238 | 0.000 | 0.0000 |
| 3 | Hydrogen | +0.4238 | 0.000 | 0.0000 |

**Table 8-22: Bond stretching and Angle bending parameters for water model**

| Bond | Equilibrium bond length [Å] | Force constant $[\frac{kJ}{mol.Å^2}]$ |
|---|---|---|
| O-H | 1.00 | 2811.00 |
| **Angle** | **Equilibrium angle [degree]** | **Force constant** $[\frac{kJ}{mol.rad^2}]$ |
| H-O-H | 109.47 | 191.50 |

### 8.5.2 Methane models

As mentioned earlier, two different one-site and 5-site models were used for methane molecule. Interaction parameters for these models are taken from literature.

One-site methane model is a non-charged methane model in which Lennard-Jones 12-6 parameters are located on carbon(Jorgensen et al. 1984). In the five-site model all hydrogen atoms are taken into account explicitly and corresponding partial charges determined from electrostatic potential fitting (ESP) of a 6-31*G ab initio calculation are assigned to all the 5 sites(Sun et al. 1992). Intramolecular interaction parameters and non-bonded parameters (L-J

12-6 potential) were taken indirectly from Amber all-atom force field (Scott et al. 1986). This model has been used successfully by (Niall and Macelroy 2003) doing MD simulation for methane calathrate hydrate at 50, 125 and 200 K.

Interaction parameters for both one-site and 5-site models discussed above are listed in Table 8-23, Table 8-24and Table 8-25.

**Table 8-23: : one-site methane model**

| Site ID | Atom name | Charge [e] | Sigma [Å] | Epsilon [kJ/mol] |
|---|---|---|---|---|
| 1 | Carbon | 0.00 | 3.730 | 1.230 |

**Table 8-24: L-J 12-6 interaction parameters for 5-site methane model**

| Site ID | Atom name | Charge [e] | Sigma [Å] | Epsilon [kJ/mol] |
|---|---|---|---|---|
| 1 | Carbon | -0.464 | 1.9082 | 0.4577296 |
| 2 | Hydrogen | 0.116 | 1.4872 | 0.0656888 |
| 3 | Hydrogen | 0.116 | 1.4872 | 0.0656888 |
| 4 | Hydrogen | 0.116 | 1.4872 | 0.0656888 |
| 5 | Hydrogen | 0.116 | 1.4872 | 0.0656888 |

**Table 8-25: Bond stretching and Angle bending parameters for 5-site methane model**

| Bond | Equilibrium bond length [Å] | Force constant $[\frac{kJ}{mol.Å^2}]$ |
|---|---|---|
| C-H | 1.09 | 1384.904 |
| **Angle** | **Equilibrium angle [degree]** | **Force constant** $[\frac{kJ}{mol.rad^2}]$ |
| H-C-H | 109.50 | 146.440 |

### 8.5.3 Carbon dioxide model

A three-site model was used for carbon dioxide molecule. This model possesses three L-J potential sites and partial atomic charges on each atom (Brodholt and Wood 1993a). Parameters for this model are given in Table 8-26 and Table 8-27.

**Table 8-26: Three-site carbon dioxide model**

| Site ID | Atom name | Charge [e] | Sigma [Å] | Epsilon [kJ/mol] |
|---|---|---|---|---|
| 1 | Carbon | 0.594 | 2.785 | 0.24112 |
| 2 | Oxygen | -0.297 | 3.014 | 0.69092 |
| 3 | Oxygen | -0.297 | 3.014 | 0.69092 |

**Table 8-27: Bond stretching and Angle bending parameters for CO2 model**

| Bond | Equilibrium bond length [Å] | Force constant $[\frac{kJ}{mol.Å^2}]$ |
|---|---|---|
| C-O | 1.162 | 28110 |
| **Angle** | **Equilibrium angle [degree]** | **Force constant** $[\frac{kJ}{mol.rad^2}]$ |
| O-C-O | 180 | 144 |

# 9 Simulation

## 9.1 Primary and reference systems

Many interesting conclusions can be made once enough comparable data are available in any study. In this regard, it was critically important for this thesis to decide about some appropriate reference systems, in order to carry out comparative analysis at the end of simulation.

In order to perform the MD simulation in current study, the simulation box was divided into two different parts. First part was occupied by liquid phase (including the aqueous amine solution) and the second part contained the gases components ($CO_2$ and/or $CH_4$). These two brought into contact with one another within a gas-liquid interface, so that the absorption process could take place across this interfacial surface.

Primary system was considered to contain the aqueous amine solution as a liquid phase; in addition to a mixture of methane and carbon dioxide at 100 bar as a gas phase. This system attracted main focus of current thesis, four reference systems were also chosen to be run in parallel with primary system. This was necessary to be able to perform some comparative analysis at the end of simulation. All the simulation systems – including both primary and reference systems – ran at about 298.15 K. which is close enough to the temperature of the systems from which speciation of the solution was determined (Section7). Aforementioned reference systems are introduced as following:

1. **Amine solution:** This system only contains the liquid phase including water as the dominant solvent plus all the amine molecules dissolved in water. The main reason for performing this simulation was to investigate distribution of the carbon dioxide absorbents molecules inside the solution excluding the effect of the interface. Doing this, hydrophobic-hydrophilic characters of each species in addition to their affinity towards each other can be studied.
2. **Amine solution + Carbon dioxide in 100 bar:** This system was chosen in order to study affinity of carbon dioxide towards the amine molecules by pushing the system into the liquid phase. This led the $CO_2$ molecules to be more available in vicinity of amine solvents. Therefore it was easier to observe some of expected phenomena.
3. **Amine solution + Carbon dioxide in 60 bar:** To study behavior of carbon dioxide in more realistic condition, the same system as reference system No.2 was conducted but this time in lower pressure, so that carbon dioxide does not stay in liquid phase

anymore. Therefore, pure carbon dioxide gas phase possessing 60 bar pressure was exposed to the amine solution. Evaluation of amine distribution in presence of the interface in addition to the process of carbon dioxide absorption was expected from this system.

4. **Water + carbon dioxide + methane:** In order to study influence of amine solution on the absorption of carbon dioxide in addition to undesired trapping of methane, current tertiary system was conducted. Considering that this system did not contain the amine solution, it was a good scale for comparing solubility of carbon dioxide and methane inside the pure liquid water with those belonging to the amine system. The same was also true for investigation of surfactant effect of the amine solvents. Comparison between interfacial tensions of this system with interfacial tensions of the primary system could demonstrate surfactant effect of the amine solvents.

### 9.1.1 Estimation of molecular population

Canonical ensemble – which has been used in this work - keeps the volume constant. Hence, density of the system is calculated once the numbers of particles are determined. As explained earlier, in current study, simulation box is divided into two liquid and gas parts. Therefore, the quantities of particles for each part have to be decided upon separately. In order to perform the MD simulation in current thesis rectangular simulation box possessing dimensions $60.529 \times 60.529 \times 110.529$ Å was chosen, so that $60.529 \times 60.529 \times 60.529$ Å was occupied initially by the amine solution and the rest by the carbon dioxide and methane (mostly in gas phase).

For the amine solution, approximate number of 4000 molecules and species was considered in total, so that the quantity of each molecule or specie could be determined easily based on the mole fractions given in Table 7-3. Considering this, following numbers of molecules/species were determined for the amine solution.

**Table 9-1: Calculated population**

**Of each molecule/specie in the liquid phase**

| Specie | quantity of molecule |
|---|---|
| $N_{PZ}$ | 44 |
| $N_{PZH^+}$ | 44 |
| $N_{PZCOO^-}$ | 44 |
| $N_{MDEA}$ | 556 |
| $N_{H_2O}$ | 3311 |
| $N_{liq.}^{tot.}$ | 3999 |

To determine the number of methane and carbon dioxide molecules, slightly complicated calculations were essential. Considering variety of mixtures ($CO_2 + CH_4$ , pure $CO_2$and pure $CH_4$) applied in primary or reference systems in this study, composition of each mixture had to be calculated separately based on thermodynamic condition of the that specific system. In this regard, underlying procedure was followed for all the reference systems.

#### 9.1.1.1 Reference system No.1

Reference system No.1 does not contain any gas phase and merely comprises of the amine solution. Composition of the amine solution and quantity of each molecule/specie were explained above in Table 9-1. Exactly the same amine part (in terms of the system size and number of constituents) was used for all the primary and reference systems that contain the amine solution. Therefore, in following sections composition of the amine solution will not be explained over again and attention will be paid only to the gas phase.

#### 9.1.1.2 Reference system No. 2

In this system, the carbon dioxide pressure was 100 bar (10 MPa) and temperature was set at 298.15 K. According Span-Wagner equation of state, melting temperature of carbon dioxide in this pressure is at 218.60 K (Span and Wagner 1996). Therefore, having temperature of 298.15 K, the system stays in liquid phase.

Considering the state of the system at T=298.15 K and P=10 MPa, corresponding liquid density was calculated, by interpolation of tabulated density data based on Span-Wagner EOS (Span and Wagner 1996). Doing this, density was found to be equal 816.8085 $kg/m^3$. Considering the volume of carbon dioxide part fixed at $60.529 \times 60.529 \times 50$ Å, the mass of

the liquid $CO_2$ was calculated. This value was finally converted to the number of carbon dioxide molecules using molecular weight and Avogadro's number.

$$m_{CO_2} = \rho_{CO_2} \times v = 816.8085 \left[\frac{kg}{m^3}\right] \times 10^{-27} \times (60.529 \times 60.529 \times 50)[\text{Å}]$$
$$\approx 1.4962 \times 10^{-19}[gr]$$

Which is approximately $3.3998 \times 10^{-21}$ mole carbon dioxide. Considering Avogadro's number as the number of molecules per mole of matter, quantity of carbon dioxide molecules was calculated to be equal 2047.4667. Since number of the molecules had to be an integer, this value was rounded down to 2047. Doing this, the density and consequently temperature of the system had to be recalculated in an opposite manner. So that having this number of molecules, firstly, new mass of the carbon dioxide was calculated and from that, new density of $CO_2$was determined again which was equal ~816.6222 $kg/m^3$. Finally, by this new density, new temperature of the system was obtained from Span-Wagner tabulated data which was equal to ~298.173 $K$.

Therefore the new state of the system (liquid $CO_2$) was identified to be equal: T=298.173 K, P=10 MPa and $N_{CO_2}$=2047.

Ultimately, carbon dioxide part of the system was connected to the amine solution segment in MD 5.1, in such a way that interaction between two parts of the reference system was possible. Figure 9-1 illustrates the preliminarily prepared reference system No.2 before starting the simulation. Here, we can see the rectangular simulation box in which the upper part is occupied by carbon dioxide and the lower part is filled with amine solution. The gap between the two parts is to provide enough space for expansion of the system without getting any overlap by the molecular tails which may come out from two sides of the interface due to PBC. Hence, each side can be expanded slowly to fill the gap gradually. In this way two phases are brought into contact to start interacting with one another.

Figure 9-2 illustrates the same system, a short time after starting the simulation. This figure clearly shows the amine species started to spread into the liquid carbon dioxide.

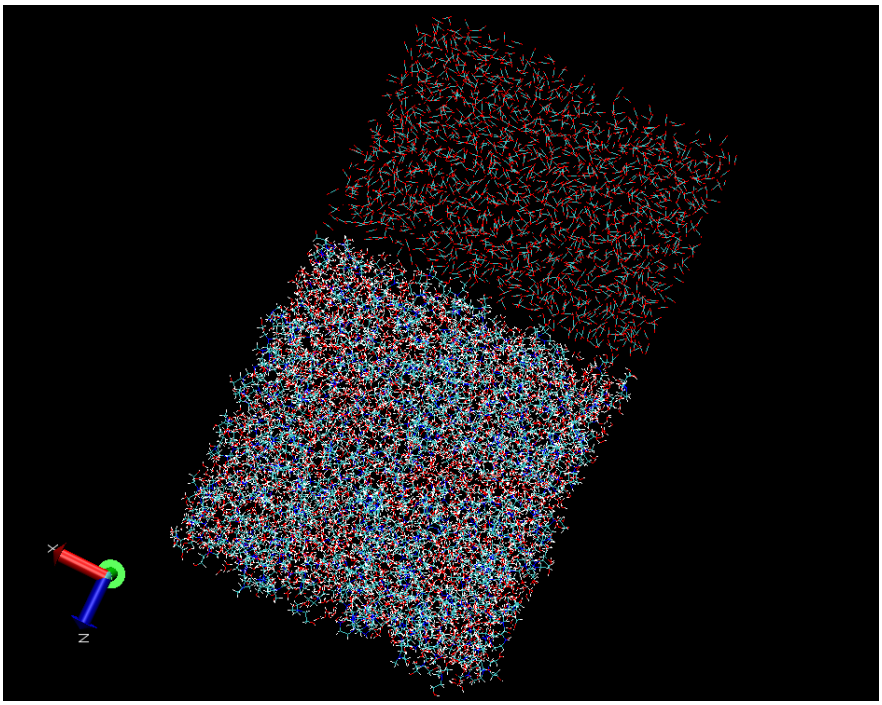

**Figure 9-1: Reference system number 2 before MD simulation is switched on**

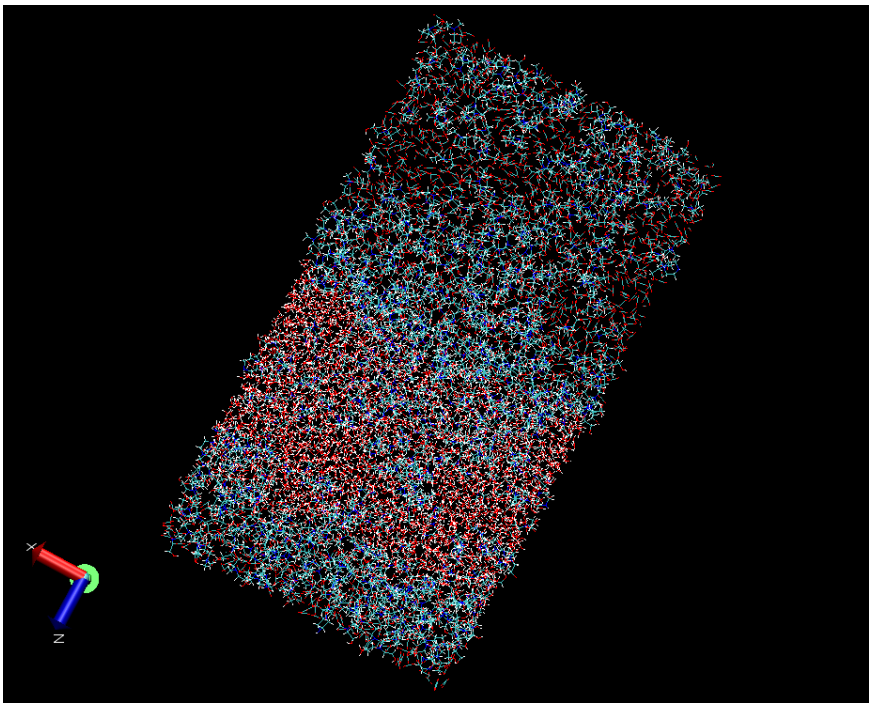

**Figure 9-2: Reference system number 2 short time after MD simulation is switched on**

#### 9.1.1.3 Reference system No. 3

The same approach was chosen to estimate quantity of carbon dioxide molecules for reference system No.3, except in this system carbon dioxide should exist in gas phase. State of the system here was defined as T=298.173 K and P=6 MPa.

According Span-Wagner EOS, saturation temperature at 6MPa equals 295.128 K(Span and Wagner 1996), therefore having temperate of 298.173 for the system, gas phase criterion is satisfied. Same procedure as reference system No.2 was employed to calculate the density of the gas phase, in addition to the quantity of carbon dioxide molecules and new temperature of the system, which slightly differed with the one from target temperature 298.173. As explained for reference No.2, this was due to the fact that the quantity of the molecules always had to be an integer and any decimal number for that should be round off to the nearest integer number. Final calculated results for reference No.3 are as following: $\rho_{CO_2}$=193.085 $kg/m^3$, T=298.163 K, P=6 MPa, $N_{CO_2}$=484.

#### 9.1.1.4 Reference system No.4

Reference system No.4 contains a mixture of methane and carbon dioxide at T=298.173 K and P=10 MPa as gas phase, in addition to the pure liquid water serving as the solvent instead of amine solution in liquid phase. Therefore, the quantity of each gaseous component in the gas phase and water molecules in the liquid phase had to be determined separately.

For the gaseous mixture similar procedure as the other reference systems was chosen. UniSim Design Suite and Peng-Robinson EOS were employed to calculate density of the methane-carbon dioxide mixture at T=298.173, P=10 MPa, $y_{CH_4}$=89% and $y_{CO_2}$=11%. $y_{CH_4}$and $y_{CO_2}$are mole fractions of each gaseous component at a sample operating condition. Consequently, density of the gaseous mixture as well as quantities of methane and carbon dioxide molecules were calculate, so that $\rho_{mixture}$=95.61 $kg/m^3$, $N_{CH_4}$=491 and $N_{CO_2}$=61.

It should be noted here, that the same $CH_4 - CO_2$ gas mixture was exposed to the amine solution in primary system as well. This was due to the similar thermodynamic condition of the gas phase for both systems. Therefore, calculation of the gas phase composition will not be repeated for primary system again.

In reference system No.4, the number of water molecules were estimated using ideal liquid density of pure water (998 $kg/m^3$). Having density of water in addition to size of the liquid part (which is $60.529 \times 60.529 \times 60.529$Å), the number of water molecules can be calculated easily. Unfortunately, the pressure of water in liquid phase is unknown before starting the MD simulation, therefore, more precise determination of water density at true pressure and temperature was impossible. Ultimately, the number of water molecules in liquid phase was estimated to be equal $N_{H_2O}$ =7396.

In order to summarize configurations of the all primary and reference systems, Table 9-2 was provided.

**Table 9-2: Summary of systems specifications**

| System | Primary System | | Ref. system No.1 | | Ref. system No.2 | | Ref. system No.3 | | Ref. system No.4 | |
|---|---|---|---|---|---|---|---|---|---|---|
| Segment | Amine sol. | $CH_4 + CO_2$ | Amine sol. | --- | Amine sol. | Liquid $CO_2$ | Amine sol. | Gaseous $CO_2$ | Water | $CH_4 + CO_2$ |
| Temperature [K] | 298.173 | 298.173 | 298.173 | --- | 298.173 | 298.173 | 298.163 | 298.163 | 298.173 | 298.173 |
| Pressure [MPa] | Determined by MD | 10 | Determined by MD | --- | Determined by MD | 10 | Determined by MD | 6 | Determined by MD | 10 |
| Density [$kg/m^3$] | 1042.3 | 95.61 | 1042.3 | --- | 1042.3 | 816.622 | 1042.3 | 193.085 | Determined by MD | 95.61 |
| Quantity of constituents | Table 9-1 | $CH_4 = 491$ $CO_2 = 61$ | Table 9-1 | --- | Table 9-1 | $CO_2 = 2047$ | Table 9-1 | $CO_2 = 484$ | $H_2O$ =7396 | $CH_4 = 491$ $CO_2 = 61$ |

## 9.2 Simulation set-up and initial preparations

### 9.2.1 General considerations

Once all the molecules and species are modeled and quantity of them are decided, initial set-up of the simulation for the systems can be made.

In this regard, first step was to determine computational requirement of the simulations for each system (primary and reference systems). This was itself dependent on the system size and population of the atoms and molecules. The two largest systems among the above mentioned primary and reference systems are the primary system, which was using five-site methane model, and the reference system No.2 (Section 9.1.1.2) which contains amine solution and liquid carbon dioxide. To be able to imagine how tremendous computational requirements are in this research, these two largest systems have been compared in Table 9-3.

**Table 9-3: Atomic population of the two largest simulation systems**

| | **Amine solution + liquid $CO_2$ ref.system** | **Primary system** |
|---|---|---|
| Number of molecules | 6046 | 4551 |
| Number of total sites | 29994 | 26491 |
| Number of covalent bonds | 27391 | 25383 |
| Number of angles | 25731 | 26691 |
| Number of torsions | 29336 | 29336 |
| Number of degrees of freedom | 62558 | 79470 |

This still does not include number of Lennard-Jones and electrostatic interactions. It is obvious from this comparison that computational requirements of the current research were expected to be enormous. To be able to cope with this difficulty, *Hexagon* a super computer at BCCS (The Bergen Center for Computational Science) was employed. Using high performance computers with 1024 processors was a great help towards the progress of simulation. Still several limitations declined the expected progress. First of all, number of available processors for every user in BCCS is limited to 1024. Therefore capacity of these available processors had to be shared among all the assigned computational jobs for above mentioned systems. Moreover, due to the compilation limitation in MD5.1[12], not more than 212 processors could be used in parallel for each simulation job. In total, average speed of 4.6

[12] MD5.1 is the acronym for MDynaMix Ver. 5.1 which was used in this work for MD simulation of the system.

steps per second was achieved for different simulations during this research. Given 1 fs as time step, for 30 ns simulation of the system approximately 77 days were required.

### 9.2.2 M.DynaMix Ver. 5.1 as simulation tool

To perform molecular dynamics simulation in current work, MDynaMix Ver. 5.1 was employed (Lyubartsev and Laaksonen 2000). This is a general purpose MD code for simulation of mixtures written in standard Fortran-77. The code supports both sequential and parallel execution. Interactions are computed using an "AMBER-like" force field within periodic cell. MDynaMix is suitable for simulation of rigid and flexible molecules. For rigid molecules, the SHAKE algorithm is used to constrain the covalent bonds and for flexible molecules double time step algorithm is included. Ewald summation for calculation of electrostatic interactions is employed. NVE, NVT and NPT statistical ensembles are supported. The code also contains some tools to facilitate some calculation such as calculation of pair distribution function.

### 9.2.3 Simulation set-up and preliminary run

Unless it is explained otherwise, following set-up was applied for simulation of all primary and reference systems:

In this work rectangular cell with dimensions $60.529 \times 60.529 \times 110.529$ Å was employed initially. The liquid phase occupied $60.529 \times 60.529 \times 60.529$ Å of the box and the gas phase positioned in the left $60.529 \times 60.529 \times 50$ Å of the space. Density was fixed for each simulation considering volume of the box and quantity of the molecules/species were constant during the simulation. Total number of molecules and species in the amine solution was decided to be roughly 4000 and quantity of methane and carbon dioxide molecules was calculated separately based on thermodynamic conditions of each system (Section 9.1.1).

Simulation ran using constraint dynamics, fixing the bond length of all covalent bonds within a $1.0 \times 10^{-4}$ Å tolerance. This was done to speed up the simulation and to be able to choose a longer time step. As it was mentioned in Section 4.2.2.2, by using constraint dynamics flexibility of the molecules is neglected and high frequency motions is not taken into account any more so that we can increase length of the time step. Unfortunately, MD5.1 is very sensitive against application of constraint dynamics in such a way that the simulation failed several times due to the application of this feature. In this work, constraint dynamics was kept off for a while after starting the simulation until the system gets stable and then it was switched on for the rest of simulation.

Time step equal to 1 fs was chosen unless the constraint dynamics was off and double time step algorithm was used. In this case only, long time step equal to 0.2 fs was applied and number of short time steps per long time step was decided to be equal 10.

Ewald sum was employed to treat the electrostatic interactions. Default parameters from MD 5.1 were kept for this feature.

Cut-off radius for Lennard-Jones interaction in long and short time steps was decided to be 10 Å and 5 Å respectively.

Canonical ensemble (NVT) was employed in current work. Temperature was kept constant at approximately 298.173 K by scaling the velocities during the equilibration phase. Later on, Nose-Hoover thermostat was used to obtain more accurate scaling for the target temperature. In the case of velocity scaling, admissible deviation was set to 5 K and in the case Nose-Hoover thermostat the relaxation time was set to to be 50 fs.

In principle, simulation starts once there are available resources for the submitted job at Hexagon. In the start-up request, required number of processors as well as the wall time has to be defined for each simulation run. In this study, *face centered cubic* (FCC) was chosen as initial configuration of the molecules for each simulation. This feature is implemented in MD5.1, so that, molecular center of masses are positioned on a FCC lattice. As mentioned earlier, this is only an initial configuration and cannot be valid naturally. Molecules and species rearrange themselves based on molecular interactions upon starting the simulation. This is usually a difficult time and attentions have to be paid, since the molecular geometries, molecular orientations, orders and intermolecular distances are not optimized yet. In this stage, simulation is very sensitive to towards application of any constraint. If the initial set-up of simulation is not precisely chosen, simulation will fail soon after beginning. In general, the system needs some time to get stable. This phase is usually called equilibration phase in MD simulation. In this work constraint dynamics was switched off during equilibration phase and velocity scaling was used as the temperature scaling method instead of Nose-Hoover thermostat. During the equilibration phase molecules spread through the simulation box and try to find their own optimized geometry and intermolecular distances based on governing forces. They also fill the artificial gap between two different initial phases to form the true interface between them (recall Figure 9-1 and Figure 9-2). After this phase, the system enters the production phase. This is the main and long part of the simulation when the time evolution of the system can be followed and true processes can be investigated. During this stage,

constrained dynamics was switched on and Nose-Hoover thermostat employed. Production phase may take several months or even more depending on the defined simulation goals. In the case of current thesis, gross time for the simulation run was about 4 months.

# 10 System evolution, results and discussion

In this chapter, time evolution of the primary and reference systems will be discussed in details and simulation results will be compared between them. The systems are non-uniform and not in equilibrium in global thermodynamic sense but have been run for long times and expected to be mechanically stable in terms of molecular simulations. For these reasons average ensemble values can only be used for some features and the analyses - to a large extent - relate to visual observations as sampled and treated through the use of VMD. Depending on each observation, they will be quantified by calculating density profiles of the systems and/or pair radial distribution functions. At the same time, hydrogen bonds network of the solution will be investigated, since it has important effect on the molecular distribution in the liquid phase. Pair correlation functions - specifically - will be employed in combination with calculated coordination numbers to describe some of the expected structures and molecular affinities. This will be used to specify whether there is any competition between gaseous components ($CO_2 - CH_4$) towards the active sequences of amine solvents or not. These data will be used to provide more insight into the overall process of carbon dioxide absorption and undesired trapping of methane. Finally, interfacial tension will be calculated for each gas-liquid system to demonstrate surfactant effect of the amine solvents.

## 10.1 Reference system No.1

As mentioned in Section 9.1.1.1, this system contained aqueous amine solution including molecular piperazine, protonated piperazine, piperazine carbamate, MDEA and water. Visual observation after $\sim$0.48 ns displayed a non-uniform solution in X direction. The solution started to form some *water free cavities* so that PZH and PZCOO stayed inside the water while at the same time, MDEA and PZ agglomerated with one another away from water to fill these cavities. This implied that hydrophobic-hydrophilic characteristic of the solutes is an important factor which strongly affect molecular distribution of the system. Due to the existing dipole moments in the molecular structure of water, significance of hydrophobic-hydrophilic behavior was expected. Recall water is the dominant solvent in the solution standing for approximately 83% of the existing molecules. Considering PZH and PZCOO carry formal positive and negative charges respectively, they prefer to stay inside the polar solvent (water), while PZ and MDEA which are neutral molecules repel the water by demonstrating their hydrophobic behavior. This leads to formation of the water free cavities inside the solution. These cavities evolved over the simulation time so that gradually they formed two separate phases after $\sim$10.66 ns. These two dominated water and dominated

MDEA phases were separated by an almost static interface. By static it is meant that shape of the interface did not change significantly over the time.

X-Y cross-section of the system is shown by Figure 10-1 which illustrates time evolution of the water free cavities towards the complete phase separation.

**a) 0.48 ns**

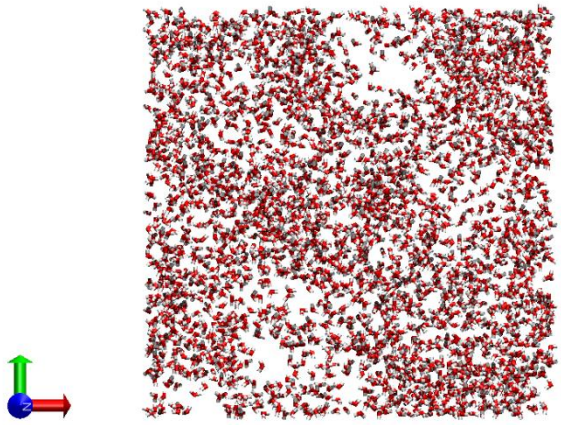

**b) 4.84 ns**

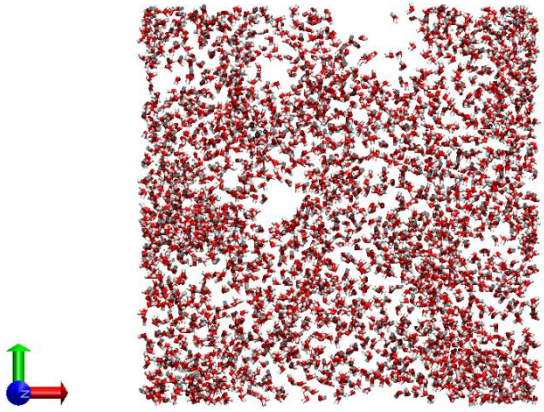

**c) 6.84 ns**

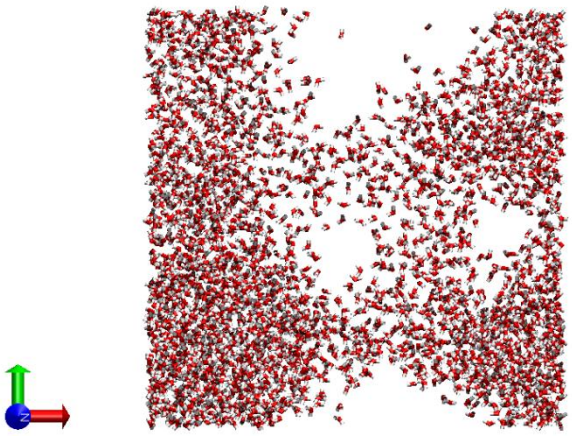

**d) 10.66 ns**

**e) 14.36 ns** **f) 17.36 ns**

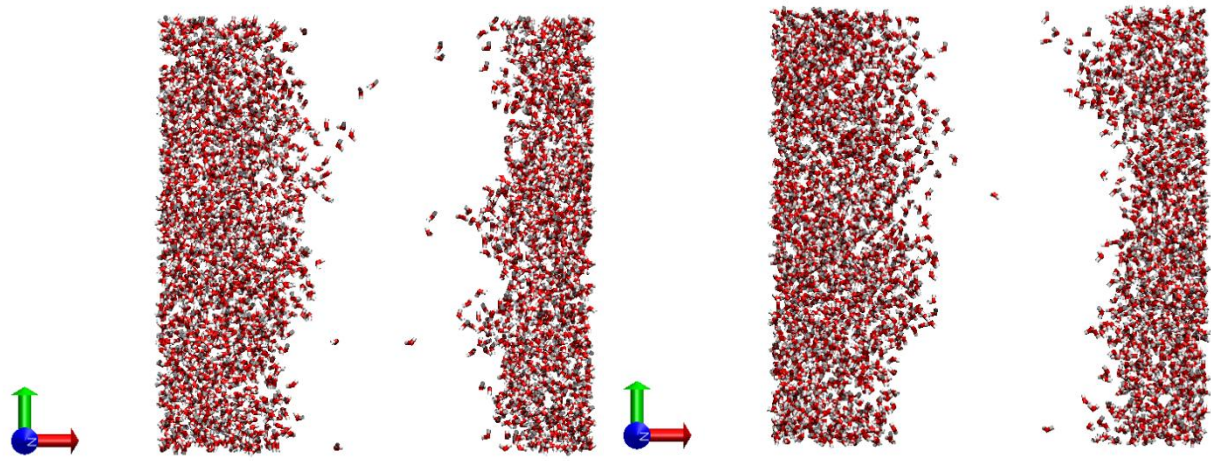

**Figure 10-1: Evolution of the free water cavities leading to the phase separation in X direction**

**a) 6.48 ns** **b) 17.36 ns**

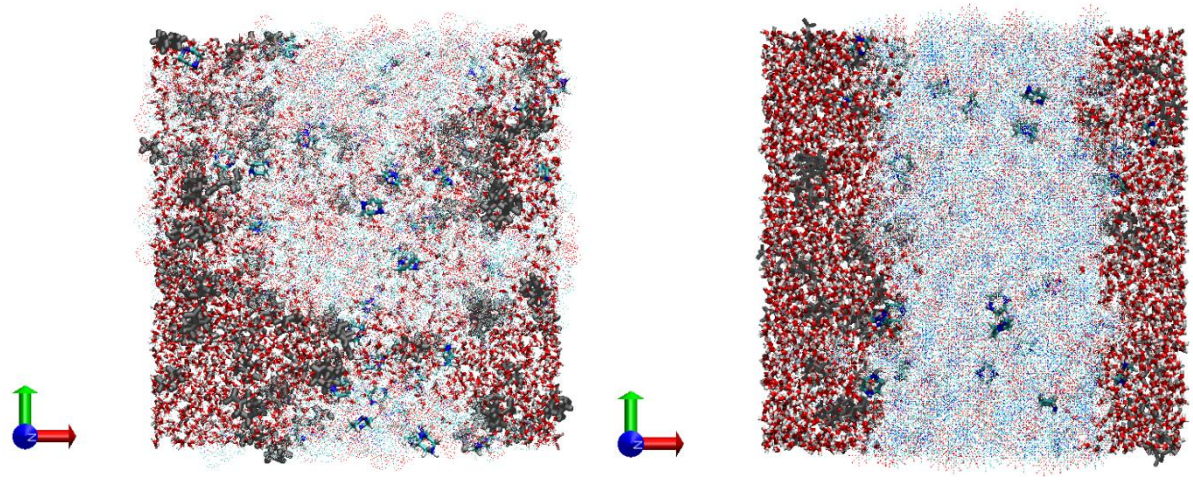

**Figure 10-2: X-Y cross-section of the system for molecular distribution of the amine solution**

In Figure 10-1, illustration of the amine molecules is excluded but they are presented in Figure 10-2. The latter figure illustrates molecular distribution of the amine solution for two time sections 6.48 ns and 17.36 ns. Here, water molecules have been demonstrated with same representation as Figure 10-1, light dotted distribution belongs to MDEA phase, blue rings represent the PZ molecules and gray rings show the PZH and PZCOO species together. This

figure supports the above mentioned argument for distribution of the charged and uncharged species inside the water.

Similarly, the density profile of the system stayed consistent with the molecular distribution illustrated above in Figure 10-1 and Figure 10-2. Using an in-house MATLAB code, two dimensional density profile of the system was averaged over 0.2 ns along X direction for configurations corresponding to the beginning (Figure 10-1 (a)) and end of the simulation (Figure 10-1 (f)). Density profile of the reference system No.1 is illustrated by Figure 10-3 and Figure 10-4.

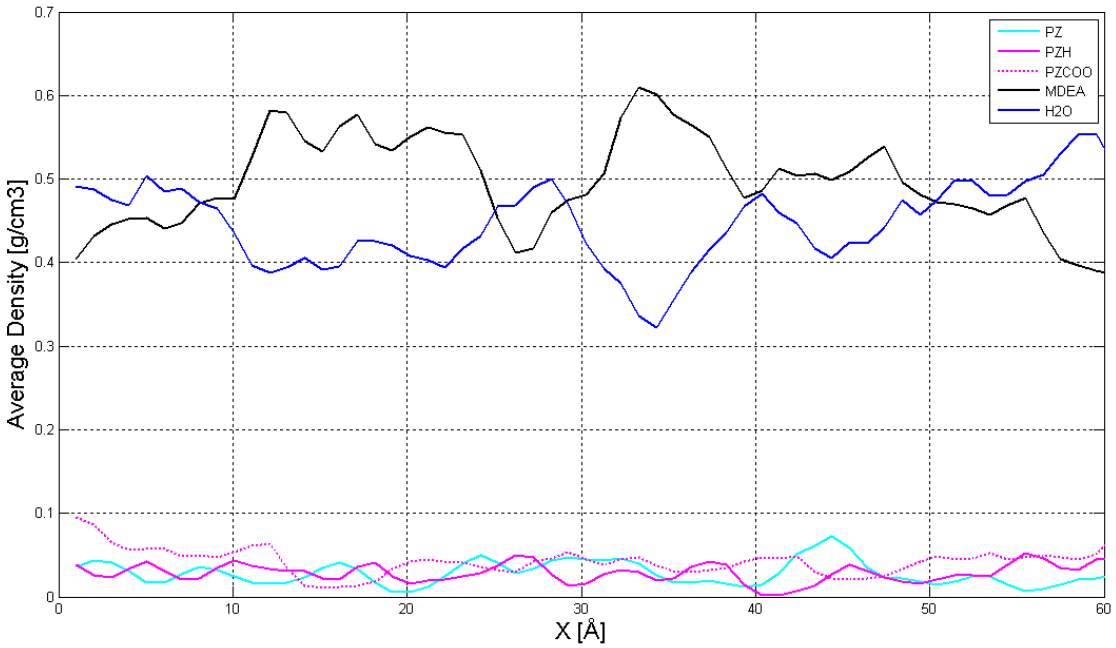


**Figure 10-3: Density profile of the system averaged over 0.2 ns for beginning of the simulation**

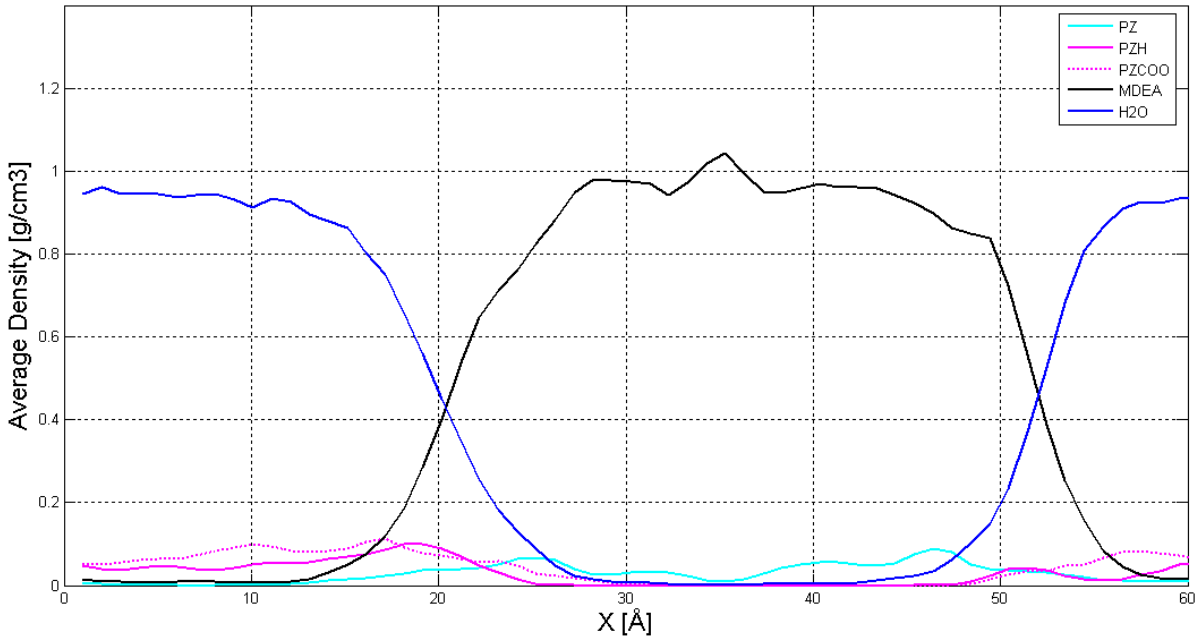


**Figure 10-4: Density profile of the system averaged over last 0.2 ns of the simulation**

Figure 10-3 illustrates density profile of the system at early simulation (around 0.48 ns). As it is clear here, phase separation has not occurred yet and the solution is pretty mixed but even in this mixed system hydrophobic character of the MDEA is detectable. In this figure black line (MDEA) always opposes position of the blue one (H2O) meaning when concentration of water increases somewhere in the box, the one for MDEA decreases and vice versa. However, due to the low concentrations of piperazine species hydrophobic-hydrophilic behavior of them is not recognizable in the mixed system. Going to the end of simulation (Figure 10-4) everything is clearer. Around 17.36 ns, phase separation is completed. Density profile of the system demonstrates dramatic decrease in concentration of water at the middle of box (between ~21-53 Å) while at the same time concentration of MDEA increases within this distance to a large extent. The same happens for PZ concentration which increases where water almost does not exist, while PZH and PZCOO remain inside the polar phase showing their hydrophilic characteristic.

Phase separation of the system was observed to be a favorable distribution based on computed potential energies of the system from MD5.1. Table 10-1 demonstrates variation of total potential energy of the system during production phase which is clearly decreasing. It proves

that development of the system towards the phase separation is companied by increased stability of that.

**Table 10-1: Variation of total potential energy of the system during production phase**

| Time [ns] | 8.67 | 10.66 | 11.36 | 14.36 | 17.36 |
|---|---|---|---|---|---|
| $E_P^{tot}$ [kJ/mol] | -21.8±0.1 | -21.9±0.1 | -21.9±0.1 | -22.0±0.1 | -22.1±0.1 |

To provide more evidence for molecular distribution of the system, hydrogen bonds network was investigated by determination of hydrogen bonds among different species with water. Calculation was performed using a script written for VMD program. Geometric definition of the hydrogen bond was employed (Chowdhuri and Chandra 2002). Distance and angle cut-off were set to be equal 3 Å and 24° respectively. Amine solution was scanned for the last 4000 configurations of the system so that all the hydrogen bonds within the cut-off criteria were determined, one time for water as a donor and another time as an acceptor. Results are given in Table 10-2.

**Table 10-2: Average number of hydrogen bonds per simulation frame**

| Molecular Pair | H2O-MDEA | H2O-PZ | H2O-PZH | H2O-PZCOO |
|---|---|---|---|---|
| Number of Hbond | 108.15 | 9.25 | 44.25 | 142.61 |

These data can explain preference of PZH and PZCOO for water phase. Considering relatively high number of hydrogen bonds between these two charged species with water molecules in addition to quantity of them inside the system (44 for each of them), it is clear that all of them has succeeded to form hydrogen bonds with surrounding water. Hence, water will be a favorable environment for them so that they are encouraged to stay inside the water bulk. This is logical and one of the purposes of the reactive addition to MDEA to react with absorbed $CO_2$ and dissolve the ionic reaction products into the bulk water phase.

In the case of PZH, additional proton connected to one of the nitrogens was observed to be highly favorable to participate in formation of hydrogen bond with water. The same was true for the nitrogens of PZH, connected with hydrogens of water within a hydrogen bond. In the

case of PZCOO, both oxygens in carboxylate group in addition to the nitrogens were quite eager to establish hydrogen bonds with hydrogens of water. Similarly for MDEA, central nitrogen and both oxygens from alcohol groups indicated their tendency to form hydrogen bonds with hydrogens in water. Figure 10-5 illustrates formation of hydrogen bonds between above mentioned molecules and water. Snap shots were taken from the last frame of MD simulation for reference system No.1.

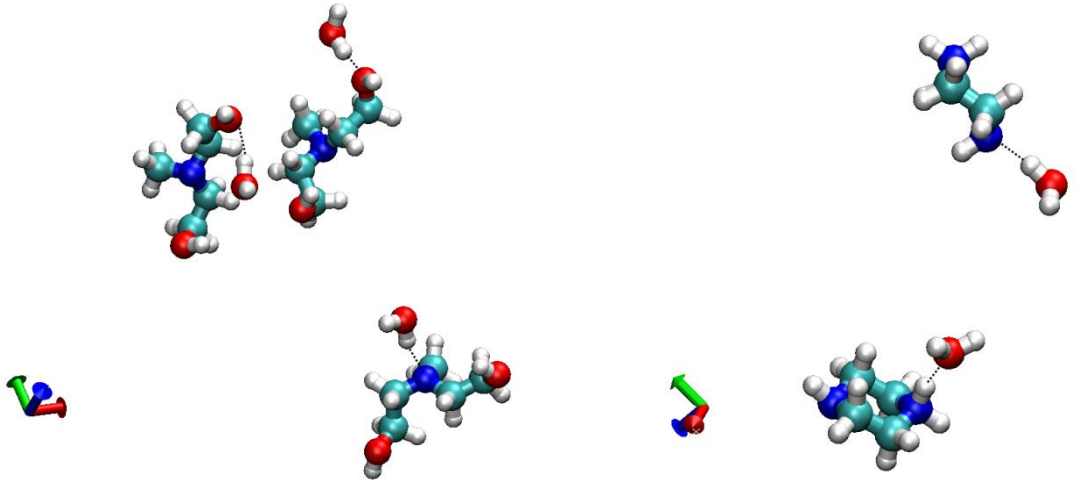

**a)** **b)**

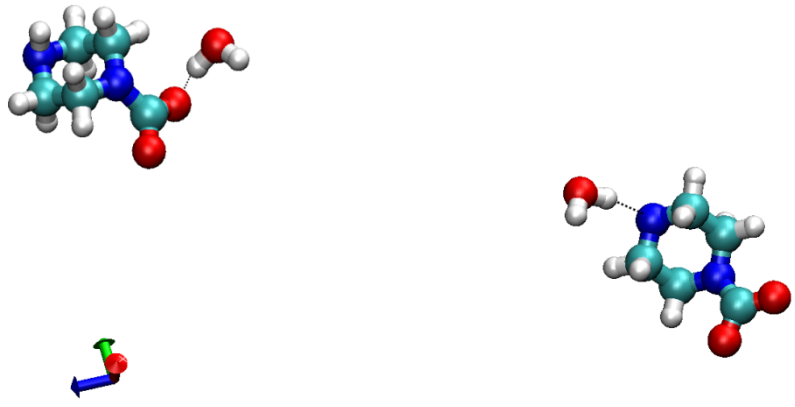

**c)**

**Figure 10-5: Formation of hydrogen bonds between a) MDEA b) PZH and c) PZCOO with water**

The last point which is needed to be explained is relatively high number of hydrogen bonds between MDEA and water. This is related to the existence of three active sites in MDEA

molecule (central nitrogen and two alcohol group's oxygens) in addition to the formation of vast interface between MDEA and water in the system. Sample MDEA-water molecules involved in formation of hydrogen bonds are illustrated in Figure 10-6. Size of the molecules is exaggerated in this figure in comparison with the overall molecular distribution in background. Red color dotted area shows the water phase, while the blue color dotted distribution represents the MDEA phase. This figure demonstrates most of the MDEA-water molecules involved in formation of hydrogen bonds exist along the interface.

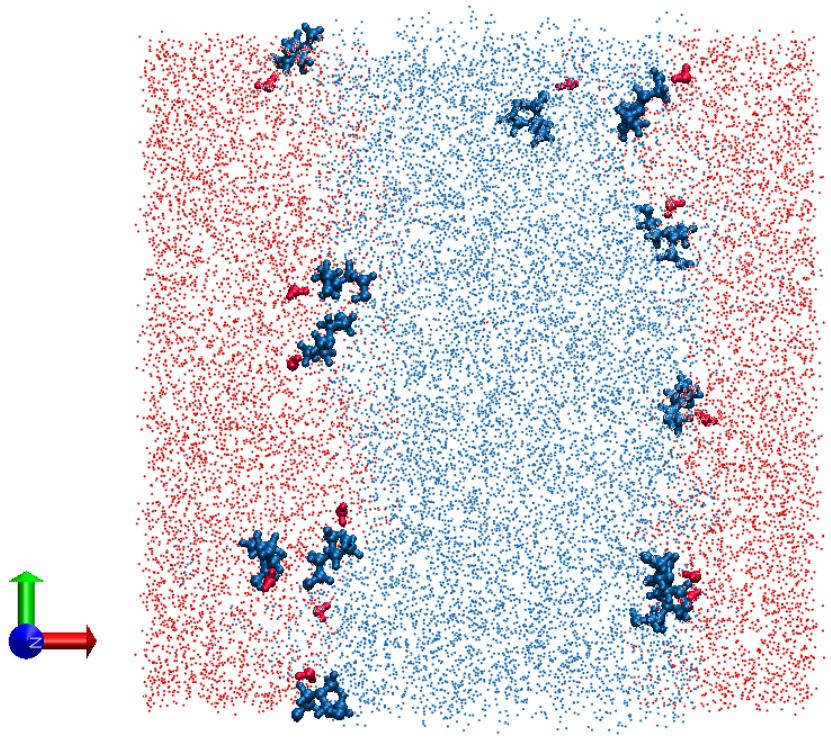

**Figure 10-6: Favorable distribution of MDEA-water molecules along the interface for hydrogen bonds formation**

To summarize, various evidence was provided in this section to explain the observed molecular distribution of the system in addition to separation of the phases based on hydrophilic-hydrophobic characteristics of each molecule/specie. This will help when subsequent reference and primary systems are to be discussed.

## 10.2 Reference system No.2

Current reference system contained aqueous amine solution in addition to liquid carbon dioxide, so that at the beginning of simulation two separate $CO_2$ and amine solution phases was connected together artificially (Look at Section 9.1.1.2). Once the simulation was initiated, these two phases started to interact with one another. As observed in reference

system No.1, molecular distribution of the system was strongly affected by the hydrophobic-hydrophilic characteristics of different species. Similarly here in reference system No.2, such an effect was detectable. Considering the liquid carbon dioxide in this reference system, one would assume that hydrophobic species would prefer to travel away from water molecules into the carbon dioxide bulk, and this is exactly what was observed in current system. At the beginning of simulation, amine solution and carbon dioxide phase were completely separated but as the simulation progressed MDEA and PZ started to move away from water phase and dissolve in the liquid carbon dioxide, while PZH and PZCOO preferred to stay with water. At the same time, small degree of common dissolution of carbon dioxide in water was observed. Figure 10-7 Illustrates time evolution of the system by which above mentioned description for molecular distributions is recognizable. In this figure red spheres represent carbon dioxide molecules; blue dotted area is water phase; magenta dotted area illustrates MDEA distribution; big gray molecules demonstrate both PZH and PZCOO and big green representation belongs to PZ molecules.

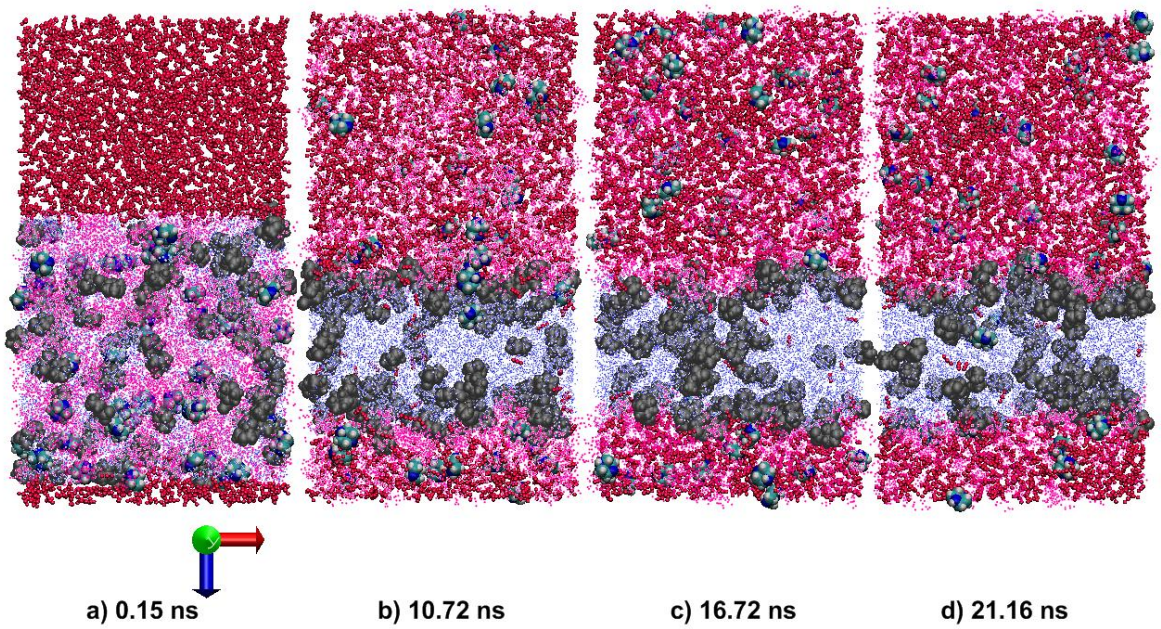


**Figure 10-7: X-Z cross-section of the system which illustrates time evolution of the reference system No.2**

Furthermore, density profile of the last 1000 configurations of the system demonstrated the same fact as Figure 10-7(d). Density of different components of the solution was averaged over the last 0.2 ns of the simulation along entire system in Z direction. Results are presented in Figure 10-8.

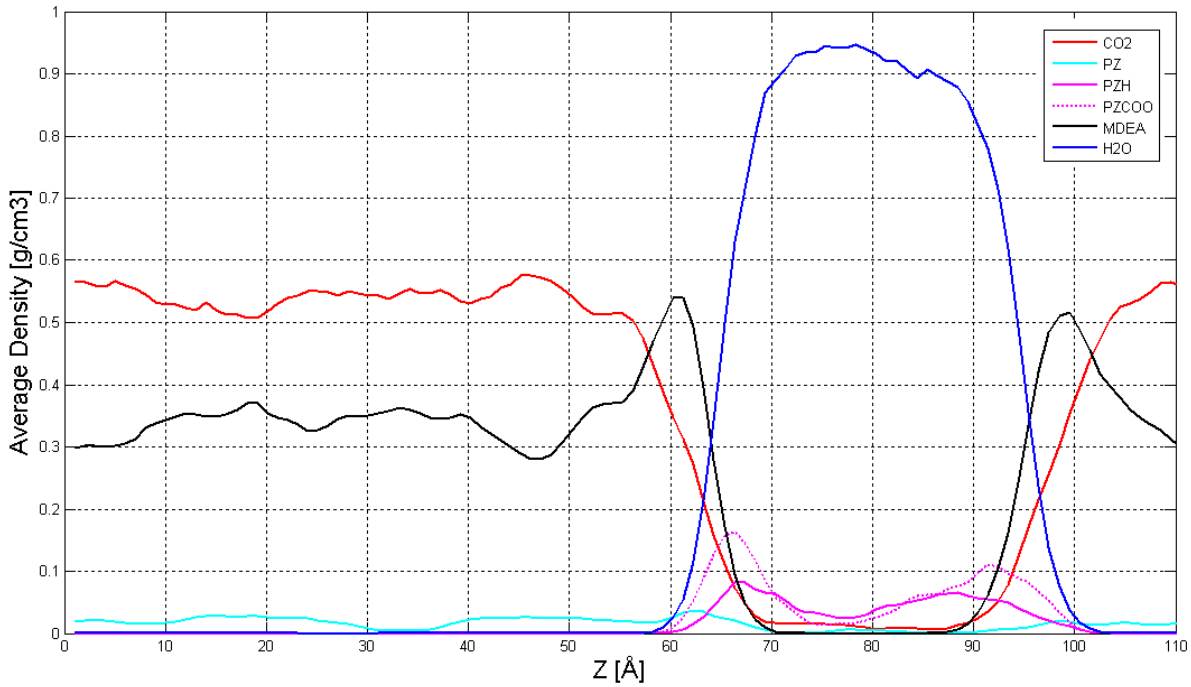


**Figure 10-8: Density profile of the system averaged over the last 0.2 ns of simulation**

Again, the separation of hydrophobic molecules (MDEA and PZ) from water and coexistence of hydrophilic species (PZ and PZH) with water are obvious. As we see, concentration of MDEA and PZ is almost zero between ~70-89 Å, while PZH and PZCOO are dominant dissolved amines in water. Moreover, even if PZH and PZCOO are ions and inside the aqueous phase, they still have an increased concentration close to the interface (60-70Å and 90-100Å) due to the non-polar segments of the ions.

Furthermore, solubility of carbon dioxide inside the water phase was observed to be very small, as expected from experimental determinations. However, the most interesting observation was affinity of carbon dioxide and MDEA. As it stems from Figure 10-8, high concentration of these two components was observed to be always together. It was important to know how MDEA performs in connection with carbon dioxide. This might help to get more insight for understanding the mechanisms which act in absorption of carbon dioxide in other reference systems as well as the primary system. To investigate affinity of carbon dioxide towards MDEA, further investigations were carried out by means of pair correlation function and calculation of coordination number between the active sequences of MDEA (amine and alcohol groups) with carbon dioxide.

In this regard, Figure 10-9 demonstrates pair correlation function between nitrogen from amine group in MDEA and carbon atom from carbon dioxide.

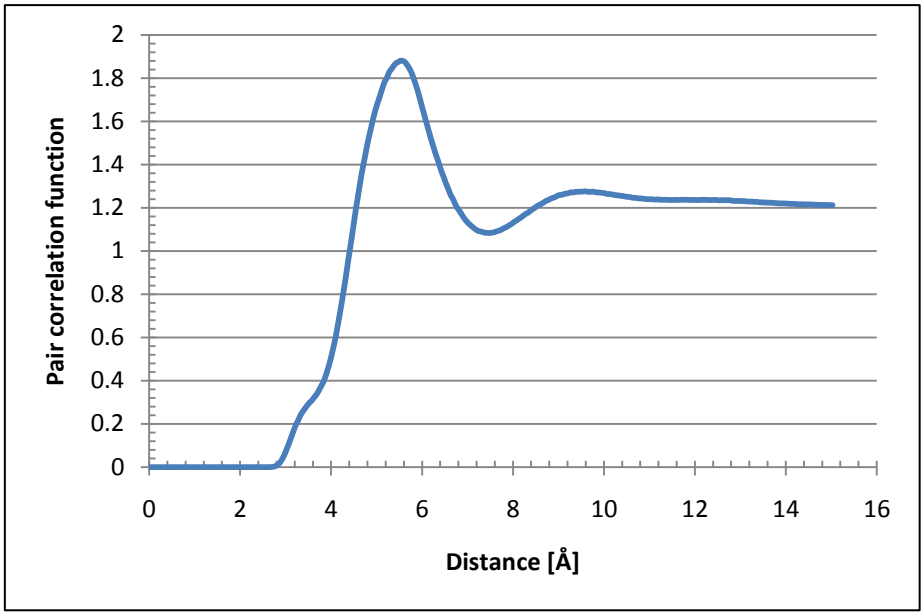


**Figure 10-9: Nitrogen-Carbon pair correlation function between MDEA and $CO_2$ molecules**

In this figure, position of the small curvature before the first peak is very close to the minimum L-J interaction distance for N-C pair which is equal to 3.415 Å. Minimum L-J interaction distance is the inter-atomic separation in which L-J potential is minimum and can be calculated directly from L-J interaction formula. Equation (10-1) shows the calculated distance for minimum L-J potential.

$$r_{min.\ pot.} = \sqrt[6]{2}\,\sigma_{ij} \qquad \textbf{(10-1)}$$

Where $\sigma_{ij}$ is the collision diameter given by Lorentz-berthelot's rule.

Therefore, the small curvature comes from the lowest short range interactions between N-C pair. The first peak possessing significant height of 1.8795 happens at 5.525 Å. Integration of pair correlation function over distance until the first minimum (first minimum is equal to 1.0826 and occurs at 7.475 Å) gives the number equal to 10.6462 which signifies quantity of the carbon dioxide molecules around nitrogen atom within the first shell. This demonstrates affinity of carbon atom possessing partial charge equal +0.5940 [e] from carbon dioxide towards nitrogen with partial atomic charge equal to -0.46258 [e] from MDEA. Figure 10-10 illustrates integration of the above pair correlation function to the first minimum.

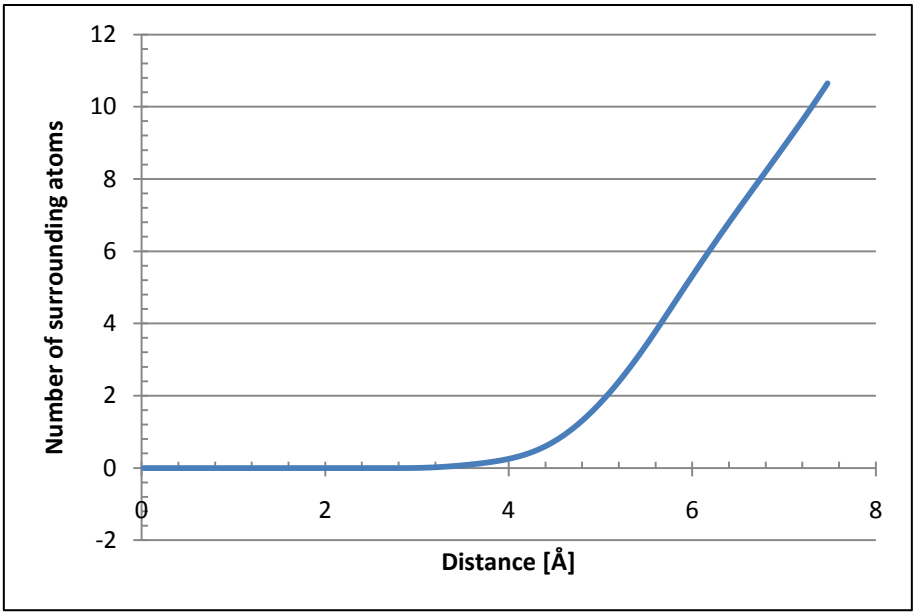


**Figure 10-10: Number of surrounding carbon atoms ($CO_2$) around nitrogen (MDEA)**

To investigate affinity of carbon dioxide for alcohol groups in MDEA, pair correlation function between oxygen from alcohol group and carbon from carbon dioxide was also calculated which is shown in Figure 10-11.

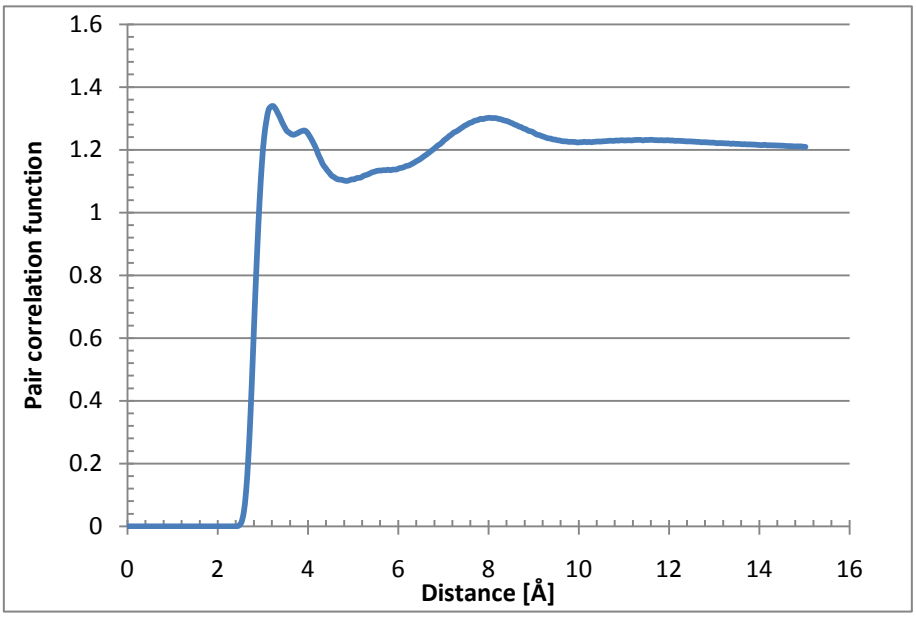


**Figure 10-11: Oxygen-Carbon pair correlation function between MDEA and $CO_2$ molecules**

In this figure, three maxima exist. Positions of the first and second maxima are very close to each other and also close to the minimum L-J potential distance ($r_{\text{min. } pot.}$) for O-C pair which is equal 3.286 Å. These two peaks are of the similar origin. Due to the very small separation

between the first and second maxima - which is actually only 0.7 Å - they cannot considered being completely independent. Most probably they come from combination of direct and indirect short range interactions. This means the first peak is due to direct interactions between oxygen-carbon pair, while the second peak may just represent indirect effect of some other carbon atoms in vicinity of the oxygen but slightly further compared to the first group. This should not be counted as a new shell meaning that both peaks should be treated as a single shell. These two peaks reflect an average structuring/packing of $CO_2$. Such a molecular structuring might happen to relocate the carbon dioxide molecules around the oxygen to find the most favorable position and orientation. Consequently, the first and second peaks together represent first shell of carbon distribution around oxygen atom and the third peak illustrates the second atomic shell. As a result, to find the quantity of atoms within the first shell, integration of pair correlation function was performed to the second minimum in the Figure 10-11. This minimum is located at 4.825 Å. Calculated coordination number for the first shell amounts to 2.3491 which is shown in Figure 10-12. On the other hand, to calculate quantity of surrounding carbon atoms in the second shell, integration of pair correlation function has to be extended to the third minimum which is far at 9.975 Å. This integration results in 25.486 carbon atom around oxygen in alcohol group (Look at Figure 10-12). The above mentioned, signify strong affinity of carbon from carbon dioxide for oxygen from alcohol groups which gives rise to the formation of two separate atomic shells around oxygen.

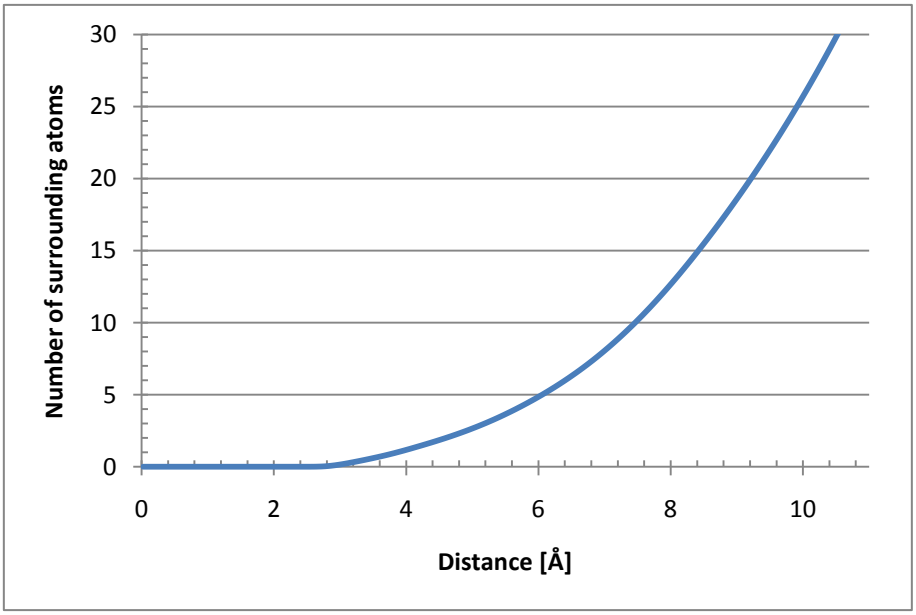


**Figure 10-12: Number of surrounding carbon atoms ($CO_2$) around oxygen (MDEA)**

Apart from intermolecular interactions, molecular structure can impose some geometric constraints on the neighboring molecular distribution. To elaborate, in the case of aforementioned N-C pair between MDEA and carbon dioxide, the latter cannot surround nitrogen within a very close distance; however they are highly attracted by their significant opposite partial charges. This is because of the structural limitation around nitrogen atom in MDEA molecule. As we know, nitrogen in MDEA is connected to three branches so that at least two of them are quite long. These branches are $-CH_3$ and $-(CH_2-CH_2-OH)_2$ which are illustrated in Figure 10-13. In this sense it is physically impossible for carbon dioxide molecules to form the first atomic shell around nitrogen within very short radii. That is why position of the first shell is fairly far (5.525 Å) in Figure 10-9.

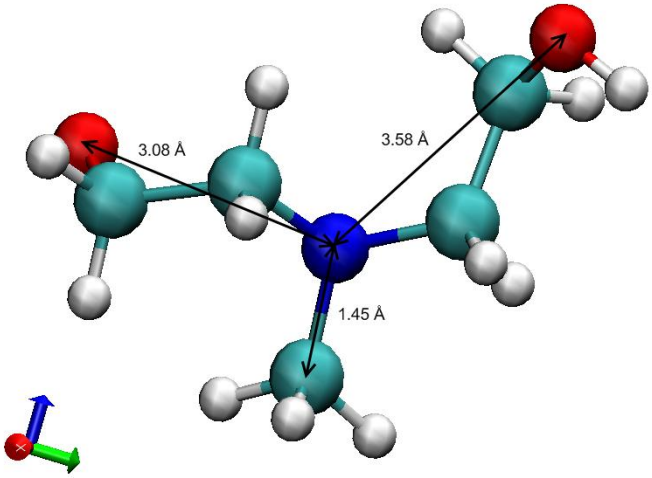


**Figure 10-13: N-O and N-C branches in MDEA molecular structure**

In contrary, such a limitation does not exist for carbon dioxide to surround the oxygen in alcohol group. Oxygen atoms are located at the end of two long tails of MDEA and it is quite feasible for carbon dioxide molecules to approach them. This is what was observed by finding the first shell very close to oxygen (3.925 Å) which is illustrated by Figure 10-11. Consequently, it sounds reasonable to conclude that central nitrogen in addition to oxygens of alcohol groups are active sequences of MDEA for absorption of carbon dioxide.

As the simulation progressed, an agglomeration of carbon dioxide was observed around the piperazine rings. This is obvious from Figure 10-7 (d). To be able to illustrate more details of carbon dioxide agglomeration around PZ molecules, one close-up snapshot from time section 21.16 ns was provided in Figure 10-14.

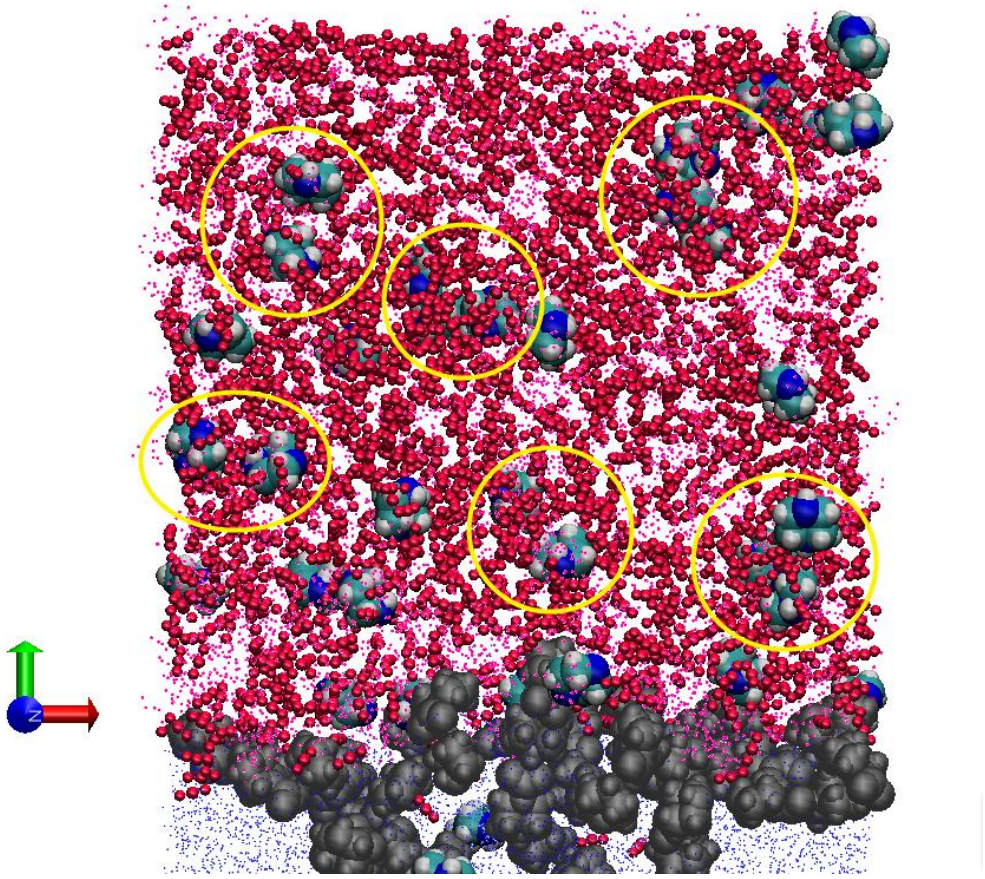

**Figure 10-14: Agglomeration of carbon dioxide around PZ molecules**

Such an agglomeration can be explained based on the strong affinity of $CO_2$ for amine groups in piperazine rings and thus expected. It has been already proved by other researchers that PZ accelerates absorption of carbon dioxide and increases solubility of $CO_2$inside the amine solution. To quantify the observations in Figure 10-14, pair correlation function between nitrogen of each amine groups in PZ molecule and carbon atom from carbon dioxide was calculated. Subsequently quantity of surrounding carbons (from $CO_2$) around the nitogens was obtained. Results from this part are presented in Figure 10-15 and Figure 10-16.

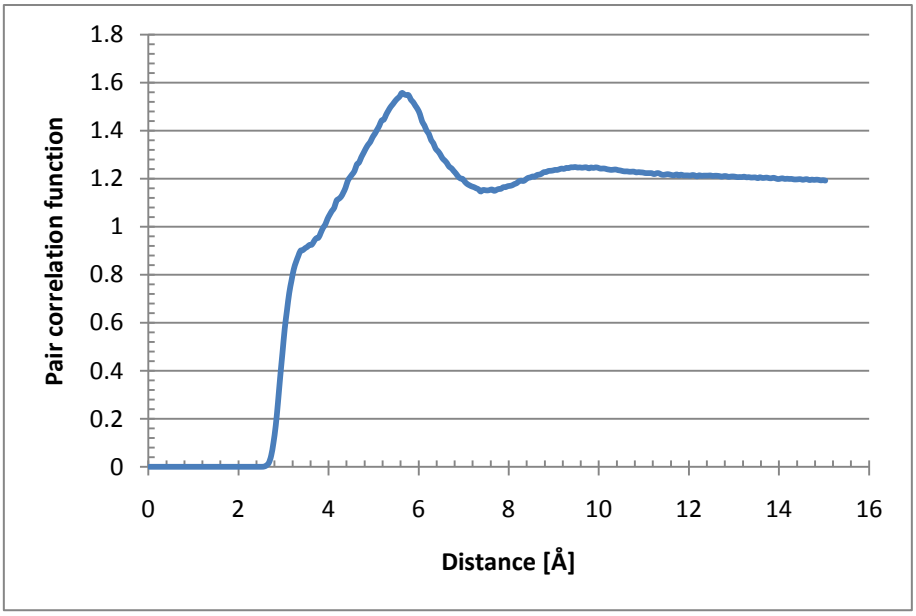


**Figure 10-15: Nitrogen-Carbon pair correlation function between PZ and $CO_2$**

Pair correlation function in Figure 10-15 illustrates one maximum which happen at 5.625 Å possessing magnitude of 1.5563. Small bulge happens at 3.325 Å before the first maximum which is close to the minimum L-J potential distance for N-C pair ($r_{min.\ pot.} = 3.415$ Å). Corresponding minimum occurs at 7.375 Å which is equal to 1.1459. As we see, there is only one layer of surrounding $CO_2$molecules around each nitrogen in PZ ring. Considering that nitrogen in amine group is highly electronegative (approximately -0.58 [e]), strong electrostatic interaction between this pair is expected. Integration of the pair correlation function to the first minimum amounts 10.2391 which is clearly consistent with $CO_2$accumulation around PZ molecules observed in Figure 10-14. Integration of pair correlation function is presented in Figure 10-16.

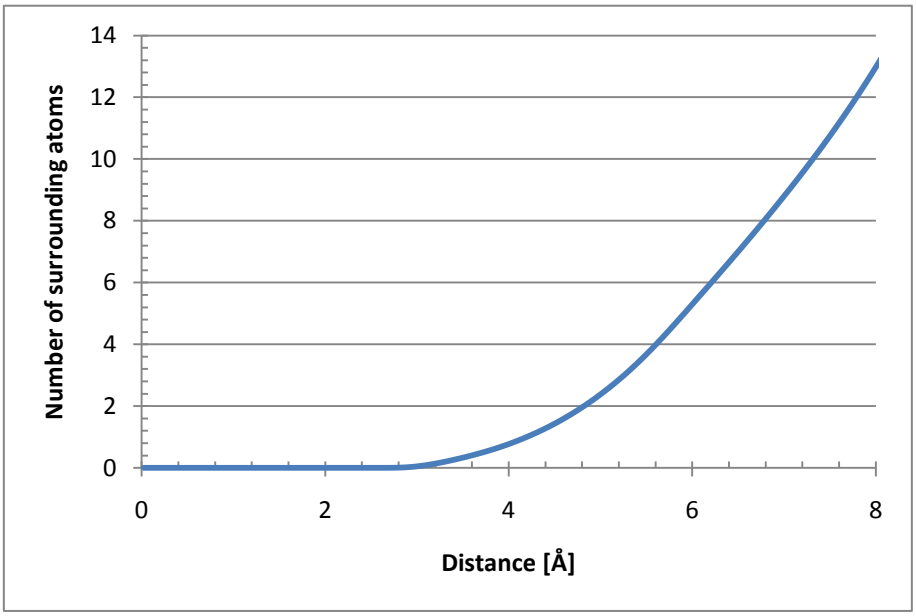

**Figure 10-16: Number of surrounding carbon atoms ($CO_2$) around nitrogens in PZ ring**

For this reference system, hydrogen bonds network was also studied. Considering existence of liquid carbon dioxide in this system providing a suitable field for MDEA and PZ to spread through that, following hydrogen bond distribution was obtained. Again, geometric definition of the hydrogen bonds was used. Distance and angle cut-off were set to be equal 3Å and 24° respectively. Moreover, VMD scan was performed over the last 13000 configurations of the system one time for water molecules as donor and another time as acceptor. Results are presented in Table 10-3.

**Table 10-3: Average number of hydrogen bonds per simulation frame**

| Molecular Pair | H2O-MDEA | H2O-PZ | H2O-PZH | H2O-PZCOO |
|---|---|---|---|---|
| Number of Hbond | 52.87 | 3.20 | 40.84 | 133.88 |

Data from this table demonstrate coexistence of charged species (PZH and PZCOO) with water is favorable so that they can build considerable number of hydrogen bounds with surrounding water molecules. To compare with reference system No.1, only the average number of hydrogen bonds between water and MDEA has changed significantly and shows 50% decrease. This might be explained based on different structures of the water-MDEA interface in these two systems. Comparison between Figure 10-2 (b) and Figure 10-7 shows that some parts of the interface in reference system No.2 are shielded by PZH and PZCOO so that MDEA molecules are not physically accessible for water.

## 10.3 Reference system No.3

In this reference system, gaseous carbon dioxide was exposed at 60 bar to the aqueous amine solution (Look at Section 9.1.1.3). Considering affinity of $CO_2$towards MDEA and PZ (demonstrated clearly by reference system No.2), and on the account of having carbon dioxide in gas phase, absorption of $CO_2$was expected to be detectable in reference system No3. Simulation was run for 20.70 ns. Carbon dioxide molecules started to show their affinity towards the interface where MDEA and PZ molecules had been agglomerated. Absorption process was observed, so that $CO_2$ molecules clustered around the amine groups in PZ rings (recall same phenomenon from reference system No.2). $CO_2$ was absorbed into the solution

and stayed inside the MDEA phase. Evolution of the absorption process was monitored during the simulation which is illustrated in Figure 10-17. Same molecular representations as for Figure 10-7 have been used here.

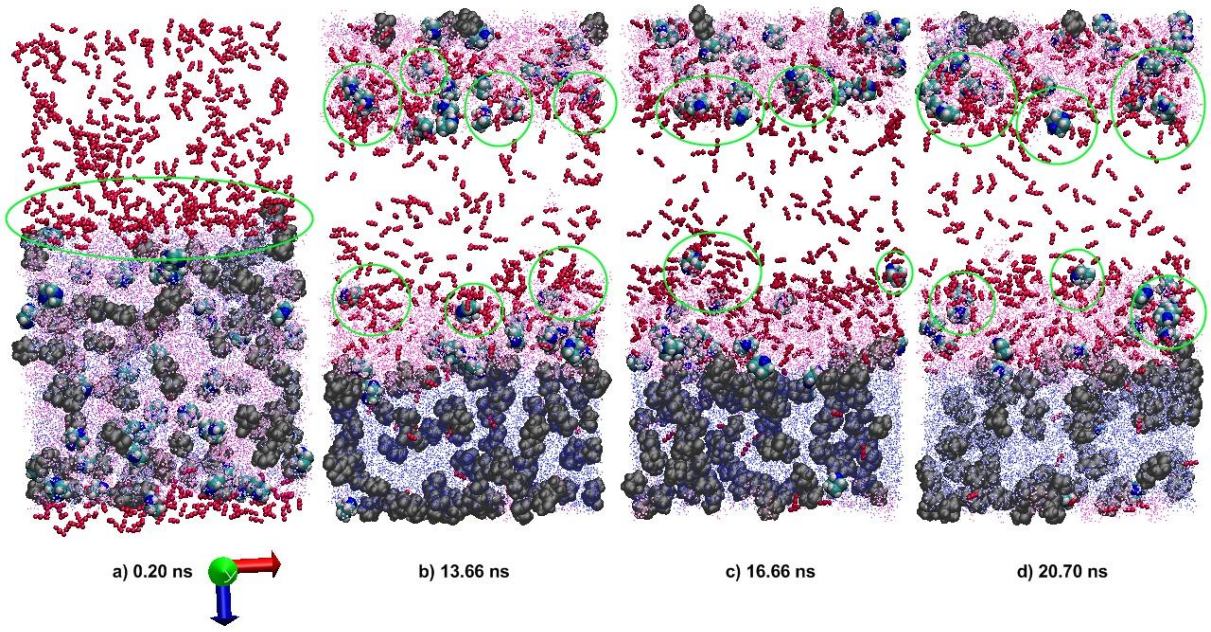


**Figure 10-17: X-Z cross-section of the reference system No.3 which illustrates process of $CO_2$ absorption**

As one can see, once the simulation was initiated, carbon dioxide molecules started to invade the interface where high concentration of amine was available for them (Figure 10-17 (a)). As the simulation progressed, separation of MDEA and water occurred due to the hydrophobic character of MDEA. This kind of separation resulted in formation of a new interface. So that two MDEA-water and MDEA-$CO_2$(gas phase) interface were formed in the system. This phase separation was expected based on what had been observed in reference system No.1 and No.2. In almost the same way, hydrophobic-hydrophilic characteristics of piperazine species divided them between MDEA phase and water bulk, so that PZ molecules stayed inside MDEA and PZH in addition to PZCOO preferred water (Figure 10-17 (b)). After 13.66 ns of simulation, PZ molecules were observed to position themselves along the $CO_2$-MDEA interface (gas-liquid interface) so that carbon dioxide molecules started to cluster around PZ rings. This is a very informative observation consistent with theories of carbon dioxide absorption, and at the same time in line with experimental results. As explained earlier in Section 3.2.1, absorption of $CO_2$ by MDEA is rate limiting, so that there will be "queues" of

$CO_2$molecules behind the gas-liquid interface in the gas side waiting to enter the interface[13]. On the other hand, PZ has high rate of reaction with carbon dioxide which leads to the formation of PZCOO (remember Equation (3-11)). As such, PZ removes $CO_2$molecules (in the form of PZCOO) from interface and carry them away into the liquid bulk[14]. This is a process parallel to diffusion of carbon dioxide into the interface and further. The conversion to carbamate is exothermic and will also have an immediate effect of expanding the local environment in order that give space for the newly formed (larger and more complex) carbamates. The increase in temperature as well as the reorganizations will significantly affect the efficient average diffusivity of carbon dioxide into the interface and through that.

High concentration of $CO_2$molecules behind the interface is obvious from Figure 10-17 (a). In addition, carbon dioxide clusters were observed around PZ molecules during entire simulation (indicated by green circles in Figure 10-17 (b), (c) and (d)). This signifies $CO_2$ affinity for PZ molecules leading to the formation of PZCOO. Indeed, $CO_2$ agglomeration around PZ rings is one stage prior to starting the chemical reaction between PZ and $CO_2$. The chemical reaction itself cannot be simulated by molecular dynamics; however such a complex simulation for chemical reaction can be performed using quantum chemistry to provide some insight into the reaction.

At the end, observation of dissolved PZH and PZCOO inside the water bulk demonstrates the final stage of $CO_2$absorption from gas-liquid interface into the liquid bulk. Recall from Section 3.4.1, that importance of piperazine carbamate was explained for absorption of $CO_2$ based on experimental data (Bishnoi and Rochelle 2000; Idem et al. 2009). This is what was observed here. To summarize, current research was able to demonstrate overall process of carbon dioxide absorption based on its own observations and add further proofs of the facts which are related to this process.

Furthermore, it has been already emphasized by other researchers (Samanta and Bandyopadhyay 2007; Bottinger et al. 2008) that MDEA has a high stoichiometric loading capacity for removal of $CO_2$ (Section 3.3.3 ). This is again what was observed in current simulation. At the end of simulation (time 20.70 ns) quantity of $CO_2$molecules dissolved in the water bulk (blue dotted area in Figure 10-17 (d)), in addition to quantity of those absorbed into the MDEA phase (magenta dotted area in Figure 10-17 (d)) was estimated by VMD.

[13] Also look at Figure 10-17 (a) where PZ molecules are not positioned along the interface yet and long queues of $CO_2$molecules were formed behind the gas-liquid boundary.
[14] Recall all the PZCOO were observed to be inside the water phase.

Results from this estimation are interpreted as a support for the high capacity of MDEA in $CO_2$removal. Compared to 23 $CO_2$molecules observed in the water bulk, 228 $CO_2$molecules were found to be inside the MDEA phase. In other words, 47.11% of total $CO_2$molecules were absorbed into the MDEA phase while at the same time only 4.75% of them dissolved in water. It means that in total, 51.86% of the carbon dioxide molecules were absorbed from gas phase into the amine solution after 20.70 ns simulation.

To quantify what mentioned above, pair correlation function and density profile of the system were calculated. The former demonstrates clustering of carbon dioxide around piperazine ring (Figure 10-18) and the latter gives illustration for high capacity of MDEA in removal of $CO_2$(Figure 10-22).

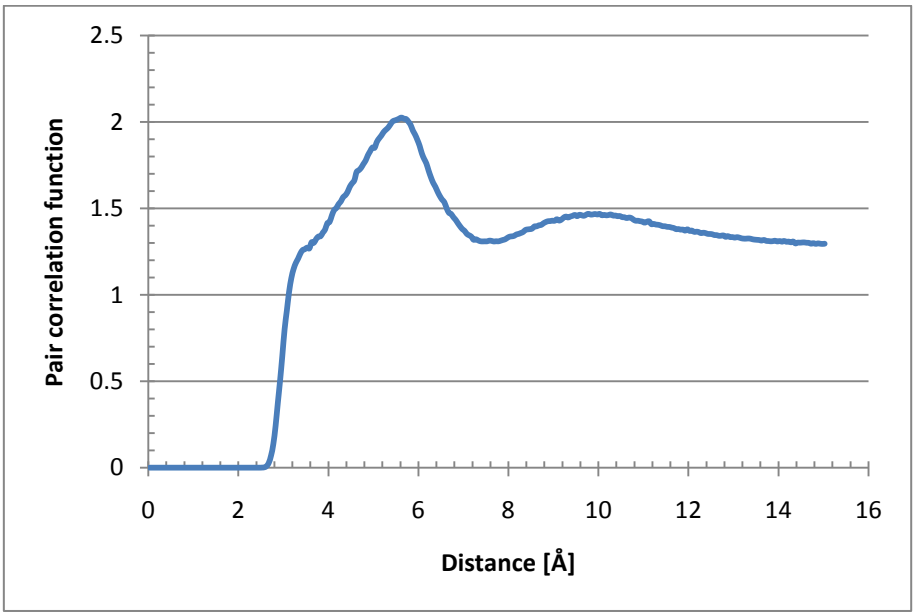


**Figure 10-18: Nitrogen-Carbon pair correlation function between PZ and $CO_2$**

Shape of the pair correlation function for N-C pair between PZ and carbon dioxide in reference system No.3 is slightly similar to the one belonging to reference system No.2. However, they are different in terms of magnitude of the peak and minimum in addition to the position of them. Figure 10-18 demonstrates one peak at 5.625 Å which its magnitude equals 2.0242. Before the first maximum, there is a bulge at 3.325 Å which is close to the minimum L-J potential distance ($r_{min.\ pot.}$=3.415 Å). The minimum occurs at 7.675 Å possessing magnitude of 1.3075. Quantity of surrounding carbon atoms from carbon dioxide molecules around nitrogen was also calculated by integrating the pair correlation function to the first

minimum which amounted to 3.3924. Result for coordination number is illustrated by Figure 10-19.

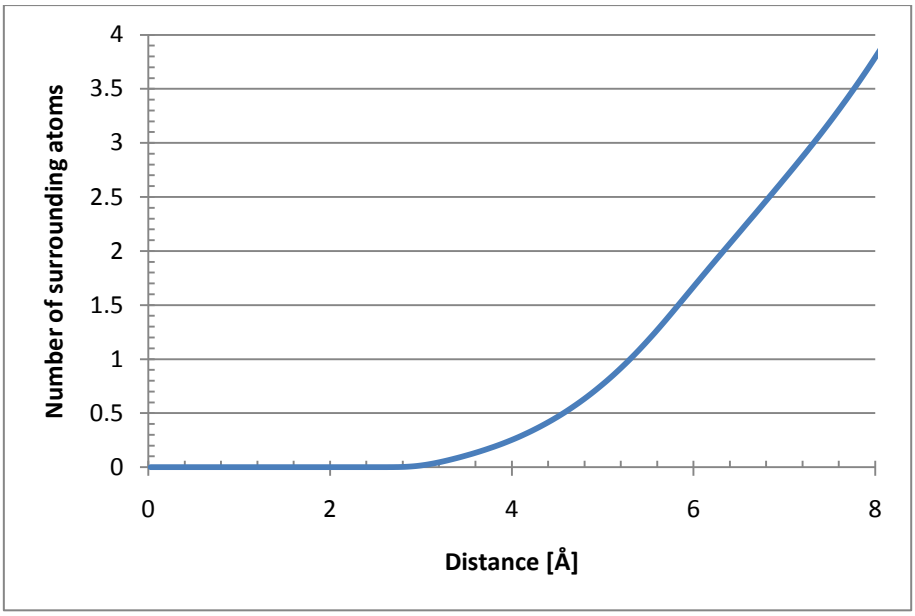


**Figure 10-19: Number of surrounding carbon atoms ($CO_2$) around nitrogens in PZ ring**

Comparing with reference system No.2, the bulge and the maximum occur in the same radius but their magnitude in current system has larger values than the reference system No.2. Position of the minimum point in reference system No.3 is slightly shifted to the right while it possesses larger value at the same time.

The most important difference - in this comparison - is found in the coordination numbers which show quantity of surrounding carbon atoms in the first shell around nitrogens of PZ. Coordination number for reference system No.3 is much smaller than previous system which is 3.3924 against 10.2391 respectively. However this was completely expected and reasonable considering reference system No.2 contains high pressure liquid carbon dioxide (at 100 bar) with 2047 carbon dioxide molecules while reference system No.3 contains 484 carbon dioxide molecules at the gas phase (60 bar). It is clear that fewer number of carbon dioxide molecules are available in reference system No.3 for electronegative nitrogens of PZ to absorb them. Moreover, this comparison signifies importance of pressure for absorption of carbon dioxide in amine systems. This conclusion is also consistent with experimental determinations.

For the sake of simplicity, pair correlation functions and coordination numbers of the reference systems No.2 and No.3 have been compared in Figure 10-20 and Figure 10-21.

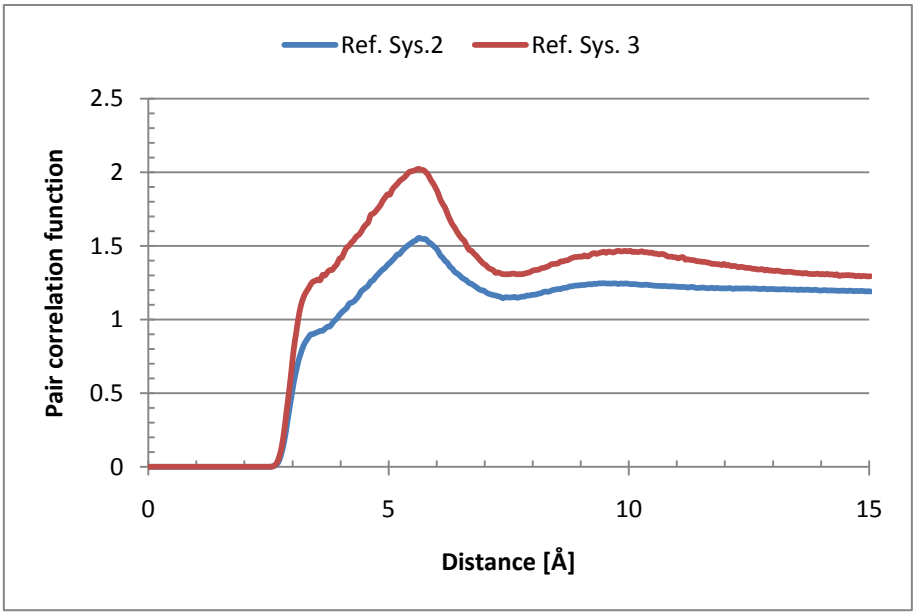


**Figure 10-20: Comparison for N-C pair correlation function between ref. sys. No.2 and No.3**

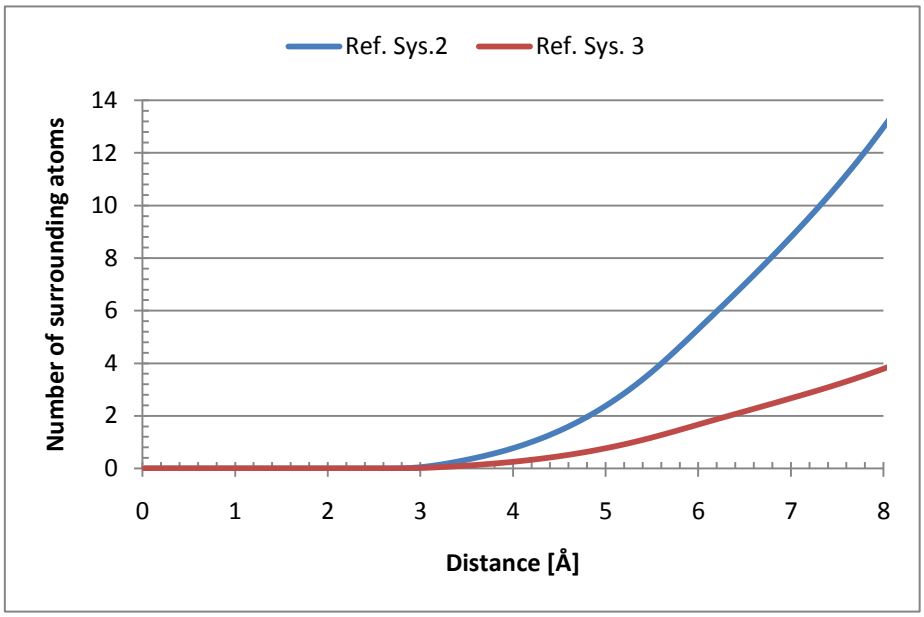


**Figure 10-21: Comparison for N-C coordination number between ref. sys. No.2 and No.3**

To illustrate further proof for the high loading capacity of MDEA in bulk removal of carbon dioxide, in addition to previously observed molecular distribution of the system (bulk and interface), density profile of the reference system No.3 was calculated for the last 1000 configurations of simulation which is presented by Figure 10-22.

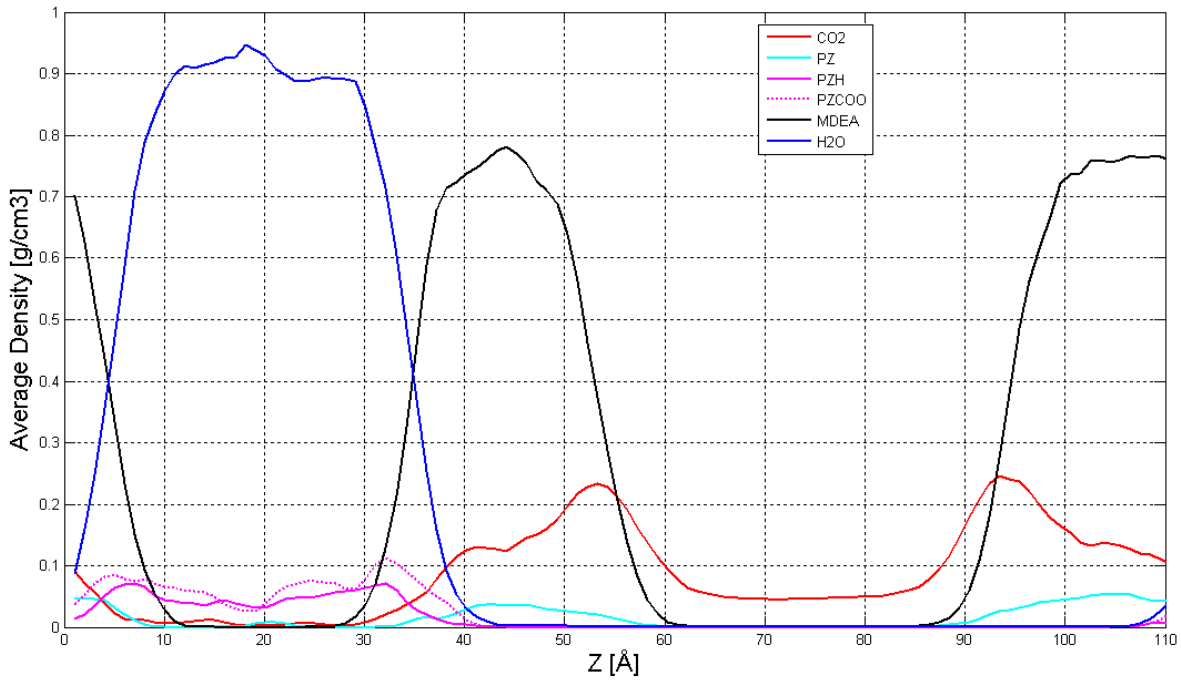


**Figure 10-22: Density profile of the reference system No.3**

As we can see, the above mentioned qualitative explanations regarding absorption of carbon dioxide is highlighted by density profile of the system. In other words, visual observations of the system are completely consistent with quantitative results from calculation of density profile. According Figure 10-22, high concentration of carbon dioxide exists simultaneously with high concentration of MDEA between 30-60 Å and 90-110 Å of the simulation box signifying high loading capacity of MDEA for $CO_2$removal. At the same place, system experiences highest concentration of PZ which is positioned along the gas-liquid interface. On the other hand, $CO_2$concentration is significantly low inside the water bulk between 10-30 Å while PZH and PZCOO have their highest concentration inside the water bulk along 0-40 Å.

Since in reference system No.3 gas-liquid interface was formed for the first time, interfacial tension (IFT) was calculated to show surfactant effect of the amine solvents. Surfactants are *amphiphilic* molecules which possess both hydrophobic-hydrophilic moieties (Pashley and Karaman 2004). That is why they can stay on the interface. Surfactants decrease the interfacial tension of the system therefore cohesion-adhesion of the interface is diminished by them, meaning less energy or mechanical work is needed to move the interface. In other words, lower interfacial tension leads to a thicker and rougher interface. This may give rise to

some undesired pitfalls in amine systems such as foaming phenomenon (discussed in Section 3.4.4).

For reference system No.3 interfacial tension (IFT) was calculated based on Equation (10-2). This equation approximates the interfacial tension based on pressure tensor (Kuznetsova and Kvamme 2002).

$$\gamma_{int.} = 0.5 \times \overline{h_z}\{P_z - 0.5 \times [P_x + P_y]\} \quad \textbf{(10-2)}$$

Where $\gamma_{int.}$ is interfacial tension $[N/m]$, $\overline{h_z}$ is the system length in direction normal to the interface $[m]$, and $P_x$, $P_y$ and $P_z$ are the average system pressures $[N/m^2]$ in x, y and z directions respectively .

In current system IFT was calculated for the last 600 intermediate averages of MD simulation which corresponds to the last 3,000,000 steps of the simulation. Results from this calculation are plotted in Figure 10-23.

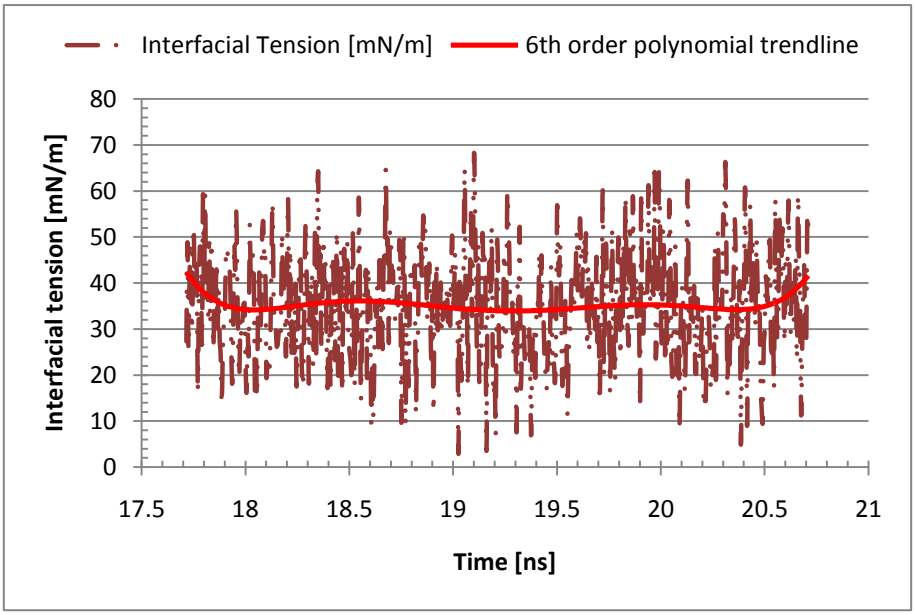


**Figure 10-23: Interfacial tension of the system over the last 600 intermediate averages of the simulation**

As seen in Figure 10-23, the total statistical average of the IFT values was equal to 35.2±0.1 mN/m during the last 3 ns of simulation. Results for IFTs contain uncertainty due to the highly dynamic nature of the interface in amine systems. Such a dynamics is also detectable in this reference system and can be seen as capillary waves on the interface in

Figure 10-17. The simple modeling used for calculation of IFTs in current thesis (Equation (10-2)) is only precise enough for the flat interfaces. Nevertheless, obtained results for this system is still in the range of experimental determinations and can be used qualitatively to a certain degree for comparison between different reference and primary systems to show the surfactant effect of the amine solvents.

## 10.4 Reference system No.4

Reference system No.4 did not contain amine solution and the liquid phase only contained the pure water. On the other hand, the gas phase contains mixture of 11 mol% $CO_2$-89 mol% $CH_4$. Thermodynamic condition was set to be similar with primary system (T=298.173 K, P=10 MPa) so that results for solubility of $CO_2$and $CH_4$ inside pure water can be compared with those related to the primary system. This comparison will demonstrate the positive role of activated amine solution in absorption of carbon dioxide by enhancing the $CO_2$solubility in water. At the same time it will show negative effect of such a solution in undesired trapping of $CH_4$.

Initially five-site methane model was used for simulation of current reference system. But after 10.85 ns, decision was made to replace the five-site model of methane with the one-site OPLS model due to the extraordinary observed solubility of methane inside water. In other words, five-site $CH_4$model was not able to replicate true solubility of methane in water in comparison with carbon dioxide. So that calculated solubility of methane in water after 10.85 ns was slightly larger than the one for carbon dioxide, while we know from experimental determinations that solubility of $CO_2$ should be much higher than $CH_4$. Therefore, results from simulation based on the five-site methane model could not be reliable.

Time evolution of the system is presented by Figure 10-24.

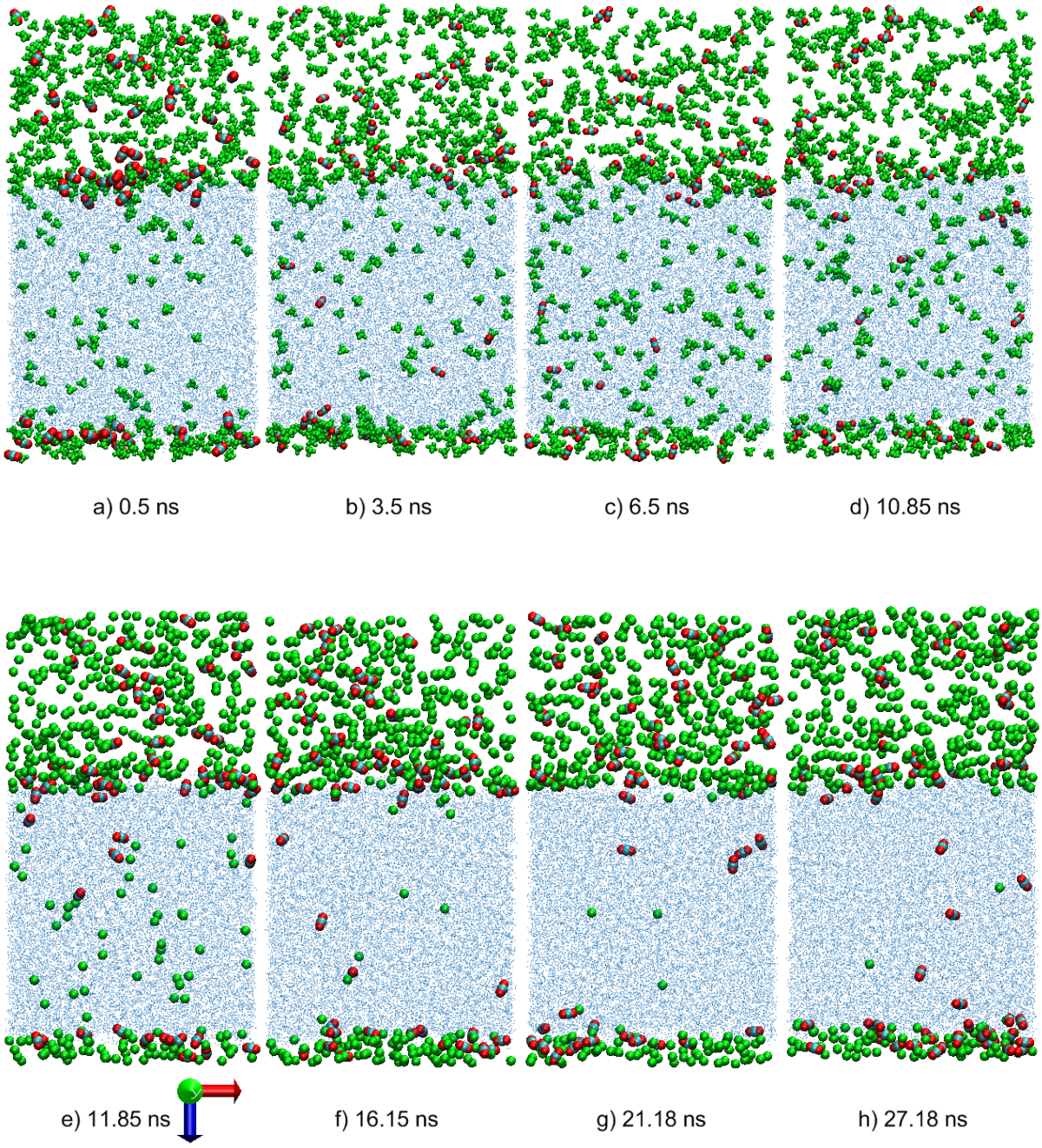


**Figure 10-24: Time evolution of the reference system No.4**

In this figure, methane molecules (either 5-site or one-site) are represented by green balls. Small red bars indicate the carbon dioxide molecules and blue dotted area demonstrates the water bulk. First four figures (Figure 10-24 (a) – (d)) illustrate the system containing 5-site methane model and the last four figures (Figure 10-24 (e) – (h)) show the system containing one-site methane model. Considering the first four pictures, solubility of methane molecules inside the water is unusually high even at the beginning of simulation (Figure 10-24 (a)), while at the same time there is no $CO_2$ dissolved in water and we know from

experimental determinations that solubility of $CO_2$ in pure water should be higher than the one for methane. When new one-site methane model was used instead of the 5-site model, solubility of methane fell down dramatically (Figure 10-24 (e) compared to Figure 10-24 (d)). After a short period of equilibration phase for the system following replacement of the 5-site methane model with the one-site model, system started to replicate more realistic (compared to solubility of real methane in real water) solubility of methane inside the water bulk, so that at the end of simulation (27.18 ns) only two methane molecules existed inside the water. Relative solubility of carbon dioxide and methane ($Solub._{CO_2}/Solub._{CH_4}$) was calculated after finishing the simulation at 27.18 ns. Result was equal to ~17.16 showing significantly higher solubility of carbon dioxide in water compared to methane, as we did know from independent experimental observations.

To be able to quantify solubility of the gaseous components inside the water solution after using the one-site methane model, density profile of the system was determined for the last 1000 configurations of the system. Density profile of the reference system No.4 is shown by Figure 10-25.

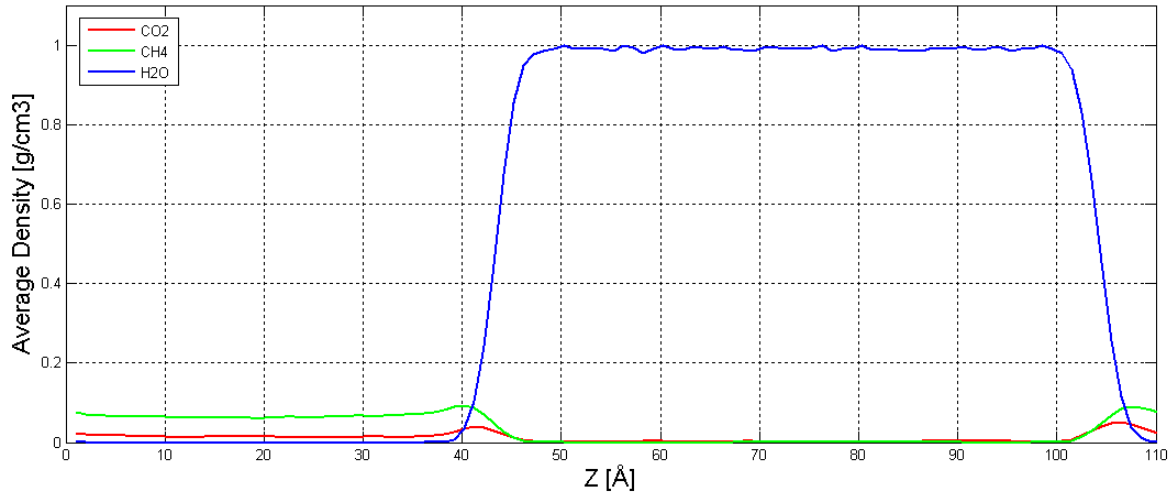


**a)**

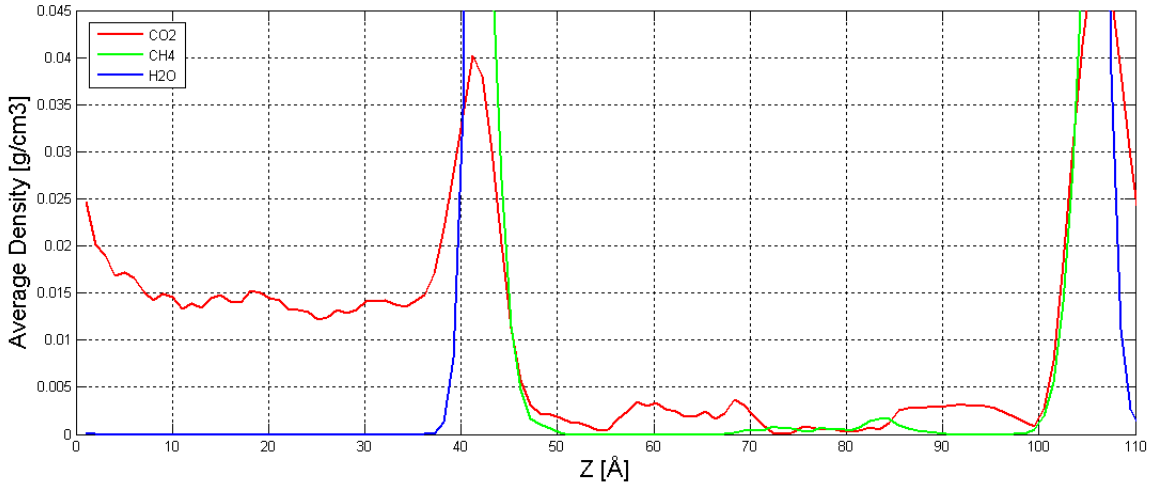


**b)**

**Figure 10-25: Density profile of the reference system No.4 (a) Overall view (b) magnified view**

As it is obvious from this figure, carbon dioxide and methane possess low solubility inside the pure water in thermodynamic conditions of interest (Figure 10-25 (a)) so that solubility of methane is much lower than the one for carbon dioxide (Figure 10-25 (b)).

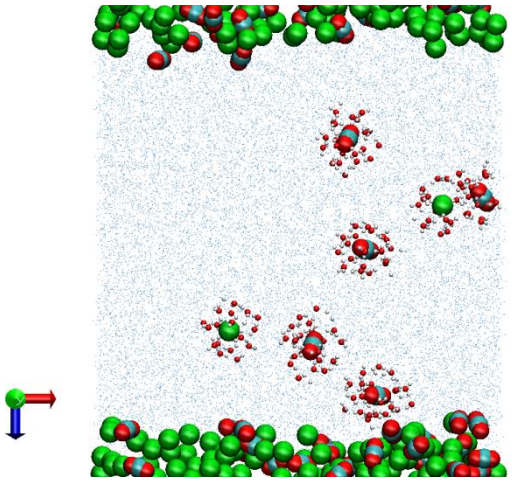

**Figure 10-26: $CH_4$/$CO_2$-water correlation**

Furthermore, to demonstrate correlation of the one-site methane model with water molecules (Figure 10-26), pair correlation function as well as coordination number of methane-water pair were calculated and compared with other simulation studies of water-methane system. Figure 10-27 compares pair correlation function for one-site methane model with the one for 5-site model in this work. In addition, Figure 10-28 illustrates pair correlation function from an independent simulation (Junfang and et al. 2009).

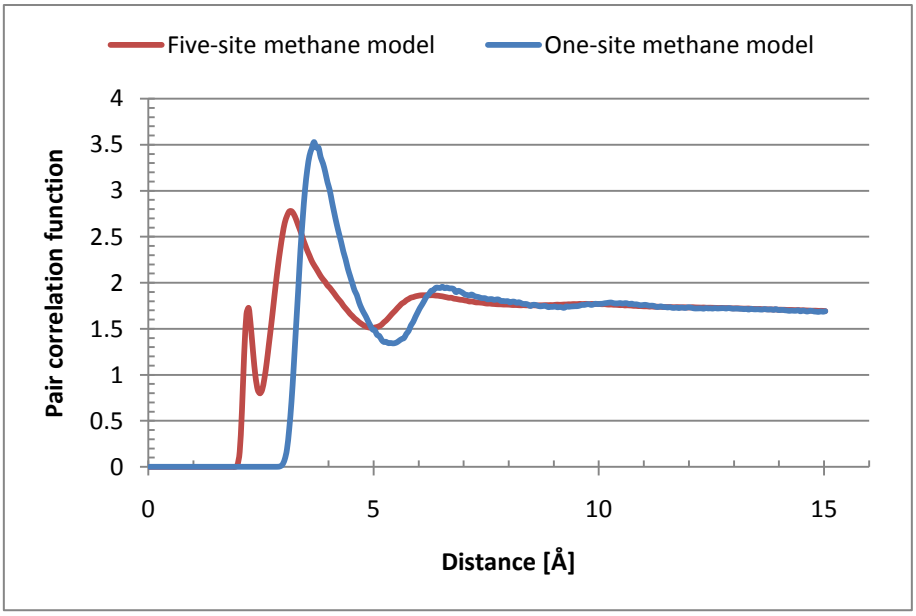


**Figure 10-27: Methane(Carbon)-water(Oxygen) pair correlation functions from current thesis**

Compared to Figure 10-28, Figure 10-27 demonstrates unreliability of five-site methane model again, while at the same time it signifies true correlation of one-site model with surrounding aqueous environment.

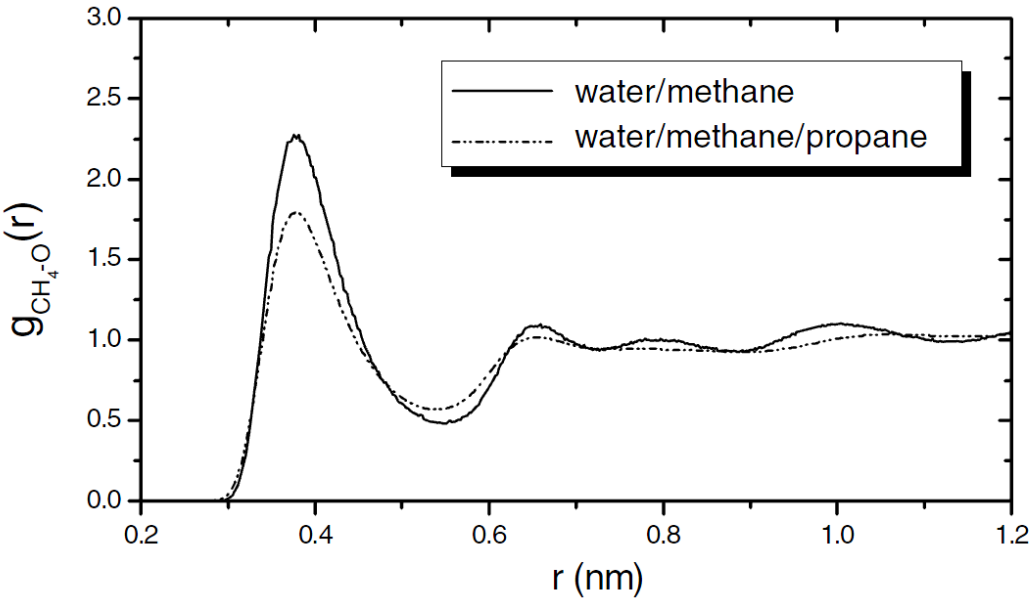


**Figure 10-28: Methane-water (Oxygen) pair correlation function (Junfang and et al. 2009)**

Similarly, Table 10-4 compares one-site and 5-site methane models with independent researches from literature using coordination numbers in water-methane system.

**Table 10-4: Methane-water coordination numbers**

| Current simulation | | Other simulations | | Hydrate (Sloan 1998) | |
|---|---|---|---|---|---|
| **One-site $CH_4$** | **Five-site $CH_4$** | **(Junfang and et al. 2009)** | **(Swaminathan et al. 1978)** | **Type I (small cavity)** | **Type II (small cavity)** |
| 20.72 | 0.6325 | 19.1 | 19.35 | 20 | 20 |

According information given in Table 10-4, one-site methane model reproduces a great degree of accuracy for coordination number.

Consequently based on what presented above, reliability of one-site methane model was found to be convincing. Hence, this model was chosen for calculation of methane solubility as well as the interfacial tension when they are going to be compared with primary or other reference systems.

To be able to express surfactant effect of the amine solvents on the interfacial tension of the gas-liquid system, a proper basis was required. This basis was provided by calculating the interfacial tension for reference system No.4 which does not contain any amine solvent. Consequently, comparison between this reference system with primary and reference system No.3 will be possible, so that influence of amine solvents on the interfacial tension of the system can be explained. Figure 10-29 illustrates interfacial tension for reference system No.4.

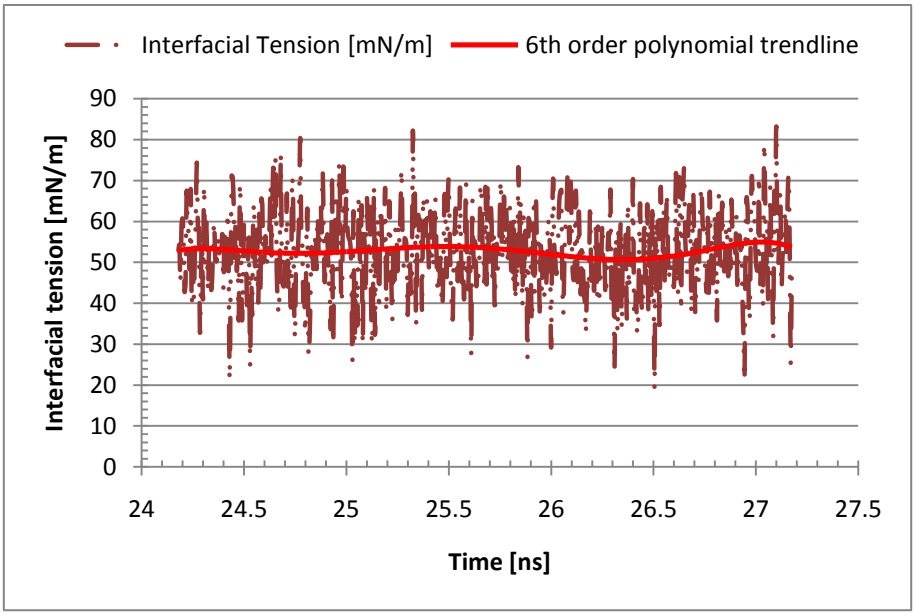


**Figure 10-29: Interfacial tension of the system over the last 600 intermediate averages of the simulation**

Interfacial tension was calculated by Equation (10-2) over the last 600 intermediate averages, corresponding to the last 3 ns of simulation. The total statistical average was equal to 52.8±0.1 mN/m which is obviously higher than the one for reference system No.3 (35.2±0.1 mN/m). As explained earlier, reduction in IFT values of reference system No.3 compared to current system is due to the surfactant effect of amine solvents.

## 10.5 Primary system

In this research, the primary system was used to obtain insight into phenomena occurring during the industrial absorption of carbon dioxide from a simplified mixture of natural gas in which its impurity contents were disregarded. Moreover, our goals included the investigation on to undesired trapping of methane molecules during process of $CO_2$ absorption. Therefore, aqueous piperazine activated MDEA solution at T=298.173 K was brought into contact with gaseous mixture of 11 mol% $CO_2$-89 mol% $CH_4$ at 10 MPa. In this system, simulation was run for 41.44 ns in total. Results were used to investigate distribution of gaseous components inside the amine solution and to understand the mechanisms responsible for interaction of $CO_2$ and $CH_4$ with amine solvents in the liquid phase.

As in the reference system No.4, five-site methane model was used initially in the primary system but after 25.14 ns, this model was replaced by the previously described OPLS one-site methane model in Section 10.4. One-site model was quite successful in reproducing methane behavior in a variety of other studies as well. Time evolution of the system after switching to

one-site methane model is shown by Figure 10-30. Molecular representations are similar to Figure 10-17 and Figure 10-24 for reference systems No.3 and No.4 respectively.

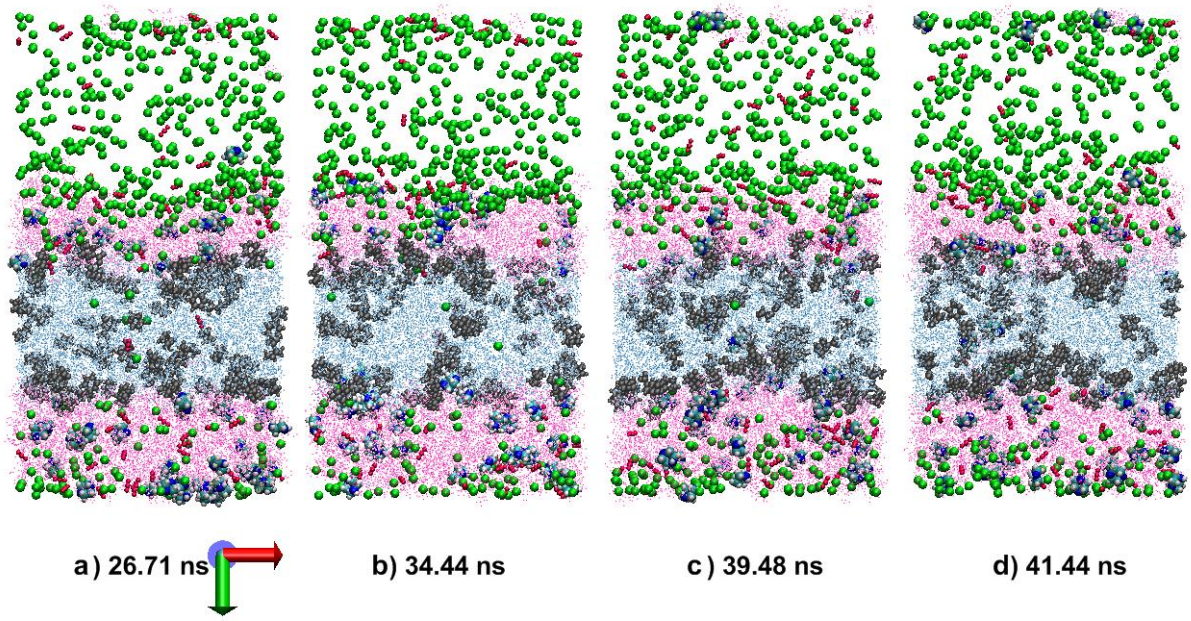


**Figure 10-30: Time evolution of the primary system for the last 14.73 ns of simulation**

As one can see, the phase separation between water and MDEA occurred in this system similar to reference systems No.1, No.2 and No.3. The distribution pattern was exhibited by the piperazine species (PZ, PZH and PZCOO) matched those obtained in the first three reference systems and agreed well their hydrophobic-hydrophilic characteristics. Visual observations during the last 14.73 ns of simulation demonstrated essentially the same process of carbon dioxide absorption as in the reference system No.3 (Look at Figure 10-30 (a)-(d)). The only difference in this system was much lower concentration of $CO_2$ due to the dominating presence of methane as the main constituent of natural gas. Once again, MDEA demonstrated its high loading capacity for removal of $CO_2$, since a large amount of carbon dioxide absorbed into the MDEA phase during this time. To quantify the molecular distribution of the liquid phase, density profile of the primary system was calculated for the last 1000 configurations of the simulation and shown in Figure 10-31.

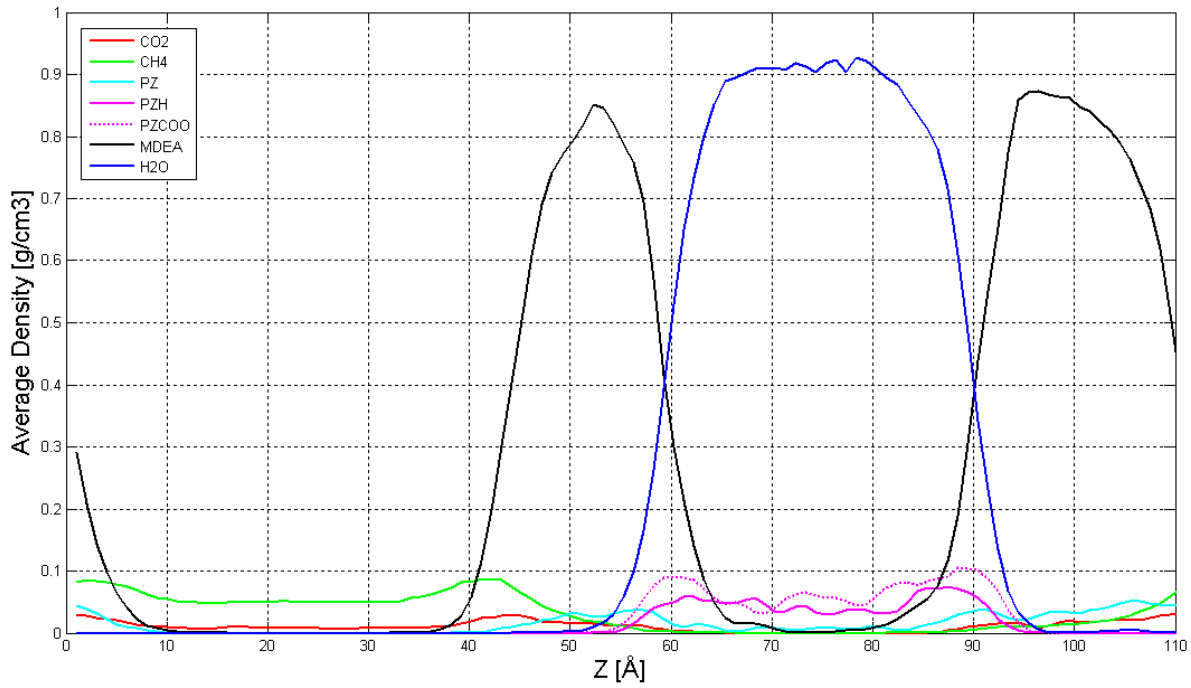


**a)**

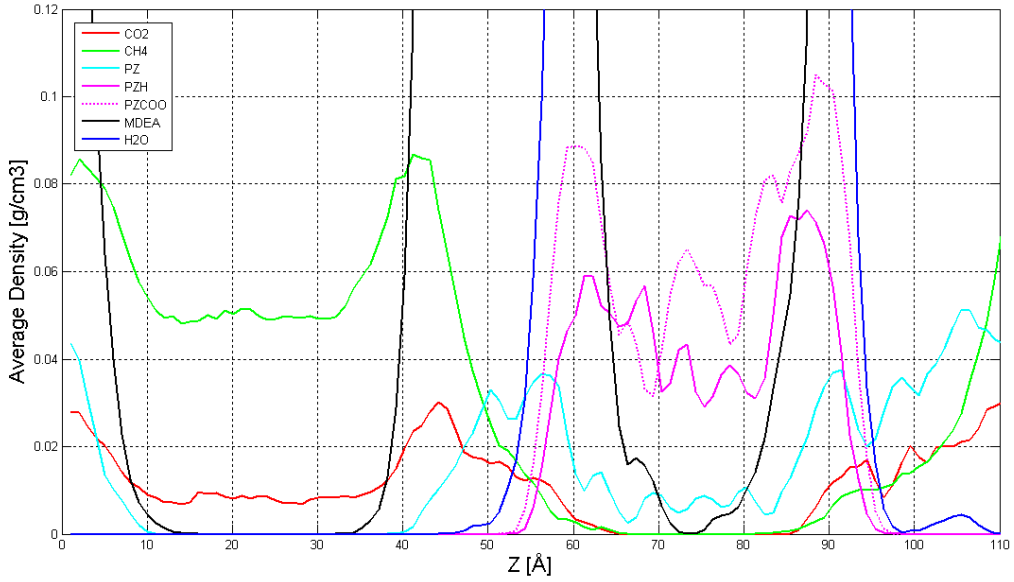


**b)**

**Figure 10-31: Density profile of the primary system (a) Overall view (b) magnified view**

The magnified view of the above density profile shows molecular distribution of the system in more detail. As illustrated, PZ (cyan line) showed a distinct preference for remaining either

along the gas-liquid interface (0-10 Å) or at the MDEA-water interface (40-70 Å and 80-110 Å). This clearly demonstrates the affinity of PZ molecules towards $CO_2$ and illustrates how PZ molecules can potentially interact with carbon dioxide within the gas-liquid interface to produce PZCOO. On the other hand, the distribution of PZCOO (dotted magenta) inside the water bulk (52-98 Å) explains how carbon dioxide molecules are absorbed into the liquid bulk in the form of piperazine carbamate and thus transported away from the interface. At the same time, density profile of the system shows high capacity of MDEA for carbon dioxide loading (look at red line between 0-8 Å, 38-65 Å and 85-110 Å).

One of the most important observations in this thesis was trapping of methane molecules by the activated amine solution. This phenomenon was easily detectable by visual observations (Figure 10-30 (a)-(d)) and density profiles of the system (Figure 10-31). Green line (methane concentration) provides the concrete evidence for trapping of methane into the liquid phase so that high concentration of this molecule is observed inside the MDEA bulk (between 0-5 Å, 40-60 Å and 90-110 Å).

Considering the aforementioned explanations, it was concluded that MDEA not only has a high loading capacity for removal of carbon dioxide but it possesses similar ability to retain methane inside the solution.

The trapping of methane is an undesired phenomenon for the industry, making it technically and economically very important in gas treating plants. Nowadays, tremendous efforts are being made within industrial sector to solve this problem; however the mechanism responsible for this process is not understood yet. As the results of this simulation show, PZ activated solution of MDEA can lead to undesired trapping of methane to a high degree. At the end of simulation (41.44 ns), relative number[15] of methane molecules trapped into the amine solution was measured by VMD and compared with the reference system No.4. It clearly demonstrated the augmentative effect of amine solution for trapping of methane. The same comparison was conducted for the absorbed $CO_2$ molecules to show the effectiveness of activated amine solution for absorption of carbon dioxide. The results are presented in Table 10-5.

[15] For $CH_4$ and $CO_2$this number is calculated from $\frac{\text{quantity of trapped } CH_4 into\ the\ solution}{initial\ quantity\ of\ CH_4\ in\ the\ gas\ phase}$ and $\frac{\text{quantity of absorbed } CO_2 inside\ the\ solution}{initial\ quantity\ of\ CO_2\ in\ the\ gas\ phase}$ respectively.

**Table 10-5: Relative number of $CH_4$ / $CO_2$ molecules trapped / absorbed into the solution, compared between primary and reference system No.4**

| Gas component | Reference system No.4 | Primary system |
|---|---|---|
| Methane | 0.40% | 26.88% |
| Carbon dioxide | 6.56% | 57.38% |

This comparison shows that the aqueous solution of PZ activated MDEA is a good promoter for absorption of carbon dioxide, so that the relative number of absorbed $CO_2$ molecules was enhanced by 50.82% . Similarly, the current activated amine solution contributes heavily to the undesired trapping of methane, in such a way; the relative number of trapped $CH_4$ molecules was increased by 26.48%. Nevertheless, these values emphasize a higher relative absorption of carbon dioxide in comparison with trapping of methane.

Precise understanding of the trapping mechanism needs an independent research; however, this work attempts to provide a clearer view of the problem – which itself never discussed in the literature – and attempts to present certain insights which may be used for further investigations.

As shown in Table 10-5, $CO_2$has higher relative absorption compared to relative trapping of methane into the solution. Although, the solubility of methane in aqueous blends of PZ and MDEA is not available in literature for comparison with the one for carbon dioxide, experimental observations for aqueous MDEA explain higher solubility of carbon dioxide compared to methane consistently (Jou et al. 1998; Xu et al. 1998; Schmidt et al. 2008). The existence of already absorbed carbon dioxide molecules inside the amine solution can increase diffusivity and mobility of methane into the system, so that this higher diffusivity may provide potential events for trapping of methane. As such, in a more general view, it may appear that methane molecules follow the carbon dioxide into the solution.

With this in mind, average number of methane molecules around central atom of carbon dioxide inside the liquid phase was calculated for the last 5 million steps of simulation in primary system (last 25000 configurations of the system). Resulting pair correlation function is plotted in Figure 10-32.

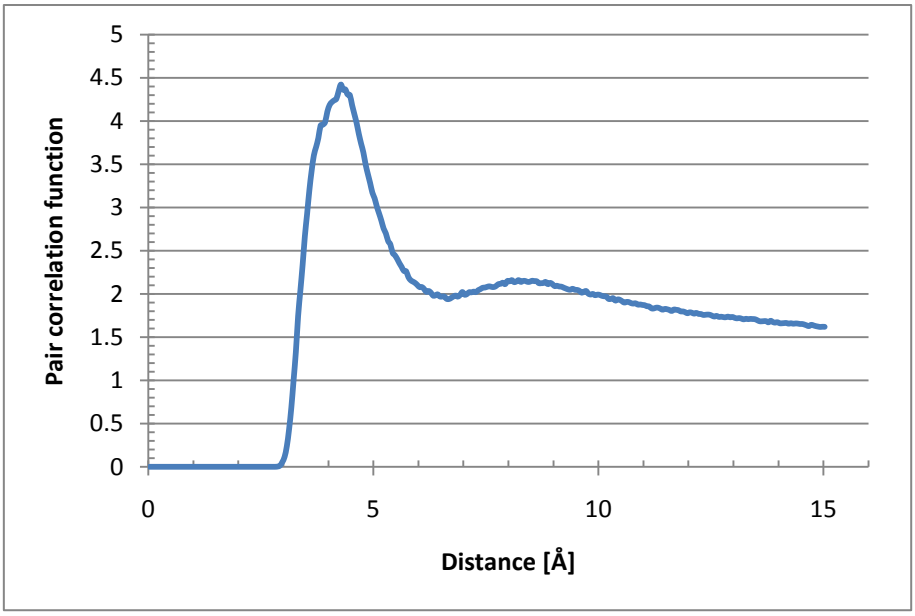


**Figure 10-32: Carbon-Carbon pair correlation function between $CO_2$ and $CH_4$**

As we can see, there is a distinct peak at 4.275 Å, signifying the first shell. This position is slightly beyond the minimum L-J potential distance ($r_{min.\ pot.}$=3.656 Å). Integration of the RDF to the first minima at 6.675 Å gives coordination number equal to 1.5665. This means at such a close distance as 4.275 Å, always 1.5665 methane molecules (at average) are following the carbon dioxide. While, this is not a proof for the aforementioned hypothesis; it can be considered as an indication that methane will tend to follow carbon dioxide inside the solution due to the diffusivity.

At this place, a hypothesis concerning entrapment of methane molecules during absorption of carbon dioxide by activated amine solution must be discussed. Credit for this theory goes to my supervisor Prof. Bjørn Kvamme.

This hypothesis involves a packing structure, consisting of two piperazine rings and a methane molecule, with the methane sandwiched between the piperazines. The mechanism promoting this configuration is same as the one responsible for SELEXOL selectivity for carbon dioxide. To elaborate, two oppositely charged sites from two different PZ rings position themselves so that the empty space between two rings provides a suitable condition for entrapment of methane molecule. In the ideal case, the piperazine molecules would form a sandwich structure in space so that the piperazine rings align with one another with their nitrogen-nitrogen axes orthogonal. It was expected that the parallel PZ rings should be

separated by about 7.297 Å. This was calculated based on the minimum L-J interactions distance between $N_{PZ} - C_{CH_4}$pair (Equation(10-1)) for the models which have been used in this work in addition to the average $N_{PZ} - N_{PZ}$ separation in molecular structure of piperazine ring. Figure 10-33 illustrates schematic diagram of packing structure.

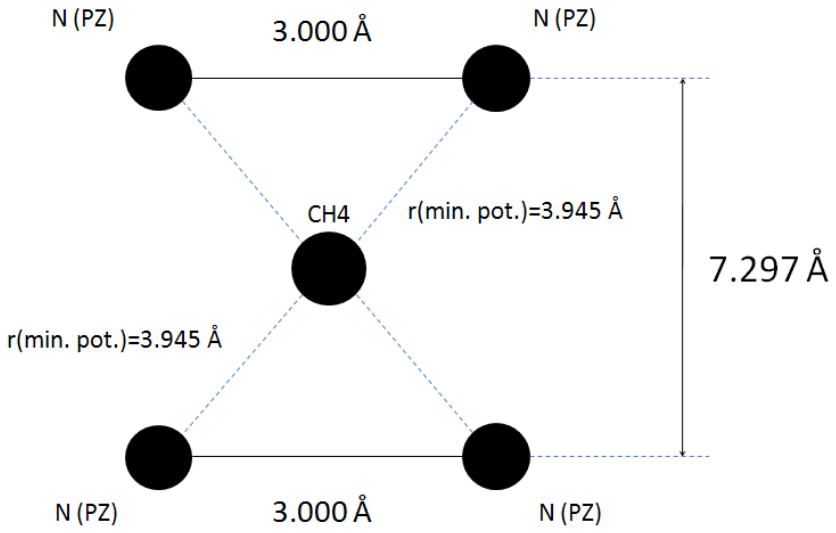


**Figure 10-33: Schematic diagram of packing structure**

**(true ratios in the figure are disregarded )**

Current thesis does not provide an evidence for the validity of this theory. Information provided in current section serves as a collection of indications which can be used as departure point for the further investigations. In order to provide concrete evidence for this hypothesis, sophisticated computer programming is required. That is necessary to make some tools to search for exact sandwich packing of methane molecules. These tools have to be used complementarily with MD51 and VMD program. This part itself can be an independent work that needs extensive knowledge of computer programming which was beyond the scale of current thesis.

Figure 10-34 shows two PZ rings close to the ideal orientation of them to form sandwich structure. There is also a methane molecule next to the structure which might be a potential candidate for entrapment if it was inside the space between two PZ molecules. This situation was observed at 26.71th ns of the simulation.

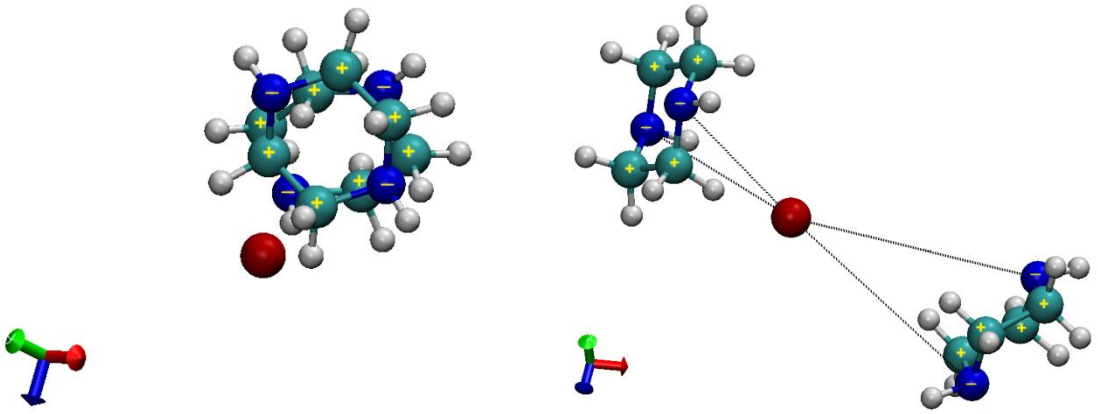

**Figure 10-34: a potential sandwich packing structure**

Random visual observations for different time sections of the simulation revealed that this can be a quite possible structure. However, due to the low concentration of PZ molecules in the current system, it was highly problematic to find them among millions of simulation frames. That was a very time consuming procedure and required sophisticated computer programming to deal with. In such a way, all the PZ and methane molecules have to be checked for every single frame during the entire simulation (41.44ns) to satisfy the necessary geometric criteria of the sandwich structure. The search for sandwich structure was also impeded due to the use of uncharged methane model (one-site model) in this thesis. Lacking partial atomic charges on the molecular structure of methane decreased the intermolecular interactions between PZ and $CH_4$only to the L-J interactions, so that effect of long range electrostatic interactions was completely disregarded. Consequently, application of a validated 5-site methane model can be beneficial. Since, the electrostatic interactions between two PZ and methane molecules are counted, this increases the chance for entrapment of methane molecules by the expected sandwich structure.

Some of the other snap-shots related to the observation of sandwich packing of methane molecules have been illustrated by Figure 10-35.

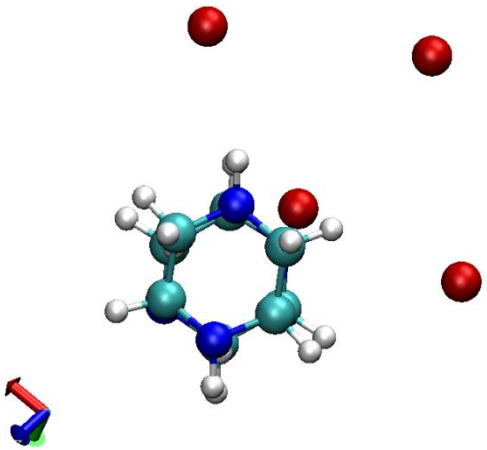

**(a) Front view**

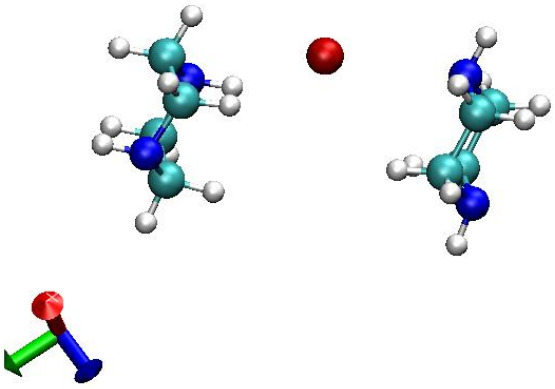

**(a) Side view**

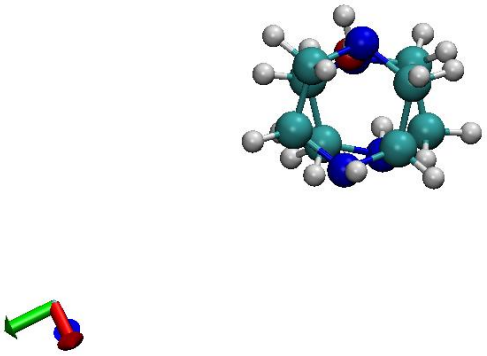

**(b) Front view**

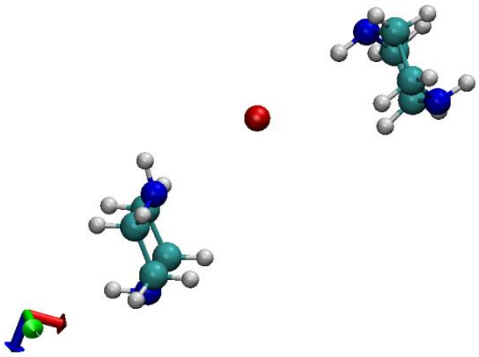

**(b) Side view**

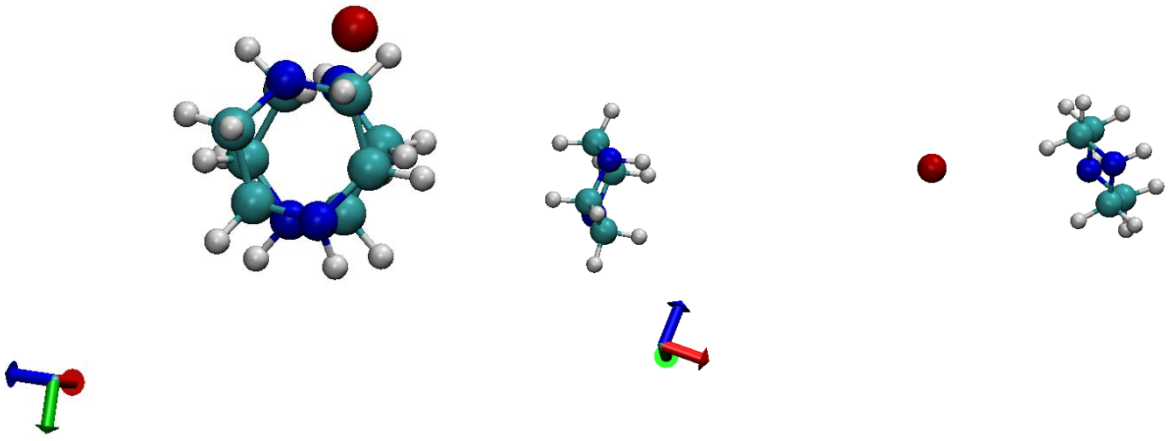

**(c) Front view** **(c) Side view**

**Figure 10-35: Potential candidates for sandwich packing of methane (a) 31.40 ns (b) 31.44 (c) 36.48 ns**

In order to identify cases that can be called *sandwich packing structures* with certainty, an *orientation analysis* is necessary. Meaning we have to particularly search for the specific relative molecular orientations from which we expect a sandwich structure, rather than many possible molecular orientations of PZ molecules around methane. To do so, a *molecular pair correlation function* instead of atomic pair correlation function has to be implemented into the MD51 original code or programmed as a script for VMD. Complication involved in this investigation brought it beyond the scale of current research; however a script for VMD was developed which generates a list of potential candidates for possible sandwich structures. This list contains all the methane and PZ molecules participating in candidate structures for sandwich packing under the specified geometric constraints. These constraints ask for the methane molecules which are positioned within the specific distances from both PZ's center of masses. The next step would be to perform an orientation analysis for this list of the candidates. This will be suggested for further works.

Above mentioned script was programmed in the Tcl language, using "orient Ver. l.0" and the "The Hume Linear Algebra Tcl Package (La) Ver. 1.01". The former calculates the principal axes of the molecules and orients the molecule to align the first, second, and third principal axes to the x, y, and z directions. This script was written by Paul Grayson[16]. The latter script consists of Tcl procedures for the manipulation of vectors and matrices[17]. Combination of

[16] Paul Grayson can be contacted within this address: pgrayson@ks.uiuc.edu
[17] Available at: http://www.hume.com/la/

these two scripts with specific requirements of the current research was implemented to the new script. I benefited greatly in this part from Bjørnar Jensen who helped to implement everything into one script.

To clarify how this script works, following flowchart presented in Figure 10-36.

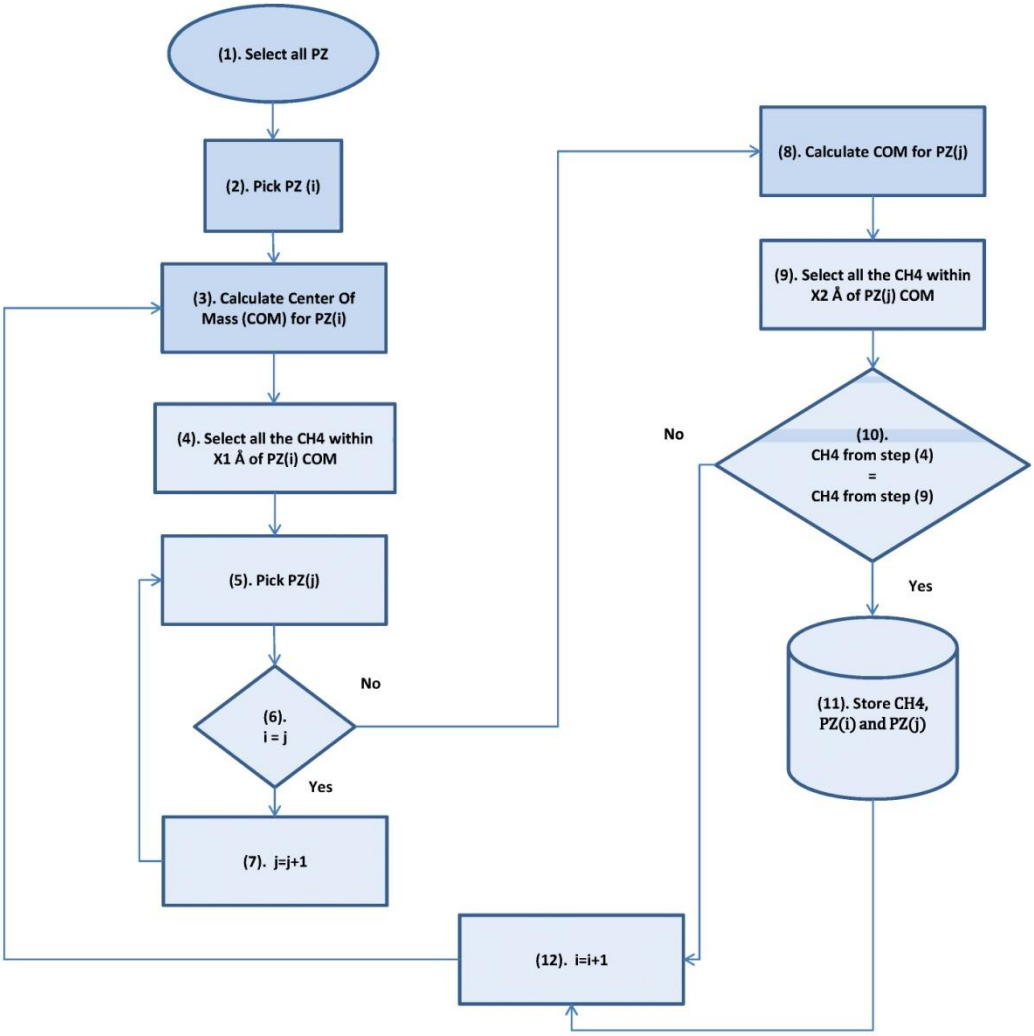


**Figure 10-36: Flowchart for VMD script which selects potential candidates for sandwich structure**

Using the described script, the last 79000 configurations of the system was explored for candidates of the sandwich structure. Geometric constraints were set, so that each methane molecule had to be simultaneously within 4 Å of both PZ's center of masses. At the end, only

31 candidates were found which satisfied the criteria. This step has to be followed by performing orientation analysis. But even if all of these configurations could correspond to an exact sandwich structure, nothing will be proven yet. This is due to the really low concentration of PZ in the solution (recall that the total mole fraction of PZ species in the solution was only 0.033). Nevertheless, we may conclude that sandwich structure cannot be the main reason for trapping of methane at low loadings. For the higher loadings, same investigation has to be repeated. It would be also a good idea to use aqueous PZ solution instead of PZ-MDEA blends to increase the chance of finding the sandwich structure. Thus, it would be easier to prove or dismiss the hypothesis.

To analyze the distribution and affinity of carbon dioxide and methane around the amine and alcohol groups in MDEA, pair correlation functions for nitrogen-carbon and oxygen-carbon pairs inside the solution were calculated. Pair correlation functions between nitrogen from MDEA and carbon from $CO_2/CH_4$ are plotted in Figure 10-37.

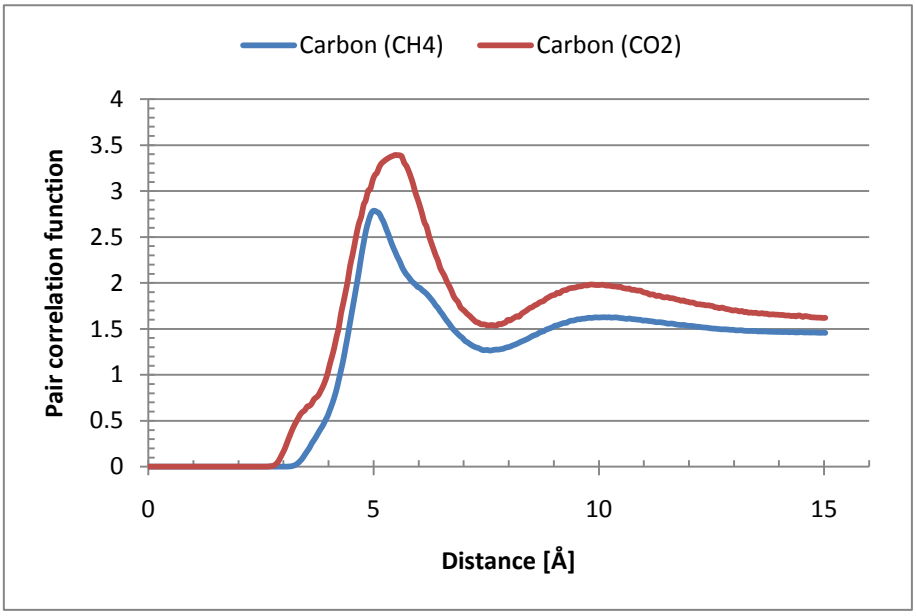


**Figure 10-37: Nitrogen-Carbon pair correlation function between MDEA and $CH_4/CO_2$**

Interesting insights can be inferred from this figure. As seen, both gaseous components have their first peaks approximately at same distance from nitrogen, so that two peaks are only 0.45 Å away from one another. But carbon dioxide molecules display a higher peak compared to methane. Looking at Figure 10-37, it becomes clear that probability of finding of $CO_2$ within the first shell is approximately 21.84% higher than the one for methane molecules. Considering population of carbon dioxide in the system is only 12.4% of methane molecules,

a higher affinity of carbon dioxide towards amine group of MDEA can be concluded. Integration of pair correlation functions over the radius is illustrated by Figure 10-38.

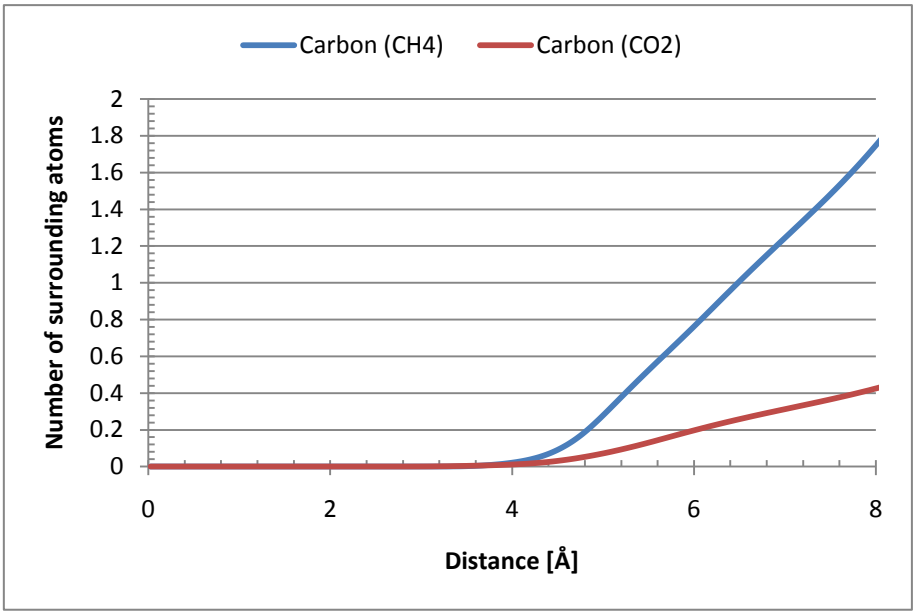


**Figure 10-38: Number of surrounding carbon atoms around nitrogen in MDEA**

Integration of RDFs to the first minima which occur at the same distance for both $CO_2$and $CH_4$, yielded to 0.3908 and 1.5188 respectively. The smaller coordination number of $CO_2$in this figure is definitely due to the lower concentration of that in the system.

Same investigation was carried out for oxygen-carbon pair inside the solution. In this selection, oxygen belongs to the alcohol groups of MDEA and carbon is the central atom in carbon dioxide and methane. The corresponding pair correlation functions are shown in Figure 10-39.

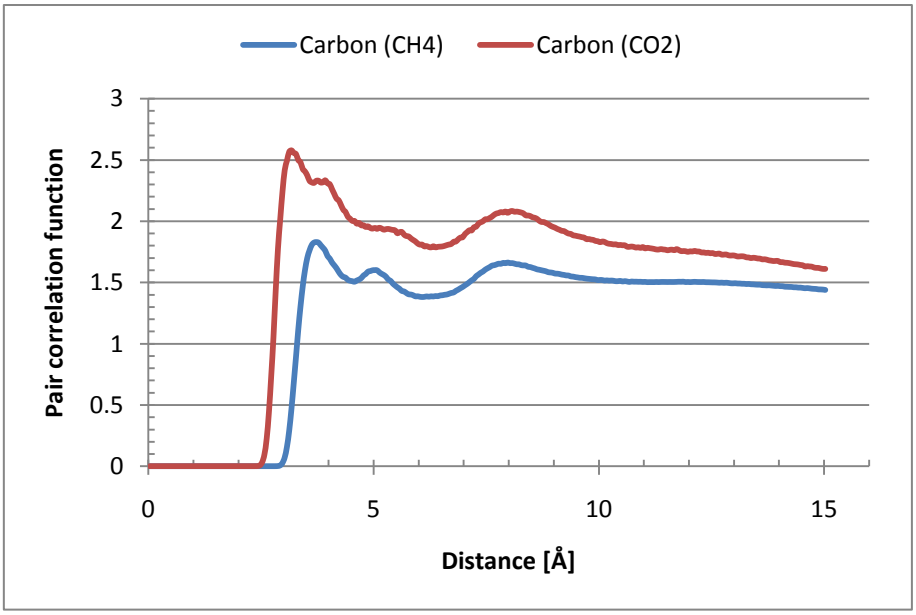


**Figure 10-39: Oxygen-Carbon pair correlation function between MDEA and $CH_4/CO_2$**

This figure indicates the presence of three molecular shells for methane around the oxygen atom, while it appears that carbon dioxide only forms two distinct shells around the oxygen. Although, carbon dioxide demonstrates a small bulge after the first peak, it does not seem to be an independent molecular shell and most probably it is the same phenomenon which was previously observed for similar pair of atoms in reference system No.2 (Figure 10-11). In general, Figure 10-39 pictures the same situation as Figure 10-37. Carbon dioxide molecules have higher probabilities of being found everywhere in comparison with methane molecules, despite their lower concentration in the system and inside the interface. According this figure, $CO_2$molecules have 40% higher probability to be found within the first shell compared to methane. Coordination number for carbon dioxide is 0.1942 while this value for methane is 0.2376 reflecting higher concentration of methane in the system and within the interface. Integration of above mentioned RDFs over the distance are presented in Figure 10-40.

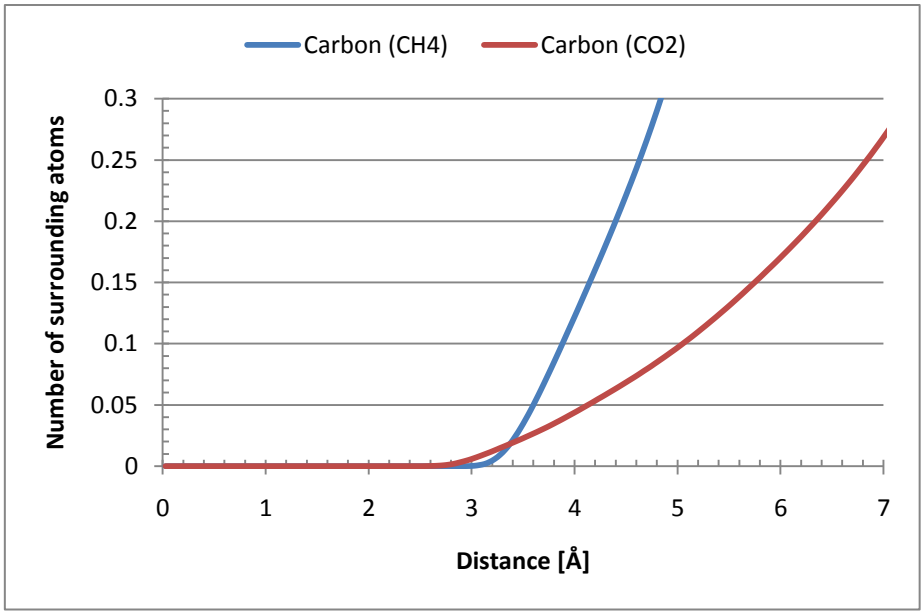


**Figure 10-40: Number of surrounding carbon atoms around oxygens in MDEA**

The above findings, clearly indicate the higher affinity of carbon dioxide towards the alcohol groups in MDEA. On the other hand, a very low coordination number of methane, despite its high concentration within the interface, signifies that $CH_4$appears to be inert with regards to alcohol group. It can be summarized at this point that MDEA with its three functional groups, (one amine and two alcohol groups) all possessing high relative affinity for carbon dioxide is capable of loading large amount of $CO_2$ during removal of carbon dioxide from natural gas.

A similar approach was chosen to compare the relative affinities of carbon dioxide and methane towards amine groups in piperazine. Pair correlation functions for nitrogen-carbon pair between PZ and $CO_2$/$CH_4$inside the solution were calculated which is shown by Figure 10-41.

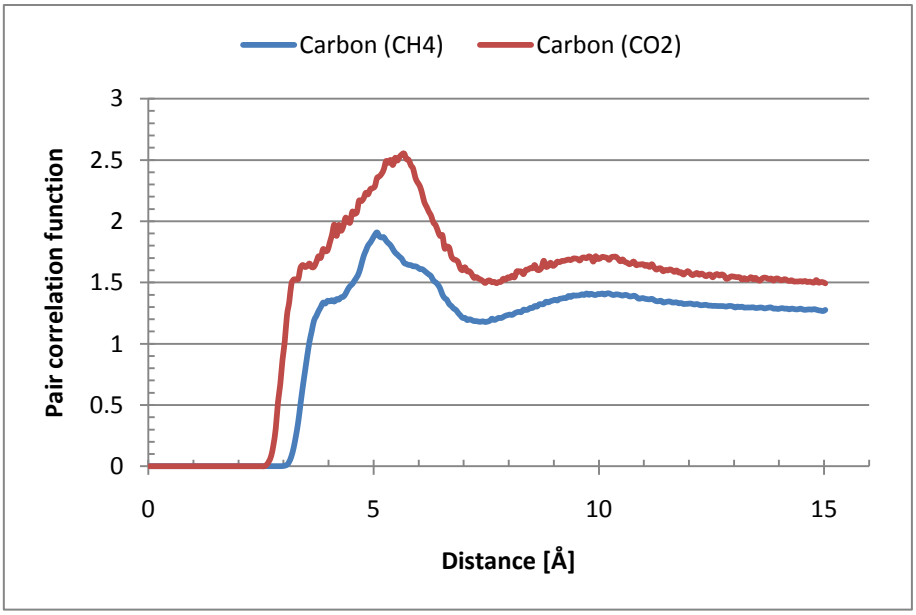


**Figure 10-41: Nitrogen-Carbon pair correlation function between PZ and $CH_4/CO_2$**

The results from this figure are consistent with those outlined earlier. In spite of the fact that carbon dioxide has a lower concentration inside the system and through the gas-liquid interface, it shows higher probability of finding by 33.73% in comparison with methane. Coordination numbers of the indicated RDFs have been illustrated by Figure 10-42. They are equal to 0.3539 and 1.3225 for carbon dioxide and methane respectively.

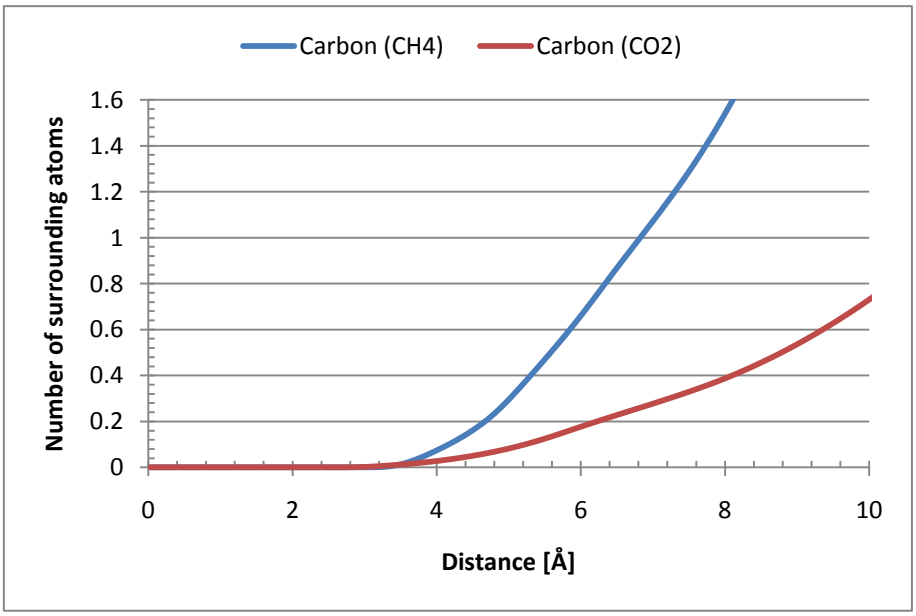


**Figure 10-42: Number of surrounding carbon atoms around nitrogens in PZ**

One important point that should be stressed here, concerns the significance of nitrogen – carbon ($CH_4$) coordination numbers. Comparing all the pair correlation functions explained above for MDEA and PZ, methane molecules always possess coordination numbers larger

than one around the amine groups, regardless of molecular structure and availability of nitrogen in MDEA or PZ. At the same time, methane has really small coordination number around the alcohol groups in MDEA, despite availability of alcohol group due to molecular structure of MDEA. Hence, it should be much easier for methane molecules to surround the oxygen. In regard to trapping of methane molecules, this may be yet another indication that amine groups (no matter in which molecule) bear the main responsibility for entrapment of methane.

The interfacial tension of the primary system was calculated based on pressures obtained from the last 600 intermediate averages of the system corresponding to the last 3 ns of simulation. Figure 10-43 illustrates variation of interfacial tension over this time.

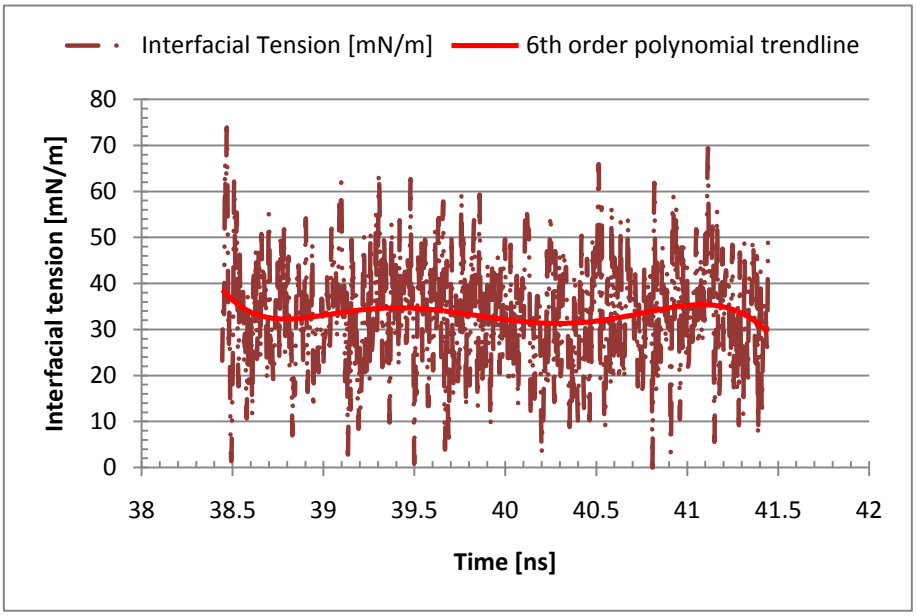


**Figure 10-43: Interfacial tension of the system over the last 600 intermediate averages of the simulation**

As illustrated by Figure 10-43, the total statistical average of the interfacial tension over the last 3 ns of simulation was equal to 33.4±0.1 mN/m. Comparing to reference system No.4 which did not contain carbon dioxide absorbents, the primary system exhibited a much lower average interfacial tension which can be ascribed to the surfactant effect of the amine solvents. Comparison between reference system No.3, reference system No.4 (amine free system) and primary system over the last 3 ns simulation of each system is given in Figure 10-44 and Table 10-6.

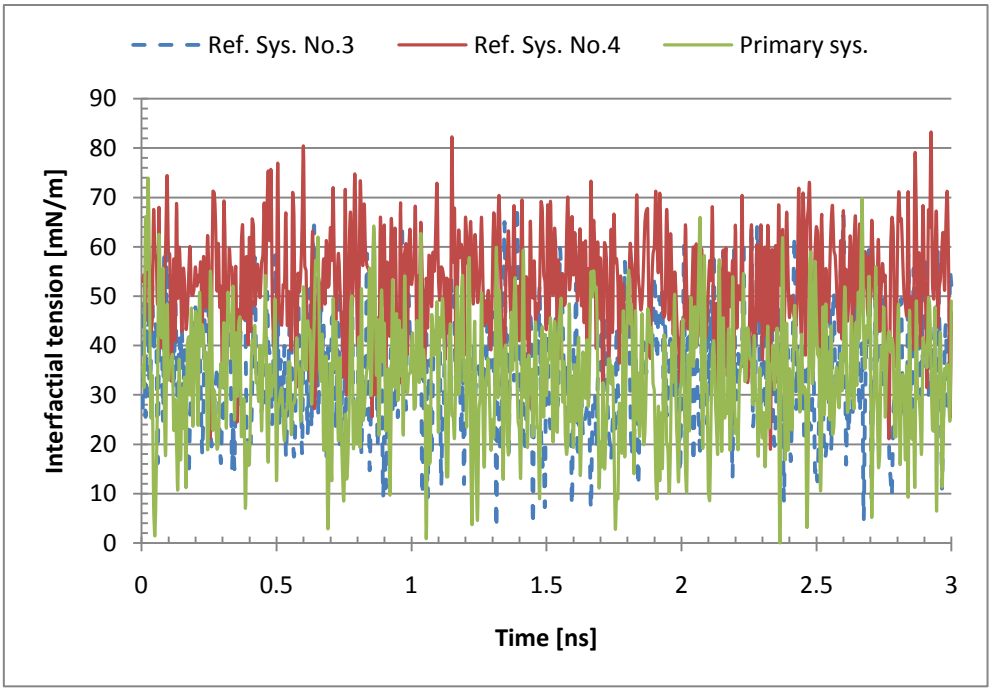


**Figure 10-44: Comparison between IFTs in reference system No.3, reference system No.4, and primary system**

**Table 10-6: Comparison between total average IFTs of ref. sys. No.1, No.3 and primary system**

| System name | Ref. sys. No.3 | Ref. sys. No.4 | Primary sys. |
|---|---|---|---|
| Average interfacial tension [mN/m] | 35.2±0.1 | 52.8±0.1 | 33.4±0.1 |

# 11 Conclusion

For this research, a lengthy molecular dynamics simulation was performed to study five different reference and primary systems, so that 41.44 ns simulation was achieved only for primary system (26 ns in average for each system). Molecular characteristics of aqueous PZ activated MDEA solution was analyzed and quantified. The Effectiveness of the applied blend for absorption of carbon dioxide from natural gas was demonstrated and deficiency of such a solution in undesired trapping of methane during purification of natural gas was indicated.

Molecular distribution of the amine solution was studied in reference system No.1. Formation and distribution of hydrogen bonds between different constituents of the solution were investigated. Hydrogen bond analysis signified that MDEA, PZH and PZCOO are capable of forming hydrogen bonds with water. All the nitrogens in amine groups, oxygens in carboxylate and alcohol groups in addition to the ionic hydrogen in protonated PZ were quite active in this regard, so that 19.45% of MDEA molecules, 100% of PZH, 324.11%[18] of PZCOO were able to from hydrogen bond with surrounding water molecules in average per each frame. While at the same time, only 21% of PZ molecules could establish hydrogen bond with water. It was observed that MDEA and PZ were separated from aqueous phase and also it was indicated that ionic nature of PZH and PZCOO made them dissolve in water. It was shown that this phase separation was energetically favorable.

High loading capacity of MDEA for carbon dioxide removal was observed in all the systems containing this gas component (Ref. sys. No2, No.3 and primary system). Specifically, affinity of carbon dioxide for the amine and alcohol groups of MDEA was demonstrated by calculating pair correlation function in reference system No.2. Therefore, considering that each MDEA molecule possesses three functional groups with high $CO_2$ affinity, noticeable capacity of MDEA for absorption of carbon dioxide was found to be conclusive. Density profile of the system quantified this capacity while at the same time it emphasized low solubility of the $CO_2$ inside the water bulk. Density profile of carbon dioxide in reference system No.2 rose even to ~0.45 g/cm3 in MDEA bulk, however it was almost zero in water.

The affinity of amine groups in PZ molecule for carbon dioxide was analyzed using pair correlation function in reference system No.2 and No.3. The coordination number for reference system No.2 was 3 times larger than the reference system No.3 that was due to the initial higher pressure and larger concentration of $CO_2$ in the former system. It was deduced

[18] Numbers more than 100% signifies more than one hydrogen bond per molecule in average.

that such an affinity is because of electronegativity of amine groups in PZ molecule that will give rise to absorption of carbon dioxide. Comparing reference system No.2 and No.3; it was shown that gas pressure has an undeniable effect on the availability of absorbate molecules around the solvents, so that it can directly affect the absorption rate of carbon dioxide.

A complete process of carbon dioxide absorption was observed in reference system No.3. It was demonstrated that distribution of PZ species through the system plays an important role for accelerating the absorption process. Considering this pattern, it was concluded that PZ and PZCOO have important effect in absorption of carbon dioxide at low loading based on Equation (3-11) which dictates absorption rate of the system. This conclusion was also found to be consistent with experimental observations (Bishnoi and Rochelle 2000; Derks 2006). It was highlighted that aqueous blend of PZ activated MDEA solution is quite effective for absorption of carbon dioxide by calculating the relative number of absorbed $CO_2$molecules, in such a way 51.85% carbon dioxide molecules had been absorbed into the amine solution. It was also shown that capability of MDEA for $CO_2$ loading was 9.9 times higher than water. To summarize, it was demonstrated satisfactorily how absorption of carbon dioxide can be promoted by adding small amount of PZ as the so-called activator, accelerator or promoter into the traditional aqueous solution of MDEA.

The surfactant effect of amine solvents was analyzed by comparing the interfacial tension between reference system No.4 (amine free system) with reference system No.3 and primary system. Average interfacial tension of the primary system was 36.93 % lower than the free amine system. This value for reference system No.3 was equal to 33.33%. Due to the lower interfacial tensions, systems containing amine solvents were expected to have more extended interfaces, which was also consistent with roughness and thickness of the interface in reference system No.3 and primary system (illustrated by Figure 10-17 and Figure 10-30). Moreover, in connection with entrapment of methane observed in primary system, it was concluded that low interfacial tension - or in other words - more dynamic interfaces can be one of the reasons which may encourage this phenomenon.

Relative number of dissolved carbon dioxide and methane molecules was calculated for reference system No.4 in absence of amine solution. Later in Section 10.5, this calculation was expanded to the primary system which contained activated amine solution. Comparison between these two systems emphasized influence of aqueous piperazine activated MDEA solution on the absorption of carbon dioxide as well as trapping of methane. Entrapment of

methane in primary system was 67.2 times larger than amine free system. Similarly, absorption of carbon dioxide in primary system was 8.75 times higher than the common solution of $CO_2$ in water in reference system No.4. Considering this, it was deduced that aqueous blend of PZ and MDEA is beneficial for absorption of carbon dioxide and simultaneously has great impact on the undesired trapping of methane.

In regard with trapping of methane, sandwich packing of this molecule with pair of piperazine rings was investigated. Some indications were collected for this hypothesis to specify approximate population of potential candidates for sandwich structure and to evaluate roughly its overall impact on the undesired trapping of methane. In pursuit of the expected structure, last 79000 configurations of the simulation were searched but only 31 candidate structures were found under the specified geometric criteria. Some of these candidates were chosen randomly to be evaluated by visual observation. It was observed that some of them were very close to the ideal structure for trapping of methane. However, due to low concentration of PZ species in the solution, it was deduced that sandwich structure most probably cannot be dominant mechanism for trapping of methane at low loading of carbon dioxide.

Comparing pair correlation functions between carbon dioxide and methane versus different amine and alcohol groups in PZ and MDEA molecules, higher affinity of carbon dioxide was concluded. Since methane was found to be inert towards the alcohol group and showed an unusually high coordination number around the amine groups - for both PZ and MDEA - it was ascertained that this functional group carries the main responsibility for entrapment of methane.

# 12 Suggestions for further work

Further works for this research can be proposed as following category:

i. Model development:

- Molecular modeling part of this work should be extended. Current study only employed species with higher molecular concentrations which are dominating the ongoing reactions inside the solution. Other ionic species either those with low concentrations or the reaction intermediates should be included. This is especially relevant if various thermodynamic conditions or different loading factors are going to be applied in further simulations. Because, different conditions change the reaction rates and consequently lead to variation of molecular concentrations. For instance, hydonium, hydroxyl, protonated piperazine carbamate (zwiterion ion), piperazine bicarbamate and protonated MDEA are worthwhile of study. Further accuracy can be achieved by modeling of the carbonate and bicarbonate ions. This will result in more realistic simulation outcomes. At the same time it might be an option to consider natural gas impurities in the system. Specifically, some important phenomena such as foaming can be simulated only if effects of impurities in the gas mixture are taken into account. Finally, it would also be advisable to build a new 5-site model for methane molecule, considering importance of partial atomic charges in methane molecule which can be very crucial in some cases such as investigation of sandwich packing structure.
- All the models require to be validated against relevant experimental evaluations to ensure that they can replicate true behavior of the molecules in actual life. To be specific, X-ray or electron diffraction techniques are proposed.

ii. New Simulation set-ups:

Simulation set up is proposed to be extended over the systems having higher loading factors and different PZ-MDEA blends. Comparison of these reference systems can be very instructive. Due to the low concentration of PZ species and because of the low loading factor (0.07 mole $CO_2$/mole amine) in the current study, it was very problematic to detect some of the phenomena such as sandwich structure or affinity of $CO_2$for some functional groups. Therefore, increasing the loading value in addition to using higher concentration of PZ would be beneficial for further studies having similar motivations.

iii. Additional reference systems:

Simulation of two new reference systems might be advisable. A system containing aqueous MDEA as the amine solution rather than the activated solution of MDEA. This will allow one to investigate the influence of MDEA in absorption of carbon dioxide independently. It would be also possible to determine whether there is any impact on the entrapment of methane molecules. Another reference system which can be considered would be a similar activated blend using SELEXOL instead of MDEA. Considering that SELEXOL is a popular physical solvent with high loading capacity for removal of carbon dioxide and hydrogen sulfide, it would be of great interest to know if it is possible to improve the absorption process by decreasing deficiencies of the current PZ-MDEA solution (regeneration cost and methane trapping) and at the same time keeping the advantages of that (high absorption rate and large $CO_2$solubility).

iv. Improvement of analysis methods:

Analytical techniques in current study need to be improved in some parts. This can be listed as following:

- Evaluation of hydrogen bonds can be carried out using an alternative technique such as energetic definition of hydrogen bonding rather than geometric definition which was used in this work. Investigation of hydrogen bonds based on energetic definition provides useful information about dynamics of hydrogen bonds. This can be accomplished by calculating *pair interaction energy* (Chowdhuri and Chandra 2002) between donors and acceptors within specific cut-off distance by means of MD simulation. Results from this alternative method can be then compared with the one from geometric evaluation in this thesis.
- Solubility of carbon dioxide and methane can also be calculated using an alternative approach. Solubility values are proposed to be obtained based on estimation of chemical potentials for dissolved $CO_2$ and dissolved $CH_4$ using *particle insertion method*. This estimation should reflect observed solubility of the gases components inside the solution.
- Investigation of interface can be carried out based on *capillary wave theory* which samples the interface free energy instead of interfacial tension. This is necessary because investigation of very dynamic interfaces in gas-liquid systems (such as the one in this thesis) involves some complications and needs more sophisticated theories to handle behavior of the interface in such systems.

- As explained in Section 10.5, to provide concrete evidence for observation of sandwich packing structure of methane molecules by pair of PZ rings, molecular pair correlation function has to be implemented into the simulation code or has to be programmed as a separate script for VMD application. In this subroutine, orientation of different molecules in respect to each other can be investigated so that ideal orientation of two planar surfaces from two PZ rings in addition to orientation of nitrogen-nitrogen axes of them can be compared.

v. Investigation targets:

- Pressure reduction and degassing:

  With the current setup it is possible to reduce pressure and implement samplings of diffusivities so that also relative diffusive transport rates of $CO_2$ and $CH_4$ out from the solvent can be studied. An even more advanced approach would be to use a grand canonical simulation (VTμ) with reservoirs of methane and carbon dioxide kept at chemical potentials corresponding to gas mixture properties or alternatively similar hybrid techniques with Monte Carlo method for the mass transfer between system and reservoirs.

# Reference


Álvaro Pérez-Salado, K., et al. (2003). "Solubility of CO2 in (H2O+piperazine) and in (H2O+MDEA+piperazine)." AIChE Journal **49**(10): 2662-2670.

Apple, M., et al. (1982). Removal of CO2 and/or H2S and/or COS from gases containing these constituents. United State of America, BASF Aktiengesellschaft, Fed. Rep. **US Patent Nr 4336233**.

Atkins, P. W. and R. S. Friedman (2005). Molecular Quantum Mechanics. New York, Oxford University Press.

Baker, J. (1985). "Classical chemical concepts from ab initio SCF calculations." Theoretical Chemistry Accounts: Theory, Computation, and Modeling (Theoretica Chimica Acta) **68**(3): 221-229.

Barnes, G. T. and I. R. Gentle (2005). An Introduction to Interfacial Science. New York, Oxford University Press.

Berendsen, H. J. C., et al. (1987). "The missing term in effective pair potentials." The Journal of Physical Chemistry **91**(24): 6269-6271.

Berendsen, H. J. C., et al. (1984). "Molecular dynamics with coupling to an external bath." The Journal of Chemical Physics **81**(8): 3684-3690.

Bishnoi, S. and G. Rochelle, T. (2002b). "Absorption of carbon dioxide in aqueous piperazine/methyldiethanolamine." AIChE Journal **48**(12): 2788-2799.

Bishnoi, S. and G. T. Rochelle (2000). "Absorption of carbon dioxide into aqueous piperazine: reaction kinetics, mass transfer and solubility." Chemical Engineering Science **55**(22): 5531-5543.

Bishnoi, S. and G. T. Rochelle (2002a). "Thermodynamics of piperazine/methyldiethanolamine/water/carbon dioxide." Industrial & Engineering Chemistry Research **41**(3).

Bottinger, W., et al. (2008). "Online NMR Spectroscopic Study of Species Distribution in MDEA-H2O-CO2 and MDEA-PIP-H2O-CO2." Industrial & Engineering Chemistry Research **47**(20): 7917.

Brodholt, J. P. and B. J. Wood (1993a). "Molecular dynamics simulations of the properties of CO2-H2O mixtures at high pressures and temperature." American Mineralogist **78**: 558-564.

Chowdhuri, S. and A. Chandra (2002). "Hydrogen bonds in aqueous electrolyte solutions: Statistics and dynamics based on both geometric and energetic criteria." Physical Review E **66**(4): 041203.

Cramer, C. J. (2004). Essentials of Computational Chemistry: Theories and Models. West Sussex, John Wiley & Sons Ltd.

da Silva, E. F. (2005). Computational Chemistry Study of Solvents for Carbon Dioxide Absorption. Naturvitenskap og Teknologi. Trondheim, Norwegian University of Science and Technology. **PhD:** 288.

Derks, P. W. J. (2006). Carbon dioxide absorption in piperazine activated N-methyldiethanolamine. Enschede, University of Twente. **PhD:** iv,4,46,48,105-111,.

Dill, K. A. and S. Bromberg (2003). Molecular Driving Forces – Statistical Thermodynamics in Chemistry and Biology. New York, Garland Science

Ermatchkov, V., et al. (2003). "Chemical equilibrium constants for the formation of carbamates in (carbon dioxide + piperazine + water) from 1H-NMR-spectroscopy." The Journal of Chemical Thermodynamics **35**(8).

Field, M. J. (2007). A Practical Introduction to the Simulation of Molecular Systems. New York, CAMBRIDGE UNIVERSITY PRESS.

Freeman, S. A., et al. (2009). "Carbon dioxide capture with concentrated, aqueous piperazine." Energy Procedia **1**(1): 1489-1496.
Frenkel, D. and B. Smit (2001). Understanding Molecular Simulation: From Algorithms to Applications. San Diego, Academic Press.
Hinchliffe, A. (2008). Molecular Modelling for Beginners. Chippenham, Wiltshire.
Hohenberg, P. and W. Kohn (1964). "Inhomogeneous Electron Gas." Physical Review **136**(3B): B864.
Hoover, W. G. (1985). "Canonical dynamics: Equilibrium phase-space distributions." Physical Review A **31**(3): 1695.
Idem, R., et al. (2009). "Kinetics, modeling, and simulation of the experimental kinetics data of carbon dioxide absorption into mixed aqueous solutions of MDEA and PZ using laminar jet apparatus with a numerically solved absorption-rate/kinetic model." Energy Procedia **1**(1): 1343,1345,.
Jakobsen, J. P., et al. (2005). "Liquid-Phase Composition Determination in CO2−H2O−Alkanolamine Systems: An NMR Study." Industrial & Engineering Chemistry Research **44**(26): 9894-9903.
Jensen, B. (2009). Modeling Trapping Mechanism for PCB Adsorption on Activated Carbon. Department of Physics and Technology. Bergen, University of Bergen (UiB). **Master of Science:** 121.
Jensen, F. (2006). Introduction to Computational Chemistry. West Sussex, John Wiley & Sons Ltd.
Jensen, K. P. and W. L. Jorgensen (2006). "Halide, Ammonium, and Alkali Metal Ion Parameters for Modeling Aqueous Solutions." Journal of Chemical Theory and Computation **2**(6): 1499-1509.
Jorgensen, W. L., et al. (1984). "Optimized intermolecular potential functions for liquid hydrocarbons." Journal of the American Chemical Society **106**(22): 6638-6646.
Jorgensen, W. L., et al. (1996). "Development and Testing of the OPLS All-Atom Force Field on Conformational Energetics and Properties of Organic Liquids." Journal of the American Chemical Society **118**(45): 11225-11236.
Jorgensen, W. L. and N. A. McDonald (1998). "Development of an all-atom force field for heterocycles. Properties of liquid pyridine and diazenes." Journal of Molecular Structure: THEOCHEM **424**(1-2): 145-155.
Jorgensen, W. L., et al. (2004). "Free Energies of Hydration from a Generalized Born Model and an All-Atom Force Field." The Journal of Physical Chemistry B **108**(41): 16264-16270.
Jou, F.-Y., et al. (1998). "Solubility of Methane and Ethane in Aqueous Solutions of Methyldiethanolamine." Journal of Chemical & Engineering Data **43**(5): 781-784.
Jou, F.-Y., et al. (2003). "Solubility of Ethane in N-Formyl Morpholine." Journal of Chemical & Engineering Data **48**(2): 224-225.
Junfang, Z. and et al. (2009). "A molecular dynamic study of water/methane/propane." Journal of Physics B: Atomic, Molecular and Optical Physics **42**(3): 035302.
Kelly, C. P., et al. (2005). "SM6: A Density Functional Theory Continuum Solvation Model for Calculating Aqueous Solvation Free Energies of Neutrals, Ions, and Solute−Water Clusters." Journal of Chemical Theory and Computation **1**(6): 1133-1152.
Kohl, A. L. and R. B. Nielsen (1997). Gas Purification. Houston, Gulf Publishing Company.
Kutepov, A. M., et al. (2001). "Interfacial Mass Transfer in the Liquid–Gas System: An Optical Study." Theoretical Foundations of Chemical Engineering **35**(3): 213-216.
Kuznetsova, T. and B. Kvamme (2002). "Thermodynamic properties and interfacial tension of a model water-carbon dioxide system." Physical Chemistry Chemical Physics **4**(6): 937-941.

Leach, A. R. (1996). Molecular Modelling: Principles and Applications. Edinburgh, Longman.

Lebedev, Y., et al. (1997). "Effect of foaming on hydrodynamics of masstransfer contact devices." Chemistry and Technology of Fuels and Oils **33**(6): 332-334.

Liu, H.-B., et al. (1999). "A Study on Equilibrium Solubility for Carbon Dioxide in Methyldiethanolamine−Piperazine−Water Solution." Industrial & Engineering Chemistry Research **38**(10): 4032-4036.

Lowdin, P.-O. (1950). "On the Non-Orthogonality Problem Connected with the Use of Atomic Wave Functions in the Theory of Molecules and Crystals." The Journal of Chemical Physics **18**(3): 365-375.

Lyubartsev, A. P. and A. Laaksonen (2000). "M.DynaMix - a scalable portable parallel MD simulation package for arbitrary molecular mixtures." Computer Physics Communications **128**(3): 565-589.

Mahdi, N. and R. C. Dannie (2007). Interaction Of Process Design, Operating Conditions And Corrosion In Amine Systems. CORROSION 2007. Nashville, Tennessee, NACE International.

Marenich, A. V., et al. (2007). "Self-Consistent Reaction Field Model for Aqueous and Nonaqueous Solutions Based on Accurate Polarized Partial Charges." Journal of Chemical Theory and Computation **3**(6): 2011-2033.

Martyna, G. J., et al. (1992). "Nose-Hoover chains: The canonical ensemble via continuous dynamics." The Journal of Chemical Physics **97**(4): 2635-2643.

McDonald, N. A. and W. L. Jorgensen (1998). "Development of an All-Atom Force Field for Heterocycles. Properties of Liquid Pyrrole, Furan, Diazoles, and Oxazoles." The Journal of Physical Chemistry B **102**(41): 8049-8059.

Melissa, L. P. P., et al. (2001). "Gas-phase and liquid-state properties of esters, nitriles, and nitro compounds with the OPLS-AA force field." Journal of Computational Chemistry **22**(13): 1340-1352.

Mulliken, R. S. (1955). "Electronic Population Analysis on LCAO[Single Bond]MO Molecular Wave Functions. I." The Journal of Chemical Physics **23**(10): 1833-1840.

Niall, J. E. and J. M. D. Macelroy (2003). "Structural and dynamical properties of methane clathrate hydrates." Journal of Computational Chemistry **24**(13): 1569-1581.

Nosé, S. (1984). "A molecular dynamics method for simulations in the canonical ensemble." Molecular Physics: An International Journal at the Interface Between Chemistry and Physics **52**(2): 255 - 268.

Nosé, S. (1991). "Constant Temperature Molecular Dynamics Methods." Progress of Theoretical Physics Supplement **103**.

Olson, R. M., et al. (2007). "Charge Model 4 and Intramolecular Charge Polarization." Journal of Chemical Theory and Computation **3**(6): 2046-2054.

Pashley, R. M. and M. E. Karaman (2004). Applied Colloid and Surface Chemistry. West Sussex, John Wiley & Sons, Ltd.

Poplsteinova, J. (2004). Absorption of Carbon Dioxide - Modeling and Experimental Characterization. Department of Chemical Engineering. Trondheim, Norwegian University of Science and Technology. **PhD:** 2-3.

Rinker, E. B., et al. (2000). "Absorption of Carbon Dioxide into Aqueous Blends of Diethanolamine and Methyldiethanolamine." Industrial & Engineering Chemistry Research **39**(11): 4346,.

Rizzo, R. C. and W. L. Jorgensen (1999). "OPLS All-Atom Model for Amines: Resolution of the Amine Hydration Problem." Journal of the American Chemical Society **121**(20): 4827-4836.

Samanta, A. and S. S. Bandyopadhyay (2007). "Kinetics and modeling of carbon dioxide absorption into aqueous solutions of piperazine." Chemical Engineering Science **62**(24): 7312-7319.

Sartori, G. and D. W. Savage (1983). "Sterically hindered amines for carbon dioxide removal from gases." Industrial & Engineering Chemistry Fundamentals **22**(2): 239,243,.

Schmidt, K. A. G., et al. (2008). "Solubility of Methane in an Aqueous Methyldiethanolamine Solution (Mass Fraction 50 %)." Journal of Chemical & Engineering Data **53**(8): 1725-1727.

Scott, J. W., et al. (1986). "An all atom force field for simulations of proteins and nucleic acids." Journal of Computational Chemistry **7**(2): 230-252.

Sloan, E. D., Jr. (1998). "Physical/chemical properties of gas hydrates and application to world margin stability and climatic change." Geological Society, London, Special Publications **137**(1): 31-50.

Span, R. and W. Wagner (1996). "A New Equation of State for Carbon Dioxide Covering the Fluid Region from the Triple-Point Temperature to 1100 K at Pressures up to 800 MPa." Journal of Physical and Chemical Reference Data **25**(6): 1509-1596.

Sun, Y., et al. (1992). "Simulation of the solvation free energies for methane, ethane, and propane and corresponding amino acid dipeptides: a critical test of the bond-PMF correction, a new set of hydrocarbon parameters, and the gas phase-water hydrophobicity scale." Journal of the American Chemical Society **114**(17): 6798-6801.

Svendsen, H. F., et al. (2001). Absorption as a Method for CO2 Capture. Second Nordic Minisymposium on Carbon Dioxide Capture and Storage. Göteborg, Sweden**:** 24,25.

Swaminathan, S., et al. (1978). "Monte Carlo studies on the structure of a dilute aqueous solution of methane." Journal of the American Chemical Society **100**(18): 5705-5712.

Thompson, J. D., et al. (2002). "More reliable partial atomic charges when using diffuse basis sets." PhysChemComm **5**(18): 117–134.

van Loo, S., et al. (2007). "The removal of carbon dioxide with activated solutions of methyl-diethanol-amine." Journal of Petroleum Science and Engineering **55**(1,2): 135.

Watkins, E. K. and W. L. Jorgensen (2001). "Perfluoroalkanes: Conformational Analysis and Liquid-State Properties from ab Initio and Monte Carlo Calculations." The Journal of Physical Chemistry A **105**(16): 4118-4125.

Watson, R. T., et al. (2001). Climate Change 2001: Synthesis Report: An Assessment of the Intergovernmental Panel on Climate Change. New York, IPCC Plenary XVIII (Wembley, United Kingdom, 24-29 September 2001)**:** 398 pp.

Wolfgang, D., et al. (1997). "OPLS all-atom force field for carbohydrates." Journal of Computational Chemistry **18**(16): 1955-1970.

Xu, G.-W., et al. (1998). "Gas−Liquid Equilibrium in a CO2−MDEA−H2O System and the Effect of Piperazine on It." Industrial & Engineering Chemistry Research **37**(4): 1473-1477.

Xu, G., et al. (1992). "Kinetics study on absorption of carbon dioxide into solutions of activated methyldiethanolamine." Industrial & Engineering Chemistry Research **31**(3): 921-927.

# Appendix A

## MDynaMix Ver.5.1 sample input file for simulation of primary system

```
#
#Input file for MD simulation of Aqueous Piperazine Activated MDEA Solution
#for Absorption of CO2 from Natural Gas
#
#
Main_filename Primary_system
Verbose_level 5
Path_DB    ../../moldb
Read_restart yes
Dump_restart 5000
Check_only no

#
Molecule_types 7
CO2_elb    61
CH4       491
PZ         44
PZH        44
PZCOO      44
MDEA      556
H2O_E    3311
#
Box  60.529  60.529  110.529
#Density 1.045
Change_V no
Change_T no
Nose_thermostat 298.173 50.
#Velocity_scaling 298.173 5.0
#Barostate_NH 1. 1000.
#Barostate_anisotropic no
PBC rect
COM_check yes 0
#
Time_step  1.
Constrain 1.d-4   1  1  1  1  1  1  1
Number_steps 5000000
#Double_timestep 10
R_cutoff 10.
R_short 5.
Neighbour_list 10
Electrostatics Ewald 2.8 9.
Cut_forces 1.
#
Startup FCC
#
Output 5
Serie_avegare 5000
Average_from 3
Average_int yes
Dump_XMOL yes

Trajectory asccrd 100. 1000  all
#
RDF_calc RW 15 300
17
4  56
1  56
4  1
1 77
4 77
&2
4  17
4  19
&2
4  33
4  34
&2
4  50
```

```
4  52
&2
1  17
1  19
&2
1  33
1  34
&2
1  50
1  52
&2
77 17
77 19
&2
77 33
77 34
&2
77 50
77 52
&2
56 17
56 19
&2
33 50
34 52
&6
4 17
4 19
4 33
4 34
4 50
4 52
#
End
```

# Appendix B

## 1. MDynaMix Ver.5.1 molecular input file for MDEA

```
#================================================I
#       Molecular Dynamics Data Base             I
#       Configuration and interaction potential  I
#       OPLS-aa Forcefield                       I
#================================================I
#       Methyldiethanolamine (MDEA)              I
#================================================I
#       Number of sites
 21
#         X         Y         Z         M         Q     sigma     epsilon
#                  (A)                 (u)       (e)     (A)      (kJ/M)
 N1    -24.848   -22.482   -33.745   14.0067   -0.46258  3.3     0.71128
 C2    -25.612   -21.274   -33.975   12.0111   -0.00278  3.5     0.276144
 H3    -26.128   -20.885   -33.097    1.008     0.06274  2.5     0.06276
 H4    -24.896   -20.511   -34.279    1.008     0.06005  2.5     0.06276
 H5    -26.412   -21.354   -34.711    1.008     0.03748  2.5     0.06276
 C6    -25.438   -23.747   -34.131   12.0111    0.03249  3.5     0.276144
 H7    -26.484   -23.779   -33.824    1.008     0.02954  2.5     0.06276
 H8    -23.814   -21.853   -31.994    1.008     0.06565  2.5     0.06276
 H9    -23.424   -23.471   -32.510    1.008     0.03789  2.5     0.06276
 C10   -25.389   -23.946   -35.646   12.0111    0.06754  3.5     0.276144
 H11   -24.730   -23.263   -36.182    1.008     0.04292  2.5     0.12552
 H12   -25.055   -24.952   -35.900    1.008     0.05337  2.5     0.12552
 H13   -24.843   -24.547   -33.692    1.008     0.07352  2.5     0.06276
 O14   -26.586   -23.939   -36.392   15.9994   -0.48039  3.07    0.71128
 H15   -27.334   -24.220   -35.887    1.008     0.31673  0.0     0.0
 C16   -23.689   -22.479   -32.877   12.0111    0.06112  3.5     0.276144
 C17   -22.475   -21.929   -33.627   12.0111    0.06983  3.5     0.276144
 H18   -22.204   -22.412   -34.565    1.008     0.04852  2.5     0.12552
 H19   -22.499   -20.852   -33.791    1.008     0.05437  2.5     0.12552
 O20   -21.306   -21.986   -32.841   15.9994   -0.49044  3.07    0.71128
 H21   -20.669   -21.630   -33.442    1.008     0.32242  0.0     0.0
#    Num. of strings for the reference
 19
    OPLS-aa  reference:
    W. L. Jorgensen, D. S. Maxwell, J. Tirado-Rives, J. Am. Chem. Soc. 118,
    11225-36 (1996).
    W. Damm, A. Frontera, J. Tirado-Rives, W. L. Jorgensen, J. Comput. Chem.
    18, 1955-70 (1997).
    W. L. Jorgensen and N. A. McDonald, Theochem 424, 145-155 (1998).
    W. L. Jorgensen and N. A. McDonald, J. Phys. Chem. B 102, 8049-8059(1998).
    R. C. Rizzo and W. L. Jorgensen, J. Am. Chem. Soc. 121, 4827-4836 (1999).
    E. K. Watkins and W. L. Jorgensen, J. Phys. Chem. A 105, 4118-4125 (2001).
    M. L. P. Price, D. Ostrovsky, and W. L. Jorgensen, J. Comput. Chem., 22,
    1340-1352 (2001).
    W. L. Jorgensen, J. P. Ulmschneider, J. Tirado-Rives, J. Phys. Chem.
    B 108, 16264-70 (2004).
    K. P. Jensen and W. L. Jorgensen, J. Chem. Theory Comput. 2,
    1499-1509 (2006).
    Ab initio calculation by Schrodinger package-Jaguar Ver.7.6:
    The optimized geometry and CM4 partial charges have been computed
    by means of the Ab initio calculation using DFT-B3LYP/6-31G** and
    SM8 solvation model.
#   Num. of bonds
 20
#ID(typ)        N1      N2       Reqv(A)   Force(KJ/M/A2)
  0             1        2       1.448      1598.288
  0             1       16       1.448      1598.288
  0             2        4       1.09       1422.56
  0             6        7       1.09       1422.56
  0             6       13       1.09       1422.56
  0             9       16       1.09       1422.56
  0            10       12       1.09       1422.56
  0            14       15       0.945      2313.752
  0            17       18       1.09       1422.56
  0            17       20       1.41       1338.88
  0             1        6       1.448      1598.288
  0             2        3       1.09       1422.56
```

```
  0             2        5       1.09       1422.56
  0             6       10       1.529      1121.312
  0             8       16       1.09       1422.56
  0            10       11       1.09       1422.56
  0            10       14       1.41       1338.88
  0            16       17       1.529      1121.312
  0            17       19       1.09       1422.56
  0            20       21       0.945      2313.752
#   Num. of angles
 35
#  N1   N2      N3       Angle    Force
#                       (Degree) (KJ/M/Rad2)
   6    1       2        107.2    216.7312
  16    1       6        107.2    216.7312
   4    2       1        109.5    146.44
   5    2       1        109.5    146.44
   5    2       4        107.8    138.072
  10    6       1        109.47   235.1408
  13    6       1        109.5    146.44
  13    6      10        110.7    156.9
  12   10       6        110.7    156.9
  14   10       6        109.5    209.2
  14   10      12        109.5    146.44
   8   16       1        109.5    146.44
   9   16       8        107.8    138.072
  17   16       8        110.7    156.9
  18   17      16        110.7    156.9
  19   17      18        107.8    138.072
  20   17      18        109.5    146.44
  21   20      17        108.5    230.12
  16    1       2        107.2    216.7312
   3    2       1        109.5    146.44
   4    2       3        107.8    138.072
   5    2       3        107.8    138.072
   7    6       1        109.5    146.44
  10    6       7        110.7    156.9
  13    6       7        107.8    138.072
  11   10       6        110.7    156.9
  12   10      11        107.8    138.072
  14   10      11        109.5    146.44
  15   14      10        108.5    230.12
   9   16       1        109.5    146.44
  17   16       1        109.47   235.1408
  17   16       9        110.7    156.9
  19   17      16        110.7    156.9
  20   17      16        109.5    209.2
  20   17      19        109.5    146.44
#number of normal dihedral angles:
  0
# Special torsions specified by keyword:
  Tors1
#  Number of MM3-type torsions
#                                K1      k2      k3      k4
 40
 1       6       10      11      -4.24   -2.97   1.98    0.00
 1       6       10      12      -4.24   -2.97   1.98    0.00
 1      16       17      18      -4.24   -2.97   1.98    0.00
 1      16       17      19      -4.24   -2.97   1.98    0.00
 2       1        6       7       0.00    0.00   0.00    0.00
 2       1        6      10       1.74   -0.54   2.91    0.00
 2       1        6      13       0.00    0.00   0.00    0.00
 2       1       16       8       0.00    0.00   0.00    0.00
 2       1       16       9       0.00    0.00   0.00    0.00
 2       1       16      17       1.74   -0.54   2.91    0.00
 3       2        1       6       0.00    0.00   0.00    0.00
 3       2        1      16       0.00    0.00   0.00    0.00
 4       2        1       6       0.00    0.00   0.00    0.00
 4       2        1      16       0.00    0.00   0.00    0.00
```

```
 5       2       1       6       0.00    0.00   0.00    0.00
 5       2       1      16       0.00    0.00   0.00    0.00
 6       1      16       8       0.00    0.00   0.00    0.00
 6       1      16       9       0.00    0.00   0.00    0.00
 6       1      16      17       1.74   -0.54   2.91    0.00
 6      10      14      15      -1.49   -0.73   2.06    0.00
 7       6       1      16       0.00    0.00   0.00    0.00
 7       6      10      11       0.00    0.00   1.26    0.00
 7       6      10      12       0.00    0.00   1.26    0.00
 7       6      10      14       0.00    0.00   1.96    0.00
 8      16      17      18       0.00    0.00   1.26    0.00
 8      16      17      19       0.00    0.00   1.26    0.00
 8      16      17      20       0.00    0.00   1.96    0.00
 9      16      17      18       0.00    0.00   1.26    0.00
 9      16      17      19       0.00    0.00   1.26    0.00
 9      16      17      20       0.00    0.00   1.96    0.00
10       6       1      16       1.74   -0.54   2.91    0.00
11      10       6      13       0.00    0.00   1.26    0.00
11      10      14      15       0.00    0.00   1.47    0.00
12      10       6      13       0.00    0.00   1.26    0.00
12      10      14      15       0.00    0.00   1.47    0.00
13       6       1      16       0.00    0.00   0.00    0.00
13       6      10      14       0.00    0.00   1.96    0.00
16      17      20      21      -1.49   -0.73   2.06    0.00
18      17      20      21       0.00    0.00   1.47    0.00
19      17      20      21       0.00    0.00   1.47    0.00
 Tors3
# Number of custom torsions
#                  k1     f1      k2     f2    k3     f3      k4     f4     v1
   2
 1   6  10  14  14.42  -34.96  -12.20  0.84  14.74  15.91  17.05  -64.67  -0.8
 1  16  17  20  14.42  -34.96  -12.20  0.84  14.74  15.91  17.05  -64.67  -0.8
```

## 2. MDynaMix Ver.5.1 molecular input file for Piperazine

```
#================================================I
#       Molecular Dynamics Data Base             I
#       Configuration and interaction potential  I
#       OPLS-aa Forcefield                       I
#================================================I
#       Piperazine (PZ)                          I
#================================================I
#       Number of sites
 16
#           X        Y        Z        M          Q      sigma      epsilon
#                   (A)               (u)        (e)       (A)       (kJ/M)
 C1       2.0201   1.0300 -0.9713  12.0111    0.04385    3.5      0.276144
 C2       0.5434   1.1185 -1.3798  12.0111    0.05419    3.5      0.276144
 C3      -0.1161   0.7371  0.9195  12.0111    0.05274    3.5      0.276144
 C4       1.3603   0.6484  1.3287  12.0111    0.04359    3.5      0.276144
 H5       2.3947   2.0553 -0.7718   1.008     0.02965    2.5      0.06276
 H6       2.6185   0.6171 -1.7922   1.008     0.06333    2.5      0.06276
 H7       0.2107   0.1268 -1.7106   1.008     0.04834    2.5      0.06276
 H8       0.4203   1.8084 -2.2220   1.008     0.06377    2.5      0.06276
 H9      -0.7155   1.1516  1.7377   1.008     0.06458    2.5      0.06276
 H10     -0.4855  -0.2758  0.7164   1.008     0.04785    2.5      0.06276
 H11      1.6946   1.6504  1.6689   1.008     0.03022    2.5      0.06276
 H12      1.4811  -0.0408  2.1730   1.008     0.06275    2.5      0.06276
 N13      2.1363   0.1486  0.1921  14.0067   -0.58745    3.3      0.71128
 H14      3.1120   0.0424  0.4544   1.008     0.28535    0.0      0.0
 N15     -0.3373   1.5459 -0.2857  14.0067   -0.5813     3.3      0.71128
 H16     -0.1348   2.5209 -0.0659   1.008     0.27854    0.0      0.0
#    Num. of strings for the reference
 19
    OPLS-aa  reference:
    W. L. Jorgensen, D. S. Maxwell, J. Tirado-Rives, J. Am. Chem. Soc. 118,
    11225-36 (1996).
    W. Damm, A. Frontera, J. Tirado-Rives, W. L. Jorgensen, J. Comput. Chem.
    18, 1955-70 (1997).
    W. L. Jorgensen and N. A. McDonald, Theochem 424, 145-155 (1998).
    W. L. Jorgensen and N. A. McDonald, J. Phys. Chem. B 102, 8049-8059(1998).
    R. C. Rizzo and W. L. Jorgensen, J. Am. Chem. Soc. 121, 4827-4836 (1999).
    E. K. Watkins and W. L. Jorgensen, J. Phys. Chem. A 105, 4118-4125 (2001).
    M. L. P. Price, D. Ostrovsky, and W. L. Jorgensen, J. Comput. Chem., 22,
    1340-1352 (2001).
    W. L. Jorgensen, J. P. Ulmschneider, J. Tirado-Rives, J. Phys. Chem.
    B 108, 16264-70 (2004).
    K. P. Jensen and W. L. Jorgensen, J. Chem. Theory Comput. 2,
    1499-1509 (2006).
    Ab initio calculation by Schrodinger package-Jaguar Ver.7.6:
    The optimized geometry and CM4 partial charges have been
    computed by means of the Ab initio calculation using DFT-B3LYP/6-31G**
    and SM8 solvation model.
#   Num. of bonds
 16
#ID(typ)   N1  N2       Reqv(A) Force(KJ/M/A2)
  0         1   2       1.529   1121.312
  0         1   6       1.09    1422.56
  0         2   7       1.09    1422.56
  0         2  15       1.448   1598.288
  0         3   9       1.09    1422.56
  0         3  15       1.448   1598.288
  0         4  12       1.09    1422.56
  0        13  14       1.01    1815.856
  0         1   5       1.09    1422.56
  0         1  13       1.448   1598.288
  0         2   8       1.09    1422.56
  0         3   4       1.529   1121.312
  0         3  10       1.09    1422.56
  0         4  11       1.09    1422.56
  0         4  13       1.448   1598.288
  0        15  16       1.01    1815.856
#   Num. of angles
```

```
 30
#    N1  N2      N3        Angle    Force
#                          (Degree) (KJ/M/Rad2)
     5   1        2        110.7    156.9
     6   1        5        107.8    138.072
    13   1        5        109.5    146.44
     7   2        1        110.7    156.9
     8   2        7        107.8    138.072
    15   2        7        109.5    146.44
     9   3        4        110.7    156.9
    10   3        9        107.8    138.072
    15   3        9        109.5    146.44
    11   4        3        110.7    156.9
    12   4       11        107.8    138.072
    13   4       11        109.5    146.44
     4  13        1        107.2    216.7312
    14  13        4        109.5    146.44
    16  15        2        109.5    146.44
     6   1        2        110.7    156.9
    13   1        2        109.47   235.1408
    13   1        6        109.5    146.44
     8   2        1        110.7    156.9
    15   2        1        109.47   235.1408
    15   2        8        109.5    146.44
    10   3        4        110.7    156.9
    15   3        4        109.47   235.1408
    15   3       10        109.5    146.44
    12   4        3        110.7    156.9
    13   4        3        109.47   235.1408
    13   4       12        109.5    146.44
    14  13        1        109.5    146.44
     3  15        2        107.2    216.7312
    16  15        3        109.5    146.44
#number of normal dihedral angles:
    0
# Special torsions specified by keyword:
  Tors1
#  Number of MM3-type torsions
 42
 1       2       15        3        1.74    -0.54    2.91     0.00
 1       2       15       16       -0.79    -1.74    1.75     0.00
 1      13        4        3        1.74    -0.54    2.91     0.00
 1      13        4       11        0.00     0.00    0.00     0.00
 1      13        4       12        0.00     0.00    0.00     0.00
 2       1       13        4        1.74    -0.54    2.91     0.00
 2       1       13       14       -0.79    -1.74    1.75     0.00
 2      15        3        4        1.74    -0.54    2.91     0.00
 2      15        3        9        0.00     0.00    0.00     0.00
 2      15        3       10        0.00     0.00    0.00     0.00
 3       4       13       14       -0.79    -1.74    1.75     0.00
 3      15        2        7        0.00     0.00    0.00     0.00
 3      15        2        8        0.00     0.00    0.00     0.00
 4       3       15       16       -0.79    -1.74    1.75     0.00
 4      13        1        5        0.00     0.00    0.00     0.00
 4      13        1        6        0.00     0.00    0.00     0.00
 5       1        2        7        0.00     0.00    1.26     0.00
 5       1        2        8        0.00     0.00    1.26     0.00
 5       1        2       15       -4.24    -2.97    1.98     0.00
 5       1       13       14        0.00     0.00    1.67     0.00
 6       1        2        7        0.00     0.00    1.26     0.00
 6       1        2        8        0.00     0.00    1.26     0.00
 6       1        2       15       -4.24    -2.97    1.98     0.00
 6       1       13       14        0.00     0.00    1.67     0.00
 7       2        1       13       -4.24    -2.97    1.98     0.00
 7       2       15       16        0.00     0.00    1.67     0.00
 8       2        1       13       -4.24    -2.97    1.98     0.00
 8       2       15       16        0.00     0.00    1.67     0.00
 9       3        4       11        0.00     0.00    1.26     0.00
```

| | | | | | | | |
|---|---|---|---|---|---|---|---|
| 9 | 3 | 4 | 12 | 0.00 | 0.00 | 1.26 | 0.00 |
| 9 | 3 | 4 | 13 | -4.24 | -2.97 | 1.98 | 0.00 |
| 9 | 3 | 15 | 16 | 0.00 | 0.00 | 1.67 | 0.00 |
| 10 | 3 | 4 | 11 | 0.00 | 0.00 | 1.26 | 0.00 |
| 10 | 3 | 4 | 12 | 0.00 | 0.00 | 1.26 | 0.00 |
| 10 | 3 | 4 | 13 | -4.24 | -2.97 | 1.98 | 0.00 |
| 10 | 3 | 15 | 16 | 0.00 | 0.00 | 1.67 | 0.00 |
| 11 | 4 | 3 | 15 | -4.24 | -2.97 | 1.98 | 0.00 |
| 11 | 4 | 13 | 14 | 0.00 | 0.00 | 1.67 | 0.00 |
| 12 | 4 | 3 | 15 | -4.24 | -2.97 | 1.98 | 0.00 |
| 12 | 4 | 13 | 14 | 0.00 | 0.00 | 1.67 | 0.00 |
| 13 | 1 | 2 | 15 | 46.17 | -4.05 | 1.13 | 0.00 |
| 13 | 4 | 3 | 15 | 46.17 | -4.05 | 1.13 | 0.00 |

## 3. MDynaMix Ver.5.1 molecular input file for Piperazine carbamate

```
#================================================I
#       Molecular Dynamics Data Base              I
#       Configuration and interaction potential   I
#       OPLS-aa Forcefield                        I
#================================================I
#       Piperazine Carbamate(PZCOO-)              I
#================================================I
#       Number of sites
 18
#         X       Y        Z       M        Q    sigma     epsilon
#                (A)              (u)      (e)    (A)       (kJ/M)
 C1     2.0157  1.0879  -0.9403 12.0111  0.05474  3.5      0.276144
 C2     0.5701  1.4960  -1.2359 12.0111  0.05709  3.5      0.276144
 C3    -0.0394  1.0500   1.0606 12.0111  0.05749  3.5      0.276144
 C4     1.4020  0.6382   1.3715 12.0111  0.05403  3.5      0.276144
 H5     2.5898  2.0020  -0.6939  1.008   0.03119  2.5      0.06276
 H6     2.4689  0.6245  -1.8274  1.008   0.06266  2.5      0.06276
 H7     0.0327  0.6104  -1.6365  1.008   0.02548  2.5      0.06276
 H8     0.5252  2.2845  -1.9891  1.008   0.06889  2.5      0.06276
 H9    -0.5128  1.5248   1.9218  1.008   0.06883  2.5      0.06276
 H10   -0.6178  0.134    0.8153  1.008   0.02490  2.5      0.06276
 H11    1.9362  1.5228   1.7689  1.008   0.03180  2.5      0.06276
 H12    1.4161 -0.1471   2.1398  1.008   0.06271  2.5      0.06276
 N13    2.0432  0.1073   0.1573 14.0067 -0.58704  3.3      0.71128
 H14    3.0046 -0.1538   0.3615  1.008   0.28296  0.0      0.0
 N15   -0.0554  2.0002  -0.0317 14.0067 -0.47952  3.3      0.71128
 C16   -1.1774  2.9371  -0.1491 12.0111  0.41829  3.750    0.43932
 O17   -1.2896  3.4960  -1.2703 15.9994 -0.61708  2.96     0.87864
 O18   -1.8646  3.0796   0.8947 15.9994 -0.61741  2.96     0.87864
#    Num. of strings for the reference
 19
   OPLS-aa  reference:
   W. L. Jorgensen, D. S. Maxwell, J. Tirado-Rives, J. Am. Chem. Soc.
   118, 11225-36 (1996).
   W. Damm, A. Frontera, J. Tirado-Rives, W. L. Jorgensen, J. Comput. Chem.
   18, 1955-70 (1997).
   W. L. Jorgensen and N. A. McDonald, Theochem 424, 145-155 (1998).
   W. L. Jorgensen and N. A. McDonald, J. Phys. Chem. B 102, 8049-8059 (1998).
   R. C. Rizzo and W. L. Jorgensen, J. Am. Chem. Soc. 121, 4827-4836 (1999).
   E. K. Watkins and W. L. Jorgensen, J. Phys. Chem. A 105, 4118-4125 (2001).
   M. L. P. Price, D. Ostrovsky, and W. L. Jorgensen, J. Comput. Chem.,
   22, 1340-1352 (2001).
   W. L. Jorgensen, J. P. Ulmschneider, J. Tirado-Rives, J. Phys. Chem.
   B 108, 16264-70 (2004).
   K. P. Jensen and W. L. Jorgensen, J. Chem. Theory Comput. 2,
   1499-1509 (2006).
   Ab initio calculation by Schrodinger package-Jaguar Ver.7.6:
   The optimized geometry and CM4 partial charges have been computed
   by means of the Ab initio calculation using DFT-B3LYP/6-31++G**
   and SM8 solvation model in combination with DFT-B3LYP/6-31G** respectively.
#   Num. of bonds
 18
#ID(typ)   N1  N2       Reqv(A) Force(KJ/M/A2)
    0       1   2       1.529   1121.312
    0       1   6       1.09    1422.56
    0       2   7       1.09    1422.56
    0       2  15       1.448   1598.288
    0       3   9       1.09    1422.56
    0       3  15       1.448   1598.288
    0       4  12       1.09    1422.56
    0      13  14       1.01    1815.856
    0      16  17       1.25    2744.704
    0       1   5       1.09    1422.56
    0       1  13       1.448   1598.288
    0       2   8       1.09    1422.56
    0       3   4       1.529   1121.312
    0       3  10       1.09    1422.56
    0       4  11       1.09    1422.56
```

```
    0       4  13       1.448   1598.288
    0      15  16       1.522   1326.328
    0      16  18       1.25    2744.704
#   Num. of angles
 33
#   N1   N2     N3      Angle    Force
#                      (Degree) (KJ/M/Rad2)
    5    1       2      110.7   156.9
    6    1       5      107.8   138.072
   13    1       5      109.5   146.44
    7    2       1      110.7   156.9
    8    2       7      107.8   138.072
   15    2       7      109.5   146.44
    9    3       4      110.7   156.9
   10    3       9      107.8   138.072
   15    3       9      109.5   146.44
   11    4       3      110.7   156.9
   12    4      11      107.8   138.072
   13    4      11      109.5   146.44
    4   13       1      107.2   216.7312
   14   13       4      109.5   146.44
   16   15       2      111.1   263.592
   17   16      15      120.4   334.72
   18   16      17      126.0   334.72
    6    1       2      110.7   156.9
   13    1       2      109.47  235.1408
   13    1       6      109.5   146.44
    8    2       1      110.7   156.9
   15    2       1      109.47  235.1408
   15    2       8      109.5   146.44
   10    3       4      110.7   156.9
   15    3       4      109.47  235.1408
   15    3      10      109.5   146.44
   12    4       3      110.7   156.9
   13    4       3      109.47  235.1408
   13    4      12      109.5   146.44
   14   13       1      109.5   146.44
    3   15       2      107.2   216.7312
   16   15       3      111.1   263.592
   18   16      15      120.4   334.72
#number of normal dihedral angles:
 0
# Special torsions specified by keyword:
  Tors1
#  Number of MM3-type torsions
 44
 1      2      15       3      1.74    -0.54   2.91    0.00
 1      2      15      16      0.00     1.93   0.00    0.00
 1     13       4       3      1.74    -0.54   2.91    0.00
 1     13       4      11      0.00     0.00   0.00    0.00
 1     13       4      12      0.00     0.00   0.00    0.00
 2      1      13       4      1.74    -0.54   2.91    0.00
 2      1      13      14     -0.79    -1.74   1.75    0.00
 2     15       3       4      1.74    -0.54   2.91    0.00
 2     15       3       9      0.00     0.00   0.00    0.00
 2     15       3      10      0.00     0.00   0.00    0.00
 2     15      16      18      0.00    25.48   0.00    0.00
 3      4      13      14     -0.79    -1.74   1.75    0.00
 3     15       2       7      0.00     0.00   0.00    0.00
 3     15       2       8      0.00     0.00   0.00    0.00
 3     15      16      17      0.00    25.48   0.00    0.00
 4      3      15      16      0.00     1.93   0.00    0.00
 4     13       1       5      0.00     0.00   0.00    0.00
 4     13       1       6      0.00     0.00   0.00    0.00
 5      1       2       7      0.00     0.00   1.26    0.00
 5      1       2       8      0.00     0.00   1.26    0.00
 5      1       2      15     -4.24    -2.97   1.98    0.00
 5      1      13      14      0.00     0.00   1.67    0.00
```

```
 6       1        2         7       0.00      0.00    1.26     0.00
 6       1        2         8       0.00      0.00    1.26     0.00
 6       1        2        15      -4.24     -2.97    1.98     0.00
 6       1       13        14       0.00      0.00    1.67     0.00
 7       2        1        13      -4.24     -2.97    1.98     0.00
 7       2       15        16       0.00      0.00   -0.58     0.00
 8       2        1        13      -4.24     -2.97    1.98     0.00
 8       2       15        16       0.00      0.00   -0.58     0.00
 9       3        4        11       0.00      0.00    1.26     0.00
 9       3        4        12       0.00      0.00    1.26     0.00
 9       3        4        13      -4.24     -2.97    1.98     0.00
 9       3       15        16       0.00      0.00   -0.58     0.00
10       3        4        11       0.00      0.00    1.26     0.00
10       3        4        12       0.00      0.00    1.26     0.00
10       3        4        13      -4.24     -2.97    1.98     0.00
10       3       15        16       0.00      0.00   -0.58     0.00
11       4        3        15      -4.24     -2.97    1.98     0.00
11       4       13        14       0.00      0.00    1.67     0.00
12       4        3        15      -4.24     -2.97    1.98     0.00
12       4       13        14       0.00      0.00    1.67     0.00
13       1        2        15      46.17     -4.05    1.13     0.00
13       4        3        15      46.17     -4.05    1.13     0.00
 Tors4
# Number of custom torsions
#                    k1      f1        k2       f2       k3      f3
   2
 2  15  16  17   -0.6664  34.5829  31.2892   35.4451  0.7284   70.6008
 3  15  16  18    0.1366  43.9283  31.9823  -35.1870 -0.7327  108.0740
```

## 4. MDynaMix Ver.5.1 molecular input file for Protonated piperazine

```
#================================================I
#       Molecular Dynamics Data Base              I
#       Configuration and interaction potential   I
#       OPLS-aa Forcefield                        I
#================================================I
#       Protonated Piperazine (PZH+)              I
#================================================I
#       Number of sites
 17
#         X         Y         Z         M          Q      sigma    epsilon
#                  (A)                 (u)        (e)       (A)     (kJ/M)
 C1    -10.506    7.941   -18.098   12.0111    0.06204    3.5   0.276144
 C2    -11.550    6.832   -18.237   12.0111    0.06166    3.5   0.276144
 C3    -13.231    8.650   -18.077   12.0111    0.06123    3.5   0.276144
 C4    -12.101    9.676   -17.989   12.0111    0.06258    3.5   0.276144
 H5     -9.570    7.647   -18.573    1.008     0.08644    2.5   0.06276
 H6    -10.336    8.127   -17.037    1.008     0.10158    2.5   0.06276
 H7    -11.190    6.112   -17.502    1.008     0.06278    2.5   0.06276
 H8    -11.423    6.354   -19.209    1.008     0.08299    2.5   0.06276
 H9    -13.922    8.843   -18.897    1.008     0.08309    2.5   0.06276
 H10   -13.887    8.854   -17.230    1.008     0.06198    2.5   0.06276
 H11   -12.460   10.594   -18.455    1.008     0.08630    2.5   0.06276
 H12   -11.893    9.895   -16.942    1.008     0.10147    2.5   0.06276
 N13   -10.884    9.231   -18.635   14.0067   -0.34428    3.3   0.71128
 N14   -12.885    7.258   -17.875   14.0067   -0.56959    3.3   0.71128
 H15   -13.574    6.519   -17.886    1.008     0.29360    0.0   0.0
 H16   -10.970    9.111   -19.634    1.008     0.35686    0.0   0.0
 H17   -10.073    9.820   -18.504    1.008     0.34926    0.0   0.0
#    Num. of strings for the reference
 20
    OPLS-aa  reference:
    W. L. Jorgensen, D. S. Maxwell, J. Tirado-Rives, J. Am. Chem. Soc.
    118, 11225-36 (1996).
    W. Damm, A. Frontera, J. Tirado-Rives, W. L. Jorgensen, J. Comput. Chem.
    18, 1955-70 (1997).
    W. L. Jorgensen and N. A. McDonald, Theochem 424, 145-155 (1998).
    W. L. Jorgensen and N. A. McDonald, J. Phys. Chem.
    B 102, 8049-8059 (1998).
    R. C. Rizzo and W. L. Jorgensen, J. Am. Chem. Soc. 121, 4827-4836 (1999).
    E. K. Watkins and W. L. Jorgensen, J. Phys. Chem. A 105, 4118-4125 (2001).
    M. L. P. Price, D. Ostrovsky, and W. L. Jorgensen, J. Comput. Chem.,
    22, 1340-1352 (2001).
    W. L. Jorgensen, J. P. Ulmschneider, J. Tirado-Rives, J. Phys. Chem.
    B 108, 16264-70 (2004).
    K. P. Jensen and W. L. Jorgensen, J. Chem. Theory Comput.
    2, 1499-1509 (2006).
    Ab initio calculation by Schrodinger package-Jaguar Ver.7.6:
    The optimized geometry and CM4 partial charges have been computed
    by means of the Ab initio calculation using SM8 solvation model
    and DFT-B3LYP/6-31G**.
#   Num. of bonds
 17
#ID(typ)   N1  N2       Reqv(A) Force(KJ/M/A2)
  0         1    2       1.529   1121.312
  0         1    6       1.09    1422.56
  0         2    7       1.09    1422.56
  0         2   14       1.448   1598.288
  0         3    9       1.09    1422.56
  0         3   14       1.448   1598.288
  0         4   12       1.09    1422.56
  0        13   16       1.01    1815.856
  0        14   15       1.01    1815.856
  0         1    5       1.09    1422.56
  0         1   13       1.448   1598.288
  0         2    8       1.09    1422.56
  0         3    4       1.529   1121.312
  0         3   10       1.09    1422.56
  0         4   11       1.09    1422.56
```

```
  0        4   13       1.448   1598.288
  0       13   17       1.01    1815.856
#   Num. of angles
 33
#  N1   N2     N3        Angle    Force
#                       (Degree) (KJ/M/Rad2)
   5    1       2        110.7   156.9
   6    1       5        107.8   138.072
  13    1       5        109.5   146.44
   7    2       1        110.7   156.9
   8    2       7        107.8   138.072
  14    2       7        109.5   146.44
   9    3       4        110.7   156.9
  10    3       9        107.8   138.072
  14    3       9        109.5   146.44
  11    4       3        110.7   156.9
  12    4      11        107.8   138.072
  13    4      11        109.5   146.44
   4   13       1        107.2   216.7312
  16   13       4        109.5   146.44
  17   13       4        109.5   146.44
   3   14       2        107.2   216.7312
  15   14       3        109.5   146.44
   6    1       2        110.7   156.9
  13    1       2        109.47  235.1408
  13    1       6        109.5   146.44
   8    2       1        110.7   156.9
  14    2       1        109.47  235.1408
  14    2       8        109.5   146.44
  10    3       4        110.7   156.9
  14    3       4        109.47  235.1408
  14    3      10        109.5   146.44
  12    4       3        110.7   156.9
  13    4       3        109.47  235.1408
  13    4      12        109.5   146.44
  16   13       1        109.5   146.44
  17   13       1        109.5   146.44
  17   13      16        106.4   182.4224
  15   14       2        109.5   146.44
# number of normal dihedral angles:
  0
# Special torsions specified by keyword:
  Tors1
#  Number of MM3-type torsions
 48
 1      2      14        3      1.74    -0.54   2.91    0.00
 1      2      14       15     -0.79    -1.74   1.75    0.00
 1     13       4        3      1.74    -0.54   2.91    0.00
 1     13       4       11      0.00     0.00   0.00    0.00
 1     13       4       12      0.00     0.00   0.00    0.00
 2      1      13        4      1.74    -0.54   2.91    0.00
 2      1      13       16     -0.79    -1.74   1.75    0.00
 2      1      13       17     -0.79    -1.74   1.75    0.00
 2     14       3        4      1.74    -0.54   2.91    0.00
 2     14       3        9      0.00     0.00   0.00    0.00
 2     14       3       10      0.00     0.00   0.00    0.00
 3      4      13       16     -0.79    -1.74   1.75    0.00
 3      4      13       17     -0.79    -1.74   1.75    0.00
 3     14       2        7      0.00     0.00   0.00    0.00
 3     14       2        8      0.00     0.00   0.00    0.00
 4      3      14       15     -0.79    -1.74   1.75    0.00
 4     13       1        5      0.00     0.00   0.00    0.00
 4     13       1        6      0.00     0.00   0.00    0.00
 5      1       2        7      0.00     0.00   1.26    0.00
 5      1       2        8      0.00     0.00   1.26    0.00
 5      1       2       14     -4.24    -2.97   1.98    0.00
 5      1      13       16      0.00     0.00   1.67    0.00
 5      1      13       17      0.00     0.00   1.67    0.00
```

| | | | | | | | |
|---|---|---|---|---|---|---|---|
| 6 | 1 | 2 | 7 | 0.00 | 0.00 | 1.26 | 0.00 |
| 6 | 1 | 2 | 8 | 0.00 | 0.00 | 1.26 | 0.00 |
| 6 | 1 | 2 | 14 | -4.24 | -2.97 | 1.98 | 0.00 |
| 6 | 1 | 13 | 16 | 0.00 | 0.00 | 1.67 | 0.00 |
| 6 | 1 | 13 | 17 | 0.00 | 0.00 | 1.67 | 0.00 |
| 7 | 2 | 1 | 13 | -4.24 | -2.97 | 1.98 | 0.00 |
| 7 | 2 | 14 | 15 | 0.00 | 0.00 | 1.67 | 0.00 |
| 8 | 2 | 1 | 13 | -4.24 | -2.97 | 1.98 | 0.00 |
| 8 | 2 | 14 | 15 | 0.00 | 0.00 | 1.67 | 0.00 |
| 9 | 3 | 4 | 11 | 0.00 | 0.00 | 1.26 | 0.00 |
| 9 | 3 | 4 | 12 | 0.00 | 0.00 | 1.26 | 0.00 |
| 9 | 3 | 4 | 13 | -4.24 | -2.97 | 1.98 | 0.00 |
| 9 | 3 | 14 | 15 | 0.00 | 0.00 | 1.67 | 0.00 |
| 10 | 3 | 4 | 11 | 0.00 | 0.00 | 1.26 | 0.00 |
| 10 | 3 | 4 | 12 | 0.00 | 0.00 | 1.26 | 0.00 |
| 10 | 3 | 4 | 13 | -4.24 | -2.97 | 1.98 | 0.00 |
| 10 | 3 | 14 | 15 | 0.00 | 0.00 | 1.67 | 0.00 |
| 11 | 4 | 3 | 14 | -4.24 | -2.97 | 1.98 | 0.00 |
| 11 | 4 | 13 | 16 | 0.00 | 0.00 | 1.67 | 0.00 |
| 11 | 4 | 13 | 17 | 0.00 | 0.00 | 1.67 | 0.00 |
| 12 | 4 | 3 | 14 | -4.24 | -2.97 | 1.98 | 0.00 |
| 12 | 4 | 13 | 16 | 0.00 | 0.00 | 1.67 | 0.00 |
| 12 | 4 | 13 | 17 | 0.00 | 0.00 | 1.67 | 0.00 |
| 13 | 1 | 2 | 14 | 46.17 | -4.05 | 1.13 | 0.00 |
| 13 | 4 | 3 | 14 | 46.17 | -4.05 | 1.13 | 0.00 |